CHAPTER 1

REVIEW OF NEWTONIAN FLUID DYNAMICS

In this introductory chapter we begin by giving the equations that describe the flow of fluids. These are the "equations of change," which indicate how the mass, momentum, and energy of the fluid change with position and time. In §1.1 we present these equations in terms of the fluxes so that they are valid for any kind of fluid, and in §1.2 we specialize the equations for the "Newtonian fluid." In §1.3 we illustrate the use of the equations for solving a variety of isothermal flow problems. In §1.4 we introduce the stream-function method as a powerful analytic technique for the solution of some flow problems.

In §§1.1 and 1.2 we present all the equations that are needed for solving nonisothermal flow problems and heat conduction problems. However, no illustrative examples are given for heat transfer. Nonisothermal flows are discussed in Chapter 4 for generalized Newtonian fluids, and full use is made there of the energy equation derived in §§1.1 and 1.2.

At the end of this chapter there is a rather long set of problems. Many of these problems involve the solution of the hydrodynamic equations for Newtonian fluids. Almost all of these flow problems are encountered again in later chapters, where they are solved for polymeric fluids using "non-Newtonian" models. Then it will be very convenient to have the Newtonian fluid solutions available.

§1.1 THE EQUATIONS OF CHANGE IN TERMS OF THE FLUXES

The motion of any fluid is described by the equations of conservation of mass, momentum, and energy. These equations are shown in two forms in Table 1.1-1. Since these equations form the basis for all of the subject material of the book, it is reasonable to discuss their derivation briefly. A more elementary derivation can be found elsewhere.[1]

In the derivation we consider an arbitrary *fixed* region in space of volume V and surface S, as shown in Fig. 1.1-1; sometimes such a mathematical region is referred to as a "control volume." On every surface element dS there is an outwardly directed normal unit vector $\boldsymbol{n}$. We imagine that this fixed region is in the midst of a fluid flow field and that the fluid moves across the boundaries of the region. We now want to apply the laws of conservation of mass, momentum, and energy to the fluid contained within this fixed region. It is presumed that the reader is familiar with the material on vector and tensor notation in §§A.1-A.7.

[1] See, for example, R. B. Bird, W. E. Stewart, and E. N. Lightfoot, *Transport Phenomena*, Wiley, New York (1960), Chapts. 3 and 10.

TABLE 1.1-1

The Equations of Change in Terms of the Fluxes π and q

	In terms of $\frac{\partial}{\partial t}$	
Mass:	$\frac{\partial}{\partial t}\rho = -(\nabla \cdot \rho \boldsymbol{v})$	(A)
Momentum:	$\frac{\partial}{\partial t}\rho \boldsymbol{v} = -[\nabla \cdot \rho \boldsymbol{v}\boldsymbol{v}] - [\nabla \cdot \boldsymbol{\pi}] + \rho \boldsymbol{g}$	(B)
Energy:	$\frac{\partial}{\partial t}\rho \hat{U} = -(\nabla \cdot \rho \hat{U}\boldsymbol{v}) - (\nabla \cdot \boldsymbol{q}) - (\boldsymbol{\pi} : \nabla \boldsymbol{v})$	(C)
	In terms of $\frac{D}{Dt} = \frac{\partial}{\partial t} + (\boldsymbol{v} \cdot \nabla)$	
Mass:	$\frac{D\rho}{Dt} = -\rho(\nabla \cdot \boldsymbol{v})$	(D)
Momentum:	$\rho \frac{D\boldsymbol{v}}{Dt} = -[\nabla \cdot \boldsymbol{\pi}] + \rho \boldsymbol{g}$	(E)
Energy:	$\rho \frac{D\hat{U}}{Dt} = -(\nabla \cdot \boldsymbol{q}) - (\boldsymbol{\pi} : \nabla \boldsymbol{v})$	(F)

a. Conservation of Mass

Suppose that at the infinitesimal surface element dS the fluid is crossing the surface of V with a velocity $\boldsymbol{v}$. Then the local volume rate of flow of fluid across dS is $(\boldsymbol{n} \cdot \boldsymbol{v})dS$. If the flow is outward, then $(\boldsymbol{n} \cdot \boldsymbol{v})dS$ is positive, whereas if the flow is inward $(\boldsymbol{n} \cdot \boldsymbol{v})dS$ is negative.[2] The local mass rate of flow is then $(\boldsymbol{n} \cdot \rho \boldsymbol{v})dS$. Note that $\rho \boldsymbol{v}$ is the mass flux (i.e., mass per unit area per unit time).

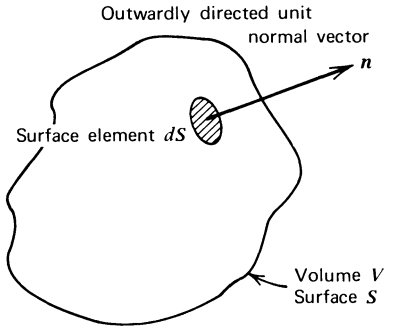

FIGURE 1.1-1. Arbitrary "control volume," fixed in space, over which mass, momentum, and energy balances are made.

[2] Recall that $(\boldsymbol{n} \cdot \boldsymbol{v})$ can be interpreted as the component of $\boldsymbol{v}$ in the direction of $\boldsymbol{n}$.

According to the law of conservation of mass, the total mass of fluid within V will increase only because of a net influx of fluid across the bounding surface S. Mathematically this is stated as

$$\frac{d}{dt}\int_V \rho\, dV = -\int_S (\boldsymbol{n}\cdot\rho\boldsymbol{v})dS \tag{1.1-1}$$

Rate of increase of mass of fluid within V | Rate of addition of mass across the surface S

When Gauss's divergence theorem (§A.5) is used, the surface integral can be transformed into a volume integral;

$$\frac{d}{dt}\int_V \rho\, dV = -\int_V (\nabla\cdot\rho\boldsymbol{v})dV \tag{1.1-2}$$

The equation may be rearranged by bringing the time derivative inside the integral. This is permissible since the volume V is fixed. This gives:

$$\int_V \left[\frac{\partial\rho}{\partial t} + (\nabla\cdot\rho\boldsymbol{v})\right]dV = 0 \tag{1.1-3}$$

We now have an integral over an arbitrary volume and this integral is equated to zero. Because of the arbitrariness of the volume, the integrand may now be set equal to zero. This gives:

$$\boxed{\frac{\partial\rho}{\partial t} = -(\nabla\cdot\rho\boldsymbol{v})} \tag{1.1-4}$$

which is called the *equation of continuity*. If the fluid has constant density, then Eq. 1.1-4 simplifies to:

$$(\nabla\cdot\boldsymbol{v}) = 0 \tag{1.1-5}$$

Use is often made of this relation for "incompressible fluids".

b. Conservation of Momentum

As pointed out above, the local volume rate of flow of a fluid across the surface element dS is $(\boldsymbol{n}\cdot\boldsymbol{v})dS$. If this is multiplied by the momentum per unit volume of the fluid, we then get $(\boldsymbol{n}\cdot\boldsymbol{v})\rho\boldsymbol{v}\, dS$; this is the rate at which momentum is carried across the element of surface dS just because the fluid itself flows across dS. This latter expression can be rearranged as $[\boldsymbol{n}\cdot\rho\boldsymbol{v}\boldsymbol{v}]dS$, and the quantity $\rho\boldsymbol{v}\boldsymbol{v}$ is the momentum flux (i.e., momentum per unit area per unit time) associated with the bulk flow of fluid. Sometimes this transport associated with bulk flow is referred to as "convective transport."

Note that there is a parallelism between the first paragraph of this subsection and the first paragraph of the preceding subsection, but that the tensorial order of the quantities involved is different. In the preceding discussion the entity being transported is mass (a scalar), and the mass flux is a vector ($\rho \boldsymbol{v}$). Here the entity being transported is momentum (a vector), and the momentum flux is a tensor ($\rho \boldsymbol{vv}$).

In addition to momentum transport by flow, there will also be momentum transferred by virtue of the molecular motions and interactions within the fluid. This additional momentum flux will be designated by the symbol $\boldsymbol{\pi}$, again a second-order tensor. We use the convention that the ij-component of this tensor π_{ij} represents the flux of positive j-momentum in the positive i-direction, associated with molecular processes. The rate of flow of momentum, resulting from molecular motions, across the element of surface dS with orientation $\boldsymbol{n}$ is then $[\boldsymbol{n} \cdot \boldsymbol{\pi}]dS$. It will be assumed throughout the entire book that $\boldsymbol{\pi}$ is a symmetric tensor (i.e., $\pi_{ij} = \pi_{ji}$). Thus far most of the kinetic theories for simple and macromolecular fluids yield symmetric momentum-flux tensors (for an exception see Example 18.4-2), and no experiments have been performed that enable one to measure any nonsymmetrical contributions.

We are now ready to write down the law of conservation of momentum. According to this law, the total momentum of the fluid within V will increase because of a net influx of momentum across the bounding surface—both by bulk flow and by molecular motions —and because of the external force of gravity acting on the fluid. When translated into mathematical terms this becomes

$$\frac{d}{dt}\int_V \rho \boldsymbol{v}\, dV = -\int_S [\boldsymbol{n} \cdot \rho \boldsymbol{vv}]dS - \int_S [\boldsymbol{n} \cdot \boldsymbol{\pi}]dS + \int_V \rho \boldsymbol{g}\, dV \tag{1.1-6}$$

Rate of increase of momentum of fluid within V	Rate of addition of momentum across S by bulk flow	Rate of addition of momentum across S by molecular motions and interactions	Force on fluid within V by gravity

where $\boldsymbol{g}$ is the force per unit mass due to gravity. Application of the Gauss divergence theorem enables us to rewrite the surface integrals as volume integrals:

$$\int_V \frac{\partial}{\partial t} \rho \boldsymbol{v}\, dV = -\int_V [\boldsymbol{\nabla} \cdot \rho \boldsymbol{vv}]dV - \int_V [\boldsymbol{\nabla} \cdot \boldsymbol{\pi}]dV + \int_V \rho \boldsymbol{g}\, dV \tag{1.1-7}$$

Then since the volume V is arbitrary, the integral signs may be removed to obtain

$$\boxed{\frac{\partial}{\partial t} \rho \boldsymbol{v} = -[\boldsymbol{\nabla} \cdot \rho \boldsymbol{vv}] - [\boldsymbol{\nabla} \cdot \boldsymbol{\pi}] + \rho \boldsymbol{g}} \tag{1.1-8}$$

and this is the *equation of motion.*

Before continuing it is appropriate to give an alternative interpretation of the tensor $\boldsymbol{\pi}$ and its components. In the derivation of Eq. 1.1-8 we could have used a somewhat different physical statement leading up to Eq. 1.1-6: the total momentum of the fluid within

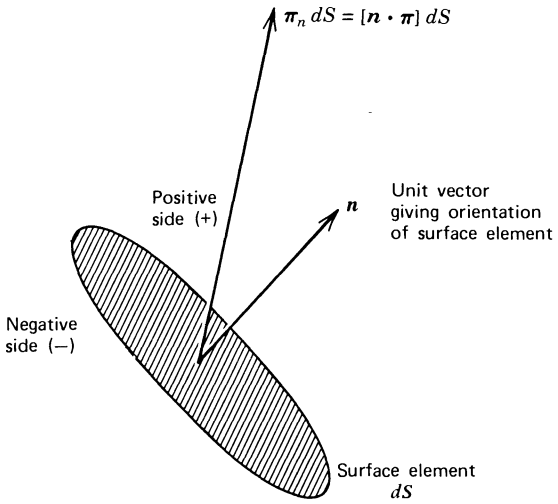

FIGURE 1.1-2. Element of surface dS across which a force $\pi_n\, dS$ is transmitted.

V will increase because of a net influx of momentum across the bounding surfaces by bulk flow, and because of the external forces acting on the fluid—both the surface force exerted by the surrounding fluid and the body force exerted by gravity. The surface force term in Eq. 1.1-6 would then have the form $-\int \pi_n\, dS$, where $\pi_n\, dS$ is a vector describing the force exerted by the fluid on the negative side of dS on the fluid on the positive side of dS (Fig. 1.1-2). Comparison of the above integral with the corresponding term in Eq. 1.1-6 shows that $\pi_n = [\boldsymbol{n} \cdot \boldsymbol{\pi}]$. That is, the force $\pi_n\, dS$ corresponding to any orientation $\boldsymbol{n}$ of dS can be obtained from the tensor $\boldsymbol{\pi}$. When this interpretation is used, it is more natural to refer to $\boldsymbol{\pi}$ as the "stress tensor" (the term "pressure tensor" is also used). The component π_{ij} is the force per unit area acting in the positive j-direction on a surface perpendicular to the i-direction, the force being exerted by the negative material on the positive material (see Fig. 1.1-3).

If one uses this viewpoint, then the integral $-\int [\boldsymbol{n} \cdot \boldsymbol{\pi}] dS$ in Eq. 1.1-6 can be reinterpreted as "force of the fluid outside V acting on the fluid inside V across S." For some purposes it is useful to think of $\boldsymbol{\pi}$ as a momentum flux, whereas in some situations the concept of stress is more natural. We shall feel free to use both interpretations and the terms "momentum flux tensor" and "stress tensor" will be used interchangeably.[3]

[3] In most treatises on applied mechanics and mechanical engineering a different convention is used for the stress tensor. A stress tensor $\boldsymbol{\sigma}$ is defined by $\pi_{-n}\, dS = -\pi_n\, dS = [\boldsymbol{\sigma} \cdot \boldsymbol{n}] dS$; that is, one thinks about the fluid on the "positive side" exerting a force on the fluid on the "negative side." The tensors $\boldsymbol{\pi}$ and $\boldsymbol{\sigma}$ are related by $\boldsymbol{\pi} = -\boldsymbol{\sigma}^{\dagger}$, where † stands for "transpose"; thus they differ in sign and in the order of the indices. Since the stress tensor is usually assumed to be symmetric, the change in the order of the indices is not particularly worrisome, but the difference in sign convention is important. We have two reasons for preferring the convention adopted here: (i) In one-dimensional heat conduction described by Fourier's law $q_y = -k(dT/dy)$, it is customary to define q_y so that it is positive when heat is moving in the $+y$-direction, that is, when the temperature decreases with increasing y. Similarly in one-dimensional diffusion, described by Fick's law, $j_{Ay} = -\mathscr{D}_{AB}\, d\rho_A/dy$, the mass flux is defined as positive when species A is moving in the $+y$-direction, in the direction of decreasing concentration. Therefore in a shear flow described by Newton's law $\pi_{yx} = -\mu\, dv_x/dy$ it seems natural to define π_{yx} so that it is positive when x-momentum is moving in the $+y$-direction, that is, in the direction of decreasing velocity. Thus the linear laws for all three transport phenomena are formulated with the same sign convention. (ii) When the total stress tensor is broken down into two parts, a pressure contribution and a viscous contribution, as shown in Eq. 1.2-1, both parts have the same sign—that is, compression is positive in both terms in accordance with the sign convention normally used in thermodynamics.

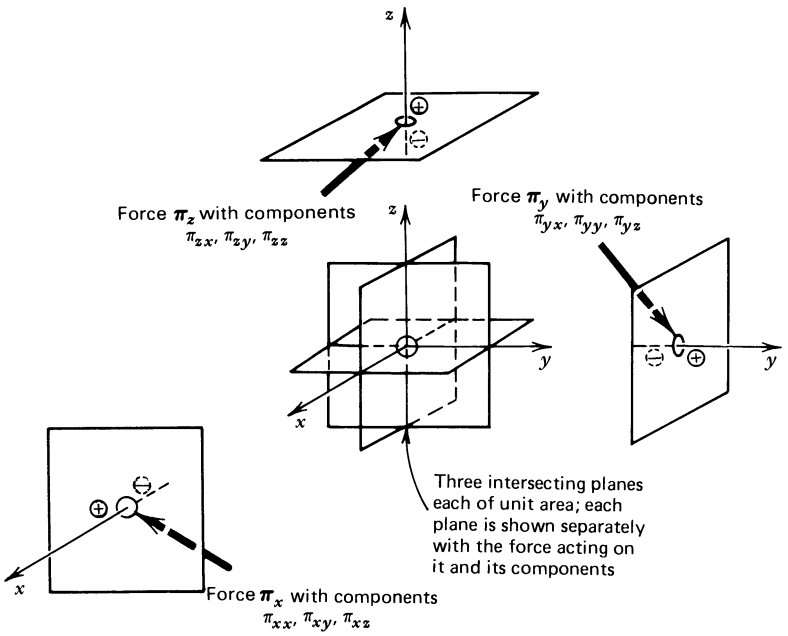

FIGURE 1.1-3. Sketch showing the sign convention and the index convention for the components of the stress tensor π.

We conclude this subsection by giving two additional equations that may be obtained from Eq. 1.1-8. By forming the dot product of the local fluid velocity vector $\boldsymbol{v}$ with the entire equation of motion and using the equation of continuity we obtain an equation of change for kinetic energy:

$$\frac{\partial}{\partial t}(\tfrac{1}{2}\rho v^2) = -(\nabla \cdot \tfrac{1}{2}\rho v^2 \boldsymbol{v}) - (\boldsymbol{v} \cdot [\nabla \cdot \boldsymbol{\pi}]) + \rho(\boldsymbol{v} \cdot \boldsymbol{g}) \tag{1.1-9}$$

Furthermore, by forming the cross product of the position vector $\boldsymbol{r}$ with the equation of motion and assuming that the stress tensor π is symmetrical we obtain an equation of change for angular momentum:

$$\frac{\partial}{\partial t}(\rho[\boldsymbol{r} \times \boldsymbol{v}]) = -[\nabla \cdot \rho \boldsymbol{v}[\boldsymbol{r} \times \boldsymbol{v}]] - [\nabla \cdot \{\boldsymbol{r} \times \boldsymbol{\pi}\}^{\dagger}] + [\boldsymbol{r} \times \rho \boldsymbol{g}] \tag{1.1-10}$$

in which the symbol † stands for the transpose of a tensor. Note that the last two equations do not introduce additional unknowns, nor do they include new information.

c. Conservation of Energy

Once again we return to the point made earlier that the local volume rate of flow of a fluid across the surface element dS is $(\boldsymbol{n} \cdot \boldsymbol{v})dS$. If this is multiplied by $\frac{1}{2}\rho v^2$, which is the kinetic energy per unit volume, then we get $(\boldsymbol{n} \cdot \frac{1}{2}\rho v^2 \boldsymbol{v})dS$, which is the rate of convective flow of kinetic energy across the surface. Similarly, if $\hat{U}$ is the internal energy per unit mass, then $(\boldsymbol{n} \cdot \rho \hat{U} \boldsymbol{v})dS$ is the rate of convective flow of internal energy across the surface element.

In addition to the flow of kinetic and internal energy across dS because of the fluid flowing across dS, there may be energy transferred by molecular motions. This additional mode of transport is associated with heat conduction, and we designate this heat flux by the symbol $\boldsymbol{q}$. Then the heat flow across dS by heat conduction will be $(\boldsymbol{n}\cdot\boldsymbol{q})dS$.

As the fluid moves outwardly across the surface of V, it will do work on the fluid outside of V. It was mentioned earlier that $[\boldsymbol{n}\cdot\boldsymbol{\pi}]dS$ is the force exerted by the fluid *inside* V on the fluid *outside* V across dS. The rate of doing work[4] by the fluid inside V on the fluid outside V will be given by the scalar product of the force and the velocity. Hence the rate of doing work across dS is $([\boldsymbol{n}\cdot\boldsymbol{\pi}]\cdot\boldsymbol{v})dS$, which may also be written $(\boldsymbol{n}\cdot[\boldsymbol{\pi}\cdot\boldsymbol{v}])dS$.

We are now in a position to write down the law of conservation of energy (or the first law of thermodynamics) in mathematical terms. According to this law, the rate of increase of the sum of the kinetic and internal energies will equal the rate of energy addition (by flow and by heat conduction) minus the rate at which the fluid inside V is doing work (this includes work against the surrounding fluid across dS and work against the external force of gravity). When translated into mathematical symbols this becomes:

$$\frac{d}{dt}\int_V (\tfrac{1}{2}\rho v^2 + \rho\hat{U})dV = -\int_S (\boldsymbol{n}\cdot(\tfrac{1}{2}\rho v^2 + \rho\hat{U})\boldsymbol{v})dS$$

Rate of increase of kinetic and internal energy within V — Rate of addition of kinetic and internal energy across S by bulk flow

$$-\int_S (\boldsymbol{n}\cdot\boldsymbol{q})dS - \int_S (\boldsymbol{n}\cdot[\boldsymbol{\pi}\cdot\boldsymbol{v}])dS + \int_V (\boldsymbol{v}\cdot\rho\boldsymbol{g})dV \qquad (1.1\text{-}11)$$

Rate of addition of energy across S by molecular motions — Rate at which fluid outside V does work against fluid inside V — Rate at which gravity does work on the fluid

Applying the divergence theorem and then removing the integral signs as before, we get

$$\frac{\partial}{\partial t}(\tfrac{1}{2}\rho v^2 + \rho\hat{U}) = -(\nabla\cdot(\tfrac{1}{2}\rho v^2 + \rho\hat{U})\boldsymbol{v}) - (\nabla\cdot\boldsymbol{q}) - (\nabla\cdot[\boldsymbol{\pi}\cdot\boldsymbol{v}]) + (\rho\boldsymbol{v}\cdot\boldsymbol{g}) \qquad (1.1\text{-}12)$$

From this equation, which is an equation of change for the sum of the kinetic and internal energies, we can subtract the equation of change for kinetic energy alone, given in Eq. 1.1-9. This gives, if we make use of the assumption that $\boldsymbol{\pi}$ is symmetrical:

$$\boxed{\frac{\partial}{\partial t}\rho\hat{U} = -(\nabla\cdot\rho\hat{U}\boldsymbol{v}) - (\nabla\cdot\boldsymbol{q}) - (\boldsymbol{\pi}:\nabla\boldsymbol{v})} \qquad (1.1\text{-}13)$$

which is the *internal energy equation.*

This completes the derivation of the three equations of change. In Table 1.1-1, where these equations are summarized, they are given in two forms: one in terms of $\partial/\partial t$, and the other in terms of D/Dt, which gives the time rate of change of a quantity as seen by an observer who is moving with the fluid. The operator $D/Dt = \partial/\partial t + (\boldsymbol{v}\cdot\nabla)$ is called the

[4] See Exercise 5 at the end of §A.1.

"substantial derivative" or the "material derivative," since it describes time changes taking place at a particular element of the "substance" or "material." It should be emphasized that there are *no* assumptions involved in going from Eqs. A, B, and C to Eqs. D, E, and F in Table 1.1-1.

The analytical solution to most of the problems in this book will begin with one of the three "boxed" equations above. Usually one will want them written out in component form in one of the standard orthogonal coordinate systems. For the reader's convenience, in Appendix B we give the equation of motion in rectangular, cylindrical, and spherical coordinates; in Appendix A many V-operations are tabulated in the same three coordinate systems and also in bipolar coordinates.

§1.2 THE EQUATIONS OF CHANGE IN TERMS OF THE TRANSPORT PROPERTIES

The equations in §1.1 are valid for any fluid. In this section we specialize these results for "Newtonian fluids" to obtain the equations of classical hydrodynamics. Then in the next section we give several examples of solutions of classical hydrodynamics problems. In doing so we select those problems that pertain to viscometry and to which we shall refer in subsequent chapters. Additional examples may be found in textbooks on transport phenomena.[1]

For structurally simple fluids such as gases, gaseous mixtures, and low-molecular-weight liquids and their mixtures, it has been established experimentally that in a simple shearing motion $v_x = v_x(y)$ the flux of x-momentum in the positive y-direction is given by "Newton's law of viscosity," $\pi_{yx} = -\mu\, dv_x/dy$, where μ is the *viscosity* of the fluid. The appropriate generalization for arbitrary, time-dependent flows is:[2,3]

$$\begin{aligned}\boldsymbol{\pi} &= p\boldsymbol{\delta} + \boldsymbol{\tau} \\ &= p\boldsymbol{\delta} - \mu[\nabla\boldsymbol{v} + (\nabla\boldsymbol{v})^{\dagger}] + (\tfrac{2}{3}\mu - \kappa)(\nabla\cdot\boldsymbol{v})\boldsymbol{\delta}\end{aligned} \tag{1.2-1}$$

where $(\nabla\boldsymbol{v})^{\dagger}$ is the transpose of the dyadic $\nabla\boldsymbol{v}$, and $\boldsymbol{\delta}$ is the unit tensor. This expression reduces to the hydrostatic pressure when there are no velocity gradients; it contains all possible combinations of first derivatives of velocity components that are allowed if one assumes that the fluid is isotropic and that the momentum flux tensor is symmetric.[2,3] The symbol p represents the thermodynamic pressure,[2] which is related to the density ρ and the temperature T through a "thermodynamic equation of state," $p = p(\rho, T)$; that is, this is taken to be the same function that one uses in thermal equilibrium.

The tensor $\boldsymbol{\tau}$ is the part of the momentum flux tensor or stress tensor that is associated with the viscosity of the fluid. We shall usually refer to it simply as the "momentum flux tensor" or "stress tensor," and use the terms "total momentum flux tensor" or "total stress tensor" for $\boldsymbol{\pi}$ when a distinction seems necessary. An equation that assigns a value to $\boldsymbol{\tau}$ is called a *constitutive equation.* Equation 1.2-1 is the constitutive equation for the Newtonian fluid.

Note that in generalizing Newton's law of viscosity to arbitrary flows an additional transport property κ, the *dilatational viscosity*, arises. The dilatational viscosity is identically

[1] See, for example, R. B. Bird, W. E. Stewart, and E. N. Lightfoot, *Transport Phenomena*, Wiley, New York (1960), Chapts. 3, 4, 10, 11.

[2] L. Landau and E. M. Lifshitz, *Fluid Mechanics*, Addison-Wesley, Reading, MA (1959), pp. 47–48, 187–188.

[3] G. K. Batchelor, *An Introduction to Fluid Dynamics*, Cambridge University Press, Cambridge (1967), Sects. 3.3 and 3.4.

zero for ideal, monatomic gases; for incompressible liquids $(\nabla \cdot \boldsymbol{v}) = 0$, and the term containing κ vanishes. Consequently the dilatational viscosity is of no importance in two key limiting cases, and no further mention will be made of it in this book.[4]

For all fluids the density ρ depends on the local thermodynamic state variables, such as pressure and temperature. However for liquids it is often a very good assumption to take the density to be constant. Such an idealized fluid is often called an "incompressible fluid", and the *momentum flux tensor* simplifies to

$$\boxed{\boldsymbol{\pi} = p\boldsymbol{\delta} + \boldsymbol{\tau} = p\boldsymbol{\delta} - \mu\dot{\boldsymbol{\gamma}}} \tag{1.2-2}$$

in which $\dot{\boldsymbol{\gamma}} = \nabla\boldsymbol{v} + (\nabla\boldsymbol{v})^{\dagger}$ is the *rate-of-strain tensor* or *rate-of-deformation tensor*. When the incompressibility assumption is made, a problem arises as to the meaning of p. For example, for a pure, incompressible fluid at constant temperature a plot of p vs. ρ is a vertical straight line; that is, the function $p(\rho)$ is many-valued. This poses no difficulty in solving hydrodynamic problems since only the gradient of p needs to be known. However, in connection with determining pressures at surfaces, an incompressible fluid theory can predict only pressure differences and not absolute values (unless, of course, the pressure on some bounding surface is specified through a boundary condition). For all discussions of Newtonian fluids in this book, Eq. 1.2-2 will be used for the momentum flux tensor; that is we will use the simple constitutive equation $\boldsymbol{\tau} = -\mu\dot{\boldsymbol{\gamma}}$ for incompressible Newtonian fluids.

The *heat flux* $\boldsymbol{q}$ for pure fluids and nondiffusing mixtures is given by "Fourier's law of heat conduction":

$$\boxed{\boldsymbol{q} = -k\nabla T} \tag{1.2-3}$$

in which k is the *thermal conductivity* and T is the temperature. For diffusing mixtures there are additional contributons to $\boldsymbol{q}$, but we do not discuss them here.[1,2]

Now that we have given the expressions in Eqs. 1.2-2 and 1.2-3 for the fluxes, let us turn to the equations of change, and particularly the *equations of change for incompressible Newtonian fluids*. These are listed in Table 1.2-1 and given in Appendix B in various coordinate systems. The equation of continuity was given earlier in Eq. 1.1-5. The equation of motion is obtained by substituting Eq. 1.2-2 into Eq. 1.1-8 and simplifying. The energy equation is obtained by first transforming Eq. 1.1-13 into an equation for temperature (by using standard thermodynamic transformations) and then inserting Fourier's law (Eq. 1.2-3) for $\boldsymbol{q}$. This process is outlined in Problem 1B.8; the final equation contains $\hat{C}_p$, which is the heat capacity at constant pressure per unit mass.

The equations of change in Table 1.2-1 are easy to interpret physically:

A and D: The *equation of continuity* states that within a small fixed volume there can be no net rate of addition of mass.

B and E: The *equation of motion* states that the mass-times-acceleration of a fluid element equals the sum of the pressure, viscous, and gravitational forces acting on the element.

C and F: The *energy equation* states that the temperature of a fluid element changes as it moves along with the fluid because of heat conduction (the k-term) and heat production by viscous heating (the μ-term).

[4] The dilatational viscosity of a liquid containing gas bubbles has been studied by G. K. Batchelor, *op. cit.*, pp. 253–255.

TABLE 1.2-1

Equations of Change for Newtonian Fluids with Constant ρ, μ, and k

	Dimensional Forms		Dimensionless Forms[a]	
Continuity	$(\nabla \cdot \boldsymbol{v}) = 0$	(A)	$(\nabla^* \cdot \boldsymbol{v}^*) = 0$	(D)
Motion[b,c]	$\rho \dfrac{D\boldsymbol{v}}{Dt} = -\nabla p + \mu\nabla^2\boldsymbol{v} + \rho\boldsymbol{g}$	(B)	$\mathrm{Re} \dfrac{D\boldsymbol{v}^*}{Dt^*} = -\nabla^* p^* + \nabla^{*2}\boldsymbol{v}^* + (\mathrm{Re/Fr})\boldsymbol{g}/g$	(E)
Energy	$\rho\hat{C}_p \dfrac{DT}{Dt} = k\nabla^2 T + \frac{1}{2}\mu(\dot{\boldsymbol{\gamma}} : \dot{\boldsymbol{\gamma}})$	(C)	$\mathrm{Pé} \dfrac{DT^*}{Dt^*} = \nabla^{*2} T^* + \frac{1}{2}\,\mathrm{Br}(\dot{\boldsymbol{\gamma}}^* : \dot{\boldsymbol{\gamma}}^*)$	(F)

[a] The dimensionless forms are based on a reference length L, reference velocity V, a reference temperature T_0, and a reference temperature difference ΔT_0. In terms of these $\boldsymbol{v}^* = \boldsymbol{v}/V$, $\nabla^* = L\nabla$, $D/Dt^* = (L/V)D/Dt$, $p^* = (L/\mu V)p$, $T^* = (T - T_0)/\Delta T_0$ and $\dot{\boldsymbol{\gamma}}^* = (L/V)\dot{\boldsymbol{\gamma}}$. The Reynolds number $\mathrm{Re} = LV\rho/\mu$, the Froude number $\mathrm{Fr} = V^2/gL$, the Péclet number $\mathrm{Pé} = \rho\hat{C}_p LV/k$, and the Brinkman number $\mathrm{Br} = \mu V^2/k\Delta T_0$ are groups that appear as a result of writing the equations in dimensionless form. Other dimensionless groups may enter through the boundary conditions.

[b] For incompressible fluids we may combine the pressure and the gravity terms as $\nabla\mathscr{P} = \nabla p - \rho\boldsymbol{g}$ where $\mathscr{P}$ is called the "modified pressure." If the velocity is specified on the entire boundary, we can conclude that the gravitational acceleration has no effect on the velocity field. If forces are specified on part of the boundary, as in free surface flow, the modified pressure is not a useful concept. The nomenclature "modified pressure" was suggested by G. K. Batchelor, *An Introduction to Fluid Dynamics*, Cambridge University Press, Cambridge (1967), p. 176.

[c] The substantial derivative is defined as $D/Dt = \partial/\partial t + (\boldsymbol{v} \cdot \nabla)$.

Before ending this section we consider in Example 1.2-1 a result that is useful when the force on an object is desired in a fluid mechanical analysis.

EXAMPLE 1.2-1 Proof that Normal Stresses of Incompressible Newtonian Fluids Are Zero at Solid Surfaces

We consider a point P on a solid surface that is in contact with an incompressible Newtonian fluid. Use a rectangular coordinate system xyz whose origin is at P and whose z-axis is normal to the surface and points into the fluid, and show that $\tau_{zz}|_{z=0} = 0$.

SOLUTION The result follows from the definition of the normal stress component τ_{zz} and the mass conservation equation:

$$\tau_{zz}\Big|_{z=0} = -2\mu \frac{\partial v_z}{\partial z}\Big|_{z=0}$$

$$= 2\mu\left(\frac{\partial v_x}{\partial x} + \frac{\partial v_y}{\partial y}\right)\Big|_{z=0} = 0 \tag{1.2-4}$$

In the last step we have used the "no slip" condition on the solid surface.

Note: The result does not apply on surfaces with slip (see Eq. 1.4-43). Also in later chapters we shall find that for polymeric liquids normal stresses are *not* zero at solid surfaces.

§1.3 SOLUTION OF ISOTHERMAL FLOW PROBLEMS

In this section we illustrate the solution of fluid flow problems with the use of the equations for incompressible Newtonian fluids under isothermal conditions. Our starting

equations are then Eqs. A and B in Table 1.2-1. These are four partial differential equations for the four unknowns: pressure and three components of velocity. Extensive experimental testing has shown that these equations describe the incompressible flow of Newtonian fluids exactly. Analytical solutions are, however, not always easy to obtain. In fact the equations are among the most challenging and extensively studied equations of mathematical physics. As a consequence we have available numerous treatises giving analytical solutions and solution procedures for Newtonian fluid mechanics.[1]

In connection with the examples we introduce two important approximate procedures: (i) in Examples 1.3-3 and 4 we use the lubrication approximation, in which the flow in a nearly constant cross section is approximated locally as flow in an equivalent constant-cross-section geometry; (ii) in Example 1.3-5 we introduce the quasi-steady-state approximation, in which an unsteady flow with small inertial effects is treated as a succession of steady-state flows.

EXAMPLE 1.3-1 Laminar Flow between Parallel Plane Surfaces

An incompressible Newtonian fluid is located in the space between two parallel plates that are separated by a distance B (see Fig. 1.3-1). The upper plate is moving in the $+x$-direction with a velocity V, thus contributing to the motion of the fluid. An additional contribution to the fluid motion is that due to a constant applied pressure gradient $\partial p/\partial x$. Find the velocity profile and the volume rate of flow. Assume that the flow is sufficiently slow that viscous heating is not important.

SOLUTION We postulate that in this system $v_x = v_x(y)$, $v_y = 0$, $v_z = 0$, $p = p(x, y)$, and T = constant. We now apply these postulates to the equations of change in order to get the differential equations that describe the system. The equations of continuity and energy are clearly unimportant. The y-component of the equation of motion just gives the vertical pressure gradient, which is of no interest here. The x-component of the equation of motion becomes:

$$0 = -\frac{\partial p}{\partial x} + \mu \frac{d^2 v_x}{dy^2} \tag{1.3-1}$$

in which $\partial p/\partial x$ was stated to be a constant. This equation has to be integrated with respect to y with the boundary conditions:

$$\text{At } y = 0: \qquad v_x = 0 \tag{1.3-2}$$

$$\text{At } y = B: \qquad v_x = V \tag{1.3-3}$$

The result is the velocity distribution:

$$v_x = V\left(\frac{y}{B}\right) - \frac{B^2}{2\mu}\frac{\partial p}{\partial x}\left[\left(\frac{y}{B}\right) - \left(\frac{y}{B}\right)^2\right] \tag{1.3-4}$$

[1] For example, H. Lamb, *Hydrodynamics*, Dover, New York (1945); L. M. Milne-Thompson, *Theoretical Hydrodynamics*, 5th ed., Macmillan, New York (1967); H. L. Dryden, F. D. Murnaghan, and M. Bateman, *Hydrodynamics*, Dover, New York (1956); R. Berker, "Intégrations des équations du mouvement d'un fluide visqueux incompressible," *Handbuch der Physik*, Vol. VIII/2, Springer, Heidelberg (1963), pp. 1-384; H. Schlichting, *Boundary Layer Theory*, McGraw-Hill, New York, 4th ed. (1960); G. K. Batchelor, *An Introduction to Fluid Dynamics*, Cambridge Univ. Press (1967); L. D. Landau and E. M. Lifshitz, *Fluid Mechanics*, Pergamon, London (1959).

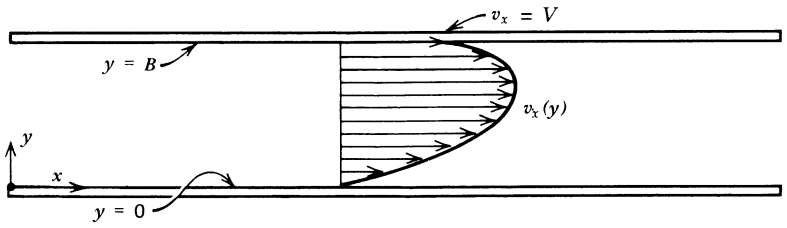

FIGURE 1.3-1. Flow between horizontal parallel planes with the upper plane moving and with an imposed pressure gradient in the flow direction.

The volume rate of flow Q for plates of width W is:

$$\begin{aligned} Q = WB\langle v_x \rangle &= \int_0^W \int_0^B v_x \, dy \, dz \\ &= WB \int_0^1 v_x d\left(\frac{y}{B}\right) \\ &= \tfrac{1}{2}WBV - \frac{WB^3}{12\mu}\frac{\partial p}{\partial x} \end{aligned} \tag{1.3-5}$$

Here the angular brackets $\langle\ \rangle$ indicate an average over the cross section. This result contains the solution for the problem where the pressure gradient and the wall motion both tend to drive the fluid in the same direction and also the problem where the pressure gradient and wall motion oppose one another. Furthermore, the solution in Eq. 1.3-5 is seen to be a sum of the solutions to the two separate problems of wall driven flow and pressure driven flow. This superposition of solutions results, of course, from the linearity of the governing equations and boundary conditions. (*Note*: It is not usually possible to perform this superposition for non-Newtonian flow problems where the governing equations are nonlinear.)

EXAMPLE 1.3-2 Laminar Flow in a Circular Tube

A fluid flows through a circular tube of radius R and length L. The tube makes an angle χ with the vertical direction. The pressures at the tube ends at $z = 0$ and $z = L$ (see Fig. 1.3-2) are $\mathscr{P}_0$ and $\mathscr{P}_L$, respectively. Find the steady-state velocity profile and the volume rate of flow, neglecting entrance and exit effects and assuming negligible viscous heating.

SOLUTION We postulate a solution of the form $v_z = v_z(r)$, $v_\theta = 0$, $v_r = 0$, and $p = p(r, \theta, z)$. The equation of continuity is satisfied identically, and only the z-component of the equation of motion is of interest:

$$0 = -\frac{\partial p}{\partial z} + \mu \frac{1}{r}\frac{d}{dr}\left(r\frac{dv_z}{dr}\right) + \rho g \cos\chi \tag{1.3-6}$$

This is to be solved with $v_z = 0$ at $r = R$ and v_z finite at $r = 0$.

Next we introduce[2] the "modified pressure" $\mathscr{P} = p - \rho g z \cos\chi$ so that

$$\frac{\partial \mathscr{P}}{\partial z} = \mu \frac{1}{r}\frac{d}{dr}\left(r\frac{dv_z}{dr}\right) \tag{1.3-7}$$

[2] In general, for incompressible fluids $\mathscr{P}$ is given by $\mathscr{P} = p + \rho g h$, where h is the distance *upward* (i.e., in the direction opposed to gravity) from some arbitrarily chosen reference plane. See also Table 1.2-1.

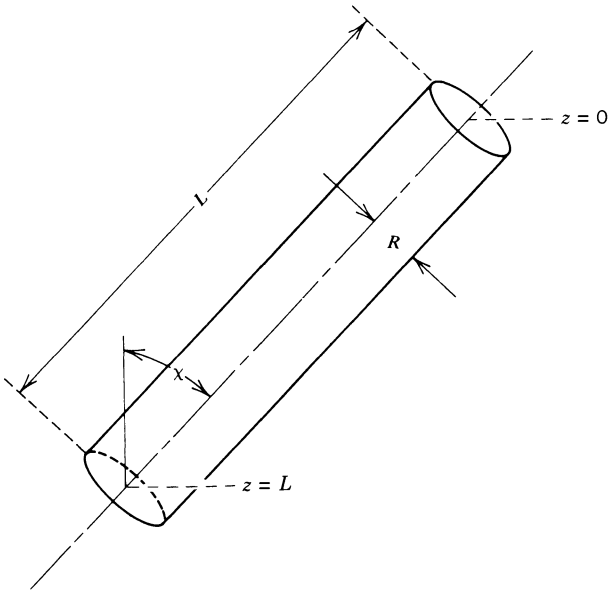

FIGURE 1.3-2. Flow through a circular tube that is inclined at an angle χ to the vertical.

The right side is a function of r alone; let us call it $F(r)$. Then

$$\mathscr{P} = F(r)z + G(r, \theta) \tag{1.3-8}$$

Application of the boundary conditions at $z = 0$ and $z = L$ gives

$$\mathscr{P} = -\frac{\mathscr{P}_0 - \mathscr{P}_L}{L} z + \mathscr{P}_0 \tag{1.3-9}$$

When this is substituted into Eq. 1.3-7, the latter can be integrated; use of the boundary conditions that $v_z = 0$ at $r = R$ and that v_z is finite at $r = 0$ then gives:

$$v_z = \frac{(\mathscr{P}_0 - \mathscr{P}_L)R^2}{4\mu L}\left[1 - \left(\frac{r}{R}\right)^2\right] \tag{1.3-10}$$

The volume rate of flow is then:

$$\begin{aligned} Q = \pi R^2 \langle v_z \rangle &= \int_0^{2\pi} \int_0^R v_z r \, dr \, d\theta \\ &= 2\pi R^2 \int_0^1 v_z \cdot \left(\frac{r}{R}\right) d\left(\frac{r}{R}\right) \\ &= \frac{\pi(\mathscr{P}_0 - \mathscr{P}_L)R^4}{8\mu L} \end{aligned} \tag{1.3-11}$$

which is the famous result of Hagen and Poiseuille.[3] This relation (accompanied by additional information about end corrections) is the basic equation needed to determine viscosity from tube flow data. It is valid for Re < 2100, where the Reynolds number $\mathrm{Re} = 2R\langle v_z \rangle \rho/\mu = 2Q\rho/\pi\mu R$, the angular brackets indicating an average over the cross section. For Re > 2100, the flow will usually be turbulent.

[3] G. Hagen, *Ann. Phys. Chem.*, **46**, 423–442 (1839); J. L. Poiseuille, *Comptes Rendus*, **11**, 961, 1041 (1840); **12**, 112 (1841).

EXAMPLE 1.3-3 Flow in a Slightly Tapered Tube

An incompressible Newtonian fluid is flowing through the horizontal tapered tube shown in Fig. 1.3-3. Show that the analysis in Example 1.3-2 for a straight tube can be applied locally to this flow, and then use that result to obtain a relationship between the volume flow rate Q and the overall pressure drop $(\mathscr{P}_0 - \mathscr{P}_L) \equiv \Delta\mathscr{P}$.

SOLUTION The taper of the tube will require a flow in the radial direction and an acceleration in the axial direction, but it is reasonable to assume that the flow will maintain axial symmetry. Therefore we assume $v_z = v_z(r, z)$, $v_r = v_r(r, z)$, and $v_\theta = 0$. The continuity equation and the r- and z-components of the Navier-Stokes equations are then (cf. Eqs. B.2-4 and 6)

$$\frac{1}{r}\frac{\partial}{\partial r}(rv_r) + \frac{\partial v_z}{\partial z} = 0 \tag{1.3-12}$$

$$\rho\left(v_r\frac{\partial v_r}{\partial r} + v_z\frac{\partial v_r}{\partial z}\right) = \mu\left[\frac{\partial}{\partial r}\left(\frac{1}{r}\frac{\partial}{\partial r}(rv_r)\right) + \frac{\partial^2 v_r}{\partial z^2}\right] - \frac{\partial\mathscr{P}}{\partial r} \tag{1.3-13}$$

$$\rho\left(v_r\frac{\partial v_z}{\partial r} + v_z\frac{\partial v_z}{\partial z}\right) = \mu\left[\frac{1}{r}\frac{\partial}{\partial r}\left(r\frac{\partial v_z}{\partial r}\right) + \frac{\partial^2 v_z}{\partial z^2}\right] - \frac{\partial\mathscr{P}}{\partial z} \tag{1.3-14}$$

The nonuniform geometry has changed the linear problem in Eq. 1.3-6 to a nonlinear one; Eqs. 1.3-12 through 14 are difficult to solve in general. However we can take advantage of the fact that the geometry changes slowly to show that these equations are dominated by only a few terms, and that if small terms are neglected, the problem is easily solved.

To see which terms must be kept and which can be neglected, we perform an *order of magnitude analysis* on Eqs. 1.3-12 through 14. First we estimate the sizes of the velocities. The axial velocity is determined by the volume flow rate and must be of order $(Q/\pi R_L^2) \equiv V$. We write this as

$$v_z \sim O(V) = O(Q/\pi R_L^2) \tag{1.3-15}$$

The size of v_r is dictated by the continuity equation. In this equation the $\partial v_z/\partial z$ term has magnitude

$$\frac{\partial v_z}{\partial z} \sim O\left(\left(\frac{Q}{\pi R_L^2} - \frac{Q}{\pi R_0^2}\right)/L\right)$$
$$= O(V(1 - (R_L/R_0)^2)/L) \tag{1.3-16}$$

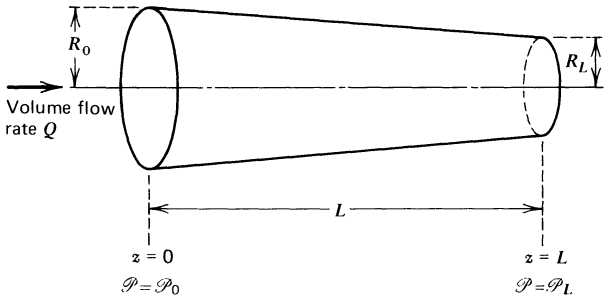

FIGURE 1.3-3. Tapered tube geometry analyzed in Example 1.3-3. The tube radius changes gradually from R_0 to R_L over a distance L. It is not necessary that dR/dz be constant as shown here, but it must be small for the analysis to hold.

Clearly we expect this derivative to be small since $(R_0 - R_L)/L \ll 1$. If we let U denote the order of v_r then the other contribution to the continuity equation is

$$\frac{1}{r}\frac{\partial}{\partial r}(rv_r) \sim O\left(\frac{U}{R_L}\right) \tag{1.3-17}$$

The radial derivative is approximated by estimating that v_r can vary from U to 0 over a distance of R_L. From the equation of continuity in Eq. 1.3-12 we may now find the relative sizes of the radial and axial velocities:

$$U = V\left(\frac{R_L}{L}\right)\left[1 - \left(\frac{R_L}{R_0}\right)^2\right] \tag{1.3-18}$$

We now look at the sizes of the contributions to the equation of motion. The viscous terms have orders:

$$\mu\frac{\partial}{\partial r}\left(\frac{1}{r}\frac{\partial}{\partial r}(rv_r)\right) \sim O\left(\mu\frac{V}{R_L L}\left[1 - \left(\frac{R_L}{R_0}\right)^2\right]\right) \tag{1.3-19}$$

$$\mu\frac{\partial^2 v_r}{\partial z^2} \sim O\left(\mu\frac{V}{L^3}R_L\left[1 - \left(\frac{R_L}{R_0}\right)^2\right]\right) \tag{1.3-20}$$

$$\mu\frac{1}{r}\frac{\partial}{\partial r}\left(r\frac{\partial v_z}{\partial r}\right) \sim O\left(\mu\frac{V}{R_L^2}\right) \tag{1.3-21}$$

$$\mu\frac{\partial^2 v_z}{\partial z^2} \sim O\left(\mu\frac{V}{L^2}\left[1 - \left(\frac{R_L}{R_0}\right)^2\right]\right) \tag{1.3-22}$$

From these results it is seen that the dashed underlined terms in Eqs. 1.3-13 and 14 are smaller than the unmarked viscous term by at least a factor of $(R_L/L)[1 - (R_L/R_0)^2] \ll 1$.

Similarly we estimate the sizes of the inertial terms:

$$\rho v_r\frac{\partial v_r}{\partial r} \sim O\left(\rho\frac{V^2 R_L}{L^2}\left[1 - \left(\frac{R_L}{R_0}\right)^2\right]^2\right) \tag{1.3-23}$$

$$\rho v_z\frac{\partial v_r}{\partial z} \sim O\left(\rho V^2\frac{R_L}{L^2}\left[1 - \left(\frac{R_L}{R_0}\right)^2\right]\right) \tag{1.3-24}$$

$$\rho v_r\frac{\partial v_z}{\partial r} \sim O\left(\rho\frac{V^2}{L}\left[1 - \left(\frac{R_L}{R_0}\right)^2\right]\right) \tag{1.3-25}$$

$$\rho v_z\frac{\partial v_z}{\partial z} \sim O\left(\rho\frac{V^2}{L}\left[1 - \left(\frac{R_L}{R_0}\right)^2\right]\right) \tag{1.3-26}$$

When the largest of these (Eqs. 1.3-25 and 26) are compared with the largest viscous term, Eq. 1.3-21, we see that all are negligible provided

$$\frac{\rho V R_L}{\mu}\left[\frac{R_L}{L}\left[1 - \left(\frac{R_L}{R_0}\right)^2\right]\right] = \tfrac{1}{2}\,\mathrm{Re}\left[\frac{R_L}{L}\left[1 - \left(\frac{R_L}{R_0}\right)^2\right]\right] \ll 1 \tag{1.3-27}$$

It is not necessary in this problem that the Reynolds number be small for the inertial terms to be negligible, since it is multiplied by a small geometric factor associated with the taper of the tube.

The pressure gradient terms are the last to be estimated. In order for the r and z components of the Navier-Stokes equations to be satisfied, the pressure gradient terms must be of the same size as the largest viscous term in each. Thus

$$\frac{\partial \mathscr{P}/\partial r}{\partial \mathscr{P}/\partial z} \sim O\left(\left(\frac{R_L}{L}\right)\left[1 - \left(\frac{R_L}{R_0}\right)^2\right]\right) \tag{1.3-28}$$

It can now be seen that if

$$\left(\frac{R_L}{L}\right)\left[1 - \left(\frac{R_L}{R_0}\right)^2\right] \ll 1 \tag{1.3-29}$$

the equation of motion is well approximated by Eq. 1.3-7, which describes flow in the straight tube. Integrating Eq. 1.3-7 with respect to r leads as before to

$$Q = \frac{\pi[R(z)]^4}{8\mu}\left(-\frac{d\mathscr{P}}{dz}\right) \tag{1.3-30}$$

Notice that we have had to hold z constant during this integration, because the boundary conditions vary with z. Although this result could easily have been adapted from Eq. 1.3-11, the above analysis serves to organize the approximation procedure and to document the limit of validity (Eq. 1.3-29) of the result. The process that we have illustrated here of adapting locally the results for a uniform geometry to a slowly varying geometry is known as the *lubrication approximation*[4]. It is a very powerful technique for estimating the flow rate vs. pressure drop relation in many complex flows.

Finally we obtain the relation between pressure drop $(\mathscr{P}_0 - \mathscr{P}_L)$ and volume flow rate. Rather than use z as the independent variable in Eq. 1.3-30, we can use $R = R_0 + (R_L - R_0)(z/L)$:

$$Q = \frac{\pi R^4}{8\mu}\left(-\frac{d\mathscr{P}}{dR}\right)\left(\frac{R_L - R_0}{L}\right) \tag{1.3-31}$$

But Q is constant for all z (and hence all R). Therefore the differential equation for $\mathscr{P}$ as a function of R can be integrated to give:

$$\begin{aligned} Q &= \frac{3\pi}{8\mu}\frac{(\mathscr{P}_0 - \mathscr{P}_L)}{L}\frac{(R_0 - R_L)}{(R_L^{-3} - R_0^{-3})} \\ &= \frac{\pi(\mathscr{P}_0 - \mathscr{P}_L)R_0^4}{8\mu L}\left[1 - \frac{1 + (R_L/R_0) + (R_L/R_0)^2 - 3(R_L/R_0)^3}{1 + (R_L/R_0) + (R_L/R_0)^2}\right] \end{aligned} \tag{1.3-32}$$

Hence the final result may be expressed as the Hagen-Poiseuille result multiplied by a correction factor.

EXAMPLE 1.3-4 The Cone-and-Plate Viscometer

The cone-and-plate geometry shown in Fig. 1.3-4 is a standard experimental arrangement for the measurement of viscosity (and other rheological properties, as we shall see later). Obtain the analytical relations needed to interpret the instrumental data:

[4] J. R. A. Pearson, *Mechanics of Polymer Processing*, Elsevier Applied Science Publishers, London (1985), pp. 165–177; R. I. Tanner, *Engineering Rheology*, Oxford Univ. Press (1985), pp. 228–236.

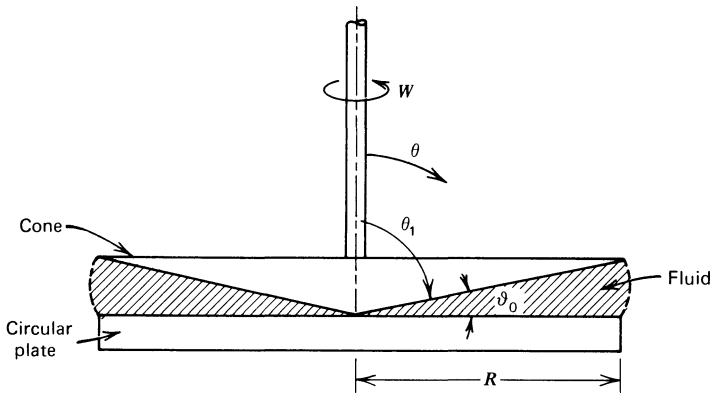

FIGURE 1.3-4. Cone-and-plate instrument; the angle ϑ_0 is usually between 0.5 and 8 degrees in commercial instruments.

a. A relation between the angular velocity W and the $\theta\phi$-component of the rate-of-strain tensor $\dot{\gamma}$ in the gap.

b. A relationship between the torque $\mathscr{T}$ and the $\theta\phi$-component of the stress tensor τ in the gap.

c. A relation giving the viscosity μ in terms of W and $\mathscr{T}$.

SOLUTION The simplest analysis of this experiment makes use of the fact that the angle ϑ_0 is so small that a lubrication approximation may be applied to the flow in the gap. In this example, however, we do not perform an order of magnitude analysis as in the previous example, but rather apply the lubrication approximation intuitively by regarding the flow to be locally that between parallel plates.

(a) The velocity v_ϕ at a radius r can be approximated by adapting Eq. 1.3-4 with $\partial p/\partial x = 0$ and with v_x replaced by v_ϕ. For the cone-and-plate system, at a distance r from the cone apex, the velocity of the cone will be Wr (this corresponds to V in Eq. 1.3-4), and the plate-cone separation will be given by $r \sin \vartheta_0 \doteq r\vartheta_0$ (this corresponds to B in Eq. 1.3-4). Hence the velocity profile will, to a good approximation, be

$$v_\phi = Wr\left(\frac{(\pi/2) - \theta}{(\pi/2) - \theta_1}\right) \tag{1.3-33}$$

The $\theta\phi$-component of the $\dot{\gamma}$-tensor is then (cf. Eq. B.3-17):

$$\dot{\gamma}_{\theta\phi} = \frac{\sin\theta}{r}\frac{\partial}{\partial\theta}\left(\frac{v_\phi}{\sin\theta}\right) \doteq \frac{1}{r}\frac{\partial}{\partial\theta}v_\phi = -\frac{W}{\vartheta_0} \tag{1.3-34}$$

The approximation made here is that θ is so close to $\pi/2$ that $\sin\theta$ can be taken to be unity; this should be an excellent approximation. We see from Eq. 1.3-34 that $\dot{\gamma}_{\theta\phi}$ is constant throughout the cone-plate gap. This is one reason why this geometry is useful for macromolecular fluids where the viscosity depends on the shear rate.

(b) The torque required to maintain the motion will be obtained by integrating the product of the lever arm r and the force $\tau_{\theta\phi}|_{\theta=\pi/2} \cdot rdrd\phi$ over the surface of the plate

$$\mathscr{T} = \int_0^{2\pi}\int_0^R \tau_{\theta\phi}\Big|_{\theta=\pi/2} r^2\, dr\, d\phi \tag{1.3-35}$$

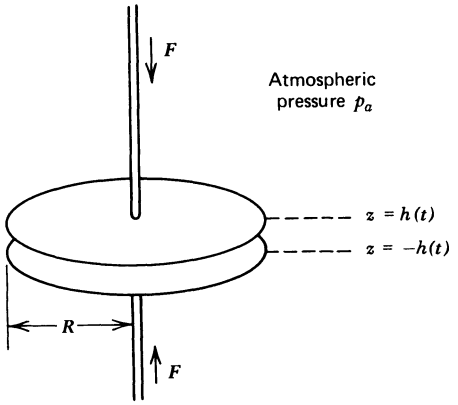

FIGURE 1.3-5. Squeezing flow between parallel disks each with radius R. The initial disk separation is $2h_0$.

Since $\dot{\gamma}_{\theta\phi}$ is constant throughout the gap, $\tau_{\theta\phi}$ will also be constant. Hence the integration is easily performed and one gets

$$\tau_{\theta\phi} = \frac{3\mathscr{T}}{2\pi R^3} \tag{1.3-36}$$

(c) Since $\tau = -\mu\dot{\gamma}$ for a Newtonian fluid, the $\theta\phi$-component of this equation, combined with Eqs. 1.3-34 and 36, gives

$$\mu = \frac{\tau_{\theta\phi}}{-\dot{\gamma}_{\theta\phi}} = \frac{3\mathscr{T}\vartheta_0}{2\pi R^3 W} \tag{1.3-37}$$

This gives the viscosity of the fluid in the gap in terms of the geometrical quantities R and ϑ_0 and the measured values of torque $\mathscr{T}$ and angular velocity W.

More complete analyses can be found elsewhere.[5] The treatment of this flow for non-Newtonian fluids is found in §10.2.

EXAMPLE 1.3-5 Squeezing Flow between Two Parallel Disks[6]

A fluid is placed in the gap between two parallel disks separated by a distance $2h_0$. The fluid completely fills the gap. A constant force F is applied to each disk as shown in Fig. 1.3-5. It is desired to obtain an expression for the change in gap separation with time. A "quasi-steady state" solution will be used; that is, at any time t the radial flow problem will be treated as a steady-state hydrodynamic problem. This means that the inertial terms in the equation of motion are neglected in the first approximation. In addition gravity is assumed negligible.

SOLUTION We introduce a cylindrical coordinate system with z-axis coinciding with the symmetry axis of the flow and with the two disks defined by $z = -h(t)$ and $z = h(t)$. Since $R \gg h$ the flow will primarily be in the r-direction so that $v_z \ll v_r$ and also $(\partial v_r/\partial r) \ll (\partial v_r/\partial z)$. Consistent with the

[5] R. B. Bird, W. E. Stewart, and E. N. Lightfoot, *op. cit.*, p. 119; S. Oka in F. R. Eirich, ed., *Rheology*, Vol. 3, Academic Press, New York (1960), Chapt. 2, pp. 61–62; K. Walters, *Rheometry*, Chapman and Hall, London (1975), Chapt. 4.

[6] J. Stefan, *Sitzungber. K. Akad. Wiss. Math. Natur. Wien*, **69**, Part 2, 713–735 (1874); see also L. Landau and E. M. Lifshitz, *op. cit.*, pp. 70–71.

quasi-steady-state approximation, we take $\rho\partial v_r/\partial t \ll \mu\partial^2 v_r/\partial z^2$. Consequently the equation of continuity and the r- and z- components of the equation of motion are well approximated by

$$\textit{Continuity}: \quad \frac{1}{r}\frac{\partial}{\partial r}(rv_r) + \frac{\partial v_z}{\partial z} = 0 \tag{1.3-38}$$

$$\textit{Motion}\,(r): \quad 0 = -\frac{\partial p}{\partial r} + \mu\frac{\partial^2 v_r}{\partial z^2} \tag{1.3-39}$$

$$\textit{Motion}\,(z): \quad 0 = -\frac{\partial p}{\partial z} \tag{1.3-40}$$

We seek a solution for the velocity field in the form $v_r = v_r(r, z, t)$ and $v_z = v_z(z, t)$. The continuity equation then demands that $v_r = rf(z, t)$. Furthermore, the equations of motion show that p must have the form $p = p_0 + p_2 r^2$, where p_0 and p_2 are constants to be determined. With these simplifications Eq. 1.3-40 is satisfied and Eqs. 1.3-38 and 39 give

$$2f + \frac{\partial v_z}{\partial z} = 0 \tag{1.3-41}$$

$$-2p_2 + \mu\frac{\partial^2 f}{\partial z^2} = 0 \tag{1.3-42}$$

The following boundary conditions are to be satisfied:

$$\partial f/\partial z = 0, \quad \text{at } z = 0; \quad f = 0, \quad \text{at } z = h \tag{1.3-43,44}$$

$$v_z = 0, \quad \text{at } z = 0; \quad v_z = \dot{h}, \quad \text{at } z = h \tag{1.3-45,46}$$

$$p = p_a, \quad \text{at } r = R \tag{1.3-47}$$

Here $\dot{h}$ stands for dh/dt. These 5 conditions suffice to determine p_0, p_2, and the 3 constants of integration of Eqs. 1.3-41 and 42. The results are

$$v_r = rf = \frac{3}{4}\frac{(-\dot{h})}{h}r\left[1 - \left(\frac{z}{h}\right)^2\right] \tag{1.3-48}$$

$$v_z = \frac{3}{2}\dot{h}\left[\left(\frac{z}{h}\right) - \frac{1}{3}\left(\frac{z}{h}\right)^3\right] \tag{1.3-49}$$

$$p - p_a = \frac{3(-\dot{h})\mu R^2}{4h^3}\left[1 - \left(\frac{r}{R}\right)^2\right] \tag{1.3-50}$$

To calculate the force on one plate all we need is the pressure distribution in Eq. 1.3-50, since we know from Example 1.2-1 that $\tau_{zz} = 0$ on the plates. Consequently we find

$$\begin{aligned} F &= \int_0^{2\pi}\int_0^R (p - p_a + \tau_{zz})\Big|_{z=h} r\,dr\,d\theta \\ &= 2\pi R^2 \int_0^1 (p - p_a)\left(\frac{r}{R}\right)d\left(\frac{r}{R}\right) \\ &= \frac{3\pi R^4\mu(-\dot{h})}{8h^3} \end{aligned} \tag{1.3-51}$$

This is the *Stefan equation*, which shows how much force $F(t)$ must be applied in order to maintain the disk motion $h(t)$.

If we now ask what the disk motion will be for a *constant applied force* F, we have to solve the differential equation for $h(t)$ in Eq. 1.3-51 to give

$$\frac{1}{h^2} - \frac{1}{h_0^2} = \frac{16Ft}{3\pi R^4 \mu} \tag{1.3-52}$$

This gives the disk separation as a function of the elapsed time, when inertial effects may be neglected.

It is possible to correct Eq. 1.3-51 for small inertial effects by means of a perturbation approach. Then the creeping flow solution in Eqs. 1.3-48 and 49 is used to evaluate the inertial term $\rho[\partial v_r/\partial t + v_r(\partial v_r/\partial r) + v_z(\partial v_r/\partial z)]$ in Eq. 1.3-39. The steps described above are then repeated to find the perturbations in v_r, v_z and p. The final result for F is

$$F = \frac{3\pi R^4 \mu(-\dot{h})}{8h^3}\left[1 + \frac{5\rho h(-\dot{h})}{7\mu} + \frac{2\rho h^2 \ddot{h}}{5\mu \dot{h}}\right] \tag{1.3-53}$$

This result[7] can be used to estimate the importance of inertial effects in lubrication squeeze films and in parallel plate plastometers.

§1.4 SOLUTION OF ISOTHERMAL FLOW PROBLEMS BY USE OF THE STREAM FUNCTION

This section is devoted to the stream function as an important analytical tool for the solution of flow problems. For simplicity we restrict our attention to flows in which we may choose a coordinate system such that only two velocity components are nonzero. Following a brief introduction to the stream function we demonstrate its use in three illustrative examples in which we solve for the flow field around a translating sphere, a rising bubble, and a rotating sphere. The last example also introduces regular perturbation methods, which we will use in later chapters.

For illustrative purposes we start by considering two-dimensional "plane" flow, for which one may choose a rectangular coordinate system so that $v_x = v_x(x, y, t)$, $v_y = v_y(x, y, t)$, and $v_z = 0$. The continuity equation then reads

$$\frac{\partial v_x}{\partial x} + \frac{\partial v_y}{\partial y} = 0 \tag{1.4-1}$$

The form of this equation suggests the introduction of a function $\psi(x, y, t)$ called the *stream function* with the property[1] that

$$v_x = -\frac{\partial \psi}{\partial y} \tag{1.4-2}$$

$$v_y = \frac{\partial \psi}{\partial x} \tag{1.4-3}$$

[7] S. Ishizawa, *JSME Bull.*, **9**, 533-550 (1966); D. C. Kuzma, *Appl. Sci. Res.*, **A18**, 15-20 (1967); A. F. Jones and S. D. R. Wilson, *J. Lubr. Technol.*, **97**, 101-104 (1975); R. J. Grimm, *Appl. Sci. Res.*, **32**, 149-166 (1976).

[1] Some authors introduce a stream function equal to the negative of the one introduced here. Our sign convention agrees with that of H. Lamb, *Hydrodynamics*, 6th ed., Cambridge University Press, Cambridge (1932); L. M. Milne-Thomson, *Theoretical Hydrodynamics* Macmillan, New York (1955); and R. B. Bird, W. E. Stewart, and E. N. Lightfoot, *Transport Phenomena*, Wiley, New York (1960), §4.2.

The use of the variable ψ in place of v_x and v_y automatically ensures that the continuity equation is satisfied. When the expressions in Eqs. 1.4-2 and 3 are inserted into the equations of motion one obtains two equations for the stream function and pressure. It is customary to eliminate the pressure between these to obtain a single equation to be satisfied by ψ. In rectangular coordinates this is done by differentiating the x-component of the equations of motion with respect to y, differentiating the y-component with respect to x and subtracting the two resulting equations. In this way the pressure is eliminated, and one obtains a single fourth-order differential equation for ψ. Various forms of this equation are shown in Table 1.4-1. In the equation of motion we have allowed for the possibility that the body force per unit volume $\boldsymbol{f}$ could depend on position. The use of a position-dependent $\boldsymbol{f}$ is illustrated in Example 1.4-3, and it will be used in connection with perturbation solutions for non-Newtonian fluids in Chapter 6. If the body force is a gravitational force or any other force that does not depend on position, it will not enter in the equation for the stream function.

EXAMPLE 1.4-1 Flow around a Translating Sphere[2]

The low Reynolds number flow around a translating sphere is an important problem in classical fluid dynamics. We consider here the limit of "creeping flow" in which the inertial terms are neglected in the equation of motion. The sphere has radius R and is moving unidirectionally with constant velocity V in an incompressible Newtonian liquid of density ρ and viscosity μ. The fluid is at rest far from the sphere.

a. Find the velocity field for the flow around the sphere.

b. From the results in **(a)** obtain the expression for the drag force on the sphere (i.e., Stokes' law).

c. Find the disturbance in a quiescent fluid due to the movement of a sphere through the fluid, in terms of the force that the sphere exerts on the fluid.

SOLUTION **(a)** In order to simplify the calculations we represent the flow in a spherical coordinate system with origin at the center of the sphere, with the fluid approaching the sphere from the positive z-direction (see Fig. 1.4-1). In this coordinate system the flow is steady and the boundary conditions far from the sphere are

$$v_r \rightarrow -V \cos \theta, \qquad \text{for } r \rightarrow \infty \tag{1.4-4}$$

$$v_\theta \rightarrow V \sin \theta, \qquad \text{for } r \rightarrow \infty \tag{1.4-5}$$

At the surface of the sphere the conditions are

$$v_r = 0, \qquad \text{at } r = R \tag{1.4-6}$$

$$v_\theta = 0, \qquad \text{at } r = R \tag{1.4-7}$$

[2] H. Lamb, *op. cit.*, pp. 602 *et seq.*; see also L. Landau and E. M. Lifshitz, *Fluid Mechanics*, Addison-Wesley, Reading, MA (1959), pp. 63–71, 95–98; G. K. Batchelor, *An Introduction to Fluid Mechanics*, Cambridge University Press (1970), pp. 229–244; and H. Villat, *Leçons sur les fluides visqueux*, Gauthier-Villars, Paris (1943), Chapt. 7.

TABLE 1.4-1

Equations for the Stream Function[a]

Type of Motion	Coordinate System	Velocity Components	Differential Equations for ψ Which are Equivalent to[b,c] $\rho \frac{D}{Dt}\boldsymbol{v} = -\nabla p + \mu\nabla^2\boldsymbol{v} + \boldsymbol{f}$ (A)	Expressions for Operators
Two-dimensional (planar)	Rectangular with $v_z = 0, f_z = 0,$ and no z-dependence	$v_x = -\frac{\partial\psi}{\partial y}$ $v_y = +\frac{\partial\psi}{\partial x}$	$\rho\left(\frac{\partial}{\partial t}(\nabla^2\psi) + \frac{\partial(\psi, \nabla^2\psi)}{\partial(x, y)}\right) = \mu\nabla^4\psi + [\nabla \times \boldsymbol{f}]_z$ (B)	$\nabla^2 \equiv \frac{\partial^2}{\partial x^2} + \frac{\partial^2}{\partial y^2}$ $\nabla^4\psi \equiv \nabla^2(\nabla^2\psi) \equiv \left(\frac{\partial^4}{\partial x^4} + 2\frac{\partial^4}{\partial x^2\partial y^2} + \frac{\partial^4}{\partial y^4}\right)\psi$ $[\nabla \times \boldsymbol{f}]_z = \frac{\partial}{\partial x} f_y - \frac{\partial}{\partial y} f_x$
	Cylindrical with $v_z = 0, f_z = 0,$ and no z-dependence	$v_r = -\frac{1}{r}\frac{\partial\psi}{\partial\theta}$ $v_\theta = +\frac{\partial\psi}{\partial r}$	$\rho\left(\frac{\partial}{\partial t}(\nabla^2\psi) + \frac{1}{r}\frac{\partial(\psi, \nabla^2\psi)}{\partial(r, \theta)}\right) = \mu\nabla^4\psi + [\nabla \times \boldsymbol{f}]_z$ (C)	$\nabla^2 \equiv \frac{\partial^2}{\partial r^2} + \frac{1}{r}\frac{\partial}{\partial r} + \frac{1}{r^2}\frac{\partial^2}{\partial\theta^2}$ $[\nabla \times \boldsymbol{f}]_z = \frac{1}{r}\frac{\partial}{\partial r}(rf_\theta) - \frac{1}{r}\frac{\partial}{\partial\theta} f_r$

Axisymmetrical	Cylindrical with $v_\theta = 0$, $f_\theta = 0$, and no θ-dependence	$v_z = -\frac{1}{r}\frac{\partial\psi}{\partial r}$ $v_r = +\frac{1}{r}\frac{\partial\psi}{\partial z}$	$\rho\left(\frac{\partial}{\partial t}(E^2\psi) - \frac{1}{r}\frac{\partial(\psi, E^2\psi)}{\partial(r, z)} - \frac{2}{r^2}\frac{\partial\psi}{\partial z}E^2\psi\right)$ $= \mu E^4\psi + r[\nabla \times \boldsymbol{f}]_\theta$ (D)	$E^2 \equiv \frac{\partial^2}{\partial r^2} - \frac{1}{r}\frac{\partial}{\partial r} + \frac{\partial^2}{\partial z^2}$ $E^4\psi \equiv E^2(E^2\psi)$ $[\nabla \times \boldsymbol{f}]_\theta = \frac{\partial}{\partial z}f_r - \frac{\partial}{\partial r}f_z$
	Spherical with $v_\phi = 0$, $f_\phi = 0$, and no ϕ-dependence	$v_r = -\frac{1}{r^2\sin\theta}\frac{\partial\psi}{\partial\theta}$ $v_\theta = +\frac{1}{r\sin\theta}\frac{\partial\psi}{\partial r}$	$\rho\left(\frac{\partial}{\partial t}(E^2\psi) + \frac{1}{r^2\sin\theta}\frac{\partial(\psi, E^2\psi)}{\partial(r, \theta)} - \frac{2E^2\psi}{r^2\sin^2\theta}\left(\frac{\partial\psi}{\partial r}\cos\theta - \frac{1}{r}\frac{\partial\psi}{\partial\theta}\sin\theta\right)\right)$ $= \mu E^4\psi + r\sin\theta[\nabla \times \boldsymbol{f}]_\phi$ (E)	$E^2 \equiv \frac{\partial^2}{\partial r^2} + \frac{\sin\theta}{r^2}\frac{\partial}{\partial\theta}\left(\frac{1}{\sin\theta}\frac{\partial}{\partial\theta}\right)$ $[\nabla \times \boldsymbol{f}]_\phi = \frac{1}{r}\frac{\partial}{\partial r}(rf_\theta) - \frac{1}{r}\frac{\partial}{\partial\theta}f_r$

[a] Adapted from R. B. Bird, W. E. Stewart, and E. N. Lightfoot, *Transport Phenomena*, Wiley, New York (1960), p. 131. Similar relations in general orthogonal coordinates may be found in S. Goldstein, *Modern Developments in Fluid Dynamics*, Oxford University Press, Oxford, England (1938), pp. 114–115; in this reference formulas are also given for axisymmetrical flows with a nonzero component of the velocity around the axis.

[b] Here the Jacobians are designated by $\frac{\partial(g, h)}{\partial(x, y)} = \begin{vmatrix} \partial g/\partial x & \partial g/\partial y \\ \partial h/\partial x & \partial h/\partial y \end{vmatrix}$.

[c] Here $\boldsymbol{f}$ denotes an arbitrary force per unit volume; its use is illustrated in Examples 1.4-3, 6.5-1, and 6.5-2.

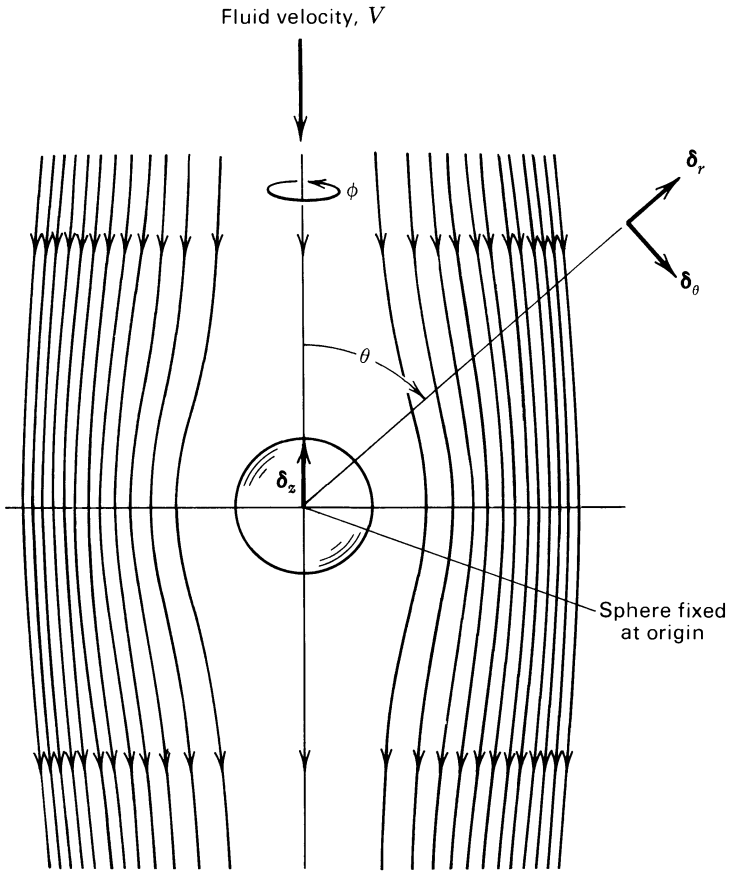

FIGURE 1.4-1. Flow around a sphere with fluid velocity $-V\boldsymbol{\delta}_z$ far from the sphere. Note that this corresponds to $v_r = (\boldsymbol{v} \cdot \boldsymbol{\delta}_r) = -V(\boldsymbol{\delta}_z \cdot \boldsymbol{\delta}_r) = -V \cos\theta$, and $v_\theta = (\boldsymbol{v} \cdot \boldsymbol{\delta}_\theta) = -V(\boldsymbol{\delta}_z \cdot \boldsymbol{\delta}_\theta) = -V(-\sin\theta)$; see Eqs. 1.4-4 and 5.

We solve the problem with the use of a stream function defined in spherical coordinates for axisymmetrical flow with no ϕ dependence. That is, according to Table 1.4-1 we use

$$v_r = -\frac{1}{r^2 \sin\theta}\frac{\partial\psi}{\partial\theta} \tag{1.4-8}$$

$$v_\theta = \frac{1}{r \sin\theta}\frac{\partial\psi}{\partial r} \tag{1.4-9}$$

Note that in terms of ψ the boundary conditions far from the sphere become

$$\psi \to \tfrac{1}{2}Vr^2 \sin^2\theta, \qquad \text{for } r \to \infty \tag{1.4-10}$$

In view of this condition we assume for ψ

$$\psi = f(r) \sin^2\theta \tag{1.4-11}$$

This expression also automatically ensures that $v_\theta = 0$ and $\partial v_r/\partial\theta = 0$ at $\theta = 0$ and π. The boundary conditions at $r = R$ then become

$$f(r) = 0, \qquad \text{at } r = R \tag{1.4-12}$$

$$f'(r) = 0, \qquad \text{at } r = R \tag{1.4-13}$$

For steady-state creeping flow the equation for ψ is (according to Eq. E of Table 1.4-1)

$$E^4\psi = 0 \tag{1.4-14}$$

where the operator E^2 is given in spherical coordinates in Table 1.4-1. If we substitute the expression for ψ in Eq. 1.4-11 into Eq. 1.4-14 we obtain

$$\left[\frac{\partial^2}{\partial r^2} + \frac{\sin\theta}{r^2}\frac{\partial}{\partial\theta}\left(\frac{1}{\sin\theta}\frac{\partial}{\partial\theta}\right)\right]\left[\sin^2\theta\left(\frac{d^2f}{dr^2} - \frac{2f}{r^2}\right)\right] = 0 \tag{1.4-15}$$

which may be rearranged to give

$$\left(\frac{d^2}{dr^2} - \frac{2}{r^2}\right)\left(\frac{d^2}{dr^2} - \frac{2}{r^2}\right)f = 0 \tag{1.4-16}$$

This is an "equidimensional" equation, known[3] to have solutions of the form $f = r^n$. If we substitute $f = r^n$ into Eq. 1.4-16, we see that n must satisfy the equation

$$[n(n-1) - 2][(n-2)(n-3) - 2] = 0 \tag{1.4-17}$$

so that $n = -1$, 1, 2, or 4. The general solution for f is then

$$f = A_1r^{-1} + A_2r + A_3r^2 + A_4r^4 \tag{1.4-18}$$

which has four constants as is appropriate for a fourth-order differential equation. The constants are determined from Eqs. 1.4-10, 12, and 13, and the stream function and velocity components become:

$$\psi = VR^2\left[\frac{1}{2}\left(\frac{r}{R}\right)^2 - \frac{3}{4}\left(\frac{r}{R}\right) + \frac{1}{4}\left(\frac{R}{r}\right)\right]\sin^2\theta \tag{1.4-19}$$

$$v_r = -V\left[1 - \frac{3}{2}\left(\frac{R}{r}\right) + \frac{1}{2}\left(\frac{R}{r}\right)^3\right]\cos\theta \tag{1.4-20}$$

$$v_\theta = V\left[1 - \frac{3}{4}\left(\frac{R}{r}\right) - \frac{1}{4}\left(\frac{R}{r}\right)^3\right]\sin\theta \tag{1.4-21}$$

(b) To find the drag force on the sphere we need the pressure $p(r, \theta)$. To obtain this we insert the above velocity field into the equations of motion; this leads to the following equations for p:

$$\frac{\partial p}{\partial r} = -3\mu VRr^{-3}\cos\theta - \rho g\cos\theta \tag{1.4-22}$$

$$\frac{1}{r}\frac{\partial p}{\partial\theta} = -\tfrac{3}{2}\mu VRr^{-3}\sin\theta + \rho g\sin\theta \tag{1.4-23}$$

where g is the gravitational acceleration acting in the negative z-direction. These equations are solved by

$$p = (\tfrac{3}{2}\mu VRr^{-2} - \rho gr)\cos\theta + p_0 \tag{1.4-24}$$

[3] C. M. Bender and S. A. Orzag, *Advanced Mathematical Methods for Scientists and Engineers*, McGraw-Hill, New York (1978), p. 12.

where p_0 is a constant. We now calculate the rr- and $r\theta$-components of the total stress tensor at the surface of the sphere

$$\pi_{rr}|_{r=R} = p|_{r=R} = (\tfrac{3}{2}\mu V R^{-1} - \rho g R)\cos\theta + p_0 \tag{1.4-25}$$

$$\pi_{r\theta}|_{r=R} = -\mu\left[r\frac{\partial}{\partial r}\left(\frac{v_\theta}{r}\right) + \frac{1}{r}\frac{\partial v_r}{\partial \theta}\right]\Bigg|_{r=R} = -\tfrac{3}{2}\mu V R^{-1}\sin\theta \tag{1.4-26}$$

Here we have used the result from Example 1.2-1 that $\tau_{rr} = 0$ at the solid surface. The force per unit area exerted by the fluid on the surface of the sphere is therefore $-[\boldsymbol{\delta}_r \cdot \boldsymbol{\pi}] = -[\pi_{rr}\boldsymbol{\delta}_r + \pi_{r\theta}\boldsymbol{\delta}_\theta]$. Certainly the net force will be in the z-direction and we therefore compute the z-component of this force:

$$-(\boldsymbol{\delta}_z \cdot [\pi_{rr}\boldsymbol{\delta}_r + \pi_{r\theta}\boldsymbol{\delta}_\theta]) = -\tfrac{3}{2}\mu V R^{-1} + \rho g R\cos^2\theta - p_0\cos\theta \tag{1.4-27}$$

where we have used $(\boldsymbol{\delta}_z \cdot \boldsymbol{\delta}_r) = \cos\theta$ and $(\boldsymbol{\delta}_z \cdot \boldsymbol{\delta}_\theta) = -\sin\theta$ (see Fig. 1.4-1). The total force in the positive z-direction on the sphere is then

$$\begin{aligned} F &= \int_0^{2\pi}\int_0^{\pi} (\boldsymbol{\delta}_z \cdot [-\boldsymbol{\delta}_r \cdot \boldsymbol{\pi}])R^2 \sin\theta\, d\theta\, d\phi \\ &= -6\pi\mu R V + \tfrac{4}{3}\pi R^3 \rho g \end{aligned} \tag{1.4-28}$$

The combination $6\pi\mu RV$ is called the drag force F_D and the combination $(4/3)\pi R^3\rho g$ is the buoyancy force. The result $F_D = 6\pi\mu RV$ is known as Stokes' law[2] and is a good approximation for Reynolds numbers $\mathrm{Re} = 2RV\rho/\mu \leq 0.1$. The expression for the drag force has been extended[4] by a perturbation method to yield

$$F_D = 6\pi\mu RV[1 + \tfrac{3}{16}\,\mathrm{Re} + \tfrac{9}{160}\,\mathrm{Re}^2 \ln \mathrm{Re} + O(\mathrm{Re}^2)] \tag{1.4-29}$$

as an improved approximation for $\mathrm{Re} < O(1)$. Experiments[5] show that an eddy forms at the back of the sphere at a Reynolds number of about 24. The eddy and wake flow begins to oscillate at $\mathrm{Re} \doteq 130$ but remains laminar until $\mathrm{Re} \doteq 200$ at which Reynolds number the flow gradually becomes turbulent.

(c) We now turn the problem around and let the fluid be at rest at infinity but let the sphere move with a constant velocity $\boldsymbol{v}_s = V\boldsymbol{\delta}_z$, with its center instantaneously at the origin (see Fig. 1.4-2). Then the velocity $\boldsymbol{v}$ of the fluid is given according to Eqs. 1.4-20 and 21 by

$$\begin{aligned} \boldsymbol{v} &= \frac{3}{4}\frac{R}{r}V(2\boldsymbol{\delta}_r\cos\theta - \boldsymbol{\delta}_\theta\sin\theta) + O\left(\frac{R^3}{r^3}\right) \\ &= \frac{3}{4}\frac{R}{r}V(\boldsymbol{\delta}_z + \boldsymbol{\delta}_r\cos\theta) + O\left(\frac{R^3}{r^3}\right) \end{aligned} \tag{1.4-30}$$

Now the force $\boldsymbol{F}_s$ exerted by the sphere on the fluid by virtue of its motion is

$$\boldsymbol{F}_s = 6\pi\mu RV\boldsymbol{\delta}_z \tag{1.4-31}$$

It is possible to express the velocity disturbance $\boldsymbol{v}$ of Eq. 1.4-30 directly in terms of $\boldsymbol{F}_s$ as follows:

$$\boldsymbol{v} = [\boldsymbol{\Omega} \cdot \boldsymbol{F}_s] + O\left(\frac{R^3}{r^3}\right) \tag{1.4-32}$$

[4] I. Proudman and J. R. A. Pearson, *J. Fluid Mech.*, **2**, 237–262 (1957).
[5] S. Taneda, *J. Phys. Soc. Jpn.*, **11**, 1104–1108 (1956).

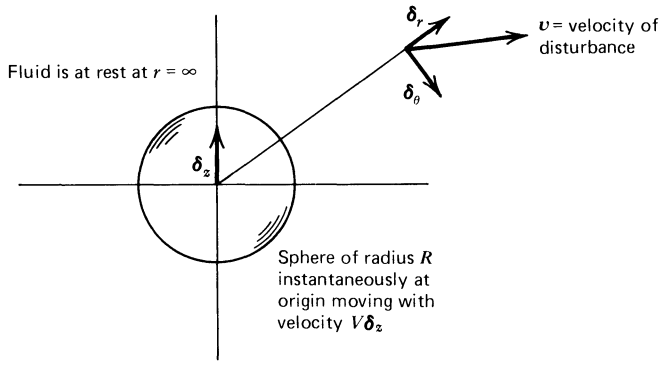

FIGURE 1.4-2. Velocity disturbance caused by a sphere moving linearly through a fluid with a constant velocity $V\boldsymbol{\delta}_z$ at that instant at which the center of the sphere is at the origin.

Here the tensor,

$$\boldsymbol{\Omega} = \frac{1}{8\pi\mu r}(\boldsymbol{\delta} + \boldsymbol{\delta}_r\boldsymbol{\delta}_r) \tag{1.4-33}$$

is called the *Oseen-Burgers tensor*[6] or *hydrodynamic interaction tensor*. It is shown in §§13.6, 14.6, and 15.4 how this tensor is used to describe the perturbation in the solvent velocity field near one part of a macromolecule because of the motion of another part of the macromolecule.

It is instructive to use the Oseen-Burgers tensor to attempt to calculate the total volume flow rate of liquid Q through the xy-plane ($\theta = \pi/2$) at the instant the sphere is at the origin. The fluid velocity at $z = 0$ and at a distance r from the origin is according to the Oseen-Burgers expression $\boldsymbol{v} = (F_s/8\pi\mu r)\boldsymbol{\delta}_z$. The volume flow rate is then

$$Q = \int_0^{2\pi}\int_R^\infty v_z r dr d\phi = 2\pi\left(\frac{F_s}{8\pi\mu}\right)\int_R^\infty dr \tag{1.4-34}$$

We see however that the integral is not convergent. This means that the Oseen tensor expression predicts that a finite force $F_s\boldsymbol{\delta}_z$ induces an infinite volume flux in the fluid. This is possible, of course, because the assumption of creeping flow is tantamount to assuming that the density of the fluid is exactly zero. The introduction of any finite fluid density, no matter how small, dramatically changes the velocity disturbance far from the sphere.[6] The slow, $O(r^{-1})$ decay of the velocity as $r \to \infty$ is then restricted to a "wake" region behind the sphere, and the Oseen-Burgers expression ceases to be a valid first approximation for the velocity disturbance far from the sphere.

EXAMPLE 1.4-2 Flow around a Rising Bubble[7]

A small spherical bubble of radius R is rising slowly in an incompressible Newtonian fluid of density ρ and viscosity μ. The fluid is at rest far from the bubble.

a. Find the velocity field for the flow around the bubble.

b. Develop a relationship between the gravitational acceleration g and the rise velocity of the bubble, V.

[6] C. W. Oseen, *Neuere Methoden und Ergebnisse in der Hydrodynamik*, Akad. Verlag, Leipzig (1927); J. M. Burgers, *Second Report on Viscosity and Plasticity*, Amsterdam Academy of Sciences, Amsterdam (1938), Chapt. 3.

[7] H. Lamb, *op. cit.*, pp. 600-601, and G. K. Batchelor, *op. cit.*, pp. 235-238, develop the solution for the flow around a translating spherical drop. In the limit as the viscosity of the drop approaches zero, these solutions then simplify to the solution given here.

SOLUTION **(a)** This flow problem is closely related to the flow around a solid sphere and we therefore adopt the same coordinate system and solution procedure illustrated in the previous example. The difference between the two situations is just in the boundary conditions at the surface of the spherical object; in this example we have the conditions

$$v_r = 0 \qquad \text{at } r = R \tag{1.4-35}$$

$$\tau_{r\theta} = -\mu\left[r\frac{\partial}{\partial r}\left(\frac{v_\theta}{r}\right) + \frac{1}{r}\frac{\partial v_r}{\partial \theta}\right] = 0 \qquad \text{at } r = R \tag{1.4-36}$$

This means that the boundary conditions for the function f of Eq. 1.4-18 are

$$f = 0 \qquad \text{at } r = R \tag{1.4-37}$$

$$-2f' + Rf'' = 0 \qquad \text{at } r = R \tag{1.4-38}$$

The four constants are now determined from Eq. 1.4-10 for $r \to \infty$ and the above equations for $r = R$ to yield

$$\psi = V(\tfrac{1}{2}r^2 - \tfrac{1}{2}Rr)\sin^2\theta \tag{1.4-39}$$

$$v_r = -V(1 - (R/r))\cos\theta \tag{1.4-40}$$

$$v_\theta = V(1 - \tfrac{1}{2}(R/r))\sin\theta \tag{1.4-41}$$

(b) To find the rise velocity we must know the pressure p. Here again we parallel the previous example to find

$$p = (\mu V R r^{-2} - \rho g r)\cos\theta + p_0 \tag{1.4-42}$$

where p_0 is a constant. The rr-component of the total stress tensor at the surface of the bubble is therefore

$$\begin{aligned}\pi_{rr}|_{r=R} &= p|_{r=R} - 2\mu\left.\frac{\partial v_r}{\partial r}\right|_{r=R} \\ &= (3\mu V R^{-1} - \rho g R)\cos\theta + p_0\end{aligned} \tag{1.4-43}$$

Notice that τ_{rr} does not vanish on the surface of the bubble as it does on the surface of the sphere. On the other hand $\pi_{r\theta}$ does vanish on the surface of the bubble. The net force per unit area in the z-direction is therefore

$$-(\boldsymbol{\delta}_z \cdot [\pi_{rr}\boldsymbol{\delta}_r]) = (-3\mu V R^{-1} + \rho g R)\cos^2\theta - p_0\cos\theta \tag{1.4-44}$$

where we have used $(\boldsymbol{\delta}_z \cdot \boldsymbol{\delta}_r) = \cos\theta$. The total force on the bubble is then

$$\begin{aligned}F &= \int_0^{2\pi}\int_0^{\pi} (\boldsymbol{\delta}_z \cdot [-\boldsymbol{\delta}_r \cdot \boldsymbol{\pi}])R^2 \sin\theta \, d\theta \, d\phi \\ &= -4\pi\mu R V + \tfrac{4}{3}\pi R^3 \rho g\end{aligned} \tag{1.4-45}$$

The first term in this expression describes the viscous drag on the bubble and the second term the buoyancy force on the bubble. The velocity of rise is found by using the condition that there is no net force on the bubble so that $V = (1/3)\rho g R^2/\mu$. Note that this gives $\pi_{rr} = p_0$ at the surface of the bubble independent of θ. This means that the bubble will remain spherical with no tendency to deform from that shape even with negligible surface tension.

For small but finite values of the Reynolds number, inertial forces will tend to deform bubbles, and the bubble shape will be given as a balance among viscous, inertial, and surface tension forces. Taylor and Acrivos[8] have derived the following expression to describe small deviations from the spherical shape:

$$R_s(\theta) = R[1 - \tfrac{5}{96}\,\mathrm{Re}\,\mathrm{Ca}\,(3\cos^2\theta - 1)] \tag{1.4-46}$$

Here $R_s(\theta)$ is the radius of the slightly deformed bubble as a function of θ, and R is the radius of an undeformed sphere of the same volume. The surface tension σ enters in the *capillary number* $\mathrm{Ca} = \mu V/\sigma$. The expression is valid when both $\mathrm{Re} = 2RV\rho/\mu \ll 1$ and $\mathrm{ReCa} \ll 1$, and it shows that inertial effects will deform the bubble into the shape of an ellipsoid flattened at the poles.

EXAMPLE 1.4-3 Rotating Sphere in a Viscous Liquid

A sphere of radius R is made to rotate with an angular velocity W in a Newtonian liquid of infinite extent, which is quiesecent far from the sphere (see Fig. 1.4-3).

a. Find the velocity distribution in the surrounding liquid when the rotation is so slow that the inertial effects may be neglected.

b. Find the secondary flow due to small inertial effects.

c. Find the torque $\mathscr{T}$ which has to be applied to the sphere in order to maintain the rotation.

SOLUTION **(a)** We describe the flow in a spherical coordinate system with the origin at the center of the sphere and with the z-axis along the axis of rotation. The boundary conditions on the velocity field are then

$$v_r = 0,\ v_\theta = 0,\ v_\phi = RW\sin\theta, \qquad \text{at } r = R \tag{1.4-47}$$

$$v_r \to 0,\ v_\theta \to 0,\ v_\phi \to 0, \qquad \text{for } r \to \infty \tag{1.4-48}$$

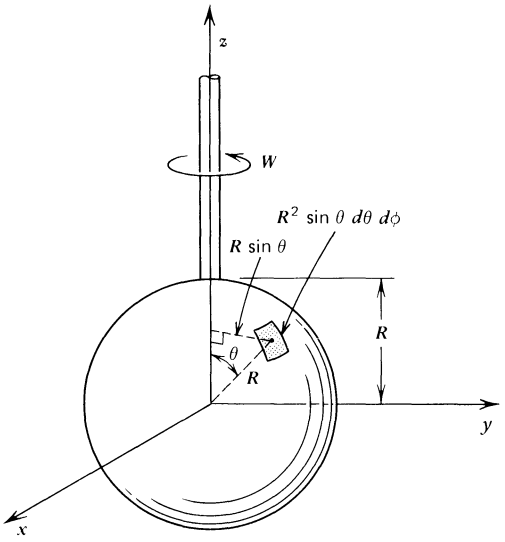

FIGURE 1.4-3. A sphere of radius R rotates with constant angular velocity W about the z-axis in an incompressible Newtonian fluid. The fluid is at rest far from the sphere.

[8] T. D. Taylor and A. Acrivos, *J. Fluid Mech.*, **18**, 466-476 (1964).

In view of these conditions we look for a solution to the creeping flow problem in the form $v_r = 0$, $v_\theta = 0$, $v_\phi = v(r) \sin\theta$ and with the modified pressure $\mathscr{P}$ being constant. The ϕ-component of the equation of motion with the inertial terms neglected then shows that $v(r)$ must satisfy

$$\frac{d}{dr}\left(r^2 \frac{dv}{dr}\right) - 2v = 0 \tag{1.4-49}$$

This is an equidimensional equation, which may be solved by the same technique that was used in Examples 1.4-1 and 2. The result is the following expression for the creeping flow around the rotating sphere

$$v_{0r} = 0; \quad v_{0\theta} = 0; \quad v_{0\phi} = \frac{R^3}{r^2} W \sin\theta \tag{1.4-50}$$

A subscript zero has been added to the velocity components to indicate that these correspond to very slow flow.

(b) To find the secondary flow due to small inertial effects we use a perturbation method. The perturbation parameter that describes the importance of the inertial effects is a Reynolds number $\mathrm{Re} = R^2 W\rho/\mu$. For $\mathrm{Re} \ll 1$ we assume then that the velocity field $\boldsymbol{v}$ and the pressure field p are

$$\boldsymbol{v} = \boldsymbol{v}_0 + \mathrm{Re}\, \boldsymbol{v}_1 + \cdots \tag{1.4-51}$$

$$p = p_0 + \mathrm{Re}\, p_1 + \cdots \tag{1.4-52}$$

Here $\boldsymbol{v}_0(r, \theta)$ is the velocity field given in component form in Eq. 1.4-50, and p_0 *is* $-\rho g r \cos\theta$. Since $\boldsymbol{v}_0$ satisfies the boundary conditions at the surface of the sphere and at infinity we see that $\boldsymbol{v}_1$ must satisfy

$$\boldsymbol{v}_1 = \boldsymbol{0}, \qquad \text{at } r = R \tag{1.4-53}$$

$$\boldsymbol{v}_1 \to \boldsymbol{0}, \qquad \text{for } r \to \infty \tag{1.4-54}$$

When the expansions are inserted into the steady state equation of motion and terms of first order in Re are equated, we find that $\boldsymbol{v}_1$ and p_1 must satisfy

$$-\nabla p_1 + \mu \nabla^2 \boldsymbol{v}_1 + \boldsymbol{f} = \boldsymbol{0} \tag{1.4-55}$$

where

$$\boldsymbol{f} = -\frac{\mu}{WR^2}[\boldsymbol{v}_0 \cdot \nabla \boldsymbol{v}_0] = \mu R^4 W r^{-5} \sin\theta\, (\sin\theta\, \boldsymbol{\delta}_r + \cos\theta\, \boldsymbol{\delta}_\theta) \tag{1.4-56}$$

In addition $\boldsymbol{v}_1$ must satisfy the equation of continuity. The $\boldsymbol{\delta}_r$ and $\boldsymbol{\delta}_\theta$ are unit vectors associated with the spherical coordinate system, and we have used Eq. 1.4-50 for $\boldsymbol{v}_0$. We see that Eq. 1.4-55 has the same form as Eq. A of Table 1.4-1 with $\rho = 0$. The boundary conditions that $\boldsymbol{v}_1$ must be zero at the surface of the sphere and at infinity introduce no velocity in the ϕ-direction or any ϕ-dependence. Since furthermore $f_\phi = 0$ and $\boldsymbol{f}$ has no ϕ-dependence, we expect $\boldsymbol{v}_1$ to have the same properties. We may therefore derive $\boldsymbol{v}_1$ from a stream function $\psi(r, \theta)$ for axisymmetrical spherical flow. From Eq. E of Table 1.4-1 we see that ψ must satisfy

$$E^4\psi = 6WR^4 r^{-5} \sin^2\theta \cos\theta \tag{1.4-57}$$

We assume that ψ has the form

$$\psi = f(r) \sin^2\theta \cos\theta \tag{1.4-58}$$

Then $f(r)$ must satisfy

$$\left(\frac{d^2}{dr^2} - \frac{6}{r^2}\right)\left(\frac{d^2}{dr^2} - \frac{6}{r^2}\right) f = 6WR^4 r^{-5} \tag{1.4-59}$$

This equidimensional equation is solved by the method outlined in Example 1.4-1. The general solution is

$$f = -\tfrac{1}{4}WR^4 r^{-1} + C_1 r^{-2} + C_2 + C_3 r^3 + C_4 r^5 \tag{1.4-60}$$

The boundary condition at infinity in Eq. 1.4-54 implies that C_3 and C_4 must be zero. The boundary condition at the surface of the sphere in Eq. 1.4-53 corresponds to

$$f = 0, f' = 0, \qquad \text{at } r = R \tag{1.4-61}$$

These conditions determine C_1 and C_2. The final results for the components of the secondary flow field v_1 are then

$$v_{1r} = -\tfrac{1}{8}WR^3\left(1 - \frac{R}{r}\right)^2 r^{-2}(3\cos^2\theta - 1) \tag{1.4-62}$$

$$v_{1\theta} = \tfrac{1}{4}WR^4\left(1 - \frac{R}{r}\right) r^{-3}\sin\theta\cos\theta \tag{1.4-63}$$

$$v_{1\phi} = 0 \tag{1.4-64}$$

These expressions show that inertial effects make the fluid move away from the sphere in the equatorial plane and towards the sphere along the axis in agreement with observations and physical intuition.

The rather straightforward perturbation solution given in this example is called a "regular perturbation" solution. Not all perturbation problems are equally straightforward. In particular the solutions from which the expressions in Eqs. 1.4-29 and 46 are obtained are examples of "singular perturbation" solutions, and these involve more elaborate techniques.

(c) We next find the torque $\mathscr{T}$ which must be applied to the sphere in order to maintain the rotation. The torque acting on a small elemental area $R^2 \sin\theta\, d\theta\, d\phi$ is the product of the shear force $\tau_{r\phi}|_{r=R}\, R^2 \sin\theta\, d\theta\, d\phi$ and the lever arm $R\sin\theta$ measured from the axis of rotation. Integration over the sphere surface then gives:

$$\begin{aligned}
\mathscr{T} &= \int_0^{2\pi}\int_0^{\pi} \tau_{r\phi}\Big|_{r=R} (R\sin\theta) R^2 \sin\theta\, d\theta\, d\phi \\
&= -2\pi\mu R^3 \int_0^{\pi} r\frac{\partial}{\partial r}\left(\frac{v_\phi}{r}\right)\Big|_{r=R} \sin^2\theta\, d\theta \\
&= +6\pi\mu R^3 W \int_0^{\pi} \sin^3\theta\, d\theta \\
&= 8\pi\mu R^3 W
\end{aligned} \tag{1.4-65}$$

Note that the first-order term v_1 in the expansion in Eq. 1.4-51 does not contribute to the torque. For other methods of finding the torque see Problem 1B.12.

PROBLEMS

1A.1 Volume Rate of Flow through a Circular Tube

The chlorinated biphenyl used by Sukanek and Laurence[1] in their research on viscous heating has the following properties at 313 K:

$$\mu = 400 \text{ poise} = 40 \text{ Pa} \cdot \text{s}$$

$$\rho = 1.6 \text{ g/cm}^3 = 1.6 \times 10^3 \text{ kg/m}^3$$

$$k = 9.4 \times 10^3 \text{ g} \cdot \text{cm/s}^3 \cdot \text{K} = 9.4 \times 10^{-2} \text{ W/m} \cdot \text{K}$$

$$\hat{C}_p = 0.235 \text{ cal/g} \cdot \text{C} = 983 \text{ J/kg} \cdot \text{K}$$

a. What will the volume rate of flow be for the flow of this fluid through a horizontal capillary tube of radius 3.2 mm and length 10.3 cm when the pressure drop is 1.67×10^5 Pa?

b. Compute the Reynolds number for the flow in order to verify that the flow is laminar.

c. What will happen if the radius of the tube is doubled?

Answers: **a.** 1.67×10^{-6} m^3/s
b. 1.33×10^{-2}

1A.2 Terminal Velocity of a Falling Sphere

a. By making a force balance on a sphere falling in a liquid and using the result in Eq. 1.4-28 show that the terminal velocity (the velocity attained at steady state) is

$$v_t = 2R^2(\rho_s - \rho)g/9\mu \tag{1A.2-1}$$

where ρ and ρ_s, are the densities of the liquid and the sphere, respectively.

b. What will be the terminal velocity of a steel sphere of radius 0.25 cm with density 7850 kg/m^3 falling in the liquid in Problem 1A.1?

c. Verify, by computing the Reynolds number for the flow, that it was permissible to use Eq. 1A.2-1.

d. What is the maximum radius of steel spheres that can be used so that Stokes' law can still be used for describing the viscous drag on the sphere falling in the liquid of Problem 1A.1?

Answers: **b.** 2.13×10^{-3} m/s
c. 4.26×10^{-4}
d. 1.54 cm

1A.3 Measurement of Viscosity in a Cone-and-Plate Viscometer

The system in Fig. 1.3-4 has the following geometrical measurements:

$$R = 5.2 \text{ cm} = 0.052 \text{ m}$$

$$\vartheta_0 = 0.35^\circ = 0.00611 \text{ rad}$$

[1] P. C. Sukanek and R. L. Laurence, *AIChE J.*, **20**, 474–484 (1974).

With a fluid completely filling the gap, a torque of 2.47 N·m is required to maintain an angular velocity of 1.28 rad/s.

a. What is the shear stess $\tau_{\theta\phi}$ in the gap?

b. What is $\dot{\gamma}_{\theta\phi}$ in the gap?

c. What is the viscosity of the fluid?

Answers: **a.** 8400 Pa
b. $-209\ s^{-1}$
c. 40 Pa · s

1A.4 Squeezing Flow Experiment

a. From Eq. 1.3-52 obtain a formula for the time required to squeeze out half of the material that is initially in the gap; call this quantity $t_{1/2}$.

b. For a silicone oil with a viscosity of 106 Pa·s Leider[2] found experimentally that $t_{1/2}$ was 499s for a squeezing flow system in which the disk radius was 2.54 cm, the initial disk separation (i.e., $2h_0$) was 0.01209 cm, and a mass of 4.07 kg was placed on the upper disk. What value of $t_{1/2}$ is calculated from the formula in (**a**)?

Answer: **b.** 535 s

1B.1 Flow in a Tube with a Sinusoidally Varying Cross-Section

Figure 1B.1 shows a tube with a radius of the form $R(z) = R_0[1 + \alpha \sin(\pi z/l)]$ where $|\alpha| < 1$ and R_0 is the mean radius. The pressure drop corresponding to the length of one full cycle, $2l$, is denoted by $\mathscr{P}_0 - \mathscr{P}_{2l}$.

a. When $l \gg R_0$ use a lubrication approximation to develop an expression for the volume rate of flow Q for a given average pressure gradient $(\mathscr{P}_0 - \mathscr{P}_{2l})/2l$.

b. When $|\alpha| \ll 1$ show that the expression becomes approximately

$$Q = \frac{\pi R_0^4(\mathscr{P}_0 - \mathscr{P}_{2l})}{16\mu l[1 + 5\alpha^2]} \tag{1B.1-1}$$

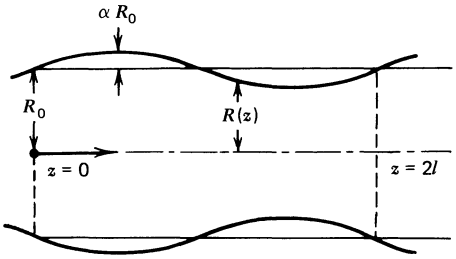

FIGURE 1B.1. Section of tube with a sinusoidally varying radius in a cylindrical coordinate system.

1B.2 Flow Between Coaxial Cylinders and Spheres

a. The space between two coaxial cylinders is filled with an incompressible, Newtonian fluid at constant temperature. The radii of the inner and outer wetted surfaces are κR and R, respectively. The angular velocities of rotation of the inner and outer cylinders are W_i and W_o. Determine the velocity distribution in the fluid, and the torques on the two cylinders needed to maintain the motion.

[2] P. J. Leider, *Ind. Eng. Chem. Fundam.*, **13**, 342–346 (1974).

b. Repeat part (**a**) for two concentric spheres. Assume that the flow is sufficiently slow that no secondary flows occur.

c. Find the torque per unit length $\mathscr{T}/L$ on a cylinder rotating slowly in an infinite sea of liquid at rest at infinity.

d. Find the torque $\mathscr{T}$ on a sphere rotating slowly in an infinite sea of liquid at rest at infinity.

Answers: **a.** $$v_\theta = \frac{\kappa R}{1-\kappa^2}\left[(W_o - \kappa^2 W_i)\frac{r}{\kappa R} + (W_i - W_o)\frac{\kappa R}{r}\right] \tag{1B.2-1}$$

b. $$v_\phi = \frac{\kappa R \sin\theta}{1-\kappa^3}\left[(W_o - \kappa^3 W_i)\frac{r}{\kappa R} + (W_i - W_o)\left(\frac{\kappa R}{r}\right)^2\right] \tag{1B.2-2}$$

c. $$\mathscr{T}/L = 4\pi\mu W R^2 \tag{1B.2-3}$$

d. $$\mathscr{T} = 8\pi\mu W R^3 \tag{1B.2-4}$$

1B.3 Laminar Newtonian Flow in a Triangular Duct[3]

A straight duct has a length L and a cross section of triangular shape, bounded by the plane surfaces $y = H$, $y = \sqrt{3}x$, and $y = -\sqrt{3}x$. Verify that the velocity profile for the laminar flow of a Newtonian fluid in a duct of this type is

$$v_z = \frac{(\mathscr{P}_0 - \mathscr{P}_L)}{4\mu LH}(y - H)(3x^2 - y^2) \tag{1B.3-1}$$

Then obtain the volume rate of flow

$$Q = \frac{\sqrt{3}(\mathscr{P}_0 - \mathscr{P}_L)H^4}{180\mu L} \tag{1B.3-2}$$

1B.4 Contraction of a Newtonian Jet at Large Reynolds Number

The behavior of Newtonian jets issuing from circular tubes has been studied experimentally by Middleman and Gavis.[4] They found that the jets swell for Re < 16 and contract for Re > 16, where the Reynolds number Re is defined as $\mathrm{Re} = 2R\langle v_z\rangle\rho/\mu$ (the angular brackets indicate an average over the tube cross section).

We assume that the flow is isothermal, and consider the equation of continuity (Eq. 1.1-4) and the equation of motion (Eq. 1.1-8) written for steady-state, incompressible flow.

a. First show that these two equations can be integrated over a volume V enclosed by a surface S to obtain

$$\int_S (\boldsymbol{n}\cdot\boldsymbol{v})dS = 0 \tag{1B.4-1}$$

$$\int_S [\boldsymbol{n}\cdot\rho\boldsymbol{vv}]dS + \int_S [\boldsymbol{n}\cdot\boldsymbol{\pi}]dS - \int_V \rho\boldsymbol{g}\,dV = 0 \tag{1B.4-2}$$

[3] L. D. Landau and E. M. Lifshitz, *Fluid Mechanics*, Addison-Wesley, Reading, MA (1959), p. 58. See also R. Berker, *Handbuch der Physik*, Vol. VIII/2, Springer, Berlin (1963), pp. 67–77, for a summary of formulas for flow in conduits of various cross sections.

[4] S. Middleman and J. Gavis, *Phys. Fluids*, **4**, 355–359 (1961).

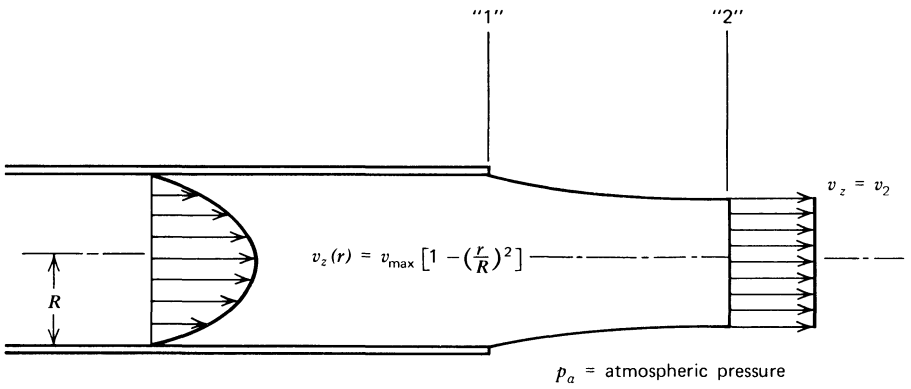

FIGURE 1B.4. Contraction of a Newtonian jet emerging from a circular tube. Within the tube the velocity profile is parabolic. At plane "2" the velocity is uniform. The cross sectional areas at "1" and "2" are S_1 and S_2, respectively. Newtonian jets have been found to contract for Re $= 2R\langle v_z\rangle\rho/\mu > 16$ and to swell for Re < 16. For Re > 100, it is found experimentally that $S_2/S_1 = \frac{3}{4}$.

When these equations are applied to the fluid contained in the region between planes "1" and "2" in Fig. 1B.4 they become

$$\langle v_z\rangle_1 S_1 - v_2 S_2 = 0 \tag{1B.4-3}$$

$$\rho\langle v_z^2\rangle_1 S_1 - \rho v_2^2 S_2 + \langle \pi_{zz}\rangle_1 S_1 - p_a S_2 + p_a(S_2 - S_1) = 0 \tag{1B.4-4}$$

where p_a is the atmospheric pressure.

b. It is desired to use the equations developed in (a) to estimate S_2/S_1 for the jet in the limit of high Reynolds number laminar flow. We do this by assuming that in this limit:

1. The flow remains parabolic up to plane "1," so that $\langle v_z^2\rangle_1/\langle v_z\rangle_1^2 = 4/3$. (Verify this numerical value.)
2. $\langle \pi_{zz}\rangle_1$ can be approximated as p_a.

Neither of these approximations has been justified. If now one solves Eqs. 1B.4-3 and 4 simultaneously then one obtains $S_2/S_1 = 3/4$; verify this. This result was obtained by Harmon.[5] The value of 3/4 agrees with the experimental results of Middleman and Gavis for Reynolds numbers of more than 100. However at Re $= 16$, it was found experimentally that $S_2/S_1 = 1$, and as the Reynolds number approaches zero, S_2/S_1 becomes about 1.13.[6]

1B.5 Parallel-Disk Viscometer

A schematic diagram is given in Fig. 1B.5 of a parallel-disk viscometer. The fluid is placed in the gap of thickness B between the two circular disks. Develop a formula for deducing the fluid viscosity from the measurement of the torque $\mathcal{T}$ required to turn the upper disk at an angular velocity W.

a. Postulate that for small values of W the velocity and pressure profiles have the form: $v_r = 0$, $v_z = 0$, and $v_\theta = zf(r)$; and $p = p(r, z)$. Write down the resulting simplified equations of continuity and motion.

[5] D. B. Harmon, *J. Franklin Inst.*, **259**, 519–522 (1955); S. Middleman and J. Gavis, *Phys. Fluids*, **4**, 355–359 (1961).
[6] R. I. Tanner in J. R. A. Pearson and S. M. Richardson, eds., *Numerical Analysis of Polymer Processing*, Applied Science Publishers, London (1983); see also R. I. Tanner, *Engineering Rheology*, Elsevier Applied Science Publishers, London (1985), pp. 322–325.

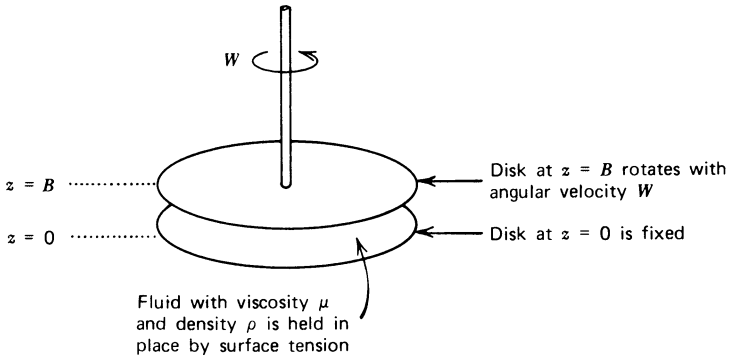

FIGURE 1B.5. Parallel-disk viscometer with two disks of radius R separated by a distance B, with dimensions such that $R \gg B$.

b. From the θ-component of the equation of motion, obtain a differential equation for $f(z)$. Solve this equation and evaluate the constants of integration. Finally obtain the velocity distribution $v_\theta = Wrz/B$.

c. Show that the torque required to turn the upper disk is $\mathscr{T} = \pi\mu WR^4/2B$.

1B.6 The Rayleigh Problem[7]

An incompressible Newtonian fluid occupies the half-space, from $y = 0$ to $y = \infty$, and is bounded at $y = 0$ by a solid plane surface. Before $t = 0$, the fluid is at rest. Then at time $t = 0$ the solid surface at $y = 0$ is made to move with constant velocity V in the positive x-direction. It is desired to find the velocity distribution $v_x = v_x(y, t)$.

a. Introduce a dimensionless velocity $\phi = v_x/V$. Inasmuch as there is no natural unit of length for the problem, and since the initial condition at $t = 0$ and the boundary condition at $y = \infty$ are the same, it seems reasonable to try a solution of the form

$$\phi = \phi(\eta) \quad \text{where} \quad \eta = \sqrt{\rho y^2/4\mu t} \tag{1B.6-1}$$

Show that with these variables the equation of motion for this flow becomes

$$\phi'' + 2\eta\phi' = 0 \tag{1B.6-2}$$

in which primes denote differentiation with respect to η. What are the boundary conditions that go with this equation?

b. Show that this equation can be solved to give

$$\phi = 1 - \frac{2}{\sqrt{\pi}} \int_0^\eta \exp(-x^2)\, dx = 1 - \operatorname{erf} \sqrt{\rho y^2/4\mu t} \tag{1B.6-3}$$

in which $\operatorname{erf} \eta$ is the error function of η.

1B.7 Steady Simple Elongational Flow and Elongational Viscosity

Here we study the type of flow that occurs when a cylindrical filament of fluid is stretched slowly in the absence of external body forces (see Fig. 1B.7). For steady-state simple elongational flow

$$v_z = \dot{\varepsilon} z \quad v_r = -\tfrac{1}{2}\dot{\varepsilon} r \quad v_\theta = 0 \tag{1B.7-1}$$

in which $\dot{\varepsilon}$ is the (constant) elongation rate.

[7] Lord Rayleigh (John William Strutt), *Phil. Mag.*, **21** (6), 697–711 (1911). See also R. B. Bird, W. E. Stewart, and E. N. Lightfoot, *op. cit.*, pp. 124–126.

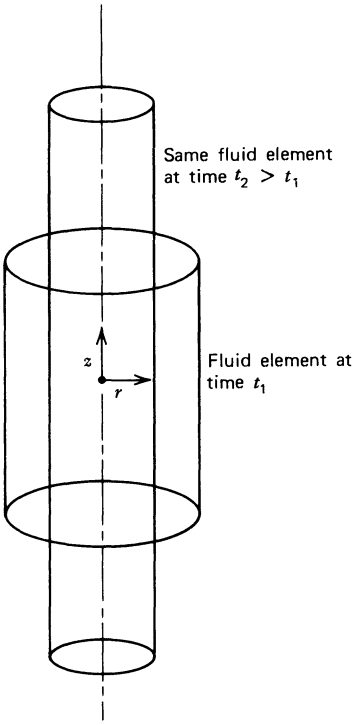

FIGURE 1B.7. Steady simple elongational flow, showing how a cylindrical portion of fluid deforms with time. The velocity components are $v_z = \dot{\varepsilon}z$, $v_r = -\frac{1}{2}\dot{\varepsilon}r$, $v_\theta = 0$, where $\dot{\varepsilon}$ is the (constant) elongation rate.

a. Verify that this velocity distribution satisfies the equation of continuity indentically. Show further that for an incompressible Newtonian fluid in steady simple elongational flow

$$\tau_{rr} = \tau_{\theta\theta} = \dot{\mu}\varepsilon; \quad \tau_{zz} = -2\mu\dot{\varepsilon} \tag{1B.7-2}$$

b. Next use the equation of motion to gain further information about the components of the stress tensor. For steady-state flow with negligible inertial terms ($[\nabla\cdot\rho\boldsymbol{vv}] = \boldsymbol{0}$) and no external forces ($\boldsymbol{g} = \boldsymbol{0}$), show that the components of $\boldsymbol{\pi}$ are constant throughout the fluid, and that specifically $p + \tau_{rr} = p_0$, where p_0 is the ambient pressure outside of the fluid fiber.

c. Show that the results of (**b**) lead to the conclusion that $\pi_{zz} - p_0 = \tau_{zz} - \tau_{rr} = -3\mu(dv_z/dz)$. The coefficient of proportionality between the normal stress difference $\tau_{zz} - \tau_{rr}$ and the negative of the elongation rate is called $\bar{\eta}$, the *elongational viscosity*[8] or *Trouton viscosity*.[9] Thus for Newtonian fluids we have the well-known result that

$$\bar{\eta} = 3\mu \tag{1B.7-3}$$

This result has been used for calculating the shape of a freely falling jet of liquid.[10]

[8] A. S. Lodge, *Elastic Liquids*, Academic Press, New York (1964), pp. 97–98, 114–118; see also §3.5.
[9] F. T. Trouton, *Proc. Roy. Soc.*, **A77**, 426 (1906).
[10] See Problem 1C.5.

1B.8 Alternative Form of the Energy Equation

It is desired to show how the energy equation in terms of the internal energy (Eq. C of Table 1.1-1) can be transformed into the energy equation in terms of the temperature (Eq. C of Table 1.2-1).

a. First show that $(\boldsymbol{\pi}:\nabla\boldsymbol{v}) = p(\nabla\cdot\boldsymbol{v}) + (\boldsymbol{\tau}:\nabla\boldsymbol{v})$ by using Eq. 1.2-1 and the definitions of the ∇-operations.

b. Next replace $\hat{U}$ by $\hat{H} - p\hat{V}$, where $\hat{H}$ is the enthalpy per unit mass. Show that

$$\frac{D}{Dt}p\hat{V} = \frac{p}{\rho}(\nabla\cdot\boldsymbol{v}) + \frac{1}{\rho}\frac{Dp}{Dt} \tag{1B.8-1}$$

by using the equation of continuity (Eq. D of Table 1.1-1). This enables us to rewrite the energy equation as an equation of change for enthalpy:

$$\rho\frac{D\hat{H}}{Dt} = -(\nabla\cdot\boldsymbol{q}) - (\boldsymbol{\tau}:\nabla\boldsymbol{v}) + \frac{Dp}{Dt} \tag{1B.8-2}$$

c. Next we asume that $\hat{H}$ can be expressed in terms of two state variables p and T, so that we can use the thermodynamic relation

$$\begin{aligned} d\hat{H} &= \left(\frac{\partial\hat{H}}{\partial T}\right)_p dT + \left(\frac{\partial\hat{H}}{\partial p}\right)_T dp \\ &= \hat{C}_p\,dT + \left[\hat{V} - T\left(\frac{\partial\hat{V}}{\partial T}\right)_p\right]dp \end{aligned} \tag{1B.8-3}$$

Use of this relation enables us to rewrite Eq. 1B.8-2 as

$$\rho\hat{C}_p\frac{DT}{Dt} = -(\nabla\cdot\boldsymbol{q}) + \left(\frac{\partial\ln\hat{V}}{\partial\ln T}\right)_p\frac{Dp}{Dt} - (\boldsymbol{\tau}:\nabla\boldsymbol{v}) \tag{1B.8-4}$$

Note that up to this point the only assumption that has been made is that $\hat{H}$ depends on only two state variables, and not on the state of strain in the system.

d. When the density is assumed constant, the $(\partial\ln\hat{V}/\partial\ln T)_p$ term in Eq. 1B.8-4 can be omitted. Next show that $(-\boldsymbol{\tau}:\nabla\boldsymbol{v})$ can be written as $+\frac{1}{2}\mu(\dot{\boldsymbol{\gamma}}:\dot{\boldsymbol{\gamma}})$ by using the expression in Eq. 1.2-2 for incompressible fluids. Then, show that introduction of Fourier's law and assumption of constant thermal conductivity leads finally to Eq. C of Table 1.2-1.

1B.9 Low Reynolds Number Flow around a Cylinder[11]

An incompressible Newtonian liquid approaches a cylinder with a constant velocity V in the positive x-direction (see Fig. 1B.9). When the equations of change are solved in the low Reynolds number regime, the following expressions are found for the pressure $p(r, \theta)$ and the fluid velocity $\boldsymbol{v}(r, \theta)$ for the region near the cylinder (they are *not* valid for large r/R):

$$p = p^0 - C\mu\frac{(\boldsymbol{V}\cdot\boldsymbol{r})}{r^2} + \rho(\boldsymbol{g}\cdot\boldsymbol{r}) \tag{1B.9-1}$$

$$\begin{aligned} \boldsymbol{v} = {} & C\boldsymbol{V}\left[\frac{1}{2}\ln\left(\frac{r}{R}\right) + \frac{1}{4} - \frac{1}{4}\left(\frac{R}{r}\right)^2\right] \\ & - C\boldsymbol{r}\frac{(\boldsymbol{V}\cdot\boldsymbol{r})}{2r^2}\left[1 - \left(\frac{R}{r}\right)^2\right] \end{aligned} \tag{1B.9-2}$$

[11] See G. K. Batchelor, *An Introduction to Fluid Dynamics*, Cambridge University Press, Cambridge (1967), pp. 244–246, 261.

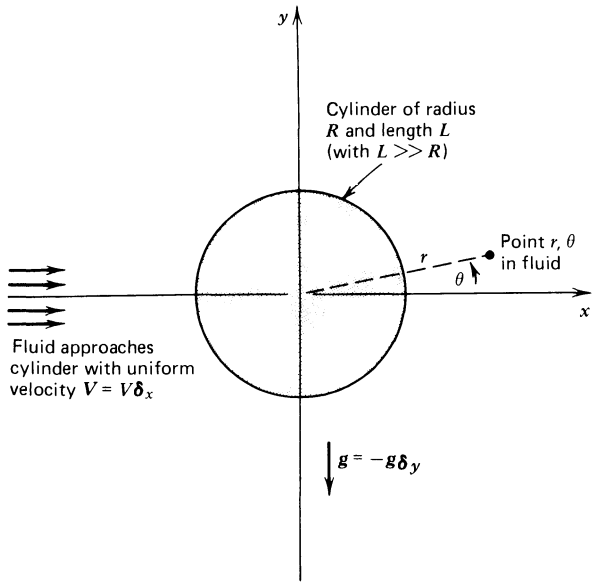

FIGURE 1B.9. Transverse flow around a cylinder, with the fluid approach velocity V and gravitational force $\boldsymbol{g}$.

In these equations the constant C is given by $C = 2/\ln(7.4/\mathrm{Re})$, in which $\mathrm{Re} = 2RV\rho/\mu$ is the Reynolds number.

a. Show that, in the absence of flow, Eq. 1B.9-1 satisfies the equation of motion.

b. Write out $p(r, \theta)$, $v_r(r, \theta)$, and $v_\theta(r, \theta)$ explicitly in terms of the scalars V and g; that is, no vectors should appear in the expressions.

c. Use the results of (**b**) to obtain p, τ_{rr}, and $\tau_{r\theta}$ at $r = R$.

d. Next show that the x-component of the stress exerted by the fluid on the solid cylinder at any point on the surface is $([-\boldsymbol{\delta}_r \cdot \boldsymbol{\pi}] \cdot \boldsymbol{\delta}_x)|_{r=R}$, and that this quantity can be simplified to

$$-p|_{r=R} \cos\theta + \tau_{r\theta}|_{r=R} \sin\theta \tag{1B.9-3}$$

e. Use the results of (**c**) and (**d**) to get the force F_x in the x-direction exerted by the fluid on a length L of the cylinder

$$F_x = 2C\pi L\mu V \tag{1B.9-4}$$

1B.10 Radial Flow between Porous Cylinders

An incompressible Newtonian liquid is made to flow radially (in the $-r$-direction in cylindrical coordinates) from a porous cylinder of radius R to another porous cylinder of radius κR (see Fig. 1B.10).

a. Write down the equations of continuity and motion for the postulates that v_r and $\mathscr{P}$ are functions of r alone.

b. Integrate the equation of continuity to get v_r as a function of r. Determine the constant of integration by writing it in terms of Q, the volume rate of flow through a length L of the outer (or inner) surface.

c. Integrate the equation of motion to get the pressure difference required to maintain a flow rate Q. Express the pressure difference in terms of ρ, μ, Q, κ, R, and L.

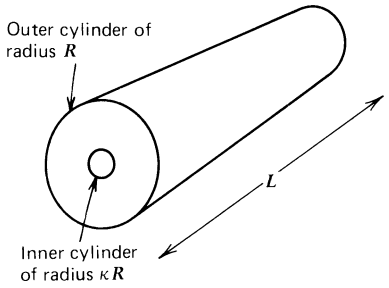

FIGURE 1B.10. Two porous cylinders, with purely radial flow from the outer cylinder to the inner cylinder.

1B.11 Flow into a Thin Slit[12]

A fluid in the region $x \geqslant 0$ flows into the slit in Fig. 1B.11, and then goes down the slit with volume flow rate Q. It is postulated that $v_\theta = 0$, $v_z = 0$, $v_r = v_r(r, \theta)$, and $\mathscr{P} = \mathscr{P}(r, \theta)$. The fluid is Newtonian and incompressible.

a. Show that the equation of continuity leads to

$$v_r = \frac{1}{r} f(\theta) \tag{1B.11-1}$$

where f is a funtion of θ, with $f(\pm \pi/2) = 0$.

b. Next write down the r- and θ-components of the equation of motion in the "creeping-flow limit" (i.e., omit the $\rho Dv/Dt$ term), using the tables in Appendix B.

c. Substitute v_r from (**a**) into the equations in (**b**). Then differentiate the r-component of the equation of motion with respect to θ, and the θ-component with respect to r. Show that this leads to

$$d^3f/d\theta^3 + 4df/d\theta = 0 \tag{1B.11-2}$$

d. Solve the equation in (**c**) to obtain an expression for $f(\theta)$ containing three constants of integration.

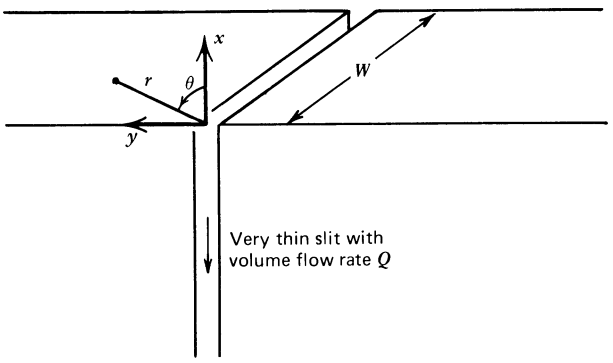

FIGURE 1B.11. A thin slit into which a fluid flows from the region $x \geq 0$. The z-direction is perpendicular to the plane of the paper.

[12] The corresponding viscoelastic problem is discussed in Problem 8C.1.

e. Determine the integration constants by using the two boundary conditions in (**a**) and the fact that the total volume flow rate through a cylindrical surface at any r must be equal Q. This gives finally

$$v_r = -(2Q/\pi Wr)\cos^2\theta \tag{1B.11-3}$$

f. Next obtain $\mathscr{P}(r, \theta)$ from the equations of motion in (**b**)

$$\mathscr{P}(r, \theta) = \mathscr{P}_\infty - \frac{2\mu Q}{\pi W r^2}\cos 2\theta \tag{1B.11-4}$$

What is the meaning of $\mathscr{P}_\infty$?

g. Next verify that the rate-of-deformation tensor is

$$\dot{\gamma} = (2Q/\pi Wr^2)[2(\boldsymbol{\delta}_r\boldsymbol{\delta}_r - \boldsymbol{\delta}_\theta\boldsymbol{\delta}_\theta)\cos^2\theta + (\boldsymbol{\delta}_r\boldsymbol{\delta}_\theta + \boldsymbol{\delta}_\theta\boldsymbol{\delta}_r)\sin 2\theta] \tag{1B.11-5}$$

h. Then obtain the total normal stress on the solid surface at $\theta = \pi/2$:

$$(p + \tau_{\theta\theta})|_{\theta=\pi/2} = p_\infty + (2\mu Q/\pi Wr^2) \tag{1B.11-6}$$

i. What is $\tau_{\theta r}|_{\theta=\pi/2}$? Is this a surprising result?

k. Find the volume rate of flow through the plane $x = 1$ by evaluating the integral $\int(\boldsymbol{n}\cdot\boldsymbol{v})\,dS$ for this surface.

j. Use the expression in Eq. 1B.11-3 to obtain $v_x(x, y)$ and $v_y(x, y)$ for this flow. Then obtain $\partial v_y/\partial x$ for $x = 0$. How does this tie in with (**i**)?

1B.12 Torque on a Rotating Sphere

In Part (**c**) of Example 1.4-3, the torque required for the slow rotation of a sphere in a Newtonian fluid was found. Here we obtain the same result by two different methods.

a. Verify that the velocity distribution in Eq. 1.4-50 can be written in vector form:

$$\boldsymbol{v} = (R/r)^3[\boldsymbol{W}\times\boldsymbol{r}] \tag{1B.12-1}$$

and that for this velocity distribution

$$\nabla\boldsymbol{v} + (\nabla\boldsymbol{v})^\dagger = -\frac{3R^3}{r^5}\{\boldsymbol{r}[\boldsymbol{W}\times\boldsymbol{r}] + [\boldsymbol{W}\times\boldsymbol{r}]\boldsymbol{r}\} \tag{1B.12-2}$$

Next show that the torque exerted by a fluid on any solid body is

$$\mathscr{T} = -\int[[\boldsymbol{n}\cdot\boldsymbol{\pi}]\times\boldsymbol{r}]dS \tag{1B.12-3}$$

where $\boldsymbol{n}$ is the outwardly directed unit normal at the solid surface. Next show that the above results may be used to get for the rotating sphere:

$$\begin{aligned}\mathscr{T} &= 3\mu R^3\int_0^{2\pi}\int_0^{\pi}(\boldsymbol{W} - [\boldsymbol{W}\cdot\boldsymbol{nn}])\sin\theta\,d\theta\,d\phi \\ &= 8\pi\mu R^3\boldsymbol{W}\end{aligned} \tag{1B.12-4}$$

which can be compared with Eq. 1.4-65.

b. The rate of work done on the rotating sphere is $\mathscr{T}W$. This has to be equal to the rate of energy dissipation in the surrounding fluid (in $R \leqslant r < \infty$):

$$\mathscr{T}W = \iiint (-\boldsymbol{\tau} : \nabla \boldsymbol{v}) r^2 \, dr \sin\theta \, d\theta \, d\phi \tag{1B.12-5}$$

Use the velocity distribution in Eq. 1B.12-1 to obtain the torque by doing the integral in Eq. 1B.12-5.

1C.1 Circulating Flow in an Annulus

A rod (radius κR) moves upward with constant velocity V through a cylindrical container (radius R) containing an incompressible viscous fluid. The fluid circulates in the cylinder, moving upward along the moving central core and moving back downward along the fixed wall. It is desired to find the velocity distribution in the annular region, away from the end disturbances (see Fig. 1C.1).

a. First consider the problem when the annular region is quite narrow—that is, κ is just slightly less than unity. In that case the annulus may be approximated by a thin plane slit, and its

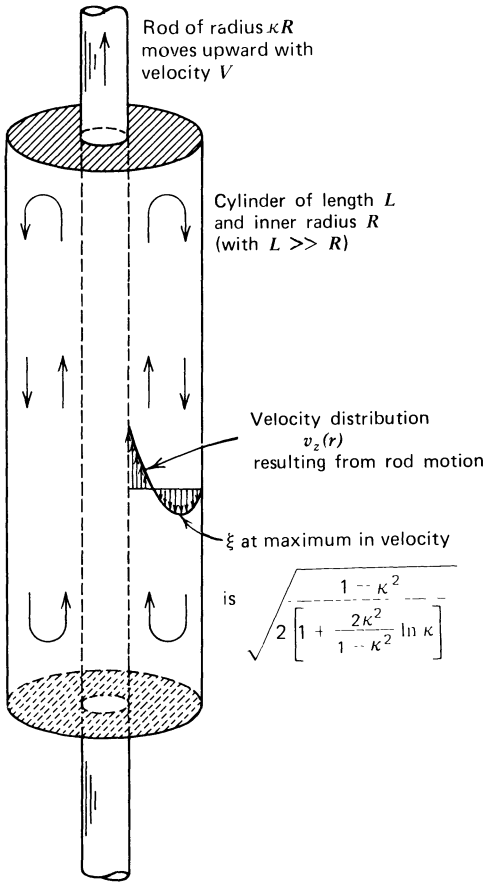

FIGURE 1C.1. Steady-state circulating flow in an annulus with the interior surface moving axially.

curvature can be neglected. Show that in this limit, the velocity distribution is given by

$$\frac{v_z}{V} = 3\zeta^2 - 4\zeta + 1 \tag{1C.1-1}$$

where $\zeta = (\xi - \kappa)/(1 - \kappa)$, and $\xi = r/R$.

b. Next, work the problem without the thin-slit asumption. Show that the velocity distribution is given by:

$$\frac{v_z}{V} = \frac{(1 - \xi^2)[1 - (2\kappa^2/(1 - \kappa^2)) \ln (1/\kappa)] - (1 - \kappa^2) \ln (1/\xi)}{(1 - \kappa^2) - (1 + \kappa^2) \ln (1/\kappa)} \tag{1C.1-2}$$

1C.2 Analysis of a Falling Cylinder Viscometer[13]

A falling cylinder viscometer consists of a long vertical cylinder (radius R) and a cylindrical slug (radius κR and height H) as shown in Fig. 1C.2. The slug is equipped with very thin fins so that its axis is maintained coincident with the axis of the tube.

The rate of descent of the cylindrical slug in the cylinder can be observed when the latter is filled with an incompressible fluid. It is desired to obtain an equation that gives the viscosity of the fluid in terms of the speed of fall V and the various geometric quantities. It is, of course, assumed that the measurement is made when a constant velocity of descent has been attained.

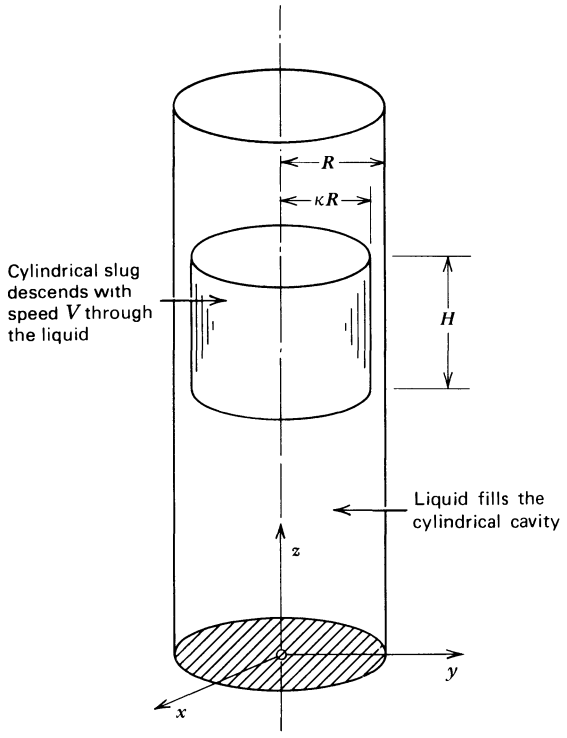

FIGURE 1C.2. Falling-cylinder viscometer, consisting of a tightly fitting cylindrical slug that descends through the liquid, which is forced upwards through the annular space.

[13] J. Lohrenz, G. W. Swift, and F. Kurata, *AIChE J.*, **6**, 547-550 (1960); *ibid.*, 7, 6S (1961); E. Ashare, R. B. Bird, and J. A. Lescarboura, *AIChE J.*, **11**, 910-916 (1965).

a. First show that the velocity distribution in the annular slit is given by

$$\frac{v_z}{V} = \frac{(1 - \xi^2) - (1 + \kappa^2)\ln(1/\xi)}{(1 - \kappa^2) - (1 + \kappa^2)\ln(1/\kappa)} \tag{1C.2-1}$$

in which $\xi = r/R$ is a dimensionless radial coordinate.

b. Make a force balance on the cylindrical slug and obtain finally

$$\mu = \frac{(\rho_0 - \rho)g(\kappa R)^2}{2V}\left(\ln\frac{1}{\kappa} - \frac{1 - \kappa^2}{1 + \kappa^2}\right) \tag{1C.2-2}$$

in which ρ is the density of the fluid and ρ_0 is the density of the slug.

c. Verify that for small slit width the result in (**b**) may be expanded in powers of $\varepsilon = 1 - \kappa$ to give

$$\mu = \frac{(\rho_0 - \rho)gR^2\varepsilon^3}{6V}(1 - \tfrac{1}{2}\varepsilon - \tfrac{13}{20}\varepsilon^2 + \cdots) \tag{1C.2-3}$$

d. Draw a sketch showing the pressure distribution in the system.

e. Which of the two forces—pressure or viscous drag—is primarily responsible for balancing the gravitational force on the slug?

1C.3 Flow Near a Sharp Corner[14]

Consider the two dimensional plane creeping flow of an incompressible Newtonian fluid near a sharp corner. Since the equations for the velocity field are linear we may consider separately the antisymmetrical and symmetrical flow shown in Fig. 1C.3. Assume that the stream function may be expanded as

$$\psi = \sum_{n=1}^{\infty} \mathscr{R}e\{A_n r^{\lambda_n} f_n(\theta)\} \tag{1C.3-1}$$

where the terms are ordered so that

$$1 < \mathscr{R}e\{\lambda_1\} < \mathscr{R}e\{\lambda_2\} < \cdots \tag{1C.3-2}$$

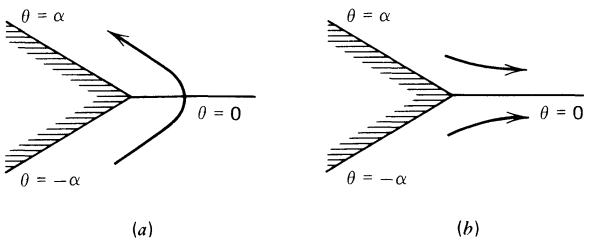

FIGURE 1C.3. Flow near a sharp corner (*a*) Antisymmetrical flow in the region $-\alpha < \theta < \alpha$; (*b*) symmetrical flow in the region $-\alpha < \theta < \alpha$. Note that situation (*b*) is also the flow in the region $0 < \theta < \alpha$ with a solid surface at $\theta = \alpha$ and a free surface at $\theta = 0$.

[14] H. K. Moffatt, *J. Fluid Mech.*, **18**, 1–18 (1964). This reference includes a careful discussion of the infinite sequence of eddies that occurs close to the corner when $2\alpha < 2\alpha_c$ (cf. Table 1C.3). Our interest here is in the flow when $2\alpha > 2\alpha_c$.

TABLE 1C.3

Values of λ_1 in Eqs. 1C.3-6 and 8 Corresponding to Sample Values of 2α.[a]

	Flow	
2α	Antisymmetrical ($2\alpha_c \doteq 146°$)	Symmetrical ($2\alpha_c \doteq 156°$)
$\pi + \varepsilon$	$2 - (2\varepsilon/\pi) + O(\varepsilon^2)$	$3 - (4\varepsilon/\pi) + O(\varepsilon^2)$
$3\pi/2$	1.544...	1.909...
$2\pi + \varepsilon$	$(3/2) + O(\varepsilon^2)$	$(3/2) - (\varepsilon/\pi) + O(\varepsilon^2)$

[a] When $2\alpha < 2\alpha_c$ the λ_1 are complex and the flow consists of a series of eddies.[14] In this table ε is a small, arbitrary number ($\varepsilon \ll 1$).

where $\mathscr{R}e\{z\}$ indicates the real part of the complex number z. Then the flow close to the corner will be dominated by the first nonzero term in the series.

a. Show that the general solution for f_n is

$$f_n = c_1 \cos \lambda_n\theta + c_2 \cos (\lambda_n - 2)\theta + c_3 \sin \lambda_n\theta + c_4 \sin (\lambda_n - 2)\theta \tag{1C.3-3}$$

where the first two terms are associated with antisymmetrical flow and the last two terms with symmetrical flow. In general the c_k are complex.

b. Show that the boundary conditions on f_n are

$$\text{At } \theta = \alpha: \quad f_n = 0; \quad f_n' = 0 \tag{1C.3-4}$$

$$\text{At } \theta = -\alpha: \quad f_n = 0; \quad f_n' = 0 \tag{1C.3-5}$$

c. When $2\alpha > 2\alpha_c$ it can be shown that λ_1 is real; therefore it is permissible to omit the real operator $\mathscr{R}e\{\ \}$ from the first term in Eq. 1C.3-1. Show that the stream function has the following asymptotic behavior near the corner for *antisymmetrical* flow:

$$\psi \sim A_1 r^{\lambda_1}[\cos(\lambda_1 - 2)\alpha \cos \lambda_1\theta - \cos \lambda_1\alpha \cos(\lambda_1 - 2)\theta] \quad (r \to 0) \tag{1C.3-6}$$

where λ_1 is the solution to

$$\sin 2(\lambda_1 - 1)\alpha = -(\lambda_1 - 1) \sin 2\alpha \tag{1C.3-7}$$

subject to the condition in Eq. 1C.3-2. Then for *symmetrical* flow show that

$$\psi \sim A_1 r^{\lambda_1}[\sin((\lambda_1 - 2)\alpha) \sin(\lambda_1\theta) - \sin(\lambda_1\alpha) \sin((\lambda_1 - 2)\theta)] \quad (r \to 0) \tag{1C.3-8}$$

where λ_1 is the solution to

$$\sin 2(\lambda_1 - 1)\alpha = +(\lambda_1 - 1) \sin 2\alpha \tag{1C.3-9}$$

d. Verify sample entries for λ_1 in Table 1C.3 and identify the entries corresponding to (1) simple shear flow, (2) flow around a 90° corner with fixed walls, and (3) flow of a jet from a slit into air with no or little change in cross section.

e. Verify that near the corner ($r \to 0$), for antisymmetrical flow

$$v_r \sim A_1 r^{\lambda_1 - 1}[\lambda_1 \cos(\lambda_1 - 2)\alpha \sin \lambda_1\theta - (\lambda_1 - 2)\cos \lambda_1\alpha \sin(\lambda_1 - 2)\theta] \tag{1C.3-10}$$

$$v_\theta \sim A_1 r^{\lambda_1 - 1}[\lambda_1 \cos(\lambda_1 - 2)\alpha \cos \lambda_1\theta - \lambda_1 \cos \lambda_1\alpha \cos(\lambda_1 - 2)\theta] \tag{1C.3-11}$$

$$p \sim -4\mu A_1 r^{\lambda_1 - 2}(\lambda_1 - 1)\cos \lambda_1\alpha \sin(\lambda_1 - 2)\theta + p_0 \tag{1C.3-12}$$

and for symmetrical flow

$$v_r \sim A_1 r^{\lambda_1 - 1}[-\lambda_1 \sin(\lambda_1 - 2)\alpha \cos \lambda_1\theta + (\lambda_1 - 2)\sin \lambda_1\alpha \cos(\lambda_1 - 2)\theta] \tag{1C.3-13}$$

$$v_\theta \sim A_1 r^{\lambda_1 - 1}[\lambda_1 \sin(\lambda_1 - 2)\alpha \sin \lambda_1\theta - \lambda_1 \sin \lambda_1\alpha \sin(\lambda_1 - 2)\theta] \tag{1C.3-14}$$

$$p \sim 4\mu A_1 r^{\lambda_1 - 2}(\lambda_1 - 1)\sin \lambda_1\alpha \cos(\lambda_1 - 2)\theta + p_0 \tag{1C.3-15}$$

where μ is the viscosity and p_0 is a constant.

f. Finally by substitution into the equation of motion show that the inertial terms are negligible compared to the viscous terms near the corner provided $\mathscr{R}e\{\lambda_1\} > 0$.

1C.4 Journal-Bearing Problem[15]

A journal-bearing system is shown in Fig. 1C.4. The journal of radius r_1 rotates with angular velocity W_1 in a stationary outer bearing of radius r_2. The journal and bearing are of length L in the z-direction, and the eccentric annular gap is completely filled with a Newtonian liquid. The origins of the rectangular and cylindrical coordinate systems are taken to be on the journal axis. The axes of the journal and bearings are separated by a distance a, and the difference in radii, $r_2 - r_1$, is called c, with $c \ll r_1$. It is desired to find the steady-state velocity distribution and pressure distribution in the system. In addition, we wish to know the torque and the force exerted by the fluid on the rotating journal.

a. We assume that the tangential flow in the annular gap can be approximated locally as that in a plane slit with one wall moving and with an imposed pressure gradient (cf. Example 1.3-1). Then at each θ we introduce a local XYZ-coordinate system with X pointing in the flow direction, Y pointing radially, and Z coinciding with z. Thus $Y = r - r_1$, and the surface at $Y = 0$ is moving with the linear velocity $W_1 r_1$, whereas the surface at $Y = B$ is fixed. Show that the local velocity profile will be

$$v_X = W_1 r_1\left(1 - \frac{Y}{B}\right) - \frac{B^2}{2\mu}\frac{dp}{dX}\frac{Y}{B}\left(1 - \frac{Y}{B}\right) \tag{1C.4-1}$$

and that the volume rate of flow will be

$$Q = \tfrac{1}{2}BLW_1 r_1 - \frac{B^3 L}{12\mu}\frac{dp}{dX} \tag{1C.4-2}$$

[15] This problem is patterned very closely after the discussion by A. Sommerfield, *Vorlesungen über Theoretische Physik*, Vol. 2, Dietrich, Wiesbaden (1947), Sect. 36. For a comprehensive theoretical treatment on lubrication see N. Tipei, *Theory of Lubrication*, Stanford University Press, Stanford, CA (1962). For an analytical solution in bipolar coordinates, see G. J. Farns, cited by R. Ehrlich and J. C. Slattery, *Ind. Eng. Chem. Fundam.*, **7**, 239–246 (1968), Appendix B; and G. H. Wannier, *Quart. J. Appl. Math.*, **8**, 1–32 (1950).

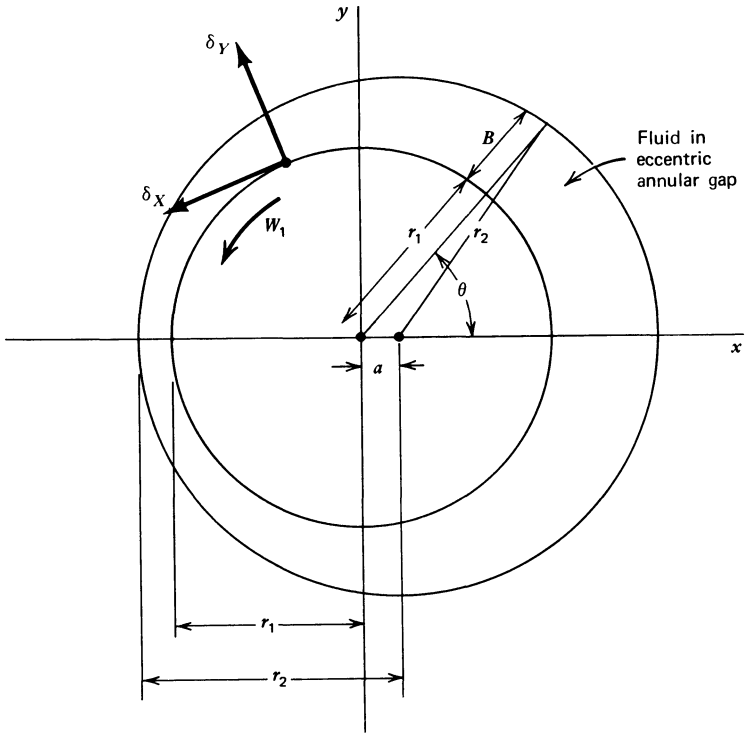

FIGURE 1C.4. Journal-bearing arrangement: cylinder of radius r_1 rotating with angular velocity W_1 in a cylindrical cavity of radius r_2. The gap width $B(\theta)$ is given approximately as $B \doteq c + a\cos\theta$, where $c = r_2 - r_1$.

In the journal-bearing problem we do not know what Q is; it is convenient to replace the unknown constant Q by an unknown constant B_0 defined by $Q = \frac{1}{2}B_0 L W_1 r_1$. Then show that

$$\frac{dp}{dX} = 6\mu W_1 r_1\left(\frac{1}{B^2} - \frac{B_0}{B^3}\right) \tag{1C.4-3}$$

$$v_X = W_1 r_1\left[1 - \left(\frac{4}{B} - \frac{3B_0}{B^2}\right)Y + 3\left(\frac{1}{B^2} - \frac{B_0}{B^3}\right)Y^2\right] \tag{1C.4-4}$$

$$\tau_{YX}\Big|_{Y=0} = -\mu\frac{\partial v_X}{\partial Y}\Big|_{Y=0} = \mu W_1 r_1\left(\frac{4}{B} - \frac{3B_0}{B^2}\right) \tag{1C.4-5}$$

b. Next apply Eqs. 1C.4-3 and 5 to the system in Fig. 1C.4 to obtain

$$\frac{1}{r_1}\frac{dp}{d\theta} = 6\mu W_1 r_1\left(\frac{1}{B^2} - \frac{B_0}{B^3}\right) \tag{1C.4-6}$$

$$\tau_{r\theta}\Big|_{r=r_1} = \mu W_1 r_1\left(\frac{4}{B} - \frac{3B_0}{B^2}\right) \tag{1C.4-7}$$

in which it is understood that $B = B(\theta)$ as described in the figure caption for Fig. 1C.4.

c. Next, in preparation for (**d**), we need to know how to evaluate the following integrals

$$J_n = \int_0^{2\pi} \frac{d\theta}{(c + a\cos\theta)^n} \tag{1C.4-8}$$

$$K_n = \int_0^{2\pi} \frac{\cos\theta\, d\theta}{(c + a\cos\theta)^n} \tag{1C.4-9}$$

Show that

$$J_1 = 2\pi(c^2 - a^2)^{-1/2} \tag{1C.4-10}$$

$$J_2 = -\frac{\partial J_1}{\partial c} = 2\pi c(c^2 - a^2)^{-3/2} \tag{1C.4-11}$$

$$J_3 = -\frac{1}{2}\frac{\partial J_2}{\partial c} = 2\pi(c^2 + \tfrac{1}{2}a^2)(c^2 - a^2)^{-5/2} \tag{1C.4-12}$$

$$J_4 = -\frac{1}{3}\frac{\partial J_3}{\partial c} = 2\pi c(c^2 + \tfrac{3}{2}a^2)(c^2 - a^2)^{-7/2} \tag{1C.4-13}$$

$$K_2 = \left(\frac{1}{a}\right)(J_1 - cJ_2) = -2\pi a(c^2 - a^2)^{-3/2} \tag{1C.4-14}$$

$$K_3 = \left(\frac{1}{a}\right)(J_2 - cJ_3) = -2\pi a(\tfrac{3}{2}c)(c^2 - a^2)^{-5/2} \tag{1C.4-15}$$

$$K_4 = \left(\frac{1}{a}\right)(J_3 - cJ_4) = -2\pi a(2c^2 + \tfrac{1}{2}a^2)(c^2 - a^2)^{-7/2} \tag{1C.4-16}$$

The expressions for J_4 and K_4 are not needed here but are given for completeness inasmuch as they will be needed in Example 6.4-2.

d. Integrate Eq. 1C.4-6 between $\theta = 0$ and $\theta = 2\pi$. Then use the fact that p has to be the same at $\theta = 0$ and $\theta = 2\pi$ in Fig. 1C.4 to obtain

$$B_0 = \frac{J_2}{J_3} = c\frac{c^2 - a^2}{c^2 + \frac{1}{2}a^2} \tag{1C.4-17}$$

e. Now obtain the torque that the fluid exerts on the rotating journal:

$$\begin{aligned}\mathscr{T} &= L\int_0^{2\pi} (-\tau_{r\theta})|_{r=r_1} r_1^2\, d\theta \\ &= -\mu L W_1 r_1^3(4J_1 - 3B_0 J_2) \\ &= -\frac{2\pi\mu L W_1 r_1^3}{\sqrt{c^2 - a^2}}\frac{c^2 + 2a^2}{c^2 + \frac{1}{2}a^2}\end{aligned} \tag{1C.4-18}$$

f. Next we want to get the components of the force that the fluid exerts on the rotating journal. We first consider the force in the positive y-direction:

$$\begin{aligned}F_y &= L\int_0^{2\pi} [-(p + \tau_{rr})\sin\theta - \tau_{r\theta}\cos\theta]|_{r=r_1} r_1\, d\theta \\ &= L\int_0^{2\pi} \left(-\frac{dp}{d\theta} - \tau_{r\theta}\right)\Big|_{r=r_1} \cos\theta\, r_1\, d\theta \\ &= -6\mu L W_1 r_1^3(K_2 - B_0 K_3) + \text{higher-order terms from } \tau_{r\theta} \\ &\doteq -\frac{6\pi\mu L W_1 r_1^3 a}{\sqrt{c^2 - a^2}(c^2 + \frac{1}{2}a^2)}\end{aligned} \tag{1C.4-19}$$

In going from the first to the second line we omit the τ_{rr} contribution, since it is zero. We also perform an integration by parts. In going from the second to the third line, we omit the $\tau_{r\theta}$ contribution, since from Eqs. 1C.4-6, 7, and 17 we see that $dp/d\theta$ is of order $(r_1/c)^2$, whereas $\tau_{r\theta}$ is of order (r_1/c).

Next show that for the force in the positive x-direction:

$$F_x = L\int_0^{2\pi} [-(p + \tau_{rr})\cos\theta + \tau_{r\theta}\sin\theta]|_{r=r_1} r_1\, d\theta = 0 \tag{1C.4-20}$$

Interpret these results.

g. Finally, integrate Eq. 1C.4-6 to obtain the pressure distribution in the system

$$\begin{aligned} p &= p_0 + 6\mu W_1 r_1^2\left[\int \frac{d\theta}{(c + a\cos\theta)^2} - B_0\int \frac{d\theta}{(c + a\cos\theta)^3}\right] \\ &= p_0 + \frac{6\mu W_1 r_1^2 a\sin\theta\,(c + \frac{1}{2}a\cos\theta)}{(c^2 + \frac{1}{2}a^2)(c + a\cos\theta)^2} \end{aligned} \tag{1C.4-21}$$

where p_0 is an arbitary constant pressure. Both integrals can be written as $\int(c + a\cos\theta)^{-1}\,d\theta +$ additional terms, and when the indicated subtraction in [ ] is performed, it is found that the coefficient of $\int(c + a\cos\theta)^{-1}\,d\theta$ is zero so that this integral does not have to be evaluated.

1C.5 Thin Filament Equation for a Vertically Falling Stream of a Newtonian Liquid[16]

A liquid flowing axially in a vertical circular tube with a volume rate of flow Q emerges from the tube and falls downward. Its radius is $R(z)$, where z is the distance downward from the end of the tube. As an approximation we assume that the axial fluid velocity v is a function of z alone, so that the velocity v and the radius of the jet R are related by $Q = \pi[R(z)]^2 v(z)$. We further assume that the radius of the filament changes gradually with axial position, so that $dR/dz \ll 1$.

a. Write a momentum balance over the fixed control volume shown in Fig. 1C.5. Include the effects of surface tension with surface tension σ and the ambient atmospheric pressure p_{atm}. Show then that

$$\rho vv' = -\frac{d}{dz}\pi_{zz} + \frac{2R'}{R}\left(\frac{\sigma}{R} - \pi_{zz}\right) + \rho g + \frac{2R'}{R}p_{atm} \tag{1C.5-1}$$

where $v' = dv/dz$ and $R' = dR/dz$.

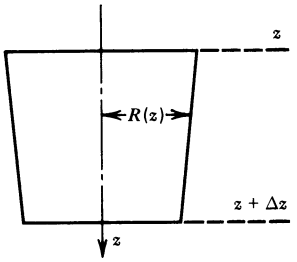

FIGURE 1C.5. Small section of liquid filament of linearly changing radius $R(z)$ within the small distance Δz.

[16] M. A. Matovich and J. R. A. Pearson, *Ind. Eng. Chem. Fundam.*, **8**, 512-520 (1969). See also C. J. S. Petrie, *Elongational Flows*, Pitman, London (1979) for an extensive discussion including bibliography. Numerical solutions of this equation have been reported and compared with data by A. Kaye and D. G. Vale, *Rheol. Acta*, **8**, 1-5 (1969), and R. J. Fisher, M. M. Denn, and R. I. Tanner, *Ind. Eng. Chem. Fundam.*, **19**, 195-197 (1980). See Example 7.4-3.

b. Introduce the boundary condition at the surface of the filament and rewrite Eq. 1C.5-1 as

$$\rho v v' = \left[-\frac{d}{dz}(\tau_{zz} - \tau_{rr}) + \frac{v'}{v}(\tau_{zz} - \tau_{rr}) \right] - \frac{\sigma}{2}\sqrt{\frac{\pi}{Qv}}\, v' + \rho g \tag{1C.5-2}$$

c. Specialize the above "thin filament equation" to Newtonian fluids to obtain

$$\rho v v' = 3\mu[v'' - (v')^2/v] - \frac{\sigma}{2}\sqrt{\frac{\pi}{Qv}}\, v' + \rho g \tag{1C.5-3}$$

d. Show that if all but viscous terms are neglected a general solution to Eq. 1C.5-3 is

$$v = c_1 \exp(-z/c_2) \tag{1C.5-4}$$

e. Show that if all but viscous and gravity terms are neglected, a solution to Eq. 1C.5-3 is:

$$v = (2\rho g/3\mu c_1) \sinh^2[\tfrac{1}{2}c_1^{1/2}(z + c_2)] \tag{1C.5-5}$$

In Eqs. 1C.5-4 and 5 the constants c_1 and c_2 are to be determined from boundary conditions.

1D.1 Oscillatory Flow of a Viscous Fluid

A viscous fluid occupies the region $y > 0$, and is bounded at the plane $y = 0$ by a solid surface that executes an oscillatory motion in the x-direction with a frequency ω and velocity amplitude V. Find the velocity distribution in the system after the initial transients fade away.

It is thus desired to solve the differential equation

$$\frac{\partial v_x}{\partial t} = \nu \frac{\partial^2 v_x}{\partial y^2} \tag{1D.1-1}$$

in which $\nu = \mu/\rho$, with the boundary conditions

$$\text{At } y = 0: \quad v_x = V \cos \omega t = V\, \mathscr{R}e\, \{e^{i\omega t}\} \tag{1D.1-2}$$

$$\text{At } y = \infty: \quad v_x = 0 \tag{1D.1-3}$$

a. Postulate a solution of the form

$$v_x(y, t) = \mathscr{R}e\, \{v^0(y) e^{i\omega t}\} \tag{1D.1-4}$$

in which $v^0(y)$ is in general complex. Show that the substitution of this function into Eq. 1D.1-1 leads to a differential equation for $v^0(y)$

$$\frac{d^2 v^0}{dy^2} - \left(\frac{i\omega}{\nu}\right) v^0 = 0 \tag{1D.1-5}$$

b. Show that this equation can be solved with the appropriate boundary conditions to give

$$v^0(y) = V e^{-(1+i)\sqrt{\omega/2\nu}\, y} \tag{1D.1-6}$$

c. Show that substitution of this result into Eq. 1D.1-4 gives for the velocity distribution

$$v_x(y, t) = Ve^{-\sqrt{\omega/2\nu}y} \cos(\omega t - \sqrt{\omega/2\nu}y) \tag{1D.1-7}$$

Sketch the result.

d. Rework the problem if the fluid, instead of extending to $y = \infty$, is bounded[17] by a fixed plane at $y = B$. Show that the velocity profiles will be very nearly linear if $\sqrt{\rho\omega/2\mu}\, B \ll 1$.

1D.2 Viscous Heating in Oscillatory Flow[18]

A Newtonian fluid of viscosity μ and thermal conductivity k is located in the region between two parallel plates separated by a distance b. Both plates are maintained at a temperature T_0. The lower plate (at $x = 0$) is made to oscillate sinusoidally in the z-direction with a velocity amplitude V and a frequency ω. The upper plate (at $x = b$) is held fixed. Estimate the temperature rise that results from viscous heating. Consider the high-frequency limit only.

Answer: $T - T_0 = (\mu V^2/4k)[(1 - e^{-2a\xi}) - (1 - e^{-2a})\xi]$
where $\xi = x/b$ and $a = b\sqrt{\rho\omega/2\mu}$

[17] See, for example, H. Schlichting, *Boundary-Layer Theory*, 4th ed., McGraw-Hill, New York (1960), p. 76.

[18] R. B. Bird, Chem. Eng. Prog., Symposium Series Number 58, **61**, 1-15 (1965); see Illustrative Example 1.

CHAPTER 2

FLOW PHENOMENA IN POLYMERIC LIQUIDS

A fluid that's macromolecular
Is really quite weird—in particular
The big normal stresses
The fluid posseses
Give rise to effects quite spectacular.

The purpose of this chapter is to demonstrate the striking qualitative difference between the behavior of Newtonian liquids and polymeric liquids. An appreciation of the qualitative behavior of polymeric liquids is important as background information for the quantitative treatments to follow in the remainder of the volumes.[1]

We begin the chapter with a brief review of the chemical constitution of polymeric liquids. It is of course this chemical composition that is responsible for the flow behavior of polymeric liquids. The treatment here is intended just to give the reader a minimum of understanding of the fluids encountered in later chapters and to provide a qualitative appreciation of the structural factors responsible for the flow properties of polymeric liquids. After this introductory section follows a sequence of six sections in which we compare and contrast the flow of polymeric liquids with Newtonian liquids. Some of the experiments presented have the character of "fun experiments." It is important to emphasize that they do not represent anomalous behavior shown by a few "strange" fluids, but are rather typical for fluids containing very large molecules. The classification of the experiments in six separate sections is to a large extent arbitrary and is done primarily for convenience. Indeed for any one polymeric liquid the behavior in the different experiments is of course related, since it is given by the underlying fundamental constitutive equation of the liquid. This connection will be explained in later chapters and some of the experiments presented here will then serve as useful reference experiments. It is also important to emphasize that the list of qualitative experiments is not intended to be exhaustive. Many other interesting flow phenomena have been observed, and still more remain to be discovered. In the final section we will briefly discuss the role of dimensionless groups in the fluid dynamics of polymeric liquids.

[1] Two interesting movies are available in which these differences are illustrated particularly well: H. Markovitz, *Rheological Behavior of Fluids*, Education Services, Inc., Watertown, MA (1965); and K. Walters and J. M. Broadbent, *Non-Newtonian Fluids*, Department of Applied Mathematics, University College of Wales, Aberystwyth, UK (1980) (the latter is available both as film and as videotape).

Polymeric fluids are sometimes called *viscoelastic fluids*. This means that the fluids have both viscous and "elastic" properties. The use of the word "elastic" to characterize a property of a fluid may seem a bit contradictory. By "elasticity" one usually means the ability of a material to return to some unique, original shape; on the other hand, by a "fluid" one means a material that will take the shape of any container in which it is left, and therefore does not possess a unique, original shape. Despite this apparent contradiction we will in this chapter show several flow situations in which polymeric fluids exhibit properties that one would describe as "elastic". In this chapter we shall use the word "elastic" to describe loosely effects associated with nonlinear or time-dependent properties of the constitutive equation, other than those associated with the non-Newtonian viscosity to be described in §2.2. Another concept that is closely tied to that of elasticity is the concept of "memory". Indeed a material that has no memory cannot be elastic, since it has no way of remembering a unique, original shape. Hence fluids exhibiting elastic properties are also often referred to as *memory fluids*.

§2.1 THE CHEMICAL NATURE OF POLYMERIC LIQUIDS[1]

A *macromolecule* (or *polymer*)[2] is a large molecule composed of many small simple chemical units, generally called *structural units*. In some polymers each structural unit is connected to precisely two other structural units, and the resulting chain structure is called a *linear* macromolecule. In other polymers most structural units are connected to two other units, although some structural units connect three or more units, and we talk of *branched* molecules. Where the chains terminate, special units called *end groups* are found. Figure 2.1-1 shows symbolic representations of linear and branched macromolecules. For the sake of completeness we mention also that in some macromolecular materials all structural units are interconnected resulting in a three-dimensional *cross-linked* or *network structure* rather than in separate molecules. Such materials, however, generally possess no fluid phase and are therefore outside the scope of this book.

It is sometimes useful to distinguish between synthetic and natural (biological) macromolecules. Many synthetic polymers are built from a single structural unit, and the polymer is then referred to as a *homopolymer*. Typical examples of synthetic homopolymers are polyethylene, polystyrene, and polyvinylchloride (see Table 2.1-1). In contrast *copolymers* are built from two or more different structural units. According to the manner in which the structural units combine, copolymers are further classified as random copolymers, block copolymers, or graft copolymers, as illustrated in Fig. 2.1-2. The motivation for producing copolymers is to obtain materials with a wider range of mechanical properties than is possible with the homopolymers alone.

Biological macromolecules, in contrast with synthetic macromolecules, generally contain a large number of different structural units. The polypeptide chains that make up proteins, for instance, consist of about 20 different structural units. Among other examples of biological macromolecules are the viruses and the interesting DNA molecules that carry

[1] Much more comprehensive treatments of the chemistry of macromolecules may be found in many standard references such as F. W. Billmeyer, Jr., *Textbook of Polymer Science*, 3rd ed., Wiley, New York (1984); P. J. Flory, *Principles of Polymer Chemistry*, Cornell University Press, Ithaca, NY (1953); and C. Tanford, *Physical Chemistry of Macromolecules*, Wiley, New York (1961).

[2] Some scientists are careful to distinguish between macromolecules (very large molecules) and polymers (macromolecules made up of repeating structural units). This fine distinction seems to be generally ignored, and we shall use the two terms synonymously in this book.

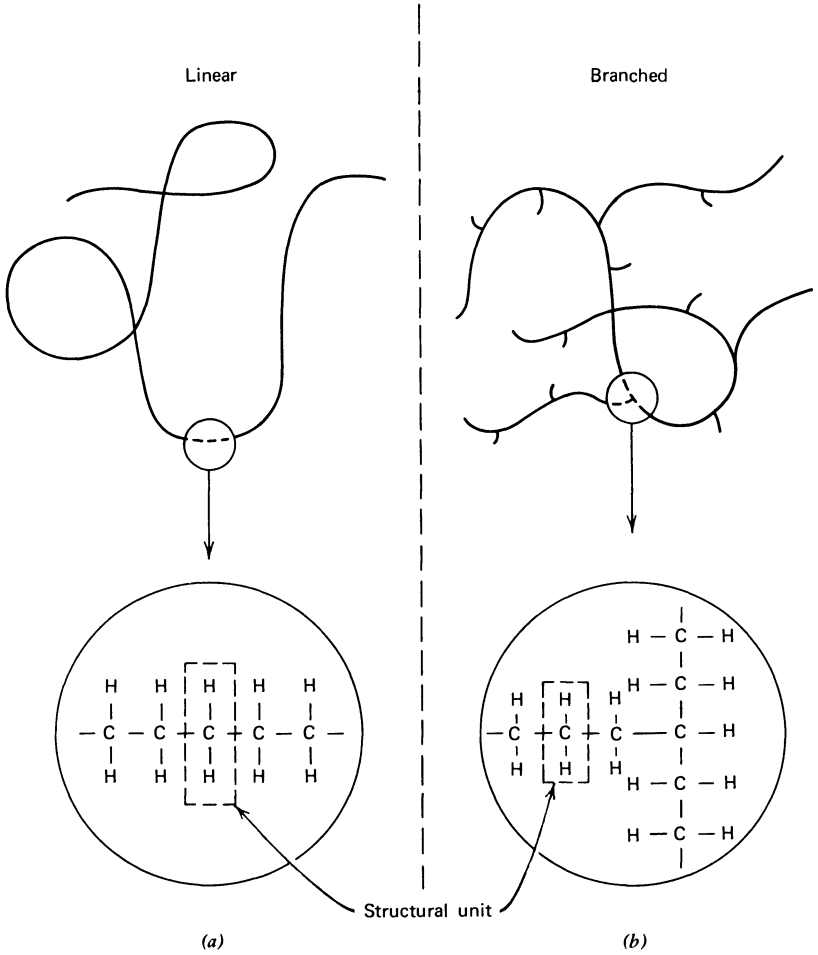

FIGURE 2.1-1. Symbolic representations of linear and branched macromolecules (high-density polyethylene and low-density polyethylene, respectively): (*a*) Linear, (*b*) branched.

in their structure the key to the inherited characteristics of organisms. More on biological polymers can be found elsewhere.[3]

Aside from unimportant corrections from end groups and branch points, the molecular weight of a macromolecule is the product of the molecular weight of a structural unit and the number of structural units in the molecule. Typical synthetic polymer molecules may have molecular weights between 10,000 and 1,000,000 g/mol. Biological macromolecules may have even larger molecular weights; for example, the molecular weight of tobacco mosaic virus is about 40,000,000 g/mol.

Naturally one can conceive of a polymer sample in which the molecular weight of all macromolecules is the same. Such a sample is called *monodisperse*. Indeed, some biological polymers are monodisperse. Synthetic monodisperse or "almost monodisperse"

[3] See, for example, C. Tanford, *Physical Chemistry of Macromolecules*, Wiley, New York (1961); H. Morawetz, *Macromolecules in Solution*, Vol. 21, High Polymers Series, Wiley, New York (1975); T. E. Creighton, *Proteins: Structures and Molecular Principles*, Freeman, New York (1983); J. King, *Protein and Nucleic Acid Structure and Dynamics*, Benjamin-Cummings, Menlo Park, CA (1985).

TABLE 2.1-1

Some Synthetic Polymers, Their Monomers and Their Structural Units

Polymer	Monomer(s)	Structural Unit
Polyethylene	$CH_2=CH_2$	$-CH_2-$
Polyvinylchloride	$CH_2=CHCl$	$-CH_2-CHCl-$
Polystyrene	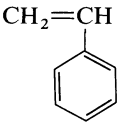	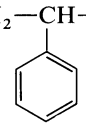
Polyacrylamide	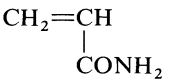	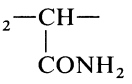
Polyisobutylene	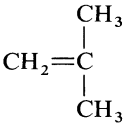	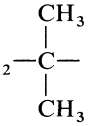
Polyisoprene (natural rubber)	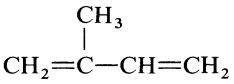	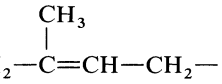
Polydimethylsiloxane	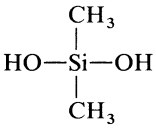	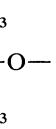
Polyethyleneoxide (Polyox)	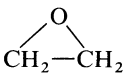	$-O-CH_2-CH_2-$
Polyhexamethylene adipamide (Nylon 66)	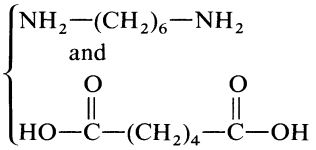	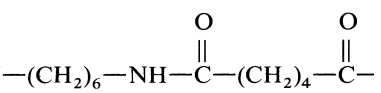
Polyethylene terephthalate (polyester)	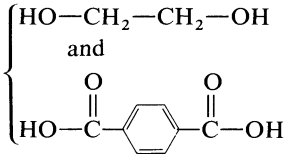	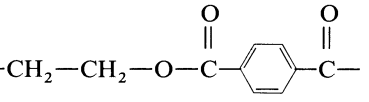

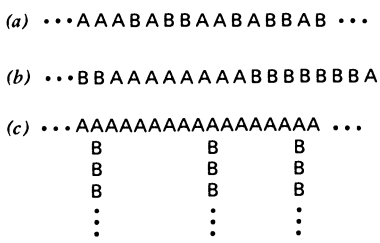

FIGURE 2.1-2. Schematic representations of (*a*) random, (*b*) block, and (*c*) graft copolymers. A and B represent two different kinds of structural units.

polymers may be prepared by special techniques, but are seldom used commercially. Most commercial polymers by contrast are *polydisperse*, that is, they contain molecules of many different molecular weights. Thus we may talk of a distribution of molecular weights.

In order to describe molecular weight distributions in simple quantitative terms, we introduce various molecular weight averages. Let us assume that we are given a polydisperse macromolecular sample, composed of a number of monodisperse fractions. Specifically let us say that fraction "1" contains N_1 moles of molecular weight M_1, fraction "2" contains N_2 moles of molecular weight M_2 and so forth. We may introduce an average molecular weight by multiplying the molecular weight of each fraction by the number of moles in that fraction, summing and dividing by the total number of moles,

$$\bar{M}_n = \frac{\sum_i N_i M_i}{\sum_i N_i} \tag{2.1-1}$$

This is called the *number-average molecular weight*; it is particularly sensitive to additions of small amounts of low molecular weight fractions. Since the mass of the ith fraction w_i is $w_i = N_i M_i$, we may alternatively form an average by weighting the M_i with respect to the mass of the fractions,

$$\bar{M}_w = \frac{\sum_i w_i M_i}{\sum_i w_i} = \frac{\sum_i N_i M_i^2}{\sum_i N_i M_i} \tag{2.1-2}$$

This average is called the *weight-average molecular weight*; it is more sensitive to the high molecular weight fractions than is $\bar{M}_n$. One may define further molecular weight averages by taking ratios of higher moments of the molecular weight distribution

$$\bar{M}_{z+j} = \frac{\sum_i N_i M_i^{3+j}}{\sum_i N_i M_i^{2+j}} \tag{2.1-3}$$

When $j = 0$ this defines the *z-average molecular weight*, and for $j > 0$ this defines the *$z + j$-average molecular weight*. For monodisperse samples all these averages are equal, but for polydisperse samples $\bar{M}_n < \bar{M}_w < \bar{M}_z < \bar{M}_{z+1}$ etc. The ratio $\bar{M}_w/\bar{M}_n$, known as the *heterogeneity index*, is often taken as a simple measure of the polydispersity of a sample (Problem 2B.1). In addition to the average molecular weights defined above, there is also the *viscosity-average molecular weight* $\bar{M}_v$ defined in Eq. 3.6-14. The average $\bar{M}_v$ lies between $\bar{M}_n$ and $\bar{M}_w$.

The chemical formulas in Table 2.1-1 serve as a useful symbolic notation for the chemist, but they do not convey any information about the extent to which the molecules

are able to change their configurations. In fact most polymers are capable of assuming a huge number of configurations by rotations around chemical bonds. Furthermore the molecules will be continually changing their configurations due to thermal motions. Such configurational changes may be either local rearrangements of the backbone or there may be large overall changes in configuration. There is consequently an entire spectrum of time constants associated with the rates at which such thermally induced configurational changes take place. We call these the *time constants for the fluid*, and we say that the fluid has a *spectrum of relaxation times*. It is these time constants that give polymeric fluids at least a partial memory. Since polymeric fluids are not chemically cross-linked they will not have a permanent memory, but there will be a finite longest relaxation time. We say that the relaxation spectrum gives the fluids a *fading memory* of duration of the longest relaxation time. It is shown in §2.8 that when the longest relaxation time is equal to or greater than the characteristic time for the macroscopic flow system, marked deviations from Newtonian behavior are observed.

In closing we add that polymers are not the only liquids that exhibit departure from Newtonian behavior. For example, detergent solutions or fine clay suspensions will form large-scale structures due to hydrogen bonding, dipole interaction, and other intermolecular forces. The time constants for the rearrangement of these structures are comparable to typical times of flow and as a result such fluids are also non-Newtonian.[4]

§2.2 NON-NEWTONIAN VISCOSITY

Probably the single most important characteristic of polymeric liquids is the fact that they have a "shear-rate dependent" or "non-Newtonian" viscosity. A quantitative definition of this property is postponed until §3.3, but a simple qualitative experiment can be performed that illustrates the property. In this first experiment, we consider two identical, vertical tubes, the bottoms of which are covered by a flat plate. The two tubes are filled with fluids, one Newtonian and the other polymeric, chosen in such a way as to have the same viscosity in an experiment involving very low shear rates. This criterion is satisfied, for example, if two identical small spheres fall through each sample at the same rate[1] (Fig. 2.2-1*a*). In addition the density of the sphere should be much larger than the densities of the fluids, so that the difference in density of the fluids may be neglected. A particularly good Newtonian liquid to use is an aqueous glycerin solution. By varying the glycerin concentration, the viscosity of the mixture can be varied from 0.001002 to 1.490 Pa·s at 293 K. In Fig. 2.1-1*b* we see that when the plate is removed from the bottoms of the tubes and the fluids are allowed to flow out by gravity, the polymeric fluid drains much more quickly than the Newtonian fluid.

We know that if both fluids were Newtonian,[1] then the fact that the two spheres drop at the same rate in experiment (*a*) would mean that the fluids have the same viscosity. This in turn means that the fluids would drain at the same rate in experiment (*b*). We might then explain the results in Fig. 2.2-1 by saying that the polymer liquid has a lower viscosity in the high shear rate part of experiment (*b*) than in experiment (*a*). The decrease in viscosity with increasing shear rate is referred to as "shear thinning," and the fluid is said to be *shear thinning* or *pseudoplastic*. This effect can be quite dramatic, with the viscosity decreasing by a factor of as much as 10^3 or 10^4. Examples of pseudoplastic fluids are molten polyethylene

[4] See W. B. Russel, W. R. Schowalter, and D. A. Saville, *Colloidal Dispersions*, Cambridge University Press (1987).

[1] For Newtonian fluids, the flow around a translating sphere is analyzed in Example 1.4-1, and flow in a circular tube is analyzed in Example 1.3-2.

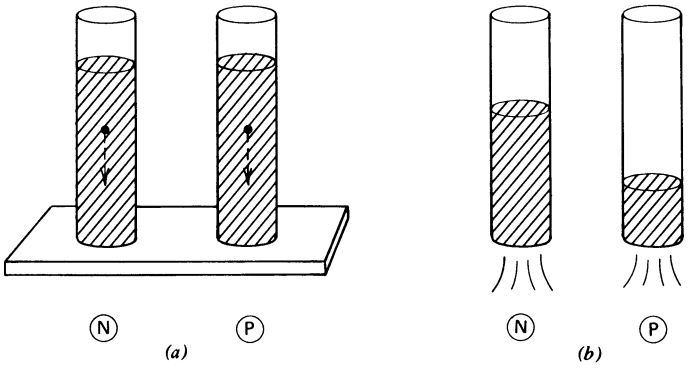

FIGURE 2.2-1. Tube flow and "shear thinning." In each part, the Newtonian behavior is shown on the left Ⓝ; the behavior of a polymer on the right Ⓟ. (*a*) A tiny sphere falls at the same rate through each; (*b*) the polymer flows out faster than the Newtonian fluid.

and polypropylene, and solutions of carboxymethylcellulose (CMC) in water, polyacrylamide in water and glycerin, and aluminum laurate in decalin and *m*-cresol. In fact almost all polymer solutions and melts that exhibit a shear-rate dependent viscosity are shear thinning.

A few fluids behave oppositely to what we have shown here, that is, they flow out of the tube in Fig. 2.2-1*b* more slowly than the corresponding Newtonian liquid. A fluid whose viscosity increases with shear rate is called *shear thickening* or *dilatant.*[2,3] This behavior is exhibited by fairly concentrated suspensions of very small particles; two reported examples are suspensions of titanium dioxide in a sucrose solution[4] and corn starch in an ethylene-glycol–water mixture.[5] As far as we know, relatively few polymer solutions have been shown to be dilatant.

Still different behavior is shown by fluids that will not flow unless acted on by at least some critical shear stress, called the *yield stress.* We call these *viscoplastic fluids.* Certain types of paints, greases, and pastes are examples of viscoplastic fluids. Carboxypolymethylene (pH 7) in water has also been reported to be viscoplastic.[6] Although the concept of yield stress has been very useful, its existence has been challenged[7] on the ground that all materials will flow provided that one waits long enough. For example, a paint film applied on a vertical wall will certainly flow, but for a good paint this process is slower than solvent evaporation and possibly chemical changes. Then the yield stress becomes a useful model property to describe the shear stress below which the flow of the paint becomes negligible. More will be said about the details of the dependence of viscosity on shear rate in the next chapter, where we discuss its measurement in polymeric fluids.

[2] A review of dilatant behavior is given by W. H. Bauer and E. A. Collins in F. R. Eirich, ed., *Rheology*, Vol. 4, Academic Press, New York (1967), Chapt. 8, pp. 423–459. See especially their Appendix II, p. 459, which contains a listing of dilatant systems.

[3] M. Reiner, *Deformation, Strain and Flow*, Interscience, New York (1960), pp. 306–309, and others use the term "dilatancy" to describe the change in volume of granular masses necessitated by a distortion. The standard example is the apparent drying of wet sand when stepped on.

[4] A. B. Metzner and M. Whitlock, *Trans. Soc. Rheol.*, **2**, 239–254 (1958).

[5] R. G. Green and R. G. Griskey, *Trans. Soc. Rheol.*, **12**, 13–25 (1968).

[6] A. G. Fredrickson, *Principles and Applications of Rheology*, Prentice-Hall, Englewood Cliffs, NJ (1964), p. 178; R. B. Bird, G. Dai, and B. J. Yarusso, *Revs. Chem. Engr.*, **1**, 1–70 (1982).

[7] H. A. Barnes and K. Walters, *Rheol. Acta*, **24**, 323–326 (1985).

§2.3 NORMAL STRESS EFFECTS

A number of important effects in the flow of polymeric liquids may be attributed to the fact that polymeric liquids exhibit normal stress differences in "shear flows" such as the flow in Fig. 1.3-1. Let us first establish some labeling conventions for referring to normal stress differences. If the fluid moves along one coordinate direction only and its velocity varies only in one other coordinate direction, then we call the direction of fluid velocity the "1" direction; the direction of velocity variation, the "2" direction; and the remaining neutral direction, the "3" direction. Then we call $\tau_{11} - \tau_{22}$ the *first normal stress difference.* Likewise, we call $\tau_{22} - \tau_{33}$ the *second normal stress difference.* In Fig. 1.3-1 the x, y, and z correspond to 1, 2, and 3 respectively. Thus the first normal stress difference is $\tau_{xx} - \tau_{yy}$ and the second normal stress difference is $\tau_{yy} - \tau_{zz}$. For Newtonian fluids the normal stress differences are exactly zero in shearing flow.

For polymeric fluids the first normal stress difference is practically always negative and numerically much larger than the second normal stress difference. This means that to a first approximation polymeric fluids exhibit in addition to the shear stresses an extra tension along the streamlines, that is, in the "1" direction. It was shown by Weissenberg[1] that the simple notion of an extra tension along streamlines may be used to obtain qualitative explanations of a large number of experiments. In terms of chemical structure, the extra tension along the streamlines in polymeric fluids arises from the stretching and alignment of the polymer molecules along the streamlines. The thermal motions make the polymer molecules act as small "rubber bands" wanting to snap back, and it is in this way that the extra tension arises. Thus there is also a structural background for Weissenberg's fundamental proposition, and we shall use it extensively in this and following sections.

The second normal stress difference has been found experimentally to be positive, but usually much smaller than the magnitude of the first normal stress difference. This means that in a shear flow the fluid exhibits a small extra tension in the "3" direction. A simple structural explanation for this extra tension is lacking, and the simplest kinetic theories of polymeric fluids are not capable of describing this effect; more elaborate theories are successful, however. We emphasize that the second normal stress difference is quite small, and it is normally observable only in situations where the first normal stress difference, for geometrical reasons, has no effect.

We now consider several experiments that enable us to see how normal stress effects manifest themselves.

a. Rod-Climbing

In this experiment we insert rotating rods into two beakers, one containing a Newtonian liquid and the other a polymer solution. In Fig. 2.3-1 we see that the Newtonian liquid near the rotating rod is pushed outward by the centrifugal force, and a dip in the liquid surface near the center of the beaker results. This is typical of the flow near the rotating shaft of a stirrer. The contrasting behavior of the polymer solution is striking. The polymer solution moves in the opposite direction, toward the center of the beaker and climbs up the rod. Moreover, for comparable rotational speeds, the response of the polymer solution can be far more dramatic than that of the Newtonian liquid, as seen in Fig. 2.3-1.

[1] K. Weissenberg, *Nature*, **159**, 310–311 (1947). In this pioneering analysis Weissenberg further proposed that the second normal stress difference should be precisely zero. This additional proposition has become known as the "Weissenberg hypothesis" and is now known not to be correct, albeit a good first approximation for some problems.

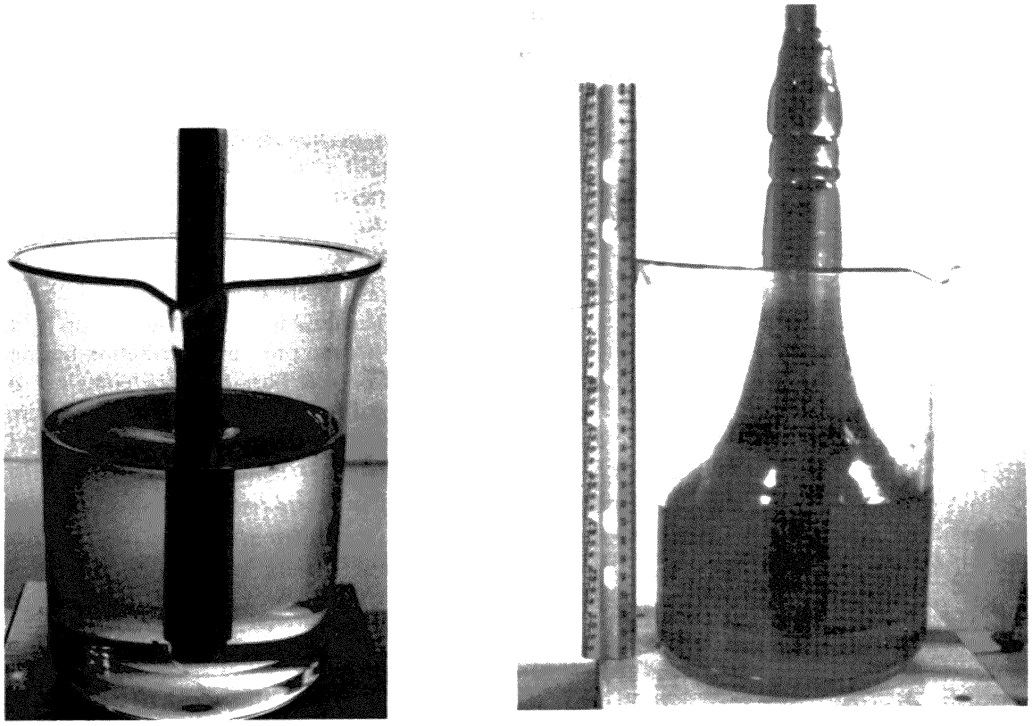

Ⓝ Ⓟ

FIGURE 2.3-1. Fixed cylinder with rotating rod. Ⓝ The Newtonian liquid, glycerin, shows a vortex; Ⓟ the polymer solution, polyacrylamide in glycerin, climbs the rod. The rod is rotated much faster in the glycerin than in the polyacrylamide solution. At comparable low rates of rotation of the shaft, the polymer will climb whereas the free surface of the Newtonian liquid will remain flat. [Photographs courtesy of Dr. F. Nazem, Rheology Research Center, University of Wisconsin-Madison.]

This phenomenon was first described by Garner and Nissan[2] and by Russel[3] but seems to have been known in the paint industry prior to its description in the scientific literature. The phenomenon may be interpreted in a rather simple fashion with the use of the notion[1] of an extra tension along the streamlines. In the rod-climbing experiment the streamlines are closed circles and the extra tension along these lines "strangulates" the fluid and forces it inwards against the centrifugal force and upwards against the gravitational force.

The above simple argument takes no account of the second normal stress difference. In Example 2.3-1 we present an analysis of the experiment based on the equations of motion, which shows that both normal stress differences actually contribute to the effect.

Finally we mention the interesting *Quelleffect*[4]. If instead of having a rotating rod in

[2] F. H. Garner and A. H. Nissan, *Nature*, **158**, 634–635 (1946).

[3] R. J. Russel, Ph.D. Thesis, Imperial College, University of London (1946) (unpublished), p. 58.

[4] K. Kirschke, *Polymères et Lubrification*, Colloques Internationaux du CNRS, No. 233, Éditions du CNRS, Paris (1974), pp. 137–144; G. Böhme, *Strömungsmechanik nicht-Newtonscher Fluide*, Teubner, Stuttgart (1981), pp. 127–128; G. R. Böhme and W. Warnecke, *Rheol. Acta*, **24**, 22–34 (1985).

the cylindrical container one rotates the bottom of the cylinder around its axis one obtains a bulge in the free surface around the axis. We expect that the extra tension along the streamlines is responsible also for this effect, which one may think of as "rod-climbing without a rod."

EXAMPLE 2.3-1 Interpretation of Free Surface Shapes in the Rod-Climbing Experiment[5]

Consider a fluid contained in the annular region between two vertical coaxial cylinders where the inner cylinder is rotating with a constant angular velocity. The fluid is bounded at the top by a "lubricated lid" that keeps the top surface flat by supporting a normal pressure distribution but no shear stress. Also the container is so deep that the influence from the bottom of the container is negligible near the lid. Use the equations of change to analyze the distribution of the normal pressure exerted by the fluid on the lubricated lid. Then by means of a simple argument explain what would cause the fluid to climb the rotating rod if the lubricated lid were replaced by a free surface. *Note*: In this experiment $1 = \theta$, $2 = r$, $3 = z$.

SOLUTION We begin by introducing a cylindrical coordinate system with z-axis coincident with the cylinder axis. Away from the bottom the only nonzero component of velocity is then v_θ. Furthermore this velocity component as well as the stress components and the pressure will be functions of r only. Hence the r- and θ-components of the equation of motion may be written, respectively,

Motion (r):
$$-\rho\frac{v_\theta^2}{r} = -\frac{1}{r}\frac{d}{dr}(r\tau_{rr}) + \frac{\tau_{\theta\theta}}{r} - \frac{dp}{dr} \tag{2.3-1}$$

Motion (θ):
$$0 = -\frac{1}{r^2}\frac{d}{dr}(r^2\tau_{r\theta}) \tag{2.3-2}$$

The normal pressure exerted on the lubricated lid is given by $p + \tau_{zz}$. An expression for the derivative of this quantity may be obtained by adding and subtracting $d\tau_{zz}/dr$ on the right side of Eq. 2.3-1, which may then be rearranged to:

$$\frac{d}{dr}(\tau_{zz} + p) = \frac{d}{dr}(\tau_{zz} - \tau_{rr}) + \frac{\tau_{\theta\theta} - \tau_{rr}}{r} + \rho\frac{v_\theta^2}{r} \tag{2.3-3}$$

We now wish to reformulate the first term on the right side of this equation so that a derivative $(d/d\tau_{r\theta})$ appears in place of (d/dr). To do this, note from Eq. 2.3-2 that

$$\frac{d\tau_{r\theta}}{dr} = -\frac{2}{r}\tau_{r\theta} \tag{2.3-4}$$

Then Eq. 2.3-3 may be formulated as

$$\begin{aligned}\frac{d(\tau_{zz} + p)}{d\ln r} &= 2\tau_{r\theta}\frac{d}{d\tau_{r\theta}}(\tau_{rr} - \tau_{zz}) + (\tau_{\theta\theta} - \tau_{rr}) + \rho v_\theta^2 \\ &= 2\tau_{21}\frac{d}{d\tau_{21}}(\tau_{22} - \tau_{33}) + (\tau_{11} - \tau_{22}) + \rho v_1^2\end{aligned} \tag{2.3-5}$$

[5] A. S. Lodge, *Elastic Liquids*, Academic Press, New York (1964), pp. 192-194; D. D. Joseph and R. L. Fosdick, *Arch. Rat. Mech. Anal.*, **49**, 321-401 (1973); D. D. Joseph, G. S. Beavers, A. Cers, C. Dewald, A. Hoger, and P. T. Than, *J. Rheol.*, **28**, 325 345 (1984).

In the second line on the right side, θ, r and z have been replaced by 1, 2 and 3 respectively. This has been done in agreement with the convention introduced at the beginning of this section with the assumption that the flow is locally a shearing flow.

For Newtonian fluids the first and second normal stress differences, $\tau_{11} - \tau_{22}$ and $\tau_{22} - \tau_{33}$, are both zero in shear flow, and Eq. 2.3-5 shows that the normal pressure exerted on the lubricated lid increases with the radius. Thus if the lid were removed we would expect that the fluid would rise near the cylinder wall and dip near the rod.

For polymeric fluids we have already indicated that $\tau_{11} - \tau_{22}$ is practically always negative with a numerical value much larger than that of $\tau_{22} - \tau_{33}$. We see that the normal stresses may cause the total normal pressure to decrease in the radial direction, and this is then consistent with the rod-climbing effect.

b. Convex Surface in a Tilted Trough

In this experiment we consider the low Reynolds number flow down an open, slightly inclined channel. The flow is driven by gravity and we observe the shape of the free surface of the fluid as shown in Fig. 2.3-2. The Newtonian fluid is seen to have a flat free surface, aside from the meniscus effect, whereas that of a typical non-Newtonian substance is slightly convex. The effect is small but reproducible. The experiment was first performed by Tanner[6] following a suggestion by Wineman and Pipkin.[7] *Note*: In this flow $1 = z$, $2 = x$, $3 = y$ (see Fig. 2.3-3).

This effect may be explained qualitatively by noting that there will be an extra tension in the y-direction. This tension will be the greatest near the vertical walls of the channel, since the velocity gradient dv_z/dx has its maximum value at the walls. Therefore the surface of the fluid will be "pulled down" near the walls and the fluid will bulge in the central region. In the following example we draw the same conclusion by using the equations of change.

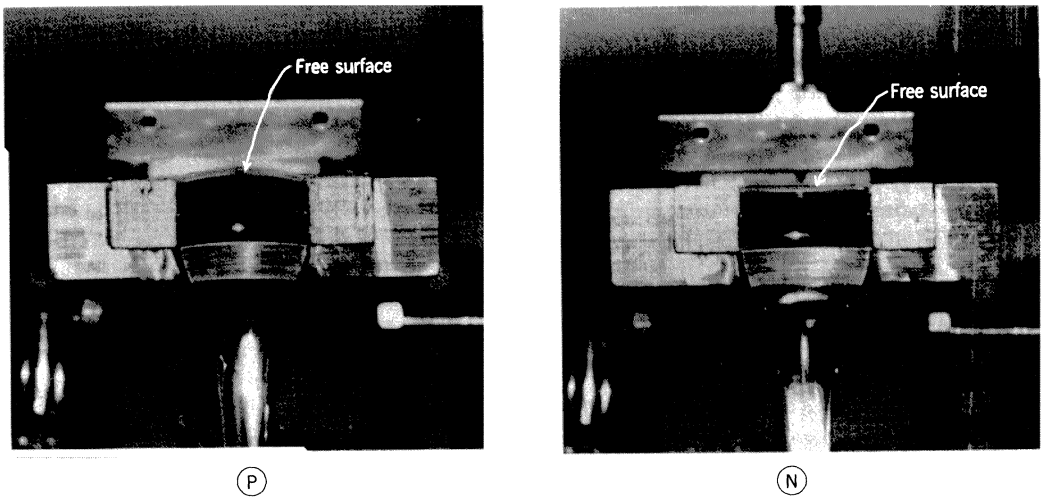

FIGURE 2.3-2. Tanner's tilted trough. A Newtonian liquid flowing down an inclined channel exhibits a flat free surface (N); the free surface of a polyisobutylene solution is convex (P). [Reproduced from R. I. Tanner, *Trans. Soc. Rheol.*, **14**, 483–507 (1970).]

[6] R. I. Tanner, *Trans. Soc. Rheol.*, **14**, 483–507 (1970); R. I. Tanner, *Engineering Rheology*, Oxford University Press (1985), pp. 102–105.

[7] A. S. Wineman and A. C. Pipkin, *Acta Mech.*, **2**, 104–115 (1966).

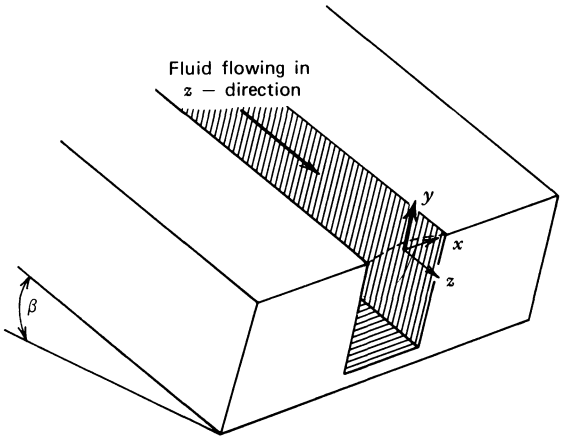

FIGURE 2.3-3. Coordinates for analysis of the tilted trough experiment. The trough is inclined at an angle β with respect to the horizontal.

EXAMPLE 2.3-2. Interpretation of Free-Surface Shapes in the Tilted Trough Experiment

For the flow in Fig. 2.3-2 explain why the free surface is flat for Newtonian liquids and convex for macromolecular fluids. To simplify the analysis, assume that the trough is very deep so that the presence of the bottom may be ignored. The trough is inclined at an angle β relative to the horizontal and has width W.

SOLUTION If the trough is very deep, we anticipate a velocity field of the form $v_z = v_z(x)$, $v_x = 0$, and $v_y = 0$ where the coordinate system is chosen as shown in Fig. 2.3-3. We further expect the stress components τ_{ij} to depend on x alone, and $p = p(x, y, z)$ since the surface is not necessarily flat. No information is gained from the continuity equation for the assumed velocity profile.

The equation of motion for this system gives

x-component:
$$0 = -\frac{\partial p}{\partial x} - \frac{d\tau_{xx}}{dx} \tag{2.3-6}$$

y-component:
$$0 = -\frac{\partial p}{\partial y} - \underline{\frac{d\tau_{xy}}{dx}} - \rho g \cos\beta \tag{2.3-7}$$

z-component:
$$0 = -\frac{\partial p}{\partial z} - \frac{d\tau_{xz}}{dx} + \rho g \sin\beta \tag{2.3-8}$$

The dashed-underlined term can be neglected if we assume that the free surface is not distorted enough to alter the stress field from that in steady shear flow between two infinite parallel plates. From these equations we can conclude that

$$\frac{\partial p}{\partial z} = 0 \tag{2.3-9}$$

and hence that

$$\tau_{xz} = (\rho g \sin\beta)x \tag{2.3-10}$$

Equation 2.3-9 is found by taking the partial derivative with respect to z of all three components of the equation of motion. From these results it can be seen that $\partial p/\partial z$ is a constant; and since $\partial p/\partial z$ is zero along the free surface, it must be zero everywhere.

Next, since π_{yy} is an analytic function of position, we may write:

$$d\pi_{yy} = \frac{\partial \pi_{yy}}{\partial x} dx + \frac{\partial \pi_{yy}}{\partial y} dy + \frac{\partial \pi_{yy}}{\partial z} dz = \frac{\partial \pi_{yy}}{\partial x} dx + \frac{\partial p}{\partial y} dy \tag{2.3-11}$$

By using Eqs. 2.3-6 and 7 together with Eq. 2.3-11, we find after integration that:

$$\pi_{yy}(x, y) = -(\tau_{xx} - \tau_{yy})|_x - \rho g(\cos \beta)y + C \tag{2.3-12}$$

where C is a constant of integration.

The total outward normal force per unit area exerted by the fluid at the free surface must be equal to the atmospheric pressure p_a. Provided the surface is not too curved, this requires that $\pi_{yy} = p_a$ and, thus, the free surface is given by the equation

$$y = \frac{-(\tau_{xx} - \tau_{yy})|_x + C - p_a}{\rho g \cos \beta} \tag{2.3-13}$$

At $x = 0$ all velocity gradients vanish so that the components of the stress tensor are all zero. For $x > 0$, if $(\tau_{xx} - \tau_{yy})|_x$ is positive, then the free surface will be lower than at $x = 0$. Thus the convex free surface shown in Fig. 2.3-2 corresponds to a positive second normal stress difference. For Newtonian fluids $(\tau_{xx} - \tau_{yy}) = 0$ for this flow, and Eq. 2.3-13 predicts a flat liquid surface as observed.

We can regard the second normal stress difference to be a function of the shear stress τ_{xz} instead of x. From Eq. 2.3-13 the total height of the fluid bulge h is given by

$$h = \frac{(\tau_{xx} - \tau_{yy})|_{\tau_{xz} = \tau_w}}{\rho g \cos \beta} \tag{2.3-14}$$

where $\tau_w = \frac{1}{2}\rho g W \sin \beta$ is the wall shear stress. Thus by measuring the size of the bulge in the fluid surface for very small values of the tilt angle β, we can measure the second normal stress difference at vanishingly small shear stresses. Since this method is restricted to low shear stress, any conclusions we have drawn about the second normal stress difference from this experiment are also limited. For larger values of shear stress, a more detailed analysis[8] has been performed to give information about the complete shape of the free surface and the onset of secondary flows.

Note that we have neglected surface tension in this analysis. If R denotes the radius (or half-width) of the channel, then the surface tension σ will not be important provided $(\rho g R^2 \cos \beta)/2\sigma \gg 1$. One of the nice results of this experiment is that it clearly establishes that the second normal stress difference is positive, at least at low shear rates.

c. Hole Pressure Effect

We now discuss measurement errors for polymeric fluids inherent in pressure transducers that are not flush-mounted.[9] To illustrate this error we consider the flow of fluids in a channel with a deep transverse slot as shown in Fig. 2.3-4. A fluid flows from left to right, driven by a pressure gradient in the x-direction. Flush-mounted pressure transducers are installed at the wall opposite the slot and at the bottom of the slot; the transducers show readings $(p + \tau_{yy})_1$ and $(p + \tau_{yy})_2$ respectively. It may be shown from the

[8] L. Sturges and D. D. Joseph, *Arch. Rat. Mech. Anal.*, **59**, 359–387 (1975).

[9] This measurement error was first confirmed by an extensive set of experiments described in J. M. Broadbent, A. Kaye, A. S. Lodge, and D. G. Vale, *Nature*, **217**, 55–56 (1968); A. Kaye, A. S. Lodge, and D. G. Vale, *Rheol. Acta*, **7**, 368–379 (1968); J. M. Broadbent and A. S. Lodge, *ibid.*, **10**, 557–573 (1972).

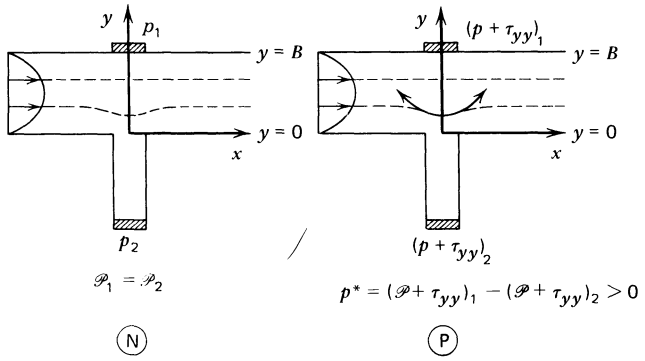

FIGURE 2.3-4. A fluid is flowing from left to right between two parallel plates across a deep transverse slot. "Pressures" are measured by flush-mounted transducer "1" and recessed transducer "2." (N) For the Newtonian fluid $\mathscr{P}_1 = \mathscr{P}_2$. (P) For polymeric fluids $(\mathscr{P} + \tau_{yy})_1 > (\mathscr{P} + \tau_{yy})_2$. The arrows tangent to the streamline indicate how the extra tension along a streamline tends to "lift" the fluid out of the hole, so that the recessed transducer gives a reading that is lower than that of the flush-mounted transducer.

equation of motion for Newtonian fluids that the centerline, $x = 0$, is a line of symmetry for the velocity field, if the flow is sufficiently slow that inertial effects may be neglected. This in turn means that the modified pressure $\mathscr{P}$ on the line of symmetry is independent of y. Thus, since τ_{yy} is zero at solid surfaces for Newtonian fluids, the modified pressures $\mathscr{P}_1$ and $\mathscr{P}_2$ are equal for Newtonian fluids, when inertial effects are negligible. On the other hand, for polymeric liquids we find[10] that generally $(\mathscr{P} + \tau_{yy})_1 > (\mathscr{P} + \tau_{yy})_2$. The difference $p^* = (\mathscr{P} + \tau_{yy})_1 - (\mathscr{P} + \tau_{yy})_2$, called the *hole pressure*, is related to the normal stresses in shear flow. For the transverse slot shown in Fig. 2.3-4 the following simple relation has been found[11] experimentally to hold

Transverse slot:
$$p^* = -\frac{1}{2}\int_0^{\tau_w} \frac{\tau_{11} - \tau_{22}}{\tau_{21}}\, d\tau_{21} \tag{2.3-15}$$

Here τ_w is the wall shear stress in the channel far from the slot. In this expression the 1, 2, and 3 directions have the meaning given at the beginning of this section, that is, in Fig. 2.3-4 we have $1 = x$, $2 = y$, $3 = z$. The stress tensor components to be used in the integral refer to the undisturbed shearing flow. The first normal stress difference is taken to be a function of shear stress. This is permissible, since we will see in Chapter 3 that both $\tau_{11} - \tau_{22}$ and τ_{21} are single-valued functions of the shear rate. Equation 2.3-15 was derived initially from theoretical arguments; however, the main justification for its continued use rests on the agreement with experiments.

Hole pressure effects occur whenever a polymeric liquid flows over a depression in a conduit wall. Two other geometries that have been studied are circular holes and long narrow slits aligned with the flow.[11] For these geometries the predicted relations are:

Circular hole:
$$p^* = -\frac{1}{3}\int_0^{\tau_w} \frac{(\tau_{11} - \tau_{22}) - (\tau_{22} - \tau_{33})}{\tau_{21}}\, d\tau_{21} \tag{2.3-16}$$

[10] D. Pike and D. G. Baird, *J. Rheol.*, **28**, 439-447 (1984); A. S. Lodge and L. de Vargas, *Rheol. Acta*, **22**, 151-170 (1983); A. S. Lodge, *Polym. News*, **9**, 242-246 (1984).

[11] K. Higashitani and W. G. Pritchard, *Trans. Soc. Rheol.*, **16**, 687-696 (1972).

Longitudinal slot:
$$p^* = \int_0^{\tau_w} \frac{(\tau_{22} - \tau_{33})}{\tau_{21}} d\tau_{21} \tag{2.3-17}$$

This last relation has been subject to much less experimental investigation than the other two formulas.

§2.4 SECONDARY FLOWS

We now turn to the first of three experiments in which a flow field may be divided into a strong primary flow field and a weak secondary flow field. Roughly speaking the primary flows are associated with the viscous properties of the fluids, and the secondary flows with inertial effects and "elastic effects." We shall find in all three experiments that the secondary flows caused by elastic effects are opposite to those caused by inertial effects. Although there is no general principle that inertial effects and elastic effects produce secondary flows in opposite directions, that does seem to be a good rule of thumb.

a. Rotating Sphere

In this experiment we consider a sphere rotating in a large sea of fluid. This situation was analyzed in Example 1.4-3 for a Newtonian fluid. The steady primary flow field (in Eq. 1.4-50) is one in which fluid particles are carried in circles concentric with the axis of rotation of the sphere. Superimposed on this is a secondary flow driven by inertial effects (given in Eqs. 1.4-62, 63, and 64) in which the fluid moves towards the sphere near the axis of rotation and away from the sphere in the equatorial plane. We understand this intuitively since the centrifugal force is largest near the equator of the sphere, thus driving the fluid away from the sphere here.

The same experiment performed with a sphere in a 5% solution of polyacrylamide was performed by Giesekus[1] as shown in Fig. 2.4-1. The photograph clearly shows a rotating primary flow but a secondary flow toward the sphere in the equatorial plane and away from the sphere near the axis of rotation. We shall return to this experiment in Example 6.5-1 where a quantitative analysis is given on the basis of a simple constitutive equation that contains both viscous and "elastic" contributions to the stress tensor.

b. Cylindrical Tank with Rotating Lid

In this experiment a flow field is produced by placing a rotating disk on top of a beaker filled with fluid. Photographs of secondary flows in this system are shown[2] in Fig. 2.4-2. The primary fluid motion is in the tangential direction because of the rotation of the disk. Moreover, the fluid at the top of the container will be rotating with a larger angular velocity than that at the bottom; consequently, the fluid near the disk will experience a large outward centrifugal force. For Newtonian fluids there are no forces to counter this, and we are not surprised to find that there is a weak secondary flow, everywhere perpendicular to the primary flow, which is directed radially outward near the disk, down the side of the beaker, inward along the bottom, and finally back up near the center, as shown in Fig. 2.4-2 Ⓝ. The magnitude of the velocity in the secondary flow is roughly 10% of that in the primary flow.

[1] H. Giesekus in E. H. Lee, ed., *Proceedings of the Fourth International Congress on Rheology*, Wiley-Interscience, New York (1965), Part 1, pp. 249–266.

[2] C. T. Hill, *Trans. Soc. Rheol.*, **16**, 213–245 (1972). See also C. T. Hill, J. D. Huppler, and R. B. Bird, *Chem. Eng. Sci.*, **21**, 815–817 (1966). Theoretical analyses have been given by J. M. Kramer and M. W. Johnson, Jr., *Trans. Soc. Rheol.*, **16**, 197–212 (1972), and J. P. Nirschl and W. E. Stewart, *J. Non-Newtonian Fluid Mech.*, **16**, 233–250 (1984).

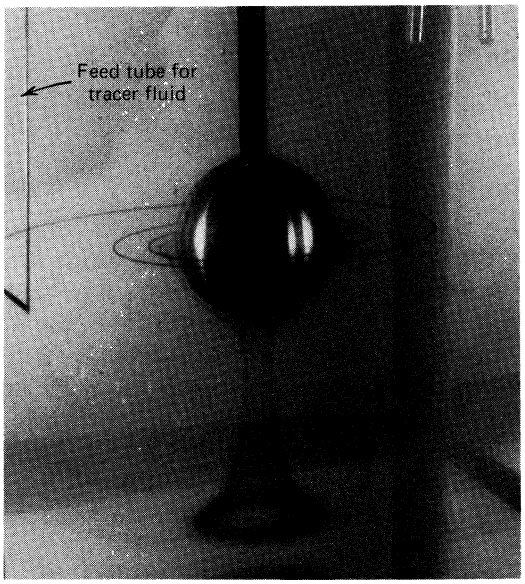

FIGURE 2.4-1. Secondary flow around a rotating sphere in a polyacrylamide solution. [Reproduced from H. Giesekus in E. H. Lee, ed., *Proceedings of the Fourth International Congress on Rheology*, Wiley-Interscience, New York (1965), Part 1, pp. 249–266.]

A polymer fluid placed in the disk and cylinder apparatus exhibits a secondary flow in the opposite direction. A typical flow pattern is shown in Fig. 2.4-2 (P) for a solution of polyacrylamide in a solvent of glycerol and water. Qualitatively we expect that the normal stresses associated with the primary flow that act to produce the rod climbing are at work here. Moreover, the normal stresses do not have to be very large in an absolute sense in order to cause a reversal in the direction of secondary flow. At polymer concentrations so low that normal stresses could no longer be detected by standard techniques, the reverse secondary flow was still clearly visible at small disk rotation speeds.

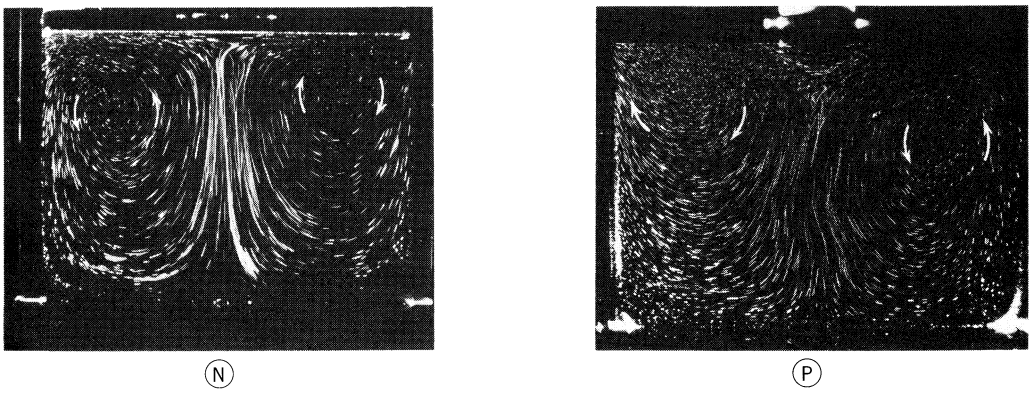

FIGURE 2.4-2. Secondary flows in the disk-cylinder system. (N) The Newtonian fluid moves up at the center, whereas (P) the viscoelastic fluid, polyacrylamide (Separan 30)-glycerol-water, moves down at the center. [Reproduced from C. T. Hill, *Trans. Soc. Rheol.*, **16**, 213–245 (1972).]

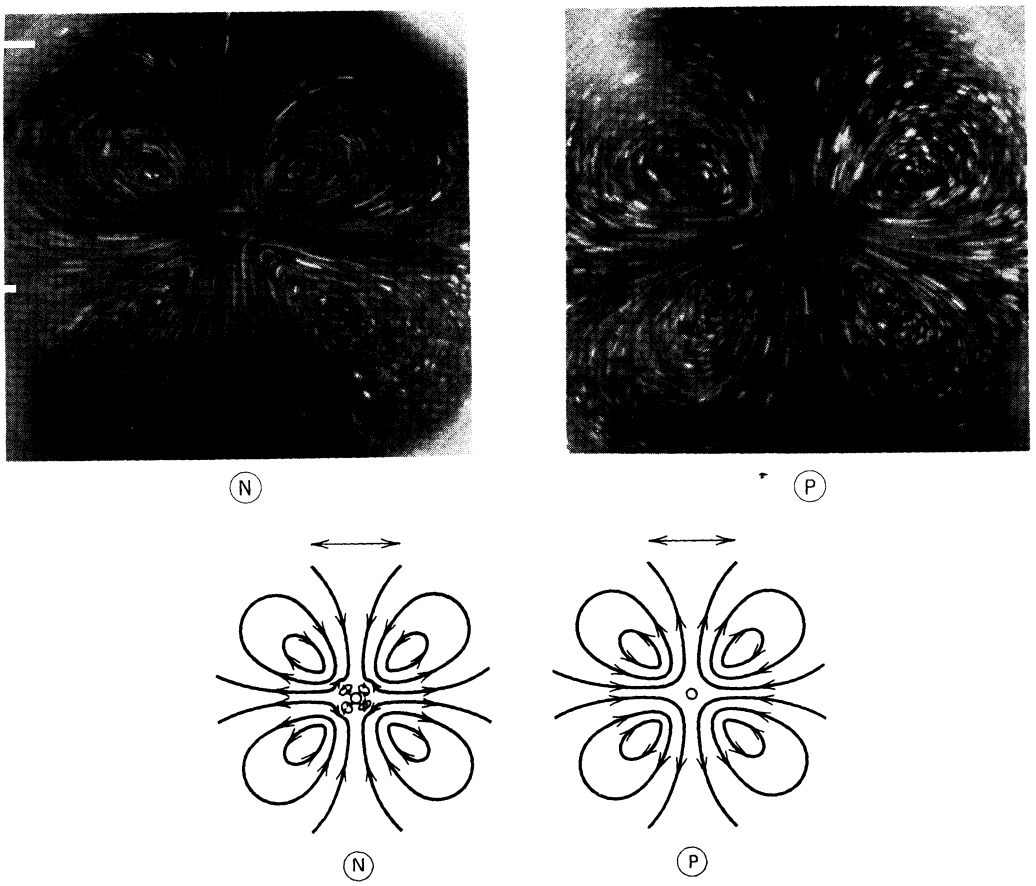

FIGURE 2.4-3. Steady streaming motion produced by a long cylinder oscillating normal to its axis. The cylinder is viewed on end and the direction of oscillation is shown by the double arrow. The photographs do not show streamlines but mean particle pathlines made visible by illuminating tiny spheres with a stroboscope synchronized with the cylinder frequency. (N) A water-glycerin mixture: (P) 100 ppm polyacrylamide in water-glycerin. [Reproduced from C. T. Chang and W. R. Schowalter, *Nature*, **252**, 686-688 (1974).]

c. Streaming Motion Produced by an Oscillating Cylinder

A long cylinder of radius R is made to oscillate with a frequency ω and amplitude δ normal to its axis. For small values of δ this produces a primary flow field of order δ with frequency ω which has mean value zero at any fixed position. In addition fluid particles will move with a nonzero time average velocity in what is known as *steady streaming motion* or, sometimes, *acoustic streaming*. Without going into detail we can describe the two kinds of contributions to this motion that may arise at order δ^2. First, since the flow field is inhomogeneous, the time average velocity of a given fluid particle will not be the same as the time average velocity at a given fixed position. Thus the primary flow field causes the fluid particles to move with a mean velocity of order δ^2. Second, nonlinear terms in the equation of motion or possibly in the constitutive equation produce a secondary flow field of order δ^2 with frequency 2ω and a nonzero mean value. This secondary flow field then directly gives a particle motion of order δ^2. The resulting steady streaming motion may be made visible by a flow visualization technique as shown in Fig. 2.4-3 for a Newtonian fluid (N) and a

polyacrylamide solution (P). For the Newtonian fluid the streaming motion is directly toward the oscillating cylinder along the axis of oscillation in an inner region, and opposite in an outer region. For the polymer solution, by contrast, there is only one region and the direction is toward the cylinder along the entire axis of oscillation.[3] Thus there is a flow reversal in most of the fluid, but we see also that the rule about the competing effects of inertia and elasticity is no more than a rule of thumb.

§2.5 OTHER ELASTIC EFFECTS

In this section we consider a further number of effects that are all in one way or another manifestations of elastic properties of polymeric fluids. However the experiments are more difficult to analyze than those encountered in the previous two sections. In addition the experiments form a more heterogeneous group in the sense that there is not one well-defined property, such as normal stresses, that is simply related to them all.

a. Extrudate Swell (also called "die swell")

In this experiment we consider a fluid that exits from a capillary of diameter D into air forming a jet of diameter D_e. For polymeric fluids it is customary to refer to the material in the jet as the *extrudate*. For Newtonian fluids D_e will be about 13% larger than D in the limit of small Reynolds number[1] and about 13% smaller than D in the limit of large Reynolds number laminar flow.[2] Hence a Newtonian fluid leaves the capillary without any dramatic change in diameter, as evidenced in Fig. 2.5-1 (N). The contrasting behavior of a

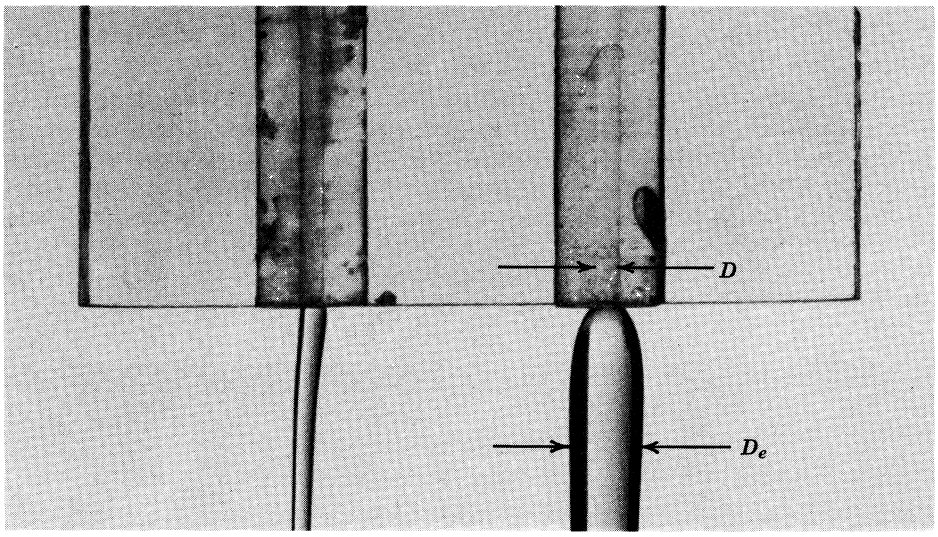

FIGURE 2.5-1. Behavior of fluids issuing from orifices. (N) A stream of Newtonian fluid (silicone fluid) shows no diameter increase upon emergence from the capillary tube; (P) a solution of 2.44 g of polymethylmethacrylate ($\bar{M}_n = 10^6$ g/mol) in 100 cm^3 of dimethylphthalate shows an increase by a factor of 3 in diameter as it flows downward out of the tube. [Reproduced from A. S. Lodge, *Elastic Liquids*, Academic Press, New York (1964), p. 242.]

[3] A detailed analysis is given by C. F. Chang and W. R. Schowalter, *J. Non-Newtonian Fluid Mech.*, **6**, 47–67 (1979).
[1] R. I. Tanner in J. R. A. Pearson and S. M. Richardson, eds., *Computational Analysis of Polymer Processing*, Applied Science, London (1983), p. 66.
[2] See Problem 1B.4.

polymeric fluid is shown in Fig. 2.5-1 Ⓟ, where D_e increases to about 300% of D. Extrudate diameters of two, three, or even four times the capillary diameter are encountered with polymers, and the phenomenon is referred to as *extrudate swell.*

A very oversimplified interpretation of extrudate swell may be obtained by using again the simple proposition of Weissenberg that flowing polymeric fluids have an extra tension along the streamlines. Once the fluid is outside the capillary this extra tension cannot be supported, and the fluid will contract axially and expand radially. Using this "elastic recoil" mechanism Tanner[3] proposed the following simple expression for extrudate swell:

$$\frac{D_e}{D} = 0.1 + \left[1 + \frac{1}{2}\left(\frac{\tau_{11} - \tau_{22}}{2\tau_{21}}\right)_w^2\right]^{1/6} \tag{2.5-1}$$

where the subscript w indicates that the stresses in steady tube flow $\tau_{11} - \tau_{22}$ and τ_{21} are to be evaluated at the wall. The simplicity of Eq. 2.5-1 and its success[4] in describing data on extrudate swell recommend its use for estimation purposes. Note, however, that the analysis in Example 2.3-1 of the rod-climbing experiment shows that one must be careful with simple arguments of this kind, and it may be that the second normal stress difference $\tau_{22} - \tau_{33}$ influences the swell ratio somewhat.

In addition to the relaxation of the normal stresses at the end of the capillary, there may be other phenomena that contribute to the extrudate swell. For example, viscous heating produces a temperature gradient across the tube cross-section. It has been demonstrated[5] that for Newtonian fluids with temperature-dependent viscosity, the viscosity near the tube wall is higher than at the center, where the temperature has a maximum, and extrudate swell results; this effect could also contribute to the extrudate swell in polymeric liquids. Still another suggestion[6] is that polymer molecules near the tube wall undergo more stretching than those near the center, and that in the extrudate the springing back of the molecules near the liquid-gas interface contributes to the jet diameter increase. It should be evident that extrudate swell is a complicated phenomenon for which no simple analysis can be entirely satisfactory.

We conclude this discussion with a few comments regarding the role of the length-to-diameter (L/D) ratio of the die. First consider a die with a very small L/D. A typical fluid element moving along the centerline begins as a short, fat cylinder in the reservoir, and then is squeezed into a long, thin cylinder within the die. Upon emerging from the die, the fluid element, "remembering" its former shape, tries to return to become short and fat again. This contribution to the extrudate swell is thus ascribed to the fluid memory of past kinematic events.

Next we consider a die with large L/D and the experiment by Lodge[7], which shows that the "memory effect" described in the last paragraph cannot give a complete explanation. He filled a tube with a large L/D with a sample of silicone "silly putty" and then allowed it to remain in the tube for a time longer than the memory of the fluid. The "silly putty" was then forced out of the tube with a plunger. As the material emerged from the tube extrudate swell was observed.

In some experiments with a die having $L/D = 150/8$, Giesekus[8] showed that with increased flow rate "delayed swell" occurs. That is, the extrudate has about the same

[3] R. I. Tanner, *J. Polym. Sci.*, **A8**, 2067–2078 (1970); R. I. Tanner, *Engineering Rheology*, Oxford University Press (1985), pp. 321–329, 338–343.
[4] J. Vlachopoulos, M. Horie, and S. Lidorikis, *Trans. Soc. Rheol.*, **16**, 669–685 (1972).
[5] H. B. Phuoc and R. I. Tanner, *J. Fluid Mech.*, **98**, 253–271 (1980).
[6] R. I. Tanner, *J. Non-Newtonian Fluid Mech.*, **6**, 289–302 (1980).
[7] A. S. Lodge, *Elastic Liquids*, Academic Press, New York (1964), pp. 243–244.
[8] H. Giesekus, *Rheol. Acta*, **8**, 411–421 (1969).

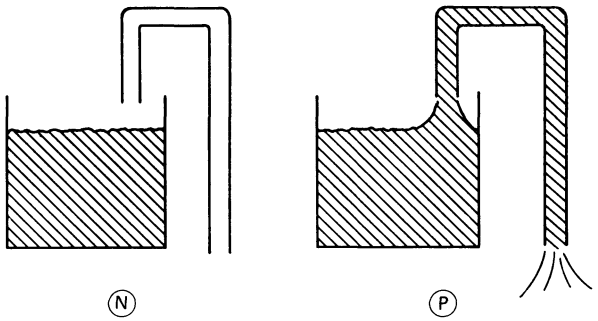

FIGURE 2.5-2. The tubeless siphon. Ⓝ When the siphon tube is lifted out of the fluid, the Newtonian liquid stops flowing; Ⓟ the macromolecular fluid continues to be siphoned.

diameter as the capillary for a distance several diameters downstream of the exit, and then at this point shows pronounced swelling.

Another interesting point is that for noncircular dies, the shape of the cross section of the extrudate is not the same as that of the die.

b. The Tubeless Siphon[9]

We turn now to an experiment involving the siphoning of Newtonian and non-Newtonian fluids. Imagine two identical experiments in which fluid is being siphoned out of a container—one experiment using a Newtonian fluid, the other a polymeric fluid (see Fig. 2.5-2). Now suppose that the tube is lifted up out of the fluid in the container. We immediately hear a slurping sound from the siphon that was in the Newtonian fluid as the liquid empties out of the tube and the siphoning stops. By contrast the non-Newtonian fluid continues to flow up to and through the siphon![10]

Photographs of fluid columns in working tubeless siphons are shown in Figs. 2.5-3 and 4. It is believed that it is the orientation and elongation of the polymer molecules along the streamlines that are responsible for the large axial stresses that make the siphon work. Note in Fig. 2.5-4 that these same stresses also prevent a bubble from rising in the fluid column.

c. The Uebler Effect

This effect was discovered in connection with the use of tiny gas bubbles in a flow visualization experiment for contraction flow. It was observed by Uebler[11] that when the diameter of the bubbles is equal to or larger than about $\frac{1}{6}$ to $\frac{1}{8}$ of the small tube diameter, a bubble moving along the centerline comes to a sudden stop right at the entrance to the small tube. Such a bubble can then remain stationary for a minute or more before finally proceeding on its journey down the tube.

[9] Tacitus relates that this effect has been utilized in connection with the harvesting of bitumen on the Dead Sea around AD 70. See *The Complete Works of Tacitus* (transl. by A. J. Church and W. J. Brodribb), The Modern Library, New York (1942), Book V, The History, p. 661. Tacitus was born AD 55. This reference, which seems to be the earliest description of a non-Newtonian flow phenomenon, was supplied by Professor Moshe Gottlieb.

[10] D. F. James, *Nature*, **212**, 754-756 (1966).

[11] A. B. Metzner, *AIChE J*, **13**, 316-318 (1967); E. A. Uebler, Ph.D. Thesis, University of Delaware, Newark (1966).

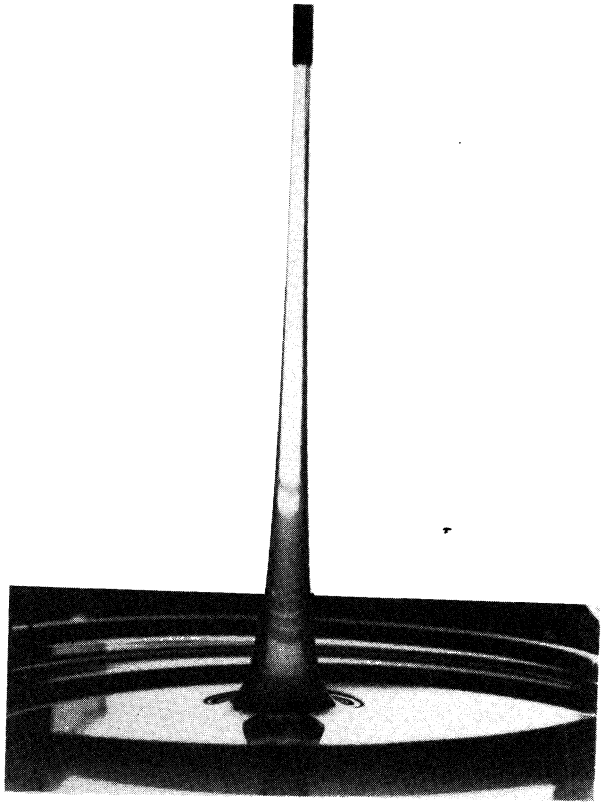

FIGURE 2.5-3. Fluid column in tubeless siphon experiment with a high molecular weight hydrocarbon polymer, AM-1 in JP-8 aviation fuel. [Reproduced from S. T. J. Peng and R. F. Landel, *J. Appl. Phys.* **47**, 4255 (1976)].

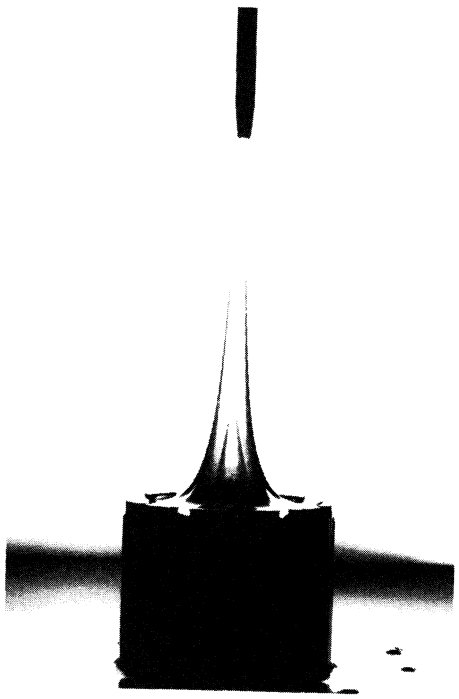

FIGURE 2.5-4. Fluid column in tubeless siphon experiment with the same polymer as in Fig. 2.5-3. Note the stable trapped bubble at the bottom of the column. [Reproduced from S. T. J. Peng and R. F. Landel in G. Astarita, G. Marrucci, and L. Nicolais, eds., *Rheology*, Vol. 2, Plenum Press, New York

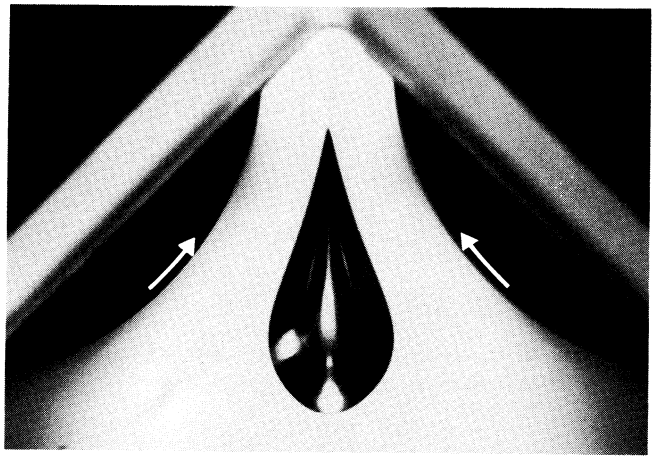

FIGURE 2.5-5. Gas bubble trapped in the flow field created by two parallel, horizontal, counter-rotating cylinders. The sense of rotation is indicated by arrows on the cylinders. In the absence of rotation the bubble passes between the cylinders. [Photograph by J. Michele in H. Giesekus, *Z. Angew. Math. Mech.*, **58**, T26–T37 (1978).]

A demonstration of this effect has been given by Giesekus,[12] who studied the flow field created by two counter-rotating cylinders immersed in a polymeric fluid as shown in Fig. 2.5-5. The axes of the cylinders are parallel and horizontal, and a flow field is generated in which fluid moves up in the region between the cylinders and down outside the cylinders. In this situation Giesekus showed that a large gas bubble may remain stationary on the upstream side of the contraction, even though common sense would suggest that both buoyancy and the flow field would make the bubble rise. As soon as the rotation of the cylinders is stopped, however, the bubble rises and escapes through the contraction. Note the similarity in the shape of this bubble and that in Fig. 2.5-4.

d. Contraction Flow

We now turn our attention to the details of the flow pattern in the neighborhood of a sudden contraction. Figure 2.5-6 shows two streak photographs taken by Giesekus[13] contrasting the velocity fields of glycerin and aqueous polyacrylamide as they flow from a large reservoir into a small tube. The Reynolds number in both photographs is very low. The behavior of the two fluids is not even qualitatively similar. A typical streamline in the Newtonian fluid is a straight line heading directly toward the entrance to the small tube; glycerin approaches the exit from a full 90 degrees in any direction about the centerline. However, for a polymer solution, only the fluid in a small conical region about the centerline moves linearly toward the entrance to the small tube. A significant portion of the polymer solution is trapped in a large circulation pattern and does not enter the small tube at all.

[12] H. Giesekus, *Z. Angew. Math. Mech.*, **58**, T26–T36 (1978).

[13] A. B. Metzner, E. A. Uebler, and C. F. Chan Man Fong, *AIChE J*, **15**, 750–758 (1969). For other photographs of converging flows of polymer solutions, see H. Giesekus, *Rheol. Acta*, **7**, 127–138 (1968); P. J. Cable and D. V. Boger, *AIChE J.*, **24**, 869–879, 992–999 (1978); **25**, 152–159 (1979); D. V. Boger and H. Nguyen, *Polym. Eng. Sci.*, **18**, 1037–1043 (1978).

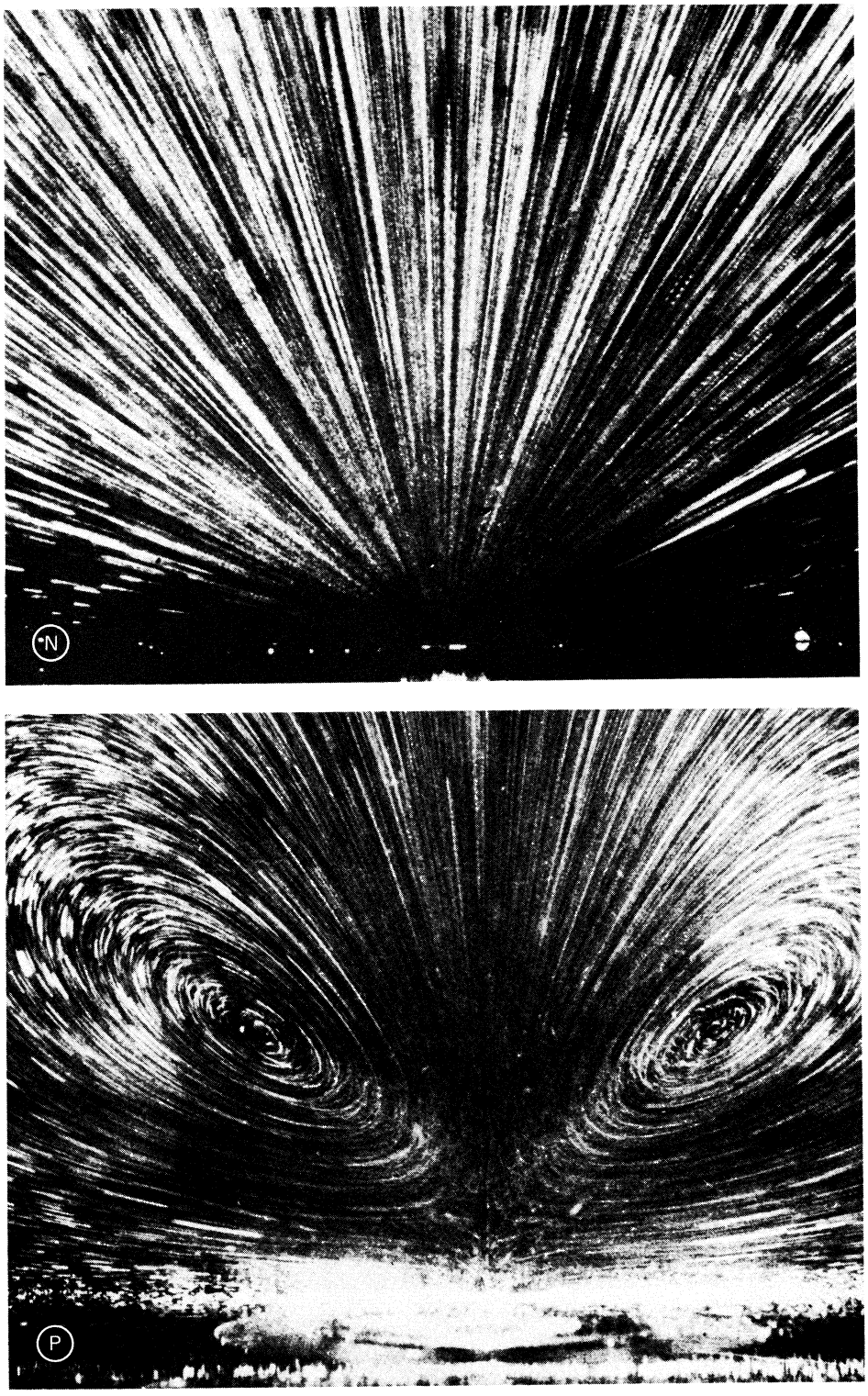

FIGURE 2.5-6. Velocity fields near a sudden contraction. The fluid moves from top to bottom in the photographs from a large reservoir into a small circular tube. (N) The streamlines in glycerin are straight and all directed toward the exit; (P) a 1.67% aqueous polyacrylamide solution shows a large toroidal vortex. [Photographs by H. Giesekus, given in A. B. Metzner, E. A. Uebler, and C. F. Chan Man Fong, *AIChE J.*, **15**, 750–758 (1969).]

Recirculation zones are generally considered detrimental in equipment for polymer processing. For this reason it is important to understand and be able to predict the conditions under which recirculation zones appear.

e. Elastic Recoil

We have referred earlier to an extra tension along the streamlines in polymeric fluids, caused by alignment and stretching of the polymer molecules. It was suggested that the tendency for the molecules to snap back when the external forces are removed produces "elastic recoil" of the fluid that could be at least partially responsible for extrudate swelling. We now turn to a number of experiments that we interpret as demonstrations of the elastic recoil effect.

The first experiment was performed by Kapoor[14] as shown in Fig. 2.5-7. In his experiment, a streak of charcoal slurry was first introduced into a 2% (weight) solution of carboxymethylcellulose in water by means of a syringe. A pressure gradient was then applied to the solution, and the deformation of the trace line was recorded in a sequence of

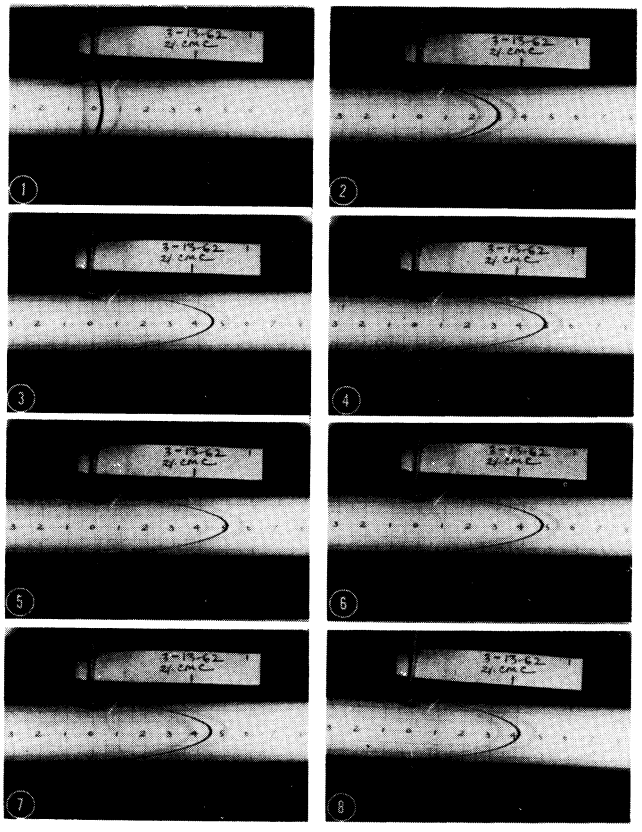

FIGURE 2.5-7. A solution of 2% carboxymethylcellulose (CMC 70H) in water is made to flow under a pressure gradient that is turned off just before frame 5. The flow and subsequent recoil are shown by the charcoal tracer line. [Reproduced from A. G. Fredrickson, *Principles and Applications of Rheology*, © Prentice-Hall, Englewood Cliffs, NJ (1964), p. 120.]

[14] N. N. Kapoor, M.S. Thesis, University of Minnesota, Minneapolis (1964); A. G. Fredrickson, *Principles and Applications of Rheology*, Prentice-Hall, Englewood Cliffs, NJ (1964), p. 120.

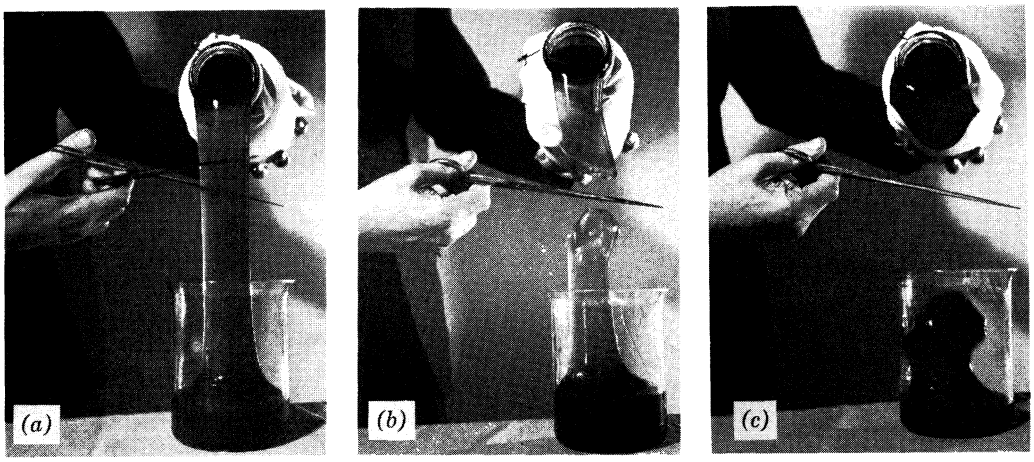

FIGURE 2.5-8. An aluminum soap solution, made of aluminum dilaurate in decalin and *m*-cresol, is (*a*) poured from a beaker and (*b*) cut in midstream. In (*c*), note that the liquid above the cut springs back to the beaker and only the fluid below the cut falls to the container. [Reproduced from A. S. Lodge, *Elastic Liquids*, Academic Press, New York (1964), p. 238. For a further discussion of aluminum soap solutions see N. Weber and W. H. Bauer, *J. Phys. Chem.*, **60**, 270-273 (1956).]

photographs. After a short time the pressure gradient was removed; the pictures taken after this time show the charcoal trace line receding as the fluid recoils. Recoil is not observed for Newtonian liquids.

In another experiment due to Lodge,[15] an aluminum soap solution is poured from a bottle into a beaker, as shown in Fig. 2.5-8 (*a*). The fluid is "pulled" out of the bottle by the weight of the entire fluid column and the tubeless siphon effect. When the fluid column is cut in two as shown in part (*b*) the top part of the column snaps back into the bottle by elastic recoil, as shown in part (*c*).

In quantitative experiments, Meissner[16] found that a filament of low-density polyethylene at 423 K which is stretched rapidly from 1 to 30 cm in length, at which point it is suddenly set free, will recover to a length of just 3 cm. The fact that the filament recovers to a length of 3 cm rather than to 1 cm shows that the "memory" of the original shape is not perfect. If the filament is held at a length of 30 cm for some time before it is set free, it will recover to some length larger than 3 cm. Finally, if the filament is held at a length of 30 cm for a long time before it is set free, there will be little or no recovery, thus demonstrating the "fading memory" of the fluid. In closing, we remark that a recovery by a factor of ten (from 30 cm to 3 cm) is very large. Typical cross-linked rubber bands cannot even be stretched by a factor of ten without breaking.

f. Filament stability

The ability of polymeric fluids to form stable filaments has been demonstrated in connection with the tubeless siphon experiment. In this section we show two further experiments that demonstrate the remarkable filament stability of polymeric fluids. Both

[15] A. S. Lodge, *Elastic Liquids*, Academic Press, New York (1964), p. 236.
[16] J. Meissner, *Rheol. Acta*, **10**, 230-242 (1971).

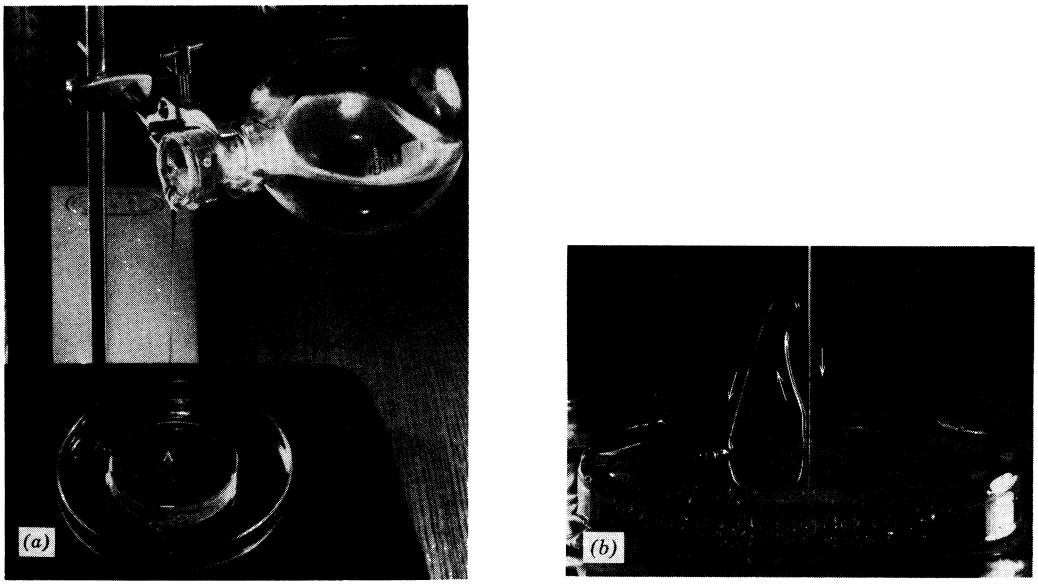

FIGURE 2.5-9. (*a*) A solution of 5.76 g of polyisobutylene ($\bar{M}_n \doteq 10^6$) in 100 cm^3 of decalin is poured onto a shallow pool of the same liquid. (*b*) A filament of the liquid stream rebounds from the pool if the stream being poured has a sufficiently small diameter. [Reproduced from A. S. Lodge, *Elastic Liquids*, Academic Press, New York (1964), p. 251.]

experiments involve very thin filaments, and surface forces are likely to contribute to the effects.

Kaye[17] has observed that when a solution of polyisobutylene in decalin is poured in a thin stream onto a shallow pool of the same liquid, the stream of liquid will bounce off the pool as shown in Fig. 2.5-9. Furthermore, the bouncing liquid stream forms a fine, continuous element. This behavior, which lasts for a period of about 1 s, alternates on a regular basis with a period of similar length, during which there is no bouncing stream. In the off-period, a small hump of liquid can be seen forming where the stream being poured strikes the surface of the pool.

Barnard and Pritchard[18] have observed that if the wall of a glass beaker, which has contained a solution of a high molecular weight polyisobutylene in low molecular weight polyisobutylene, is cleaned by tearing the polymer from the wall while wrapping it onto a glass rod, an interesting phenomenon is observed. Several very thin streams of fluid are found to emanate from irregularities on the surface of the liquid (see Fig. 2.5-10). The streams increase in length at a rate of several centimeters per second. It is believed that this is an electrically driven phenomenon. However, in Newtonian liquids of low conductivity similarly to that of the polyisobutylene, the streaming jet breaks up into a series of droplets, instead of remaining as a continuous filament such as the polymer shown here.[19]

[17] A. Kaye, *Nature*, **197**, 1001–1002 (1963).
[18] B. J. S. Barnard and W. G. Pritchard, *Nature*, **250**, 215–216 (1974).
[19] G. I. Taylor, *Proc. Roy. Soc., London*, **A313**, 453–475 (1969).

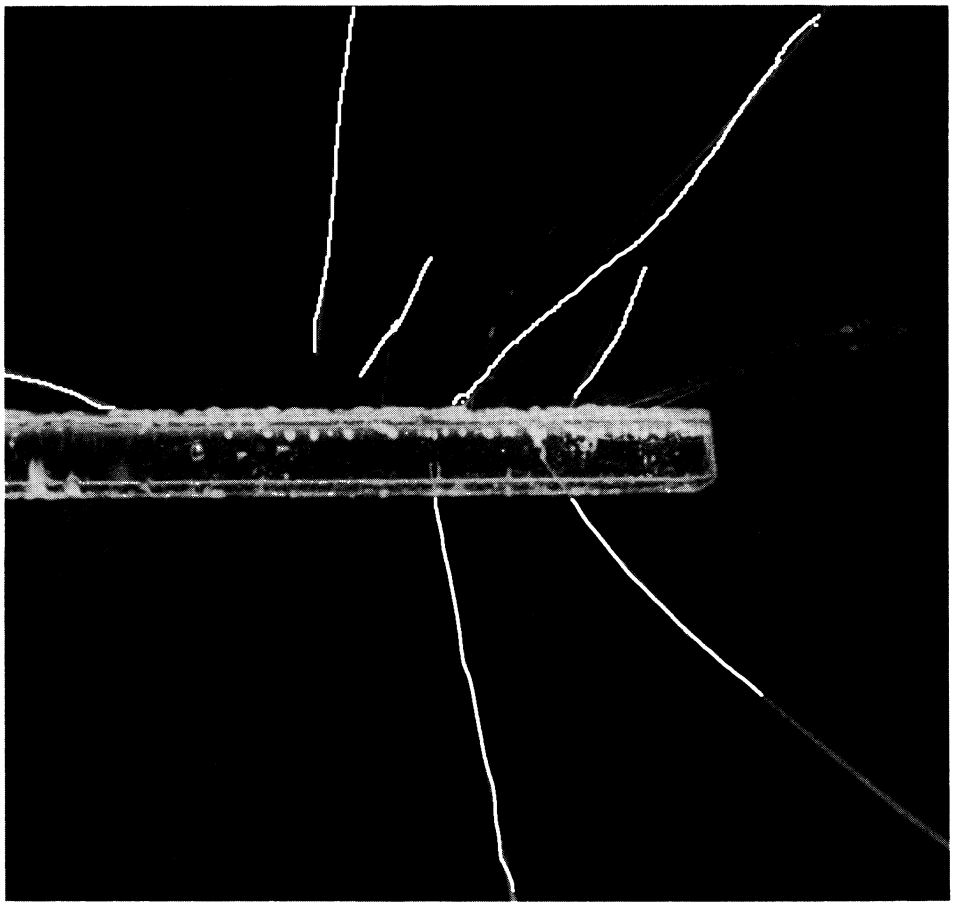

FIGURE 2.5-10. A solution of high molecular weight polyisobutylene in low molecular weight polyisobutylene forms fine, continuous streams emanating from a 6-mm glass rod. [Reproduced from B. J. S. Barnard and W. G. Pritchard, *Nature*, **250**, 215–216 (1974).]

g. Vortex Inhibition

The final experiment in this section is that of vortex inhibition.[20] The experiment is done by first filling a large tank with water, stirring the water to generate a circulation in the tank, and finally removing a plug from the center of the bottom to allow the water to drain. As the water empties from the tank, a very stable air core reaching all the way to the outlet forms, accompanied by a pronounced slurping sound (see Fig. 2.5-11 Ⓝ). Now, if a very small amount of certain polymers is added to the draining water, the air core suddenly disappears and the noise that goes with it ceases (see Fig. 2.5-11 Ⓟ). Moreover, the volume flow rate out of the tank nearly doubles after the air core is eliminated, provided that the level in the tank is kept constant.[21]

[20] R. J. Gordon and C. Balakrishnan, *J. Appl. Polym. Sci.*, **16**, 1629–1639 (1972).
[21] S. Ishikawa, Sc.D. Thesis, Massachusetts Institute of Technology, Cambridge (1979).

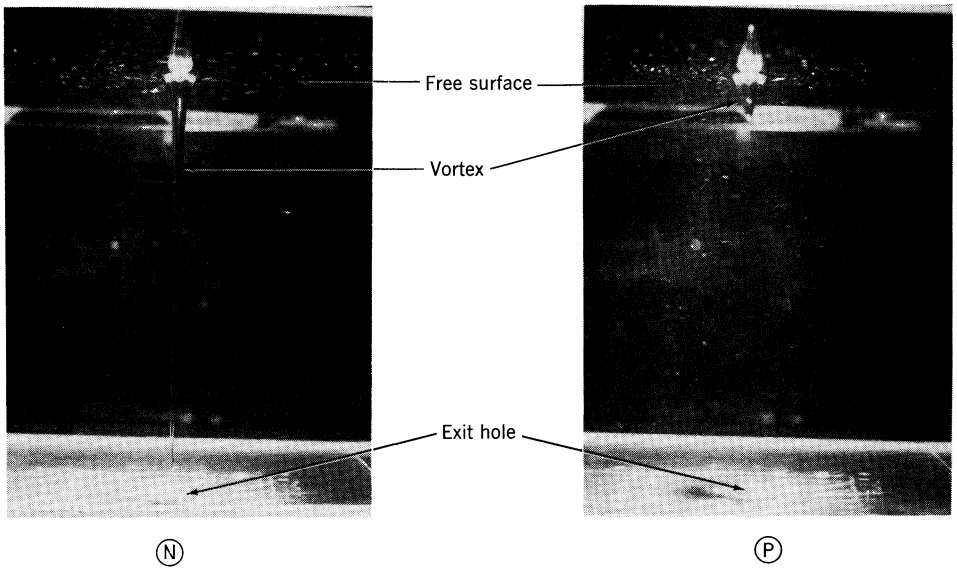

FIGURE 2.5-11. Vortex inhibition. Ⓝ shows the vortex that is formed as water drains form a tank, and Ⓟ shows the corresponding result after addition of a small amount of polymer to the water. A reflection of the vortex in the free surface of the liquid can be seen just above the vortex in both photographs. [Reproduced from photographs courtesy of Professor R. J. Gordon, Department of Chemical Engineering, University of Florida.]

Among the best polymers for vortex inhibition are polyethyleneoxide, effective at 7.5 ppm, and polyacrylamide, effective at only 3 ppm. These solutions are exceedingly dilute. It is even more interesting that the polymers that are good at vortex inhibition are generally also good in drag reduction—a dilute solution, turbulent flow phenomenon described in §2.7a. Furthermore, the same ordering in terms of effective concentrations seems to hold for both phenomena. For example, the two polymers mentioned above show significant drag reduction at concentrations of 9 and 5 ppm, respectively.

The mechanism for vortex inhibition is more amenable to understanding than that for drag reduction because the former involves laminar flow and the latter involves turbulent flow. The bulk of the flow out of the vortex tank occurs through a thin boundary layer[22] along the bottom surface of the container. As polymer molecules flow from this thin layer into the exit tube they experience very large rates of strain which are sufficient to stretch them nearly to their fully extended configuration.[21] In the fully extended configuration, the polymer molecules cause sufficient increase in the tension along streamlines near the exit hole that a larger fraction of the total flow passes through the boundary layer. This results in a slight increase in the size of the viscous core around the axis of rotation and the disappearance of the air core. This understanding of the mechanism for vortex inhibition and the close connection between effectiveness of polymers in vortex inhibition and drag

[22] The physical origin of this boundary layer is the no-slip condition on v_θ at the bottom of the container. In the bulk of the flow, an (inward) radial pressure gradient exists to counter the (outward) centrifugal force associated with the swirling flow ($v_\theta \propto 1/r$). Near the bottom wall v_θ goes to zero, and the unopposed radial pressure gradient causes an inward flow. Taylor has illustrated this boundary layer by stirring a cup of tea which contains tea leaves. When stirring is stopped, the inward flow in the boundary layer at the bottom of the cup causes the tea leaves to collect in a pile at the center. E. S. Taylor, *Illustrated Experiments in Fluid Mechanics, The NCFMF Book of Film Notes*, MIT Press, Cambridge, MA (1972), pp. 97-104.

reduction lends credence to the currently accepted belief that molecular extension is also responsible for drag reduction.

§2.6 BUBBLES AND PARTICLES

The fluid dynamics of systems with bubbles or particles is a vast subject even for Newtonian fluids.[1] When the bubbles or particles move in non-Newtonian fluids one encounters striking, new phenomena in practically every situation,[2] as exemplified by the following experiments.

a. Bubble Shapes

We now consider the buoyancy-driven rise of a gas bubble in a large container of fluid. If the fluid is Newtonian and the motion is so slow that inertial effects may be neglected then the bubble is spherical as shown in Example 1.4-2. Bubbles that rise very slowly in non-Newtonian fluids will also be spherical. However to observe spherical bubbles requires either very tiny bubbles or a very high viscosity of the fluid. Usually the bubbles will be deformed in some fashion from spherical shape, either because of inertial or elastic effects.

When bubbles in Newtonian fluids are deformed slightly due to inertial effects, they assume the shape of an ellipsoid of revolution flattened at the poles (an oblate ellipsoid). The actual deformation depends on the Reynolds number and the capillary number and is given to a first approximation in Eq. 1.4-46. By contrast bubbles in polymeric fluids that are deformed slightly due to elastic effects assume the shape of an ellipsoid of revolution that is elongated at the poles (a prolate ellipsoid) as shown in Fig. 2.6-1*a*. Qualitatively we can explain this by postulating that there is an extra tension along the streamlines that tends to squeeze the bubble at its equator and hence elongate it at the poles as shown in Fig. 2.6-1*b*. However such an extra tension could not be the result of a steady shear flow but the result of a transient stretching of the fluid elements. In Example 6.5-2 we present a quantitative computation of the deformation.

Bubbles with the shape shown in Fig. 2.6-1 are observed only when the motion is so slow that the deformation from the spherical shape is small. Larger or faster bubbles deform into a variety of shapes,[3] often with a cusp at the bottom end. An example of such a deformed shape is shown in Fig. 2.6-2. This bubble is not even rotationally symmetric but has a bottom end in the form of a knife edge, as evidenced by the two photographs of the same bubble taken at right angles. In fact the knife edge appears to continue into a thin sheet of air that eventually dissolves in the liquid. Thus one may say that the bubble in Fig. 2.6-1 is a "closed shape," whereas that in Fig. 2.6-2 is an "open shape." An important difference between bubbles with closed shapes and open shapes is that surface active impurities in the fluid may accumulate on the surface of the former but not on the latter type of bubbles. Surface-active impurities tend to immobilize bubble surfaces and hence retard the motion of gas bubbles. Thus a discontinuous change in bubble shape from a closed bubble (Fig. 2.6-1) to an open shape (Fig. 2.6-2) may be responsible for a discontinuous

[1] See J. F. Harper, *Adv. Appl. Mech.*, **12**, 59–129 (1972) and R. Clift, J. R. Grace, and M. E. Weber, *Bubbles, Drops, and Particles*, Academic Press, New York (1978).

[2] For extensive reviews see H. Giesekus, *Z. Angew. Math. Mech.*, **58**, T26–T36 (1978), and P. O. Brunn, *J. Non-Newtonian Fluid Mech.*, 7, 271–288 (1980).

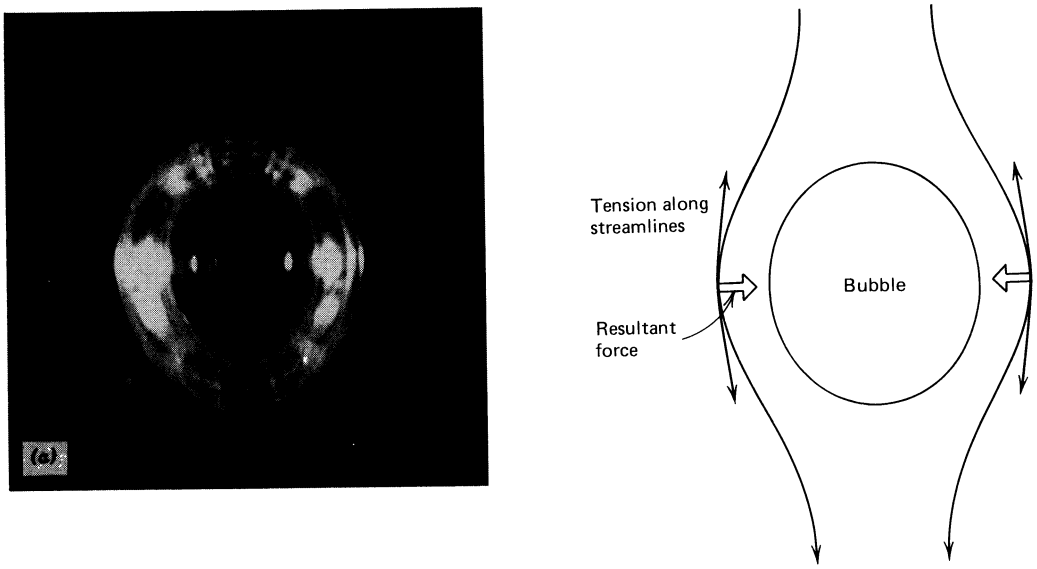

FIGURE 2.6-1. (*a*) Slightly deformed gas bubble of volume approximately 24 mm^3 rising with velocity 0.2 mm/s in a 1% solution of polyacrylamide in glycerin. [Photograph by O. Persson, Instituttet for Kemiteknik, Danmarks tekniske Højskole, Danmark]; (*b*) qualitative explanation of deformation in terms of an extra tension along the streamlines tending to squeeze the bubble at its equator. The streamlines are seen by an observer moving with the bubble.

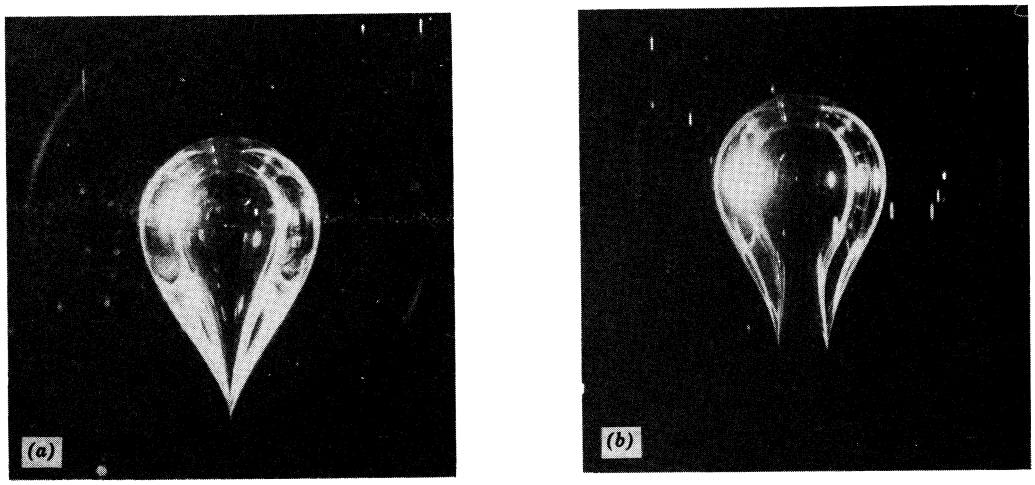

FIGURE 2.6-2. Highly distorted gas bubble of volume approximately 2100 mm^3 rising with velocity 10 mm/s in a polyacrylamide solution. The bubble is seen from two mutually perpendicular directions. Note that the bottom end is not axisymmetric. [Photographs by O. Persson, Instituttet for Kemiteknik, Danmarks tekniske Højskole, Danmark.]

increase in the rise velocity that is often encountered[3] when bubbles exceed a certain critical size.

b. Negative Wake

We now compare measurements of fluid velocity in the wakes behind gas bubbles rising in Newtonian and non-Newtonian fluids. The measurements reveal the unexpected phenomenon that the fluid velocity behind the bubbles in polymeric liquids is in the downward direction away from the rising bubbles (the velocities are referred to an observer at rest with respect to the liquid far from the bubbles). Thus the liquid velocity is opposite to the velocity in the usual wake behind objects moving in Newtonian fluids, and the phenomenon has been termed "negative wake."[4]

Consider in Fig. 2.6-3 Ⓝ the fluid velocity on the axis of a gas bubble rising in a viscous Newtonian liquid (a 99% glycerol-1% water mixture at 295 K). The position and velocity of the bubble is indicated in Fig. 2.6-3 Ⓝ by the width and height of the rectangle. The figure shows that while some fluid is pushed in front of the bubble, more fluid is pulled along behind the bubble. Consider now in Fig. 2.6-3 Ⓟ the fluid velocity on the axis of a gas bubble in a 1% solution of polyacrylamide in glycerol. The figure clearly shows that the fluid behind the bubble instead of being pulled along in the usual wake pattern is in fact "recoiling" away from the bubble. Negative wakes can be observed behind solid spheres as well as behind bubbles.[5]

c. Particle Interaction in Homogeneous Flow

A particularly simple example of a particle interaction phenomenon in non-Newtonian fluids occurs when two spheres of equal size and mass slowly settle along their line of centers in a fluid at rest far from the spheres. It is known[6] that in Newtonian fluids the two spheres will fall with the same speed so that the distance between them is constant, provided the Reynolds number is low. However in non-Newtonian fluids the two spheres will not fall with the same speed. Riddle, Narvaez, and Bird[7] discovered that if the initial separation is larger than a certain critical separation the spheres will diverge, whereas if it is smaller than this separation they will converge. The diverging of the spheres is probably related to a negative wake behind the leading sphere.

An even more spectacular interaction effect occurs in homogeneous shear flow of polymeric liquids with suspended spheres. During the shear flow, the suspended spheres rearrange to form chain structures. This effect seems to have been first described by Highgate and Whorlow.[8,9] In an investigation of the effect Michele, Pätzold, and Donis[10] used a suspension of glass spheres (60–70 μm in diameter) in a 0.5% solution of

[3] G. Astarita and G. Apuzzo, *AIChE J.*, **11**, 815–820 (1965); P. H. Calderbank, D. S. L. Johnson, and J. Loudon, *Chem. Eng. Sci.*, **25**, 235–256 (1970), L. G. Leal, J. Skoog, and A. Acrivos, *Can. J. Chem. Eng.*, **49**, 569–575 (1971), M. Coutanceau and M. Hajjam, *Appl. Sci. Res.*, **38**, 199–207 (1982).

[4] O. Hassager, *Nature*, **279**, 402–403 (1979).

[5] D. Sigli and M. Coutanceau, *J. Non-Newtonian Fluid Mech.*, **2**, 1–22 (1977); C. Bisgaard and O. Hassager, *Rheol. Acta*, **21**, 537–539 (1982); C. Bisgaard, *J. Non-Newtonian Fluid Mech.*, **12**, 283–302 (1983).

[6] J. Happel and H. Brenner, *Low Reynolds Number Hydrodynamics*, 2nd ed., Noordhoff, Leiden (1973).

[7] M. J. Riddle, C. Narvaez, and R. B. Bird, *J. Non-Newtonian Fluid Mech.*, **2**, 23–25 (1977).

[8] D. J. Highgate, *Nature*, **211**, 1390–1391 (1966); D. J. Highgate and R. W. Whorlow in R. E. Wetton and R. W. Whorlow, eds., *Polymer Systems: Deformation and Flow*, Macmillan, London (1968), pp. 251–261.

[9] D. J. Highgate and R. W. Whorlow, *Rheol. Acta*, **8**, 142–151 (1969).

[10] J. Michele, R. Pätzold, and R. Donis, *Rheol. Acta*, **16**, 317–321 (1977).

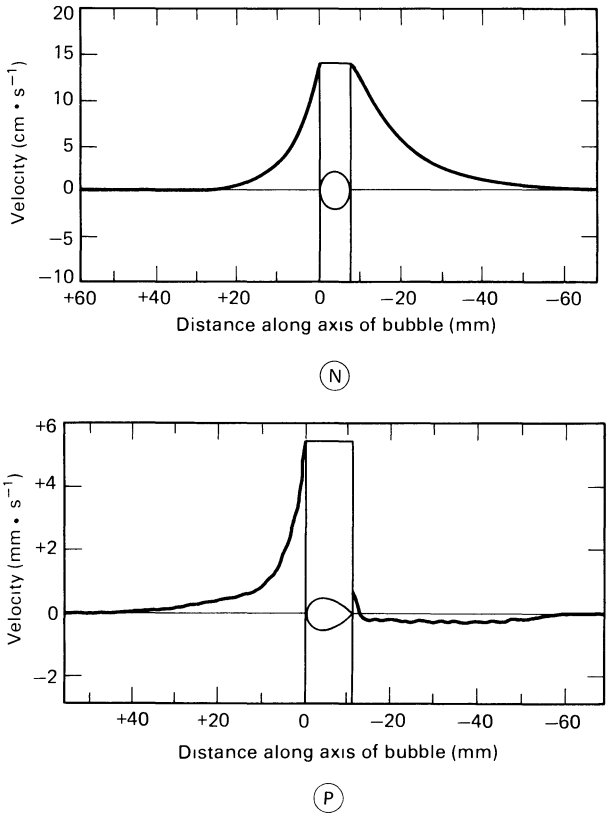

FIGURE 2.6-3. (N) Axial component of liquid velocity on the axis of a gas bubble of volume 400 mm^3 rising in a viscous Newtonian liquid (a 99% glycerol–1% water mixture at 295 K). The position of the bubble is indicated by the tall rectangle, the height of which indicates the rise velocity of the bubble (14.2 cm/s). The data are obtained from an experiment in which a bubble rising at constant speed along the axis of a glass cylinder passes a test section in which two photocells measure the rise velocity of the bubble and a laser-Doppler anemometer measures the axial component of the liquid velocity at a fixed point on the axis of the cylinder as a function of time. A third photocell in line with one of the anemometer beams indicates exactly when the bubble enters into and exits from the point of the velocity measurement. The constant rise velocity of the bubble allows a transformation of the velocity versus time record into the velocity versus space representation shown. (P) Representation of the axial component of fluid velocity on the axis of a gas bubble of volume 460 mm^3 rising in a solution of polyacrylamide in glycerol at 295 K. [Reprinted by permission from O. Hassager, *Nature*, **279**, 402–403 (1979). Copyright © 1979 Macmillan Journals Limited.]

polyacrylamide in water. A droplet of the suspension was placed between two glass plates which were squeezed together to a separation of approximately 100 μm. Figure 2.6-4*a* shows the more or less random distribution of the spheres after this process. Then the top plate was moved sideways, thus creating a shear flow between the plates. Figure 2.6-4*b* shows the distribution of the spheres after a movement of about 3 cm. Then the top plate was moved back and forth a number of times, and this gave the distribution in Fig. 2.6-4*c*. Further movement resulted in the distribution with just two chains of spheres in Fig. 2.6-4*d*. Michele, Pätzold, and Donis found that this striking alignment effect is strongly dependent on polymer concentration, being even more pronounced at higher polymer concentrations. They further concluded from, say, Fig. 2.6-4*b* that long range hydrodynamic forces must be

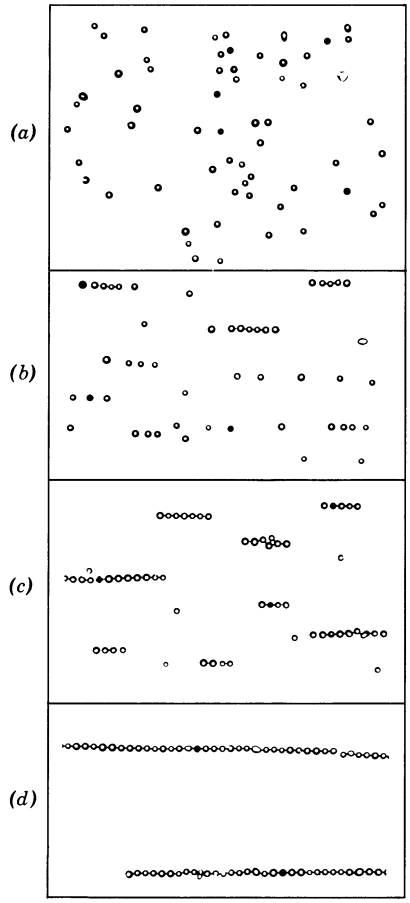

FIGURE 2.6-4. A 1.2% suspension of glass spheres (60–70 μm) in a 0.5% solution of polyacrylamide in water: (*a*) initial, random configuration; (*b*) after shearing movement of top plate of about 3 cm; (*c*) after top plate was moved back and forth several times; (*d*) and after further and faster movement of top plate. [Reproduced from J. Michele, R. Pätzold, and R. Donis, *Rheol. Acta*, **16**, 317–321 (1977).]

more important than short-range electrostatic forces between the spheres. An interpretation of the effect in terms of normal stresses has been given by Giesekus.[2]

§2.7. EFFECTS OF POLYMER ADDITIVES IN TURBULENT FLOW

Except for the discussion on vortex inhibition, we have been dealing with unusual phenomena in polymer melts and polymer solutions with concentrations roughly of the order of 0.1% and higher. Since the viscosity of such systems is usually very high, turbulence is seldom encountered. In this section we are going to see some non-Newtonian effects in solutions with polymer concentrations of the order of 10–500 ppm. With such minute amounts of polymer added to a Newtonian fluid the viscosity of the fluid is not appreciably changed when measured in laminar flow. However when the fluids undergo turbulent motion some dramatic effects are encountered, as illustrated in the following.

a. Drag Reduction

In 1948 Toms[1] discovered that if he added a very small amount of polymethylmethacrylate, approximately 10 ppm by weight, to monochlorobenzene undergoing turbulent tube flow, a substantial reduction in pressure drop at the given flow rate resulted. This reduction in pressure drop in the polymer solution relative to the pure solvent alone at the same flow rate is defined as *drag reduction.* Since then any number of polymer-solvent pairs have been found to show drag reduction. Three additional examples give an idea of the variety of possible systems: polyisobutylene in decalin, carboxymethylcellulose in water, and polyethylene oxide in water.

Drag reduction results may be presented conveniently in terms of the Fanning friction factor f:

$$f = \frac{1}{4}\left(\frac{D}{L}\right)\frac{\mathscr{P}_0 - \mathscr{P}_L}{\frac{1}{2}\rho\langle v\rangle^2} \tag{2.7-1}$$

where $\mathscr{P}_0 - \mathscr{P}_L$ is the modified pressure drop over a length L of the tube, D is the tube diameter, and $\langle v\rangle$ is the average velocity over a cross section of the tube. The friction factor is essentially a dimensionless pressure gradient, and it is a function only of the Reynolds

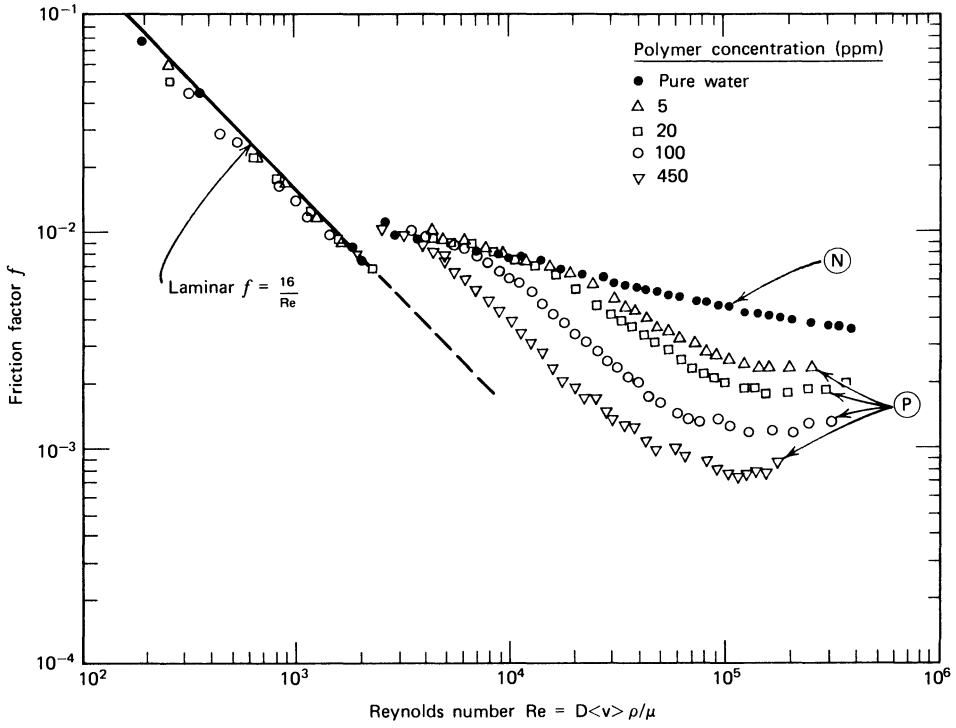

FIGURE 2.7-1. Friction factor for dilute aqueous solutions of polyethylene oxide, $\bar{M}_v = 6.1 \times 10^6$. In the turbulent regime, the curves for the polymer solutions lie below that of the solvent and illustrate drag reduction. [Data replotted from P. S. Virk, Sc.D. Thesis, Massachusetts Institute of Technology, Cambridge, MA (1966). See also C. B. Wang, *Ind. Eng. Chem. Fundam.*, **11**, 546-551 (1972).]

[1] B. A. Toms in *Proceedings of the International Congress on Rheology* (Holland, 1948), North-Holland, Amsterdam (1949), pp. II.135-II.141; *Phys. Fluids*, **20**, S3-S5 (1977). The latter reference is in a special number of the journal devoted entirely to turbulence and drag reduction. See also P. S. Virk, *AIChE J.*, **21**, 625-656 (1975); W. D. McComb and L. H. Rabie, *AIChE J.*, **28**, 547-557, 558-565 (1982). For a study of the drag-reducing properties of fish mucus, see T. L. Daniel, *Biol. Bull.*, **160**, 376-382 1981).

number $\mathrm{Re} = D\langle v\rangle\rho/\mu$ for fully developed flow of Newtonian fluids. At the very tiny polymer concentrations of interest in drag reduction, the viscosity and density of the polymer solution differ only slightly from those of the pure solvent. Nonetheless, the effect of the polymer additive is to lower the value of the friction factor at a given Reynolds number. The amount by which the friction factor is lowered is a measure of the amount of drag reduction.[2]

Figure 2.7-1 shows the friction factor for water with and without a small amount of polyethylene oxide. It is clear from this figure that the drag reduction is strictly a turbulent flow phenomenon; it does not result from maintaining laminar flow past the usual transition region. Note also that whereas the addition of only 5 ppm of polyethylene oxide to water gives a 40% reduction in f at $\mathrm{Re} = 1.0 \times 10^5$, the viscosity of the solution is only 1.0% greater than the viscosity of the water alone.

Although the mechanism producing drag reduction is not yet known, a number of polymer characteristics making for good drag reducers have been determined. A long-chain backbone and flexibility are important characteristics of good drag-reducing agents. For instance, of two polymers with the same molecular weight and same structural units, a linear one will be more effective than a highly branched one. Also, for two different polymers of similar configuration and the same molecular weight, the one with the lower molecular weight monomer will have the greater drag-reducing effect if both are utilized at the same weight concentration.

b. Effect of Polymer Additives on Heat Transfer in Turbulent Flow

Consider a fluid flowing in a pipe of diameter D at a sufficiently high Reynolds number so that the flow is turbulent. The tube is jacketed by a heater so as to provide a constant heat flux q_0 to the fluid in the region of interest. As is customary, the heat transferred from the wall to the fluid may be expressed in terms of a local Stanton number St

$$St = \frac{q_0}{(T_w - T_b)\hat{C}_p G} = \frac{h}{\hat{C}_p G} \tag{2.7-2}$$

where $(T_w - T_b)$ represents the local difference between the wall temperature and the bulk temperature of the fluid, $\hat{C}_p$ is the fluid heat capacity per unit mass, $G = \langle\rho v\rangle$ is the mass velocity, and h is the local heat transfer coefficient.[3] On the order of 25 diameters down the tube from the entrance to the heated section, the local Stanton number becomes independent of position, and it is this measure of heat transfer that is of interest here.[4]

In Fig. 2.7-2 we present some data[5] taken on a polymer solution consisting of 50 ppm of a high molecular weight polyethylene oxide in water. Both friction factor and

[2] Provided the polymer additive has negligible effect on the viscosity and density of the solvent, then the drop in f at fixed Re will agree with the definition of the amount of drag reduction given before.

[3] For more on the various ways of presenting heat-transfer results see R. B. Bird, W. E. Stewart, and E. N. Lightfoot, *Transport Phenomena*, Wiley, New York (1960), Chapt. 13.

[4] See M. K. Gupta, A. B. Metzner, and J. P. Hartnett, *Int. J. Heat Mass Transfer*, **10**, 1211-1224 (1967).

[5] These data are given by P. M. Debrule and R. H. Sabersky, *Int. J. Heat Mass Transfer*, **17**, 529-540 (1974). Other data on this problem are given among others by K. A. Smith, G. H. Keurohlian, P. S. Virk, and E. W. Merrill, *AIChE J.*, **15**, 294-297 (1969); M. Poreh and U. Paz, *Int. J. Heat Mass Transfer*, **11**, 805-818 (1968); Y. Dimant and M. Poreh, *Adv. Heat Transfer*, **12**, 77-103 (1976); C. S. Wells, Jr., *AIChE J.*, **14**, 406-410 (1968); G. Marrucci and G. Astarita, *Ind. Eng. Chem. Fundam.*, **6**, 470-471 (1967); M. K. Gupta *et al.*, *loc. cit.*, Y. I. Cho, K. S. Ng, and J. P. Hartnett, *Lett. Heat Mass Transfer*, **7**, 347-351 (1980); E. F. Mathys and R. H. Sabersky, *Int. J. Heat Mass Transfer*, **25**, 1343-1351 (1982); and E. Y. Kwack, J. P. Hartnett, and Y. I. Cho, *Wärme- und Stoffübergang*, **16**, 35-44 (1982). Data on the analogous mass-transfer effect is given by Y. I. Cho and J. P. Hartnett, *Int. J. Heat Mass Transfer*, **24**, 945-951 (1981).

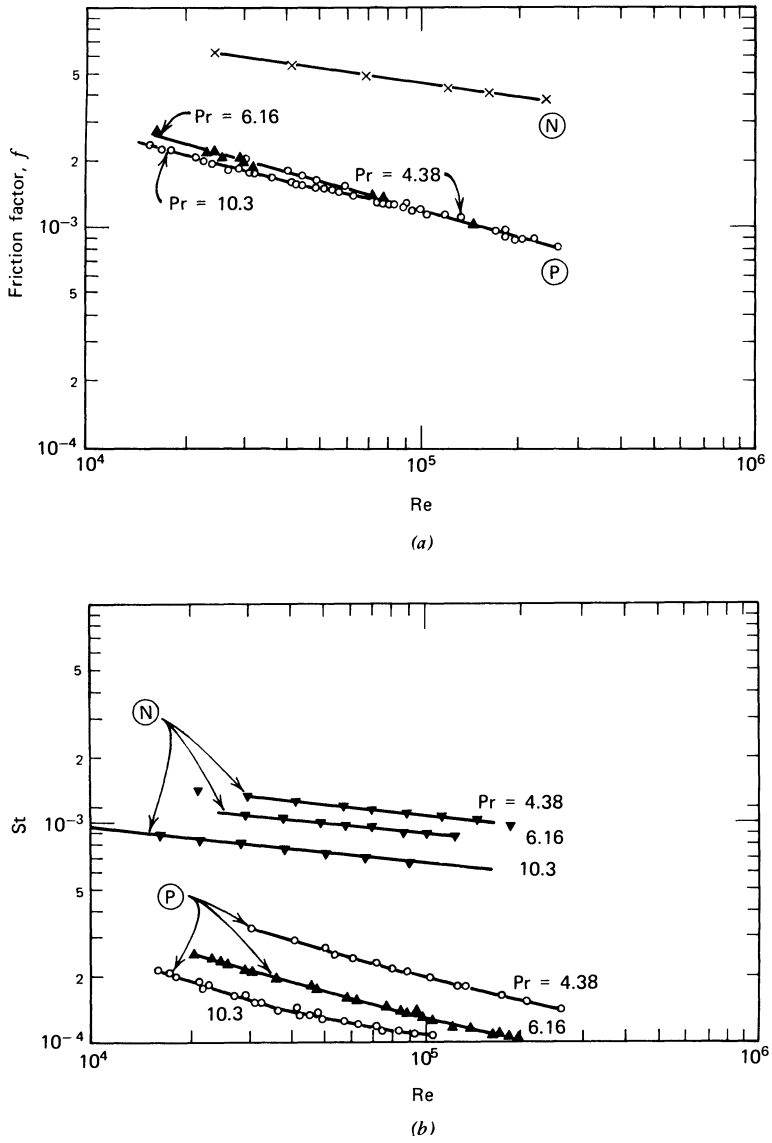

FIGURE 2.7-2. Turbulent heat transfer in water (N) and in a drag-reducing polymer solution consisting of 50 ppm polyethylene oxide in water (P). (*a*) The friction factor for water is lowered by the addition of a small amount of the polymer. The friction factor for the polymer solution shows a small dependence on the Prandtl number; the water curve is for all three values of Pr. (*b*) The decrease in Stanton number for the dilute polymer solution relative to the pure water is shown at three Prandtl numbers. [Reproduced from R. M. Debrule and R. H. Sabersky, *Int. J. Heat Mass Transfer*, **17**, 529-540 (1974).]

heat transfer results are included for comparison. The friction factor data show that drag reduction is indeed being realized. Note that varying the Prandtl number $\mathrm{Pr} = \hat{C}_p\mu/k$, where k is the thermal conductivity of the fluid, has little effect on f, as expected. The results for the Stanton number show a corresponding decrease after the addition of 50 ppm of the polymer. Even though the magnitude of the Stanton number shows a noticeable dependence on Pr, the percent decrease in St is roughly constant at a given Reynolds number. For

example, at $Re = 10^5$ the addition of 50 ppm polyethylene oxide reduces the Stanton number approximately 82% at all three Prandtl numbers shown. The decrease in St appears to be slightly more pronounced than the drop in friction factor (74% at $Re = 10^5$) for the drag-reducing system presented here. The results in Fig. 2.7-2 are for flow in a smooth tube. For a rough tube, the polymer additives produce an even larger drop in both f and St, with the Stanton number being lowered by nearly a factor of 10 by 50 ppm of polymer.

In nucleate boiling of dilute polymer solutions it has been found that polymer additives give rise to enhancement of heat transfer.[6] Photographic studies reveal differences in bubble size and bubble dynamics between pure fluids and those with polymeric additives.

c. Effect of Polymer Additives on Jet Breakup

In this final illustration we consider some high-speed photographs showing the break-up of jets.[7] In Fig. 2.7-3 we show two jets photographed 1 m from the orifice; the Newtonian jet is pure water, and the polymeric jet consists of water with 200-ppm polyethylene oxide added. Both jets are in the process of breakup, but they show a remarkable difference: around the pure water jet a number of satellite droplets appear, but

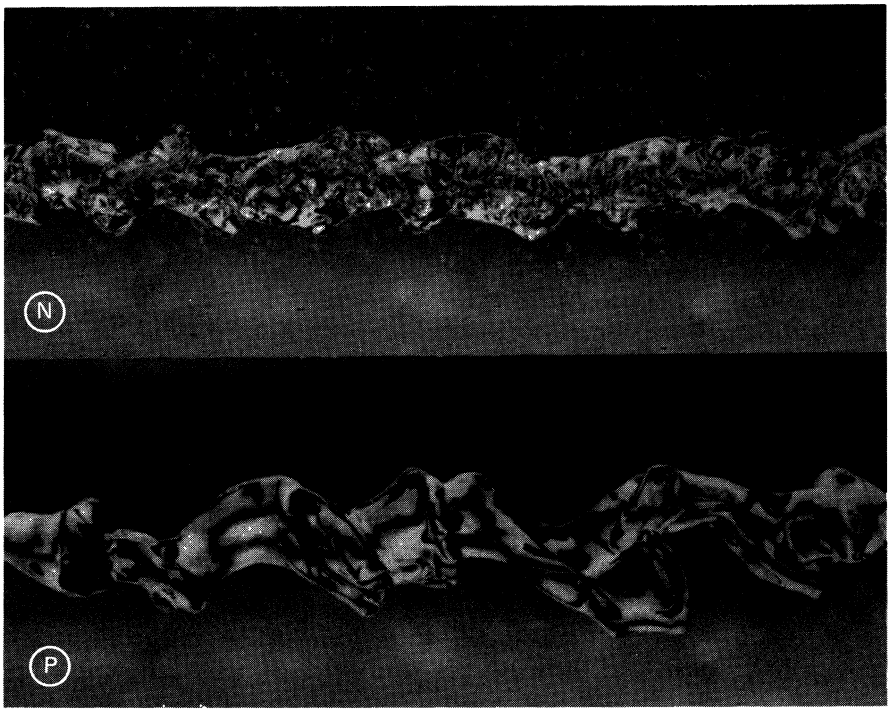

FIGURE 2.7-3. High-speed photographs of a jet 1 m from an orifice: (N) pure water and (P) 200 ppm solution of polyethyleneoxide in water. [Photographs courtesy of J. J. Taylor, Independent Consultant, Santa Barbara, CA, and J. W. Hoyt, Department of Mechanical Engineering, San Diego State University.]

[6] P. Kotchaphakdee and M. C. Williams, *Int. J. Heat Mass Transfer*, **13**, 835–848 (1970); H. J. Gannett, Jr., and M. C. Williams, *ibid.*, **14**, 1001–1005 (1971); D. D. Paul and S. I. Abdel-Khalik, *J. Rheol.*, **27**, 59–76 (1983).

[7] J. W. Hoyt and J. J. Taylor, *Phys. Fluids*, **20**, S253–S257 (1977).

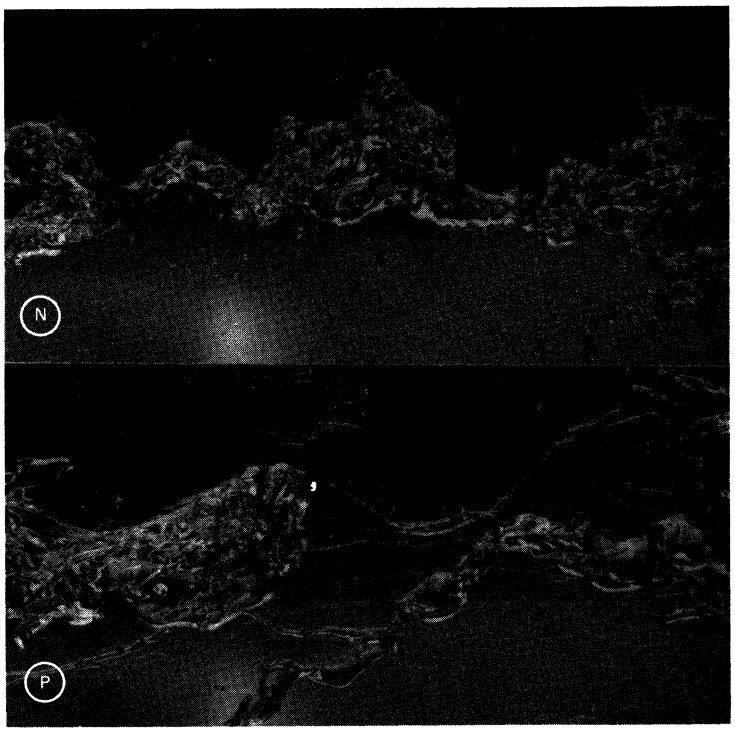

FIGURE 2.7-4. High-speed photographs taken 2 m from the orifice of the same two jets shown in Fig. 2.7-3. [Reproduced from photographs courtesy of J. J. Taylor, Independent Consultant, Santa Barbara, CA, and J. W. Hoyt, Department of Mechanical Engineering, San Diego State University.]

there are no satellite droplets near the jet with polymer additive. In Fig. 2.7-4 the same jets are shown 2 m from the orifice. Here both jets have disintegrated further. At this point some satellite droplets have also appeared in the jet with polymer additive. What is more striking, however, is that during breakup the polymer jet is pulled out into thin threads or filaments. Presumably it is the resistance of the polymer molecules to elongation that is responsible for this kind of jet breakup.

§2.8 DIMENSIONLESS GROUPS IN NON-NEWTONIAN FLUID MECHANICS

In Newtonian fluid mechanics the Reynolds number appears as a dimensionless group that may be interpreted roughly as a ratio of the magnitude of inertial forces to that of viscous forces. In any given flow situation other dimensionless numbers may arise (for example, geometric ratios), but the Reynolds number is generally the most important dimensionless group. Dimensionless groups are particularly useful for scaling arguments and also for cataloging flow regimes. For example, in tangential annular flow with the inner cylinder rotating, one can make visual observations and then determine the ranges of Reynolds numbers and radius ratios for which one has laminar flow, Taylor vortices, undulating vortices, and turbulence.

For viscoelastic fluids the key dimensionless group is the *Deborah number*, introduced by Reiner.[1] This number may be interpreted as the ratio of the magnitude of the

[1] M. Reiner, *Phys. Today*, **17**, 62 (Jan. 1964). Similar ideas (supported by experimental data on specific flow systems) were independently proposed by R. B. Bird, *Can. J. Chem. Eng.*, **43**, 161-167 (1965).

elastic forces to that of the viscous forces. It is defined as the ratio of a characteristic time (or "time scale") of the fluid, λ, to a characteristic time (or "time scale") of the flow system, t_{flow}

$$\text{De} = \lambda / t_{\text{flow}} \tag{2.8-1}$$

The characteristic time of the fluid is often taken to be the largest time constant describing the slowest molecular motions, or else some mean time constant determined by linear viscoelasticity (see Table 5.3-1); sometimes the characteristic time is chosen to be a time constant in a constitutive equation. The characteristic time for the flow is usually taken to be the time interval during which a typical fluid element experiences a significant sequence of kinematic events; sometimes it is taken to be the duration of an experiment or experimental observation. If the flow following a material particle is steady, then the characteristic time is taken to be the reciprocal of a characteristic strain rate. In Fig. 2.8-1 we show four steady-state flows and suggest useful definitions of the Deborah number.

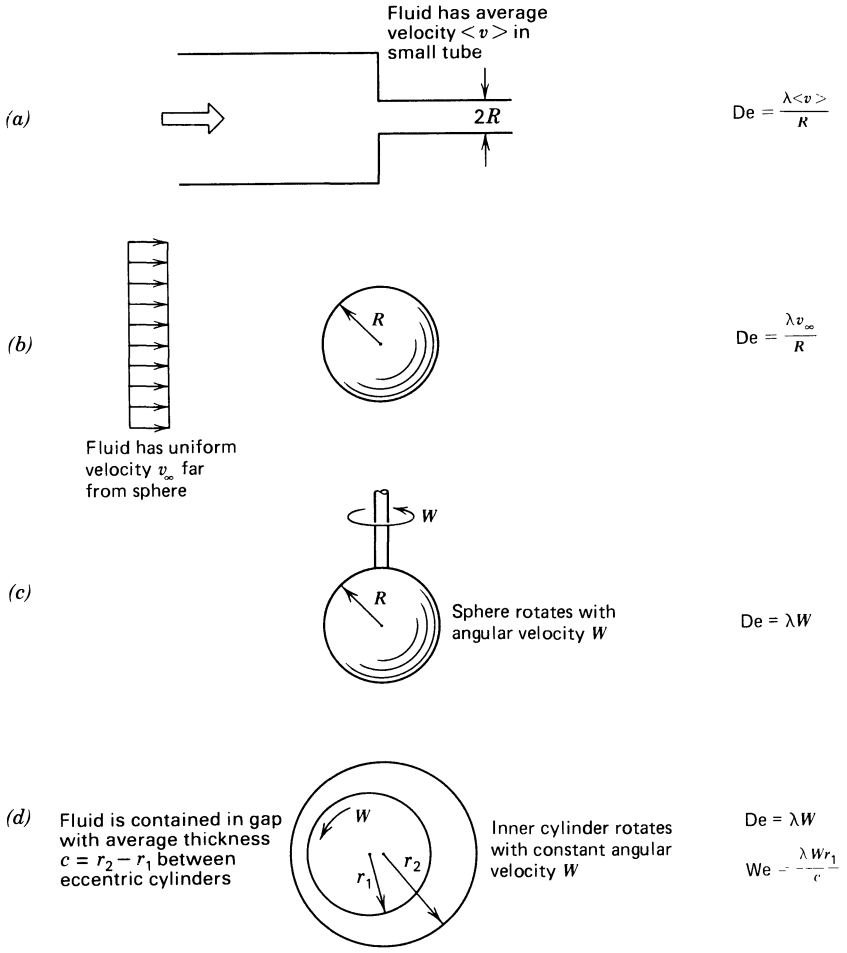

FIGURE 2.8-1. Four flow systems for illustrating the definition of De (Eq. 2.8-1) and We (Eq. 2.8-2): (*a*) flow through a sudden contraction; (*b*) flow around a sphere; (*c*) flow near a rotating sphere; and (*d*) flow between eccentric cylinders (journal bearing). Since two time scales for the flow can be identified for the eccentric cylinder flow, we use the characteristic shear rate to construct We, and the time required to execute one revolution to construct De.

For some problems there is more than one characteristic time for the flow that can be identified. For example in the eccentric cylinder flow in Fig. 2.8-1, one time scale is W^{-1} which gives the order of magnitude of the time required to move once around the cylinders; a second time scale for this problem is c/Wr_1 which is the reciprocal of the mean shear rate between the cylinders. A second dimensionless group, the *Weissenberg number*, that is sometimes used in polymer fluid dynamics involves a ratio of λ to this second characteristic time. The Weissenberg number We is defined by:

$$\text{We} = \lambda\kappa \tag{2.8-2}$$

where κ is a characteristic strain rate in the flow. For many problems, however, there is only one characteristic time that can be identified, and for these problems we choose to use the Deborah number as the dimensionless group.

Two limiting values of the Deborah number can be identified with classical mechanics. If the Deborah number is small, then thermal motions keep the polymer molecules more or less in their equilibrium configurations, and the polymeric fluid shows only minor qualitative differences from a Newtonian fluid. We say that Newtonian fluid behavior is obtained in the limit $\text{De} \to 0$. Conversely, if the Deborah number is large, polymer molecules that are distorted by the flow will not have time to relax during the time scale of the process or experiment. In the limit $\text{De} \to \infty$ the experiment happens so fast that the polymer molecules have no time to change configuration, and the fluid behaves more or less as a Hookean elastic solid. For many polymeric liquids, λ lies between 10^{-3} s for dilute solutions and 10^{3} s for concentrated solutions and melts. Since the characteristic times for flow systems are often in the same range, a wide spectrum of De values is easily obtainable. In the figures given earlier in this chapter the labeling Ⓝ and Ⓟ could just as well be replaced by the statements $\text{De} < \text{De}_{\text{crit}}$ and $\text{De} > \text{De}_{\text{crit}}$, where the actual value of the

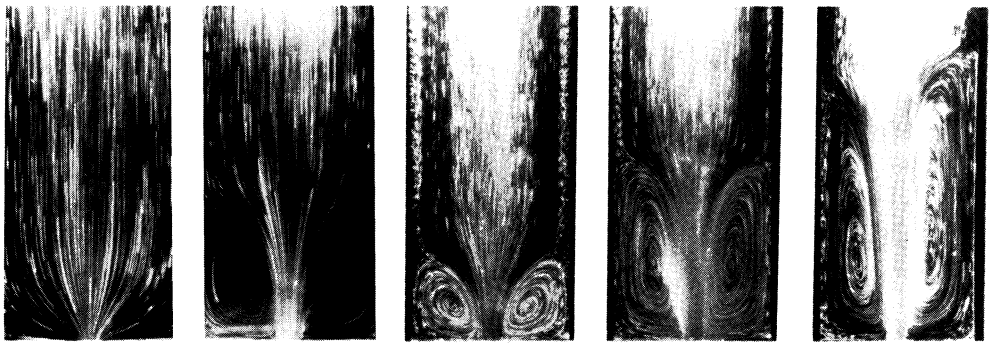

(*a*) (*b*) (*c*) (*d*) (*e*)

FIGURE 2.8-2. Streak photographs showing the streamlines for the flow downward through an axisymmetric sudden contraction with contraction ratio 7.675 to 1 as a function of De. (*a*) De = 0 for a Newtonian glucose syrup. (*b–e*) De = 0.2, 1, 3, and 8 respectively for a 0.057% polyacrylamide glucose solution. From De = 1 to 3, the non-Newtonian vortex grows, but the flow remains two-dimensional and axisymmetric. For De > 3, the vortex becomes asymmetric and a swirling component to the flow is observed. At Deborah numbers higher than 8, the flow becomes very erratic. The Deborah number is defined by $\lambda\langle v\rangle/R$ where λ is estimated as the longest relaxation time for the polyacrylamide solution and R is the small tube radius. [Reproduced from D. V. Boger and H. Nguyen, *Polym. Eng. Sci.* **18**, 1038–1043 (1978).]

critical Deborah number depends on the specific choices for λ and t_{flow}. For many systems De_{crit} has been found to be about unity.

Notice from the above discussion that there is in fact no such thing as a non-Newtonian fluid in and of itself. The value of the Deborah number which describes the extent of the non-Newtonian behavior depends on both λ and t_{flow}. It is in fact precisely this double dependence on the respective times of the fluid and the flow that motivated Reiner to name the ratio after the prophetess Deborah[1,2] who said: "The mountains flowed before the Lord." Indeed the time constants for mountain flow are so large that within the time span of human life they will behave as solids. However, the Lord has an infinite time available for observation and in this time span the mountains will flow as Newtonian fluids with $\text{De} = 0$.

We can illustrate the significance of De in two simple experiments with "silly putty." This unvulcanized silicone rubber has a time constant of the order of seconds, so that it behaves as a solid in experiments of duration much less than one second, and as a fluid in experiments lasting many minutes. For example, if we roll silly putty into a ball and bounce it on a hard surface, it will bounce like a solid rubber ball. However, if the silly putty is left in a container for an hour, it will flow so as to fill the container the way fluids do.

As an illustration of the classification of flow regimes in a complex flow by using De, we direct the reader's attention to Fig. 2.8-2. Here streak photographs by Boger and Nguyen[3] are shown for flow of a 0.057% polyacrylamide glucose solution through a sudden contraction for a series of different Deborah numbers. Since the fluid is fixed in these experiments, the time constant λ is also fixed. The Deborah number ($\lambda\langle v\rangle/R$; cf. Fig. 2.8-1) is thus varied by increasing the volume flow rate through the contraction. Note that when De is of order unity, the first very large deviations from Newtonian behavior are observed.

In a given flow problem we may define a Reynolds number in addition to the Deborah number and possibly the Weissenberg number. Then any combination of these numbers, such as their product or their ratio, is also a dimensionless number, and several such have in fact been named.[4] We make no use of these other combinations in this text.

PROBLEMS

2A.1 Calculation of Molecular Weight Averages

A polymer blend is being prepared by mixing 80 kg of one polymer sample A (number average molecular weight $\bar{M}_{n,A} = 10{,}000$ g/mol and weight average molecular weight $\bar{M}_{w,A} = 15{,}000$ g/mol) with 20 kg of another sample B ($\bar{M}_{n,B} = 20{,}000$ g/mol and $\bar{M}_{w,B} = 50{,}000$ g/mol). It is desired to

[2] From Deborah's Song, Judges, 5:5.

[3] D. V. Boger and H. Nguyen, *Polym. Eng. Sci.*, **18**, 1038–1043 (1978). More recent experiments by S. J. Muller, Sc.D. Thesis, Massachusetts Institute of Technology, Cambridge (1986) have shown that the flow transitions with increasing De are even more complex than those shown in Fig. 2.8-2. Prior to the development of the large vortex, as De is increased from small values a transition to a three-dimensional, time-periodic flow is found at De approximately equal to 0.6. The fluid is observed to undergo torsional oscillations as it moves through the contraction. For De approximately equal to unity, the flow again becomes steady state and two-dimensional. Once the flow has returned to steady state, the non-Newtonian vortex is observed. See also, J. V. Lawler, S. J. Muller, R. A. Brown, and R. C. Armstrong, *J. Non-Newtonian Fluid Mech.*, **20**, 51–93 (1986).

[4] For more on dimensionless groups, see G. Astarita and G. Marrucci, *Principles of Non-Newtonian Fluid Mechanics*, McGraw-Hill, New York (1974); J. R. A. Pearson, *Mechanics of Polymer Processing*, Elsevier, London (1985), Chapter 6; R. I. Tanner, *Engineering Rheology*, Oxford University Press (1985), pp. 190–192.

calculate the number average and weight average molecular weights of the mixture, $\bar{M}_{n,\text{mix}}$ and $\bar{M}_{w,\text{mix}}$, respectively.

Answer: $\bar{M}_{n,\text{mix}} = 1.11 \times 10^4$ g/mol

$\bar{M}_{w,\text{mix}} = 2.20 \times 10^4$ g/mol

2A.2 Comparison of Viscosity Determinations

The characteristics of two fluids, A and B, have been investigated by (1) measuring the terminal velocity of a sphere falling in a large bath of each fluid and by (2) measuring the volume flow rate of each at a specified pressure gradient. In (1) a 0.5 cm diameter sphere weighing 0.104 g fell with a terminal velocity of 0.75 cm/s in both fluids. However, in (2), fluids A and B had volumetric flow rates of 3.061×10^{-2} and 0.3455 cm^3/s, respectively, at an imposed pressure gradient of 6.857×10^4 Pa/m in a 0.210 cm diameter tube. The density of A is 1.0 g/cm^3, and the density of B is 1.014 g/cm^3. Based on these results which of the two fluids is definitely *not* Newtonian?

2B.1 The Heterogeneity Index

a. From the definitions, Eqs. 2.1-1 and 2 show that:

$$\frac{\bar{M}_w}{\bar{M}_n} - 1 = \frac{\sum_i \sum_j N_i N_j (M_i - M_j)^2}{2(\sum_i N_i M_i)^2} \tag{2B.1-1}$$

b. What does Eq. 2B.1-1 imply about the relative sizes of $\bar{M}_n$ and $\bar{M}_w$?

2B.2 Interpretation of the First Normal Stress Difference in Tangential Annular Flow[1]

a. In the limit that inertial forces are negligible, show that the equation of motion for tangential annular flow leads to:

$$\frac{d}{dr}(p + \tau_{rr}) = \frac{\tau_{\theta\theta} - \tau_{rr}}{r} \tag{2B.2-1}$$

b. Now consider the static forces that are present when a thin string wrapped around a cylinder of radius R is under tension T (see Fig. 2B.2). By making a force balance on a very short isolated segment of string, show that the reaction of the cylinder is a radial force of magnitude F_r, given by

$$\left(\frac{F_r}{l}\right) = \frac{T}{R} \qquad \left(\frac{l}{R} \ll 1\right) \tag{2B.2-2}$$

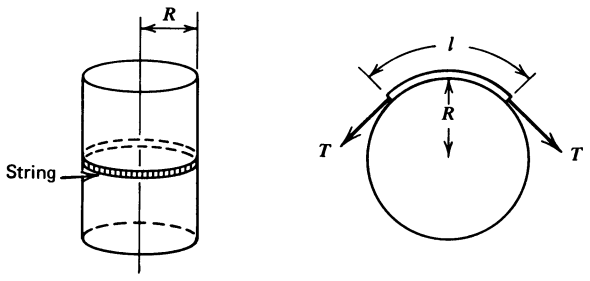

FIGURE 2B.2. Static forces acting by a string on a cylinder.

[1] This problem was suggested by A. S. Lodge, *Elastic Liquids*, Academic Press, New York (1964), p. 191.

c. Use the results from (**a**) and (**b**) to interpret physically the normal stresses in tangential annular flow. How does this relate to the rod-climbing experiment?

2B.3 Simplified Results for Hole Pressure

For many polymeric liquids the normal stress differences can be expressed as powers of the shear stress:[2]

$$\tau_{11} - \tau_{22} = -\kappa_1 |\tau_{21}|^{n_1} \tag{2B.3-1}$$

$$\tau_{22} - \tau_{33} = \kappa_2 |\tau_{21}|^{n_2} \tag{2B.3-2}$$

in which κ_1, κ_2, n_1, and n_2 are all constants. Show that for fluids in which these relations hold, the hole pressure results, Eqs. 2.3-15 to 17, simplify to

Circular hole:
$$p^* = -\frac{1}{3}\left(\frac{\tau_{11} - \tau_{22}}{n_1} - \frac{\tau_{22} - \tau_{33}}{n_2}\right)_w \tag{2B.3-3}$$

Transverse slot:
$$p^* = -\frac{1}{2n_1}(\tau_{11} - \tau_{22})_w \tag{2B.3-4}$$

Axial slot:
$$p^* = +\frac{1}{n_2}(\tau_{22} - \tau_{33})_w \tag{2B.3-5}$$

where the subscript w means "evaluated at the wall." One fluid model found in the literature, the second-order fluid, gives a value of 2 for both n_1 and n_2. The results above agree with derivations of the hole pressure made with the second-order fluid model assumed from the beginning[3] (Problem 6B.15).

2B.4 Free Surface Shape in a Tilted Trough[4]

It is desired to obtain an expression for the free surface shape of a fluid flowing down a tilted trough of semicircular cross section that is inclined at an angle β to the horizontal. To do this, parallel the development in Example 2.3-2.

a. First, consider steady flow in a tube of radius R inclined at an angle β. From the symmetry of the velocity field it can be shown that $\tau_{z\theta} = \tau_{r\theta} = 0$ for this flow (see §3.2). Combine this information with the equations of motion to show that the variation of $\pi_{\theta\theta}$ within the tube is given by

$$d\pi_{\theta\theta} = -\rho g \cos\beta \cos\theta \, r d\theta - \left(\frac{d}{dr} N_2 + \frac{N_2}{r} + \rho g \cos\beta \sin\theta\right) dr + \left(\frac{\partial p}{\partial z}\right) dz \tag{2B.4-1}$$

where $N_2 = \tau_{rr} - \tau_{\theta\theta}$ is the second normal stress difference and we have taken $\theta = 0$ to be horizontal.

b. Now imagine that the upper half of the tube and fluid is removed so that we are left with flow down a semicircular trough. The velocity profile in the trough will be identical to that in the lower half of the tube provided the normal stress distribution given in Eq. 2B.4-1 is maintained on the surface $\theta = 0$. Explain.

[2] K. Higashitani and W. G. Pritchard, *Trans. Soc. Rheol.*, **16**, 687-696 (1972).

[3] R. I. Tanner and A. C. Pipkin, *Trans. Soc. Rheol.*, **13**, 471-484 (1969), treat the transverse slot problem and E. A. Kearsley, *Trans. Soc. Rheol.*, **14**, 419-424 (1970) analyzes flow along an axial slot.

[4] A. C. Pipkin and R. I. Tanner, *Mech. Today*, **1**, 262-321 (1972); R. I. Tanner, *Trans. Soc. Rheol.*, 483-507 (1970). L. Sturges and D. D. Joseph, *Arch. Rat. Mech. Anal.*, **59**, 359-387 (1976), include surface tension in their analysis and also consider the onset of secondary flow with increasing β.

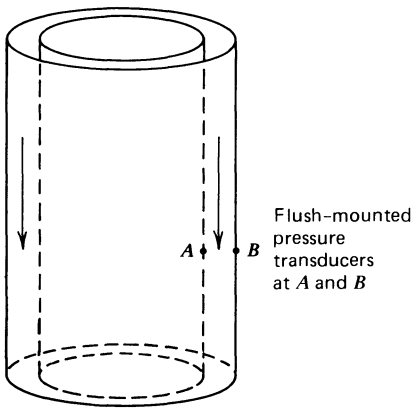

FIGURE 2B.5. Pressure measurements in axial annular flow. For a Newtonian fluid $p_A = p_B$, whereas for a polymeric fluid $\pi_{rr,A} > \pi_{rr,B}$.

c. In order to describe the free surface it is convenient to consider a Cartesian coordinate system oriented similarly to the one in Fig. 2.3-3: the z-axis is coincident with the axis of the trough, x lies in the horizontal plane, and y is positive in the upward direction. Show that the normal stress π_{yy} is given by

$$\pi_{yy}(x, y) = -\rho g y \cos\beta + \pi_{yy}(x, 0) + C$$

$$\pi_{yy}(x, 0) = -\int_0^x \frac{N_2}{x}\, dx - N_2(x) \tag{2B.4-2}$$

where C is an integration constant.

d. Show that the total bulge in the free surface of the fluid is

$$h = -\frac{\pi_{yy}(R, 0)}{\rho g \cos\beta} \tag{2B.4-3}$$

2B.5 Axial Annular Flow[5]

A fluid is pumped axially through the annular space between two concentric cylinders; the Reynolds number is small enough so that the flow is laminar. Small, flush-mounted pressure transducers (labeled A and B in Fig. 2B.5) are located on the cylinder walls opposite one another. For a Newtonian fluid, the pressure readings at A and B are found to be the same, so that $p_A = p_B$. For a viscoelastic fluid, it is found that $\pi_{rr,A}$ is slightly larger than $\pi_{rr,B}$. Use the r-component of the equation of motion to show that this difference in behavior between the Newtonian and polymeric fluids is consistent with a small, positive second normal stress difference. Assume that the two transducers are located at the same vertical position.

[5] J. W. Hayes and R. I. Tanner in E. H. Lee, ed., *Proceedings of the Fourth International Congress on Rheology*, Wiley-Interscience, New York (1965), Part 3, pp. 389-399; J. D. Huppler, *Trans. Soc. Rheol.*, **9:2**, 273-286 (1965); R. I. Tanner, *Trans. Soc. Rheol.*, **11**, 347-360 (1967). These measurements were made with hole-mounted transducers and actually showed $\pi_{rr,A} < \pi_{rr,B}$. When correction is made for the hole pressure, it is found that $\pi_{rr,A} > \pi_{rr,B}$ [A. C. Pipkin and R. I. Tanner, *Mech. Today*, **1**, 262-321 (1972)].

CHAPTER 3

MATERIAL FUNCTIONS FOR POLYMERIC LIQUIDS

Chapter 2 has demonstrated rather dramatically that Newton's law of viscosity is wholly inadequate for the description of macromolecular liquids. In this chapter we begin the task of discovering the proper way to describe these non-Newtonian fluids. The first step is the quantitative experimental characterization of their flow behavior. Recall that incompressible Newtonian fluids at constant temperature can be characterized by just two *material constants*: the density ρ and the viscosity μ. Once these quantities have been measured, the governing equations for the velocity and stress distributions in the fluid are fixed for any flow system. There are many steady-state and unsteady-state experiments from which μ can be determined.[1]

The experimental description of incompressible non-Newtonian fluids, on the other hand, is much more complicated. We can, of course, measure the density, but since we have no equation for τ analogous to Eq. 1.2-2, we do not know what other property or properties need to be measured. From the "fun experiments" that were presented in the last chapter, we know a little about what to expect. For example, if we try to measure a "viscosity" using a viscometer, this "viscosity" will not necessarily be a constant. Furthermore, we know from analyses of rod climbing and the tilted trough that normal stresses should also be measured. The recoil experiment in §2.5 indicates that unsteady-state experiments might also lead to additional information.

Whereas different isothermal experiments on a Newtonian fluid yield a single *material constant*, namely the viscosity, a variety of experiments performed on a polymeric liquid will yield a host of *material functions* that depend on shear rate, frequency, time, and so on. These material functions serve to classify fluids, and they can be used to determine constants in specific non-Newtonian constitutive equations. In this chapter, then, we shall present the standard flow patterns used in characterizing polymeric liquids and discuss the material functions that can be obtained from each. Representative fluid behavior will also be shown by means of sample experimental data. Once the reader understands the kind of fluid responses characteristic of polymeric materials in various experiments, the constitutive equations developed and used in the rest of the book will be more meaningful.

We begin this chapter with a description of the two standard kinds of flows, shear and shearfree, that are used to characterize polymeric liquids; the velocity and stress fields for these flows are described in §§3.1 and 3.2. Then in §§3.3 and 3.4 and in §3.5 we give the most common material functions that arise in these two types of flows, respectively. In §3.6

[1] A rather complete listing of standard techniques is given in J. R. Van Wazer, J. W. Lyons, K. Y. Kim, and R. E. Colwell, *Viscosity and Flow Measurement*, Wiley, New York (1963).

we present some of the most important experimental findings about the concentation, temperature, and molecular weight dependence of the material functions. Finally in §3.7 we return to the subject of kinematics and give a more detailed discussion of the identification of shear and shearfree flows.[2]

Whereas this chapter deals with the *description* of the nature and diversity of material response to simple shearing and shearfree flows, the analysis of *experimental methods* for measuring these quantities is not dealt with until Chapter 10. This discussion is deferred because constitutive equations are either helpful or necessary in the analyses.

§3.1 SHEAR AND SHEARFREE FLOWS

The two types of flows most often used to characterize polymeric liquids are *shear* flow and *shearfree* flow. We give examples of each and show that the relative motion of material particles is very different in these two types of flow. It is thus not surprising that the material information learned from the two types of flow is quite different. In this section we restrict our attention to *homogeneous* (or uniform) deformations[1] in which the velocity gradient is independent of position; in §3.7 nonhomogeneous flows are discussed.

a. Shear Flow

A *simple shear flow* is given by the velocity field

$$v_x = \dot{\gamma}_{yx} y; \quad v_y = 0; \quad v_z = 0 \tag{3.1-1}$$

in which the velocity gradient $\dot{\gamma}_{yx}$ can be a function of time. The absolute value of $\dot{\gamma}_{yx}$ is called the *shear rate*[2] $\dot{\gamma}$. For steady shear flow (sometimes called a *viscometric*[3] flow) the shear rate is independent of time; it is presumed that the shear rate has been constant for such a long time that all the stresses in the fluid are time-independent. A simple shear flow is easily generated between parallel plates as illustrated in Fig. 3.1-1. A characteristic of steady shear flows is that the distance l between two neighboring fluid particles, which are initially on the y-axis and separated by a distance l_0, is

$$l = l_0\sqrt{1 + (\dot{\gamma}\Delta t)^2} \sim l_0\dot{\gamma}\Delta t \qquad (\dot{\gamma} = \text{constant}) \tag{3.1-2}$$

after a time interval Δt; the second (approximate) expression is applicable when $\Delta t \to \infty$. The particles are seen to separate linearly in Δt for large Δt. A second distinguishing feature

[2] This section can be omitted on first reading.

[1] An extensive treatment of homogeneous deformation and flow is found in A. S. Lodge, *Elastic Liquids*, Academic Press, New York (1964); our description of kinematics has been strongly influenced by this book.

[2] The definition of shear rate $\dot{\gamma}$ given here is a special case of a more general formula that is given in Eqs. 3.7-3 and 4.1-8 and used in more complex shearing flows later in the book. The general formula gives $\dot{\gamma}$ as the magnitude of the rate-of-strain tensor (cf. Eq. A.3-21):

$$\dot{\gamma} = +\sqrt{(1/2)(\dot{\boldsymbol{\gamma}}:\dot{\boldsymbol{\gamma}})} \tag{3.1-1a}$$

so that $\dot{\gamma}$ is always a positive quantity.

[3] Viscometric flow is not restricted to $\dot{\gamma}_{yx}$ independent of position; see §3.7.

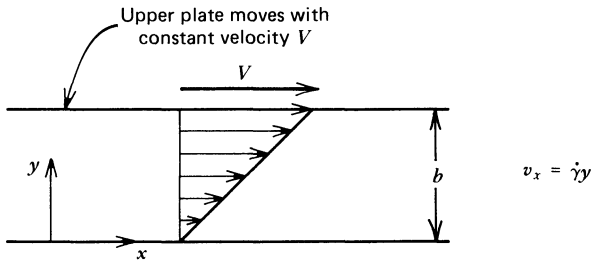

FIGURE 3.1-1. Steady simple shear flow with shear rate $\dot{\gamma} = V/b$. This flow is characterized by a one-parameter family of material surfaces, namely y = constant, which slide relative to one another.

of shear flows is that it is possible to identify a one-parameter family of material surfaces that slide relative to one another without stretching. For example, the flow in Fig. 3.1-1 is like the shearing of a deck of cards, with the family of material surfaces corresponding to the cards. Shearing flows are found in many polymer processing operations, for example, in injection molding and extrusion, and in many rheometer flows. In addition polymer melts and solutions are subjected to shear flow in transportation through ducts and in lubrication applications.

b. Shearfree Flow

Simple shearfree flows are given by the velocity field

$$\begin{aligned} v_x &= -\frac{1}{2}\dot{\varepsilon}(1+b)x \\ v_y &= -\frac{1}{2}\dot{\varepsilon}(1-b)y \\ v_z &= +\dot{\varepsilon}z \end{aligned} \tag{3.1-3}$$

where $0 \leq b \leq 1$ and $\dot{\varepsilon}$ is the *elongation rate*[4] which can depend on time. Several special shearfree flows are obtained for particular choices of the parameter b:

Elongational flow:	$(b = 0, \dot{\varepsilon} > 0)$
Biaxial stretching flow:	$(b = 0, \dot{\varepsilon} < 0)$
Planar elongational flow:	$(b = 1)$

The streamlines for elongational flow ($b = 0$) are illustrated in Fig. 3.1-2; the choice of b will affect the way the streamlines change with rotation about the z-axis. The effects of the three kinds of shearfree flow on a cube of material are illustrated for steady state in Fig. 3.1-3, where these deformations are compared with steady shearing. By steady shearfree flow we mean that $\dot{\varepsilon}$ is independent of time; it is presumed that the elongation rate has been constant for such a long time that all the stresses in the fluid are time-independent.

[4] Note that the magnitude of the rate-of-strain tensor $\dot{\gamma}$ given in Eq. 3.1-1a is equal to $\sqrt{3+b^2}|\dot{\varepsilon}|$ for simple shearfree flow.

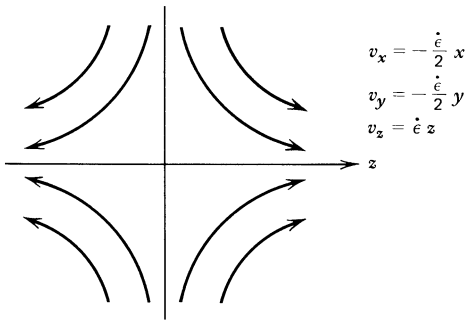

FIGURE 3.1-2. Steady elongational flow (shearfree flow with $b = 0$).

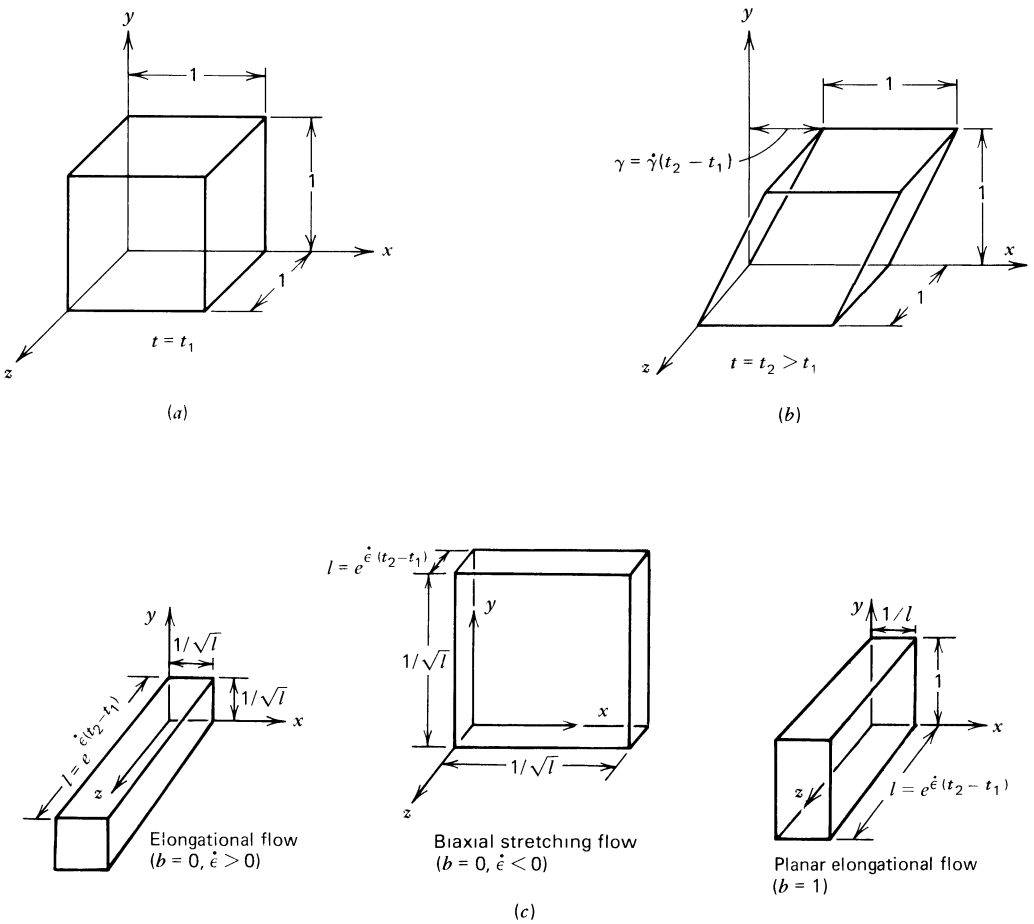

FIGURE 3.1-3. Deformation of (*a*) unit cube of material from time t_1 to t_2 ($t_2 > t_1$) in (*b*) steady simple shear flow and (*c*) three kinds of shearfree flow. The volume of material is preserved in all of these flows.

A distinguishing feature of steady shearfree flows that can be seen from Eq. 3.1-3 is that neighboring fluid elements move relative to one another at an exponential rate. For example two fluid particles on the z-axis which are initially separated by a distance l_0 will be separated by distance l after time Δt:

$$l = l_0 e^{\dot{\varepsilon}\Delta t} \qquad (\dot{\varepsilon} = \text{constant}) \tag{3.1-4}$$

This exponential rate of separation of fluid elements is much more rapid than the linear rate of separation in steady shear flow.

Shearfree flows are found in many polymer processing operations, for example, fiber spinning, film blowing, vacuum thermoforming, and sheet stretching; polymer foaming involves shearfree flow around bubbles. In addition many other flows, such as flows near stagnation points, flow through contractions, and flow around corners have a strong elongational character. Because of the shearing that must occur near the solid boundaries in these latter examples, they are not purely shearfree flows, however.

§3.2 THE STRESS TENSOR FOR SHEAR AND SHEARFREE FLOWS

Material functions relate the kinematics of a flow to the stress field needed to sustain the motion, so we must describe the stresses required for simple shear or shearfree motions. In this section we indicate how the stress tensor can be simplified for these two types of flows, and in addition we deduce which combinations of stress tensor components are experimentally accessible.

a. Shear Flows

For Newtonian liquids we know that in the shear flow of Eq. 3.1-1 only the shear stress τ_{yx} is nonzero. For non-Newtonian fluids we must assume, in the absence of a constitutive equation, that in any flow all six independent components of the stress tensor may be nonzero.[1] However, for simple shearing flows of incompressible liquids, it is possible to show that at most three independent combinations of components of the stress tensor can be measured (see Problem 3B.3). This conclusion is based on the invariance of the shear flow in Eq. 3.1-1 with respect to a 180° rotation about the z-axis and the assumptions that the fluid is isotropic, so that it has no preferred direction other than one introduced by the flow itself, and that the stress in the fluid depends only on the flow field. The most general form that the total stress tensor can have for a simple shearing flow is

$$\boldsymbol{\pi} = p\boldsymbol{\delta} + \boldsymbol{\tau} = \begin{pmatrix} p + \tau_{xx} & \tau_{yx} & 0 \\ \tau_{yx} & p + \tau_{yy} & 0 \\ 0 & 0 & p + \tau_{zz} \end{pmatrix} \tag{3.2-1}$$

[1] We will always take the stress tensor to be symmetrical. The theoretical possibility of a nonsymmetrical stress tensor is discussed by J. S. Dahler and L. E. Scriven, *Nature*, **192**, 36–37 (1961). To date no experiments have shown asymmetry in the stress tensor for amorphous liquids. Furthermore, almost all of the molecular theories for amorphous liquids give expressions for the stress tensor that are symmetrical (see §13.3 and other discussions in Volume 2).

However for incompressible fluids we cannot separate the pressure and normal stress contributions in normal force measurements on surfaces (see below Eq. 1.2-2). Hence, the only quantities of experimental interest are the shear stress and two normal stress differences. The stresses that are customarily used in conjunction with shear flow are:

Shear stress:	τ_{yx}	
First normal stress difference:	$\tau_{xx} - \tau_{yy}$	(3.2-2)[2]
Second normal stress difference:	$\tau_{yy} - \tau_{zz}$	

Hence there are only three independent, experimentally accessible quantities in simple shear flow.

b. Shearfree Flows

The shearfree flow given in Eq. 3.1-3 shows even more symmetry than does simple shear flow. From Fig. 3.1-3 it is clear that the description of the deformation is unaffected by a 180° rotation about the x-, y-, or z-axis. This symmetry coupled with the assumed fluid isotropy reduces the most general form of the stress tensor for shearfree flow to

$$\boldsymbol{\pi} = p\boldsymbol{\delta} + \boldsymbol{\tau} = \begin{pmatrix} p + \tau_{xx} & 0 & 0 \\ 0 & p + \tau_{yy} & 0 \\ 0 & 0 & p + \tau_{zz} \end{pmatrix} \tag{3.2-3}$$

When we restrict attention to incompressible fluids, there are only two normal stress differences of experimental interest:

$$\begin{matrix} \tau_{zz} - \tau_{xx} \\ \tau_{yy} - \tau_{xx} \end{matrix} \tag{3.2-4}$$

For the elongational and biaxial stretching flows for which $b = 0$ in Eq. 3.1-3, the x- and y-directions are indistinguishable so that $\tau_{xx} - \tau_{yy} = 0$ and there is only one normal stress difference to be determined for these flows.

We turn now in the next three sections to defining and describing material functions that give the three stress combinations in shear flow and the two normal stress differences in shearfree flow. A long list of material functions has been defined for these two types of flow fields, corresponding to the large variety of time-dependent $\dot{\gamma}_{yx}$ and $\dot{\varepsilon}$ that can be produced experimentally.

§3.3 STEADY SHEAR FLOW MATERIAL FUNCTIONS

As a consequence of the assumption made above that the stress tensor depends only on the flow field, we can say that the steady-state stresses in steady simple shear flow are functions only of the shear rate $\dot{\gamma}$. The *viscosity* η (also called the *non-Newtonian viscosity* or

[2] Some rheologists use N_1 to denote $-(\tau_{xx} - \tau_{yy})$ and N_2 to denote $-(\tau_{yy} - \tau_{zz})$.

shear-rate dependent viscosity) is defined analogously to the viscosity for Newtonian fluids (cf. Eq. 1.2-1):

$$\boxed{\tau_{yx} = -\eta(\dot{\gamma})\dot{\gamma}_{yx}} \tag{3.3-1}$$

Likewise, we can define normal stress coefficients Ψ_1 and Ψ_2 as follows:

$$\boxed{\tau_{xx} - \tau_{yy} = -\Psi_1(\dot{\gamma})\dot{\gamma}_{yx}^2} \tag{3.3-2}$$

$$\boxed{\tau_{yy} - \tau_{zz} = -\Psi_2(\dot{\gamma})\dot{\gamma}_{yx}^2} \tag{3.3-3}$$

The functions Ψ_1 and Ψ_2 are known as the *first* and *second normal stress coefficients*, respectively; η, Ψ_1, and Ψ_2 are sometimes collectively referred to as the *viscometric functions*. In Eq. 3.3-1 changing the sign of $\dot{\gamma}_{yx}$ will change the sign of the shear stress and therefore η must be an even function of $\dot{\gamma}_{yx}$. Similarly, in Eqs. 3.3-2 and 3 the normal stress differences will not change sign if $\dot{\gamma}_{yx}$ changes sign, so that Ψ_1 and Ψ_2 are also even functions of $\dot{\gamma}_{yx}$. This explains why η, Ψ_1, and Ψ_2 are written as function of $\dot{\gamma} = |\dot{\gamma}_{yx}|$ rather than $\dot{\gamma}_{yx}$. Sometimes it is more convenient to regard the viscometric functions as functions of the absolute value of the shear stress $\tau = |\tau_{yx}|$.

Experimentally, the viscosity is the best known of the viscometric functions. Some typical plots of $\eta(\dot{\gamma})$ are given in Figs. 3.3-1 to 4 for a polymer melt, concentrated solutions, and dilute solutions. At low shear rates, the shear stress is proportional to $\dot{\gamma}$, and the viscosity approaches a constant value η_0, the *zero-shear-rate viscosity*. At higher shear rates the viscosity of most polymeric liquids decreases with increasing shear rate.[1] For many

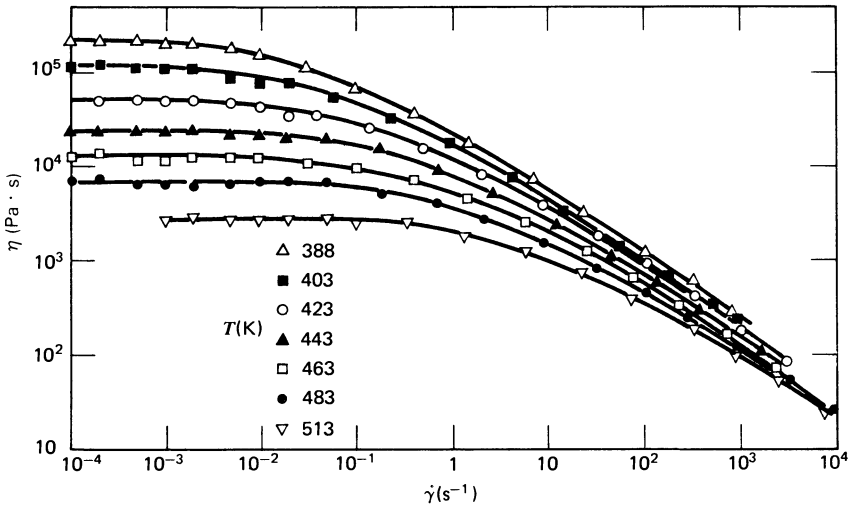

FIGURE 3.3-1. Non-Newtonian viscosity η of a low-density polyethylene melt (Melt I) at several different temperatures. The data taken at shear rates below 5×10^{-2} s^{-1} were obtained with a Weissenberg Rheogoniometer; the viscosity at higher shear rates was determined using a capillary viscometer. [J. Meissner, *Kunststoffe*, **61**, 576–582 (1971).]

[1] Almost all macromolecular fluids show this *shear thinning* or *pseudoplastic* behavior. A few fluids, called *shear thickening* or *dilatant fluids* are discussed by S. Burow, A. Peterlin, and D. T. Turner, *Polym. Lett.*, **2**, 67–70 (1964). See §2.2. For other "shear-thickening" data see M.-N. Layec-Raphalen and C. Wolff, *J. Non-Newtonian Fluid Mech.*, **1**, 159–173 (1976); they studied tube flow of dilute solutions of high molecular weight polystyrene in decalin.

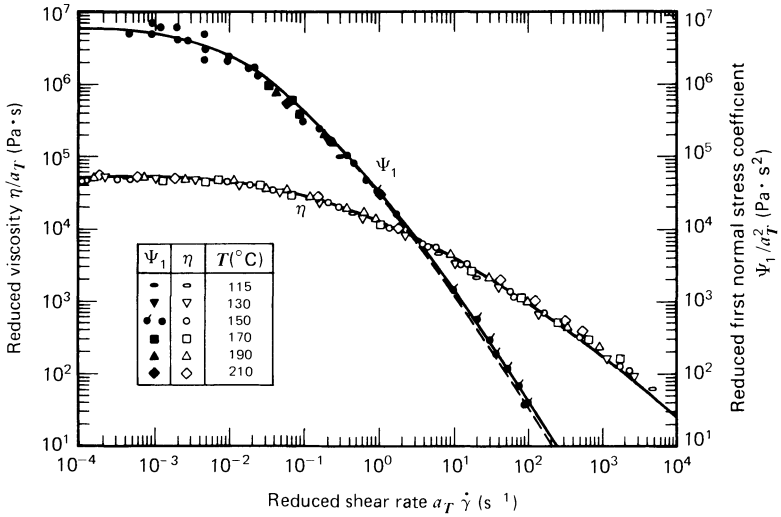

FIGURE 3.3-2. Master curves for the viscosity and first normal stress coefficient as functions of shear rate for the low-density polyethylene melt (Melt I) shown in Fig. 3.3-1. Data taken at the indicated temperatures were shifted to a reference temperature $T_0 = 423$ K. The shift factor a_T used here is given by $\eta_0(T)/\eta_0(T_0)$. The solid and dashed curves were calculated with the Wagner model described in §8.3, the solid line with a single term exponential "damping function" and the dashed line with two terms. [H. M. Laun, *Rheol. Acta*, **17**, 1-15 (1978).]

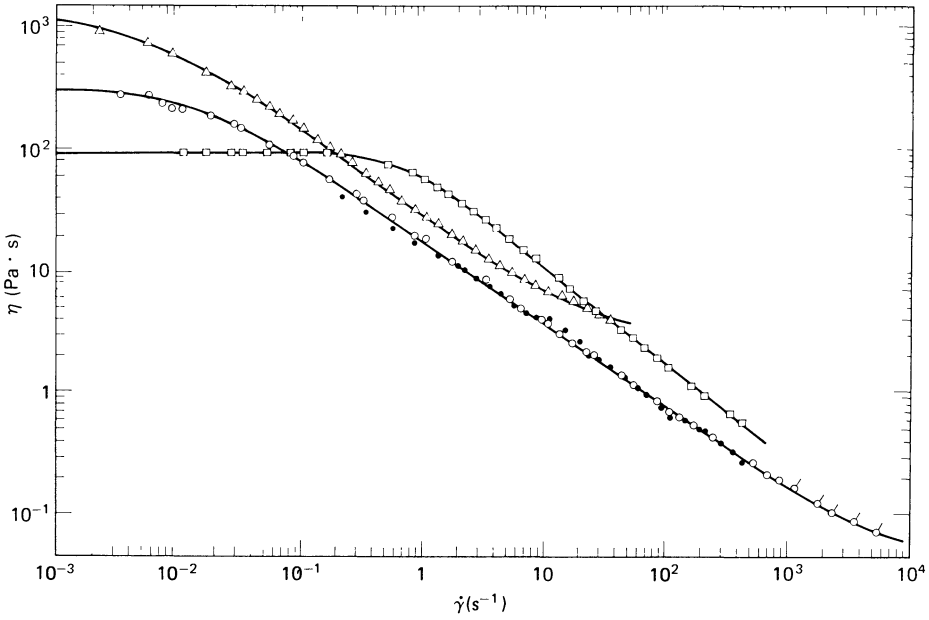

FIGURE 3.3-3. Dependence of viscosity on shear rate for two polymer solutions and an aluminum soap solution: ○ 1.5% polyacrylamide (Separan AP30) in a 50/50 mixture by weight of water and glycerin; △ 2.0% polyisobutylene in Primol; and □ 7% aluminum laurate in a mixture of decalin and *m*-cresol. The data shown by ○ were taken on a Ferranti-Shirley viscometer; all others are from a Weissenberg Rheogoniometer. All data were taken at 298 K. [Data of J. D. Huppler, E. Ashare, and L. A. Holmes, *Trans. Soc. Rheol.*, **11**, 159-179 (1967).]

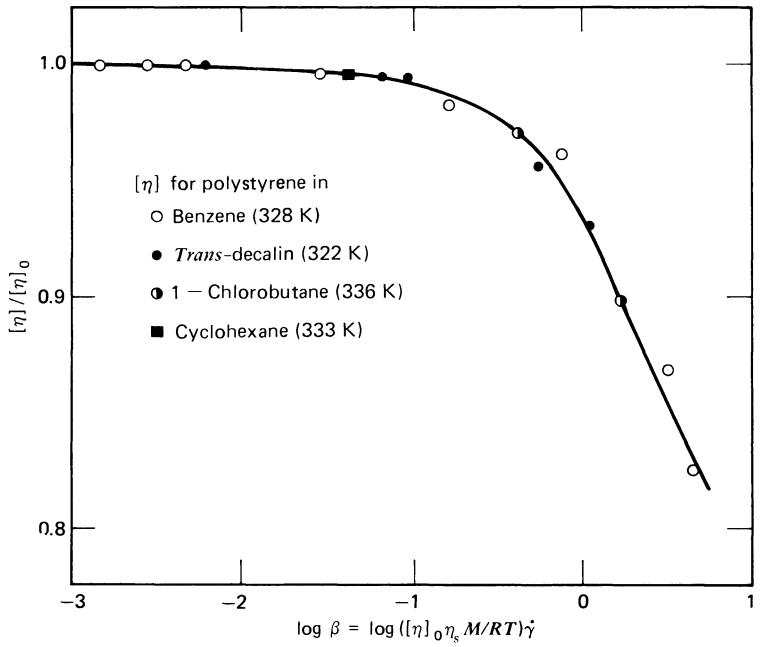

FIGURE 3.3-4. Intrinsic viscosity $[\eta]$ (see Eq. 3.3-6) of polystyrene solutions, with various solvents, as a function of reduced shear rate β. [Data of T. Kotaka, H. Suzuki, and H. Inagaki, *J. Chem. Phys.*, **45**, 2770-2773 (1966).]

engineering applications, this is the most important property of polymeric fluids. When plotted as log η versus log $\dot{\gamma}$, the viscosity vs. shear rate curve exhibits a pronounced linear region at high shear rates that can persist over several decades of decreasing viscosity. The slope of the linear section, or "power-law" region, is found experimentally to be between -0.4 and -0.9 for typical polymeric liquids. The range of shear rates over which the transition from η_0 to the power law region occurs is fairly narrow for narrow molecular weight distributions. As the molecular weight distribution of the polymer is broadened, the transition region is also broadened and shifted to lower shear rates.[2] Finally, at very high rates of shear the viscosity may again become independent of shear rate and approach η_∞, the *infinite-shear-rate viscosity*. For concentrated solutions and melts, η_∞ is not usually measurable since polymer degradation becomes a serious problem before sufficiently high shear rates can be obtained.

When viscosity data are available for a wide variety of $\dot{\gamma}$ and T, it is convenient to display the data as "master curves." This is illustrated by taking the data of Fig. 3.3-1 for $\eta(\dot{\gamma}, T)$ and replotting them in Fig. 3.3-2 as though they were all taken at a single, reference temperature. In Fig. 3.3-1, it is seen that changing the temperature does not affect the functional dependence of η on $\dot{\gamma}$; it merely alters the zero-shear-rate viscosity and the shear rate at which the transition from constant viscosity to power-law behavior occurs. As temperature is increased, η_0 decreases and the transition shear rate increases. Data obtained at various temperatures can be superposed onto a single "master curve" by plotting $\eta(T)\eta_0(T_0)/\eta_0(T)$ versus $a_T\dot{\gamma}$ where $a_T = a_T(T_0)$ is a "shift factor."[3] This means that viscosity

[2] W. W. Graessley, *Adv. Polym. Sci.*, **16**, 1-179 (1974).

[3] In $a_T(T_0)$ the subscript T denotes the temperature at which data were actually taken; and the argument T_0, the reference temperature. The T_0 argument is normally suppressed.

measured at a temperature T and a shear rate $\dot{\gamma}$ is equivalent, after correction for the temperature dependence of η_0, to viscosity measured at temperature T_0 and shear rate $a_T\dot{\gamma}$. The success of this method is shown in the resulting master curve for a polyethylene melt in Fig. 3.3-2. The value of a_T is determined primarily by $\eta_0(T)$; for example the master curves in Fig. 3.3-2 were obtained by taking $a_T = \eta_0(T)/\eta_0(T_0)$. This means that $a_T < 1$ for $T > T_0$ and $a_T > 1$ for $T < T_0$. The technique we have illustrated here is known as *time–temperature superposition* or the *method of reduced variables*. We discuss the method more fully in §3.6.

In dilute solutions, the viscosity is dominated by the solvent, so that it is difficult to discern the effect of the polymer on $\eta(\dot{\gamma})$. The polymer contribution to the viscosity can be obtained by expanding the *relative viscosity* η_{rel}, defined as the ratio of solution viscosity to solvent viscosity η_s

$$\eta_{\text{rel}} = \frac{\eta}{\eta_s} \tag{3.3-4}$$

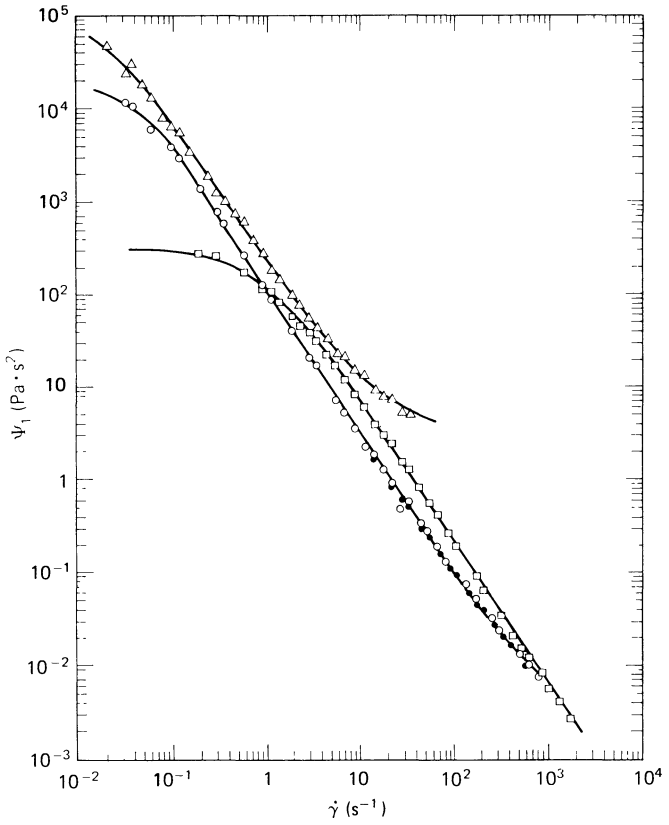

FIGURE 3.3-5. Dependence of the first normal stress coefficient on shear rate for two polymer solutions and a soap solution: ○ 1.5% polyacrylamide (Separan AP30) in a water–glycerin mixture; △ 2.0% polyisobutylene in Primol; and □ 7% aluminum laurate in decalin and *m*-cresol. All data were taken at 298 K. [Data replotted from J. D. Huppler, E. Ashare, and L. A. Holmes, *Trans. Soc. Rheol.*, **11**, 159–179 (1967).]

in a Taylor series in the mass concentration c

$$\eta_{\text{rel}} = 1 + [\eta]c + k'[\eta]^2c^2 + \cdots \tag{3.3-5}$$

in which $[\eta]$ and k' are independent of concentration. The coefficient $[\eta]$ is the *intrinsic viscosity* of the solution, and k' is the *Huggins coefficient*; it follows from Eq. 3.3-5 that

$$\boxed{[\eta] = \lim_{c\to 0}\left(\frac{\eta - \eta_s}{c\eta_s}\right)} \tag{3.3-6}$$

Note that the intrinsic viscosity has dimensions of reciprocal concentration. As shown in Fig. 3.3-4, the intrinsic viscosity depends on shear rate in much the same way as the viscosity of the polymer melt and polymer solutions.

The first normal stress coefficient is shown in Figs. 3.3-2 and 5. The polymer melt data in Fig. 3.3-2 are presented in terms of reduced variables in the same way as the viscosity (see §3.6 for more detail); the shift factors a_T are the same in both plots. It is seen that Ψ_1 is positive[4] and that it has a large power law region in which it decreases by as much as a factor of 10^6. Most often, the rate of decline of Ψ_1 with $\dot{\gamma}$ is greater than that of η with $\dot{\gamma}$. At low rates of shear the first normal stress difference is proportional to $\dot{\gamma}^2$, so that Ψ_1 tends to a constant $\Psi_{1,0}$, the zero-shear-rate first normal stress coefficient, as $\dot{\gamma}$ approaches zero. There does not seem to be a limiting value of Ψ_1 at high shear rates to correspond to η_∞. Some data do show, however, a levelling-off trend at the high shear rates.

The second normal stress coefficient is not nearly as well studied experimentally as η and Ψ_1. The most important points to note about Ψ_2 are that its magnitude is much smaller than Ψ_1, usually about 10% of Ψ_1, and that it is negative.[5] It was thought for some time that $\tau_{yy} = \tau_{zz}$ (or $\Psi_2 = 0$); this relation, called the "Weissenberg hypothesis," is now known not to be correct. In Fig. 3.3-6 we present data for Ψ_2. There it can be seen that Ψ_2 exhibits a large power-law region such as those for $\eta(\dot{\gamma})$ and $\Psi_1(\dot{\gamma})$. Values for $\Psi_{2,0}$ or $\Psi_{2,\infty}$, the zero- and infinite-shear-rate values of Ψ_2, are not observed in these data. In Fig. 3.3-7, values of the ratio $-\Psi_2/\Psi_1$ are seen to range from 0.01 to 0.2 for a polyacrylamide solution and a polyethylene oxide solution. Our knowledge about Ψ_2 is still incomplete. Furthermore, the general statements above regarding the sign and magnitude of Ψ_2 are based on data for moderately concentrated solutions of relatively few different kinds of polymers. Some data[6] suggest that Ψ_2 may even change sign and become positive at large shear rates.

[4] G. Kiss, *Phys. Today*, **37**, 15, 121 (1984), has pointed out that negative first normal stress coefficients have been observed in some liquid crystalline solutions and other systems. See G. Kiss and R. S. Porter, *J. Polym. Sci. Polym. Symp.*, **65**, 193-211 (1978); *J. Polym. Sci. Polym. Phys. Ed.*, **18**, 361-388 (1980).

[5] The first study in which Ψ_2 was reported to be negative is that of R. F. Ginn and A. B. Metzner in E. H. Lee, ed., Wiley-Interscience, *Proceedings of the Fourth International Congress on Rheology*, New York (1965), Part 2, pp. 583-601; *Trans. Soc. Rheol.*, **13**, 429-453 (1969). The uncertainty in the sign of Ψ_2 was resolved by the discovery of the hole pressure effect (see §2.3); see J. M. Broadbent, A. Kaye, A. S. Lodge, and D. G. Vale, *Nature*, **277**, 55-56 (1968); A. Kaye, A. S. Lodge, and D. G. Vale, *Rheol. Acta*, **7**, 368-379 (1968); J. M. Broadbent and A. S. Lodge, *Rheol. Acta*, **10**, 557-573 (1972). See also M. Keentok, A. G. Georgescu, A. A. Sherwood, and R. I. Tanner, *J. Non-Newtonian Fluid Mech.*, **6**, 303-324 (1980); H. W. Gao, S. Ramachandran, and E. B. Christiansen, *J. Rheol.*, **25**, 213-235 (1981); K. Walters, *IUPAC Macro 83* (Bucharest, Romania), Part 2, 227-237 (1983); S. Ramachandran, H. W. Gao, and E. B. Christiansen, *Macromolecules*, **18**, 695-699 (1985); W.-M. Kulicke and U. Wallbaum, *Chem. Eng. Sci.*, **40**, 961-972 (1985).

[6] W. G. Pritchard, *Phil. Trans. Roy. Soc. London*, **A270**, 507-556 (1971).

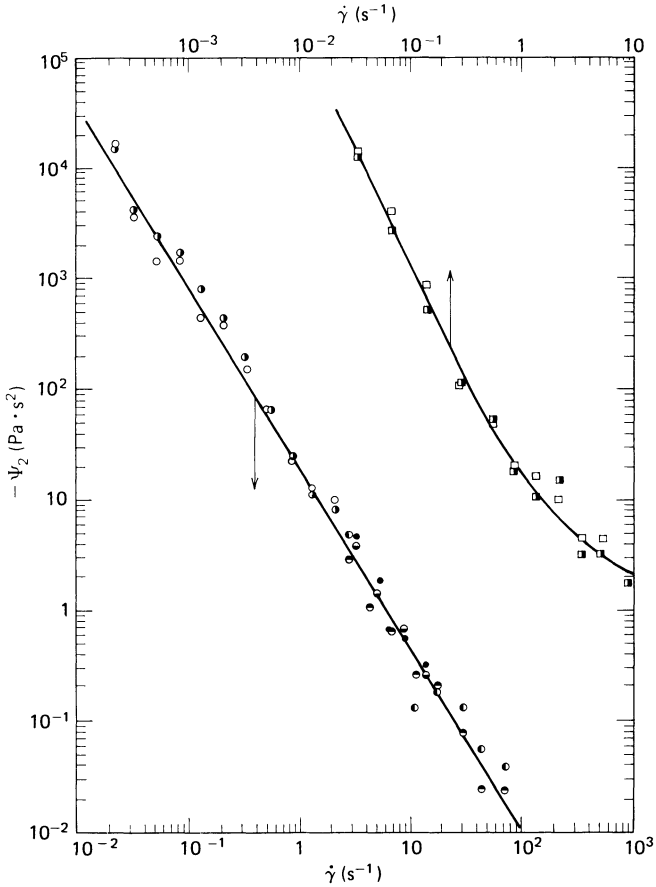

FIGURE 3.3-6. Dependence of the second normal stress coefficient on shear rate for two polymer solutions: the circles are for a 2.5% solution of polyacrylamide in a 50/50 mixture of water and glycerin, and the squares are for a 3% solution of polyethylene oxide in a 57/38/5 mixture of water, glycerin, and isopropyl alcohol. [Data replotted from E. B. Christiansen and W. R. Leppard, *Trans. Soc. Rheol.*, **18**, 65–86 (1974).]

Note that for Newtonian fluids Ψ_1 and Ψ_2 are both zero. The negative $\tau_{xx} - \tau_{yy}$ and positive $\tau_{yy} - \tau_{zz}$ can both be loosely thought of as corresponding to an extra compression in the y-direction. Consequently, in order to maintain steady shear flow between two parallel plates, a normal force must be applied to the plates to prevent them from separating when the fluid is polymeric. Only a shear stress is needed to maintain steady shear flow for a Newtonian fluid.

A measure of the 'elasticity' in the fluid is the *stress ratio*, $(\tau_{xx} - \tau_{yy})/\tau_{yx}$. This ratio is zero for Newtonian fluids, and also for non-Newtonian fluids in the limit of small shear rates. Figure 3.3-8 shows the stress ratio for a low density polyethylene melt and a polyacrylamide solution. The stress ratio for both is a monotone increasing function of shear rate with values as high as 2 to 3 being attained for the polyethylene and 20 to 30 for the polyacrylamide. Many polymers do not have stress ratios this large.

Now that we have described the steady shear flow material functions, we point out briefly one common method for measuring them by using a cone-and-plate apparatus (see Fig. 1.3-4 and Example 1.3-4). As was seen in Example 1.3-4, by using a very small cone angle ϑ_0 a very nearly uniform shear rate of W/ϑ_0 can be achieved throughout the sample

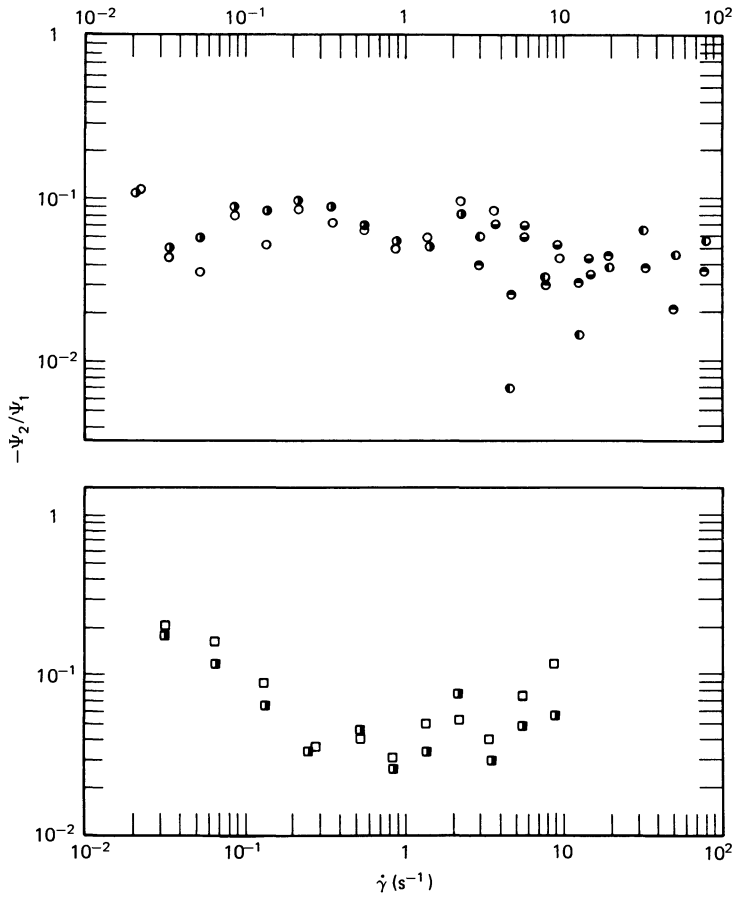

FIGURE 3.3-7. Ratio of the second normal stress coefficient to the first normal stress coefficient for the two solutions shown in Fig. 3.3-6. [E. B. Christiansen and W. R. Leppard, *Trans. Soc. Rheol.*, **18**, 65–86 (1974).]

where W is the rotation rate of the cone. This means that the shear-rate-dependent material functions η, Ψ_1, and Ψ_2 are constant throughout the gap, a result that greatly simplifies analysis of the cone-and-plate flow for non-Newtonian fluids. Since the viscosity is constant in this flow, the analysis of the shear stress from Example 1.3-4 can be taken over directly to give

$$\eta(\dot{\gamma}) = \frac{3\mathscr{T}\vartheta_0}{2\pi R^3 W} \tag{3.3-7}$$

$$\dot{\gamma} = W/\vartheta_0 \tag{3.3-8}$$

When used for polymer characterization, the cone-and-plate rheometer is normally instrumented to allow measurement of the total thrust $\mathscr{F}$ downward on the bottom plate in addition to the torque $\mathscr{T}$. From this total thrust measurement the first normal stress coefficient can be calculated by

$$\Psi_1 = \frac{2\mathscr{F}\vartheta_0^2}{\pi R^2 W^2} \tag{3.3-9}$$

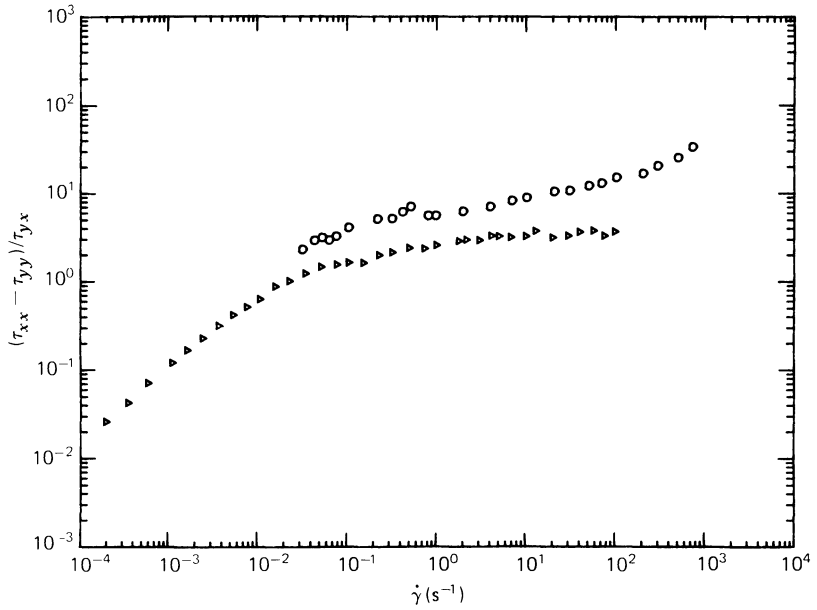

FIGURE 3.3-8. The stress ratio $(\tau_{xx} - \tau_{yy})/\tau_{yx}$ for the low-density polyethylene melt of Fig. 3.3-2 and the polyacrylamide solution of Figs. 3.3-3 and 5: ○ polyacrylamide; ▷ LDPE.

If in addition we can measure the local stress distribution across the plate surface, $\pi_{\theta\theta}(r)|_{\theta=\pi/2}$, then the second normal stress coefficient can be determined from

$$\Psi_1 + 2\Psi_2 = -\frac{1}{\dot{\gamma}^2}\frac{\partial \pi_{\theta\theta}}{\partial \ln r}\bigg|_{\theta=\pi/2} \tag{3.3-10}$$

in conjunction with the previous result for Ψ_1. In addition the second normal stress coefficient can be determined directly from the local stress $\pi_{\theta\theta}(R)|_{\theta=\pi/2}$ at the plate edge

$$\Psi_2 = \frac{p_a - \pi_{\theta\theta}(R)}{\dot{\gamma}^2} \tag{3.3-11}$$

where p_a is atmospheric pressure. A derivation of these results and a discussion of alternative methods for measuring the viscometric functions are given in Example 10.2-1.

§3.4 UNSTEADY SHEAR FLOW MATERIAL FUNCTIONS

We now consider the time-dependent behavior of polymeric liquids in unsteady simple shearing flow. A summary of the most commonly used shear flow experiments is given in Fig. 3.4-1. As in steady shear flow there are only three measurable stress quantities: the shear stress and two normal stress differences. These are represented by material functions defined analogously to η, Ψ_1, and Ψ_2 except that in the time-dependent shearing flows they can depend on time (or frequency) as well as the shear rate. A summary of the time-dependent material functions corresponding to the experiments shown in Fig. 3.4-1 is given in Table 3.4-1.

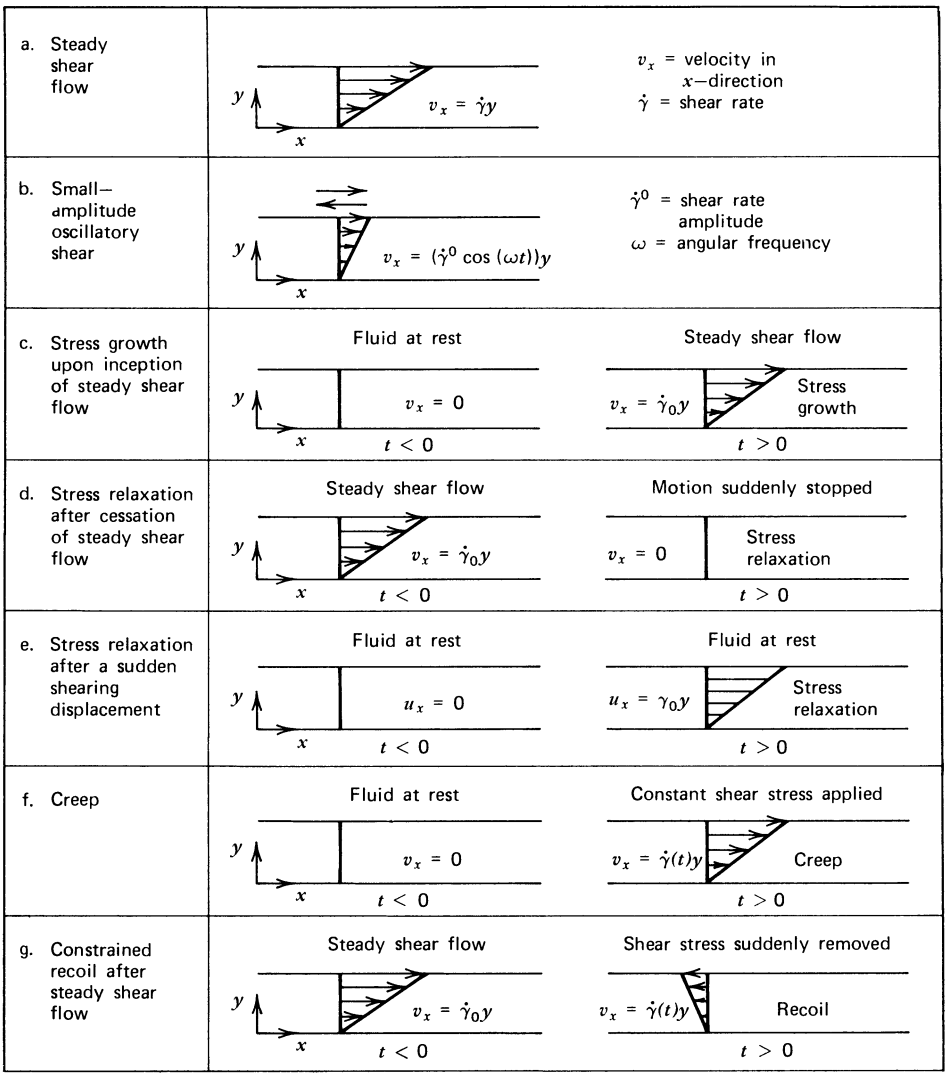

FIGURE 3.4-1. Various types of simple shear flow experiments used in rheology. For the shearing displacement experiment in (*e*), u_x is the displacement of a particle in the x-direction measured from its position just before $t = 0$; also the "magnitude of shear" γ_0 is the shear-displacement gradient and is $\gamma_0 = \int_0^t \dot{\gamma}(t')\,dt'$.

Experiment b: Small-Amplitude Oscillatory Shear Flow

The *small-amplitude oscillatory shear experiment* (Fig. 3.4-1b) involves measurement of the unsteady response of a sample that is contained between two parallel plates, the upper one of which undergoes small-amplitude sinusoidal oscillations in its own plane with frequency ω. The instantaneous velocity profile will be very nearly linear in y if $\omega\rho h^2/2\eta_0 \ll 1$, where h is the distance between the plates (see Problem 1D.1). For a linear velocity profile, the shear strain between times 0 and t, defined by $\gamma_{yx}(0, t) = \int_0^t \dot{\gamma}_{yx}(t')\,dt'$,

Table 3.4-1

Material Functions in Simple Shearing Flows $v_x = \dot{\gamma}_{yx}\, y,\ v_y = v_z = 0$

Flow	Material Function	Defining Equation
a. Steady shear flow $\dot{\gamma}_{yx} = \dot{\gamma} =$ constant	$\eta(\dot{\gamma})$ $\Psi_1(\dot{\gamma})$ $\Psi_2(\dot{\gamma})$	$\tau_{yx} = -\eta\dot{\gamma}_{yx}$ $\tau_{xx} - \tau_{yy} = -\Psi_1\dot{\gamma}_{yx}^2$ $\tau_{yy} - \tau_{zz} = -\Psi_2\dot{\gamma}_{yx}^2$
b. Small-amplitude oscillatory shear $\dot{\gamma}_{yx} = \dot{\gamma}^0 \cos\omega t$ $= \gamma^0\omega \cos\omega t$	$\eta'(\omega)$ $\eta''(\omega)$ $G'(\omega) = \eta''\omega$ $G''(\omega) = \eta'\omega$	$\tau_{yx} = -\eta'\dot{\gamma}^0 \cos\omega t$ $-\eta''\dot{\gamma}^0 \sin\omega t$ $\tau_{yx} = -G'\gamma^0 \sin\omega t$ $-G''\gamma^0 \cos\omega t$
c. Stress growth upon inception of steady shear flow $\dot{\gamma}_{yx} = \begin{cases} 0 & t < 0 \\ \dot{\gamma}_0 & t \geq 0 \end{cases}$	$\eta^+(t, \dot{\gamma}_0)$ $\Psi_1^+(t, \dot{\gamma}_0)$ $\Psi_2^+(t, \dot{\gamma}_0)$	$\tau_{yx} = -\eta^+\dot{\gamma}_0$ $\tau_{xx} - \tau_{yy} = -\Psi_1^+\dot{\gamma}_0^2$ $\tau_{yy} - \tau_{zz} = -\Psi_2^+\dot{\gamma}_0^2$
d. Stress relaxation after cessation of steady shear flow $\dot{\gamma}_{yx} = \begin{cases} \dot{\gamma}_0 & t < 0 \\ 0 & t \geq 0 \end{cases}$	$\eta^-(t, \dot{\gamma}_0)$ $\Psi_1^-(t, \dot{\gamma}_0)$ $\Psi_2^-(t, \dot{\gamma}_0)$	$\tau_{yx} = -\eta^-\dot{\gamma}_0$ $\tau_{xx} - \tau_{yy} = -\Psi_1^-\dot{\gamma}_0^2$ $\tau_{yy} - \tau_{zz} = -\Psi_2^-\dot{\gamma}_0^2$
e. Stress relaxation after a sudden shearing displacement $\dot{\gamma}_{yx} = \gamma_0\delta(t)$	$G(t, \gamma_0)$ $G_{\Psi 1}(t, \gamma_0)$	$\tau_{yx} = -G\gamma_0$ $\tau_{xx} - \tau_{yy} = -G_{\Psi 1}\gamma_0^2$
f. Creep $\tau_{yx} = \begin{cases} 0 & t < 0 \\ \tau_0 & t \geq 0 \end{cases}$	$J(t, \tau_0)$	$\gamma_{yx}(0, t) = -J\tau_0$
g. Constrained recoil after steady shear flow $\tau_{yx} = \begin{cases} \tau_0 & t < 0 \\ 0 & t \geq 0 \end{cases}$	$\gamma_r(0, t, \tau_0)$ $\gamma_\infty(\tau_0)$ $J_e^0(\tau_0)$	$\gamma_r = \int_0^t \dot{\gamma}_{yx}(t')\, dt'$ $\gamma_\infty = \lim_{t\to\infty} \gamma_r$ $\gamma_\infty = J_e^0(\tau_0)\tau_0$

and the shear rate at time t in the fluid will be independent of position and are given respectively by

$$\gamma_{yx}(0, t) = \gamma^0 \sin\omega t \tag{3.4-1a}$$

$$\dot{\gamma}_{yx}(t) = \gamma^0\omega \cos\omega t = \dot{\gamma}^0 \cos\omega t \tag{3.4-1b}$$

where γ^0 and $\dot{\gamma}^0$ are the (positive) amplitudes of the shear strain and shear rate oscillations. For Newtonian fluids the shear stress τ_{yx} is in phase with the shear rate $\dot{\gamma}_{yx}$ and there are no normal stresses. For polymeric materials, the response is shown qualitatively in Fig. 3.4-2,

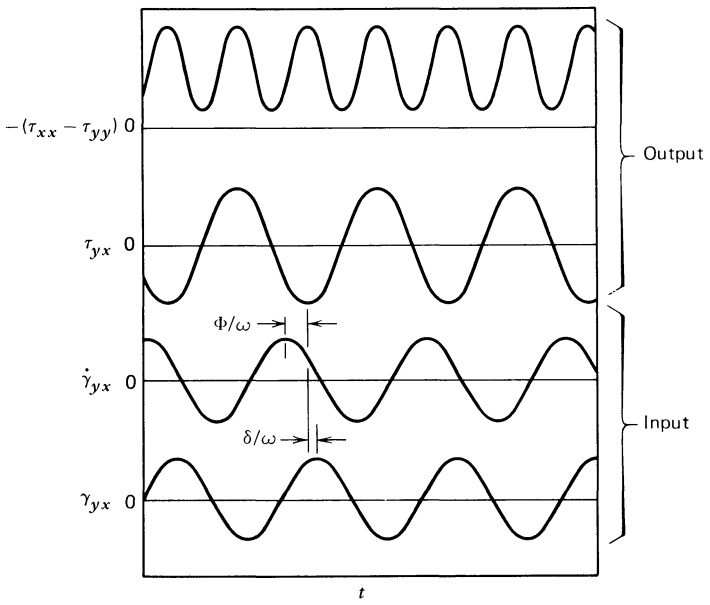

FIGURE 3.4-2. Oscillatory shear strain, shear rate, shear stress, and first normal stress difference in small-amplitude oscillatory shear flow. [After A. S. Lodge. *Elastic Liquids*, Academic Press, New York (1964), p. 113.]

where it is seen that the shear stress oscillates with frequency ω, but is not in phase with either the shear strain or shear rate, and that the normal stresses oscillate with a frequency 2ω about a nonzero mean value (see Problem 3C.1).

For shear stress one can measure the amplitude and phase shift as a function of the frequency ω. We will assume that the shear strain amplitude γ^0 is sufficiently small so that the shear stress is linear in strain or strain rate, and we write (corresponding to the two forms of Eq. 3.4-1):

$$\tau_{yx} = -A(\omega)\gamma^0 \sin(\omega t + \delta) \qquad (0 \leq \delta \leq \pi/2) \tag{3.4-2a}$$

$$\tau_{yx} = -B(\omega)\dot{\gamma}^0 \cos(\omega t - \Phi) \qquad (0 \leq \Phi \leq \pi/2) \tag{3.4-2b}$$

where $\Phi = (\pi/2) - \delta$. It is customary to rewrite Eqs. 3.4-2 to display the in-phase and out-of-phase parts of the shear stress. In this way we define the two equivalent sets of linear viscoelastic material functions G', G'' and η', η'':

$$\boxed{\tau_{yx} = -G'(\omega)\gamma^0 \sin \omega t - G''(\omega)\gamma^0 \cos \omega t} \tag{3.4-3a}$$

$$\boxed{\tau_{yx} = -\eta'(\omega)\dot{\gamma}^0 \cos \omega t - \eta''(\omega)\dot{\gamma}^0 \sin \omega t} \tag{3.4-3b}$$

It is easy to see that G', G'' are related to A, δ and that η', η'' are related to B, Φ by

$$A(\omega) = \sqrt{G'^2 + G''^2} = |G^*|, \quad \tan \delta = G''/G' \tag{3.4-4a}$$

$$B(\omega) = \sqrt{\eta'^2 + \eta''^2} = |\eta^*|, \quad \tan \Phi = \eta''/\eta' \tag{3.4-4b}$$

in which we have introduced the notation $|G^*|$ and $|\eta^*|$ for the magnitudes of the *complex modulus* G^* and *complex viscosity* η^*.[1]

Because G' and G'', or alternatively η' and η'', determine the shear stress that is linear in the strain these material functions are often called linear viscoelastic properties. They are important in characterizing the behavior of a material in small deformations (see Chapter 5). To understand the information that these material functions contain, it is useful to recall that for a perfectly elastic solid G' is equal to the constant shear modulus G, and G'' is zero, whereas for a Newtonian fluid, η' is equal to the viscosity μ, and η'' is zero. For this reason G' $(=\eta''\omega)$ is known as the *storage modulus*; it gives information about the elastic character of the fluid or the energy storage that takes place during the deformation. On the other hand, G'' $(=\eta'\omega)$ is known as the *loss modulus*; it tells about the viscous character of the fluid, or the energy dissipation that occurs in flow. The quantity η' is called the *dynamic viscosity*; and the phase angle δ between stress and strain is normally given by the *loss tangent*, $\tan\delta$. For more detail on these and other linear viscoelastic properties, standard references should be consulted.[2] We shall use both G^* and η^* in specifying the linear viscoelastic properties.

Sample data showing the complex modulus for a polymer melt, the complex viscosity for three polymer solutions, and the intrinsic complex viscosity for a dilute solution are shown in Figs. 3.4-3 to 6. The dynamic viscosity is found to approach the zero-shear-rate viscosity at low frequency; this is to be expected. Correspondingly the loss modulus is asymptotic to $\eta_0\omega$ as $\omega \to 0$. On the other hand the out-of-phase part of the complex viscosity associated with energy storage is found to approach zero linearly in ω as $\omega \to 0$; likewise the storage modulus is proportional to ω^2. Thus there is a nonzero limiting value of $\eta''/\omega = G'/\omega^2$ at low frequency. At intermediate frequencies, η' and η''/ω both show large power-law regions similar to those we have previously encountered for the viscometric functions. Finally at high frequencies, η' may approach a limiting value η'_∞. As with η_∞, this quantity is usually observed only for dilute solutions where it is found to be slightly larger

[1] The complex modulus and viscosity arise naturally in the following alternative formulas for the stress given in Eq. 3.4-3. Let us use the complex notation

$$\gamma_{yx}(0, t) = -\gamma^0 \mathscr{R}e\{ie^{i\omega t}\} \tag{3.4-1a'}$$

$$\dot{\gamma}_{yx}(t) = \dot{\gamma}^0 \mathscr{R}e\{e^{i\omega t}\} \tag{3.4-1b'}$$

where γ^0 and $\dot{\gamma}^0$ are the (real, positive) amplitudes of the oscillatory shear strain and shear rate. For small deformations the shear stress is assumed to oscillate with the same frequency, but not necessarily in phase: $\tau_{yx} = \mathscr{R}e\{\tau^0_{yx}e^{i\omega t}\}$ where τ^0_{yx} is in general complex. Then if the complex modulus G^* and the complex viscosity η^* are defined by:

$$\tau^0_{yx} = iG^*\gamma^0 \tag{3.4-3a'}$$

$$\tau^0_{yx} = -\eta^*\dot{\gamma}^0 \tag{3.4-3b'}$$

and we take

$$G^* = G' + iG'' \tag{3.4-3c}$$

$$\eta^* = \eta' - i\eta'' \tag{3.4-3d}$$

then the above formulas are equivalent to Eqs. 3.4-3a and b. Also we have $G^* = i\omega\eta^*$.

[2] J. D. Ferry, *Viscoelastic Properties of Polymers*, 3rd ed., Wiley, New York (1980); H. Leaderman in F. R. Eirich, ed., *Rheology*, Vol. 2, Academic Press, New York (1958), Chapt. 1, pp. 1–61.; A. V. Tobolsky, *op. cit.*, pp. 63–81; T. Alfrey, Jr. and E. F. Gurnee in F. R. Eirich, ed., *Rheology*, Vol. 3, Academic Press, New York (1956), Chapt. 11, pp. 387–429.

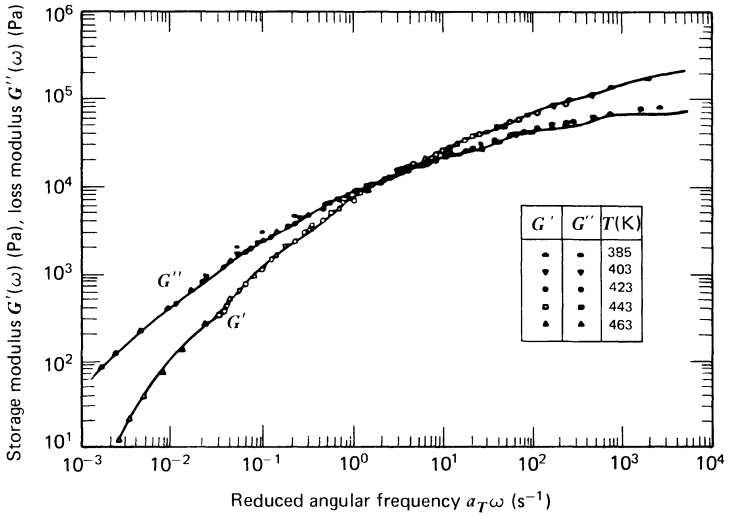

FIGURE 3.4-3. Storage and loss moduli, G' and G'', as functions of frequency ω at a reference temperature of $T_0 = 423$ K for the low-density polyethylene melt (Melt I) shown in Fig. 3.3-1. The shift factors a_T used to shift the data from the indicated temperatures to T_0 are the same as those used for the viscosity and first normal stress coefficient in Fig. 3.3-2. The solid curves are calculated from the generalized Maxwell model, Eqs. 5.2-13 through 15, with the constants tabulated in Table 5.3-2. [Data of A. Zosel (1972) as reported in H. M. Laun, *Rheol. Acta*, **17**, 1-15 (1978).]

than the solvent viscosity.[3] Also, at high frequencies η''/ω may become proportional to ω^{-2}. Since this corresponds to a storage modulus G' that is constant, the fluid becomes like a perfectly elastic solid, which indicates that there is not sufficient time for molecular rearrangements at the high frequencies.

Data for the dilute solution[4] in Fig. 3.4-6 are presented in terms of the intrinsic quantities $[\eta']$ and $[\eta'']/\omega$. These are obtained by extrapolating data for η' and η'' obtained at different polymer concentrations to zero concentration; they are thus infinite dilution properties and are dynamic analogs of the intrinsic viscosity discussed in §3.3. They are defined by:[5]

$$[\eta'] = \lim_{c\to 0}\left(\frac{\eta' - \eta_s}{c\eta_s}\right) \tag{3.4-5}$$

$$[\eta'']/\omega = \lim_{c\to 0}\left(\frac{\eta''/\omega}{c\eta_s}\right) \tag{3.4-6}$$

As seen in Fig. 3.4-2, the normal stresses oscillate about non-zero values. There are three material functions that are needed to describe each of the oscillatory normal stress differences $\tau_{xx} - \tau_{yy}$ and $\tau_{yy} - \tau_{zz}$. Not many experimental data are available for these material functions.[6]

[3] Values of η'_∞ less than η_s have also been reported for polystyrene, polyisoprene, and polybutadiene in a variety of solvents over a wide range of concentrations. See the Ph.D. Theses (Department of Chemistry, University of Wisconsin-Madison) of C. J. T. Landry (1985), D. R. Radtke (1986), T. M. Stokich (1987), and P. A. Merchak (1987); see also T. M. Stokich and J. L. Schrag, *Macromolecules*, **20** (1987).

[4] For a review of dilute solution viscoelastic properties see K. Osaki, *Adv. Polym. Sci.*, **12**, 1-64 (1973).

[5] The intrinsic quantities $[G']$ and $[G'']$ are defined similarly to $[\eta'']$ and $[\eta']$, respectively, except that the values to be extrapolated to infinite dilution are divided by c rather than $c\eta_s$. Thus $[G'] = \omega\eta_s[\eta'']$ and $[G''] = \omega\eta_s[\eta']$.

[6] See E. B. Christiansen and W. R. Leppard, *Trans. Soc. Rheol.*, **18**, 65-86 (1974).

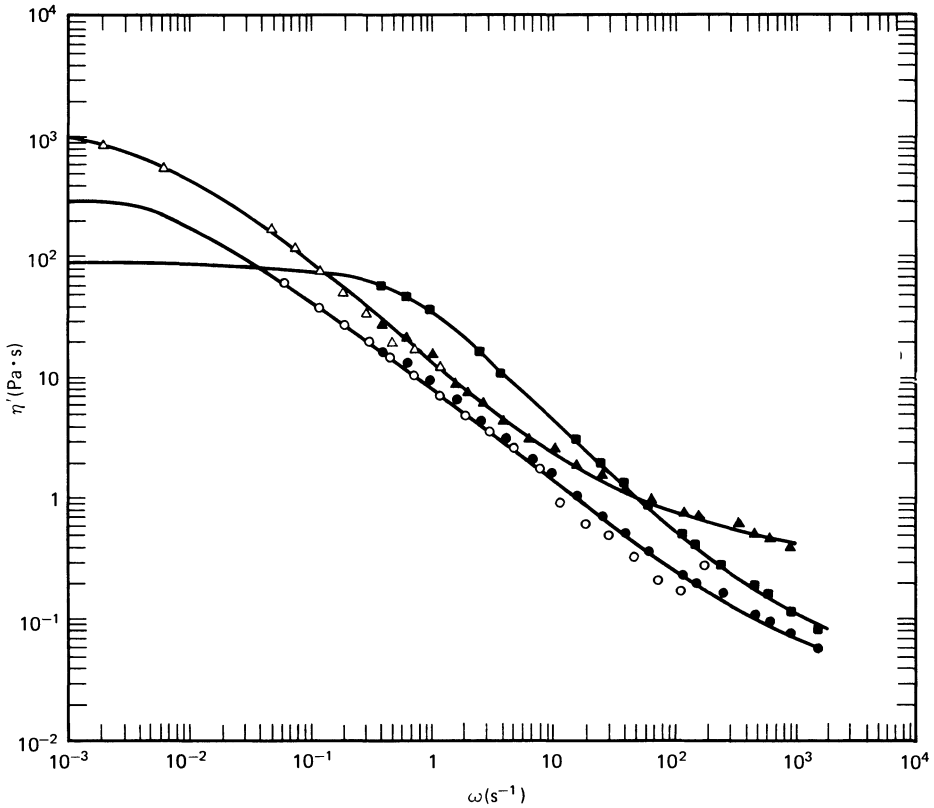

FIGURE 3.4-4. Dynamic viscosity η' as a function of frequency ω for two polymer solutions and a soap solution: ○ 1.5% polyacrylamide in a water-glycerin mixture; △ 2.0% polyisobutylene in Primol; and □ 7.0% aluminum laurate in a mixture of decalin and *m*-cresol. The hollow symbols represent data taken on a Weissenberg Rheogoniometer; the solid symbols, data taken on the Birnboim apparatus. All data were taken at 298 K. [Data of J. D. Huppler, E. Ashare, and L. A. Holmes, *Trans. Soc. Rheol.*, **11**, 159–179 (1967).]

Experiment c: Stress Growth upon the Inception of Steady Shear Flow

In a *stress growth experiment* (Fig. 3.4-1c), the fluid sample is presumed to be at rest for all times previous to $t = 0$; all components of stress are thus zero when the steady shearing is begun at time $t = 0$. For times $t \geq 0$ we denote the constant velocity gradient as $\dot{\gamma}_0$. The object of this experiment is to observe the approach of the stresses to their steady shear flow values. Material functions $\eta^+(t, \dot{\gamma}_0)$, $\Psi_1^+(t, \dot{\gamma}_0)$, and $\Psi_2^+(t, \dot{\gamma}_0)$ are defined (see Table 3.4-1) analogously to η, Ψ_1, and Ψ_2 to describe the transient shear stress and normal stress differences. The plus sign superscript emphasizes that a steady shear rate is applied for positive times. These transient properties can be measured in a cone-and-plate instrument.

Qualitatively it is found that only for vanishingly small shear rates does the shear stress approach its steady-state value monotonically. This monotone-increasing, low-shear-rate-limiting η^+ curve forms an envelope below which the η^+ curves at higher shear rates fall; it contains the same information as the linear viscoelastic properties η^* or G^*. For larger shear rates η^+ departs from the linear viscoelastic envelope, goes through a maximum, and then approaches the steady-state value, possibly after one or more oscillations about $\eta(\dot{\gamma}_0)$. The time at which η^+ departs from the linear envelope decreases as

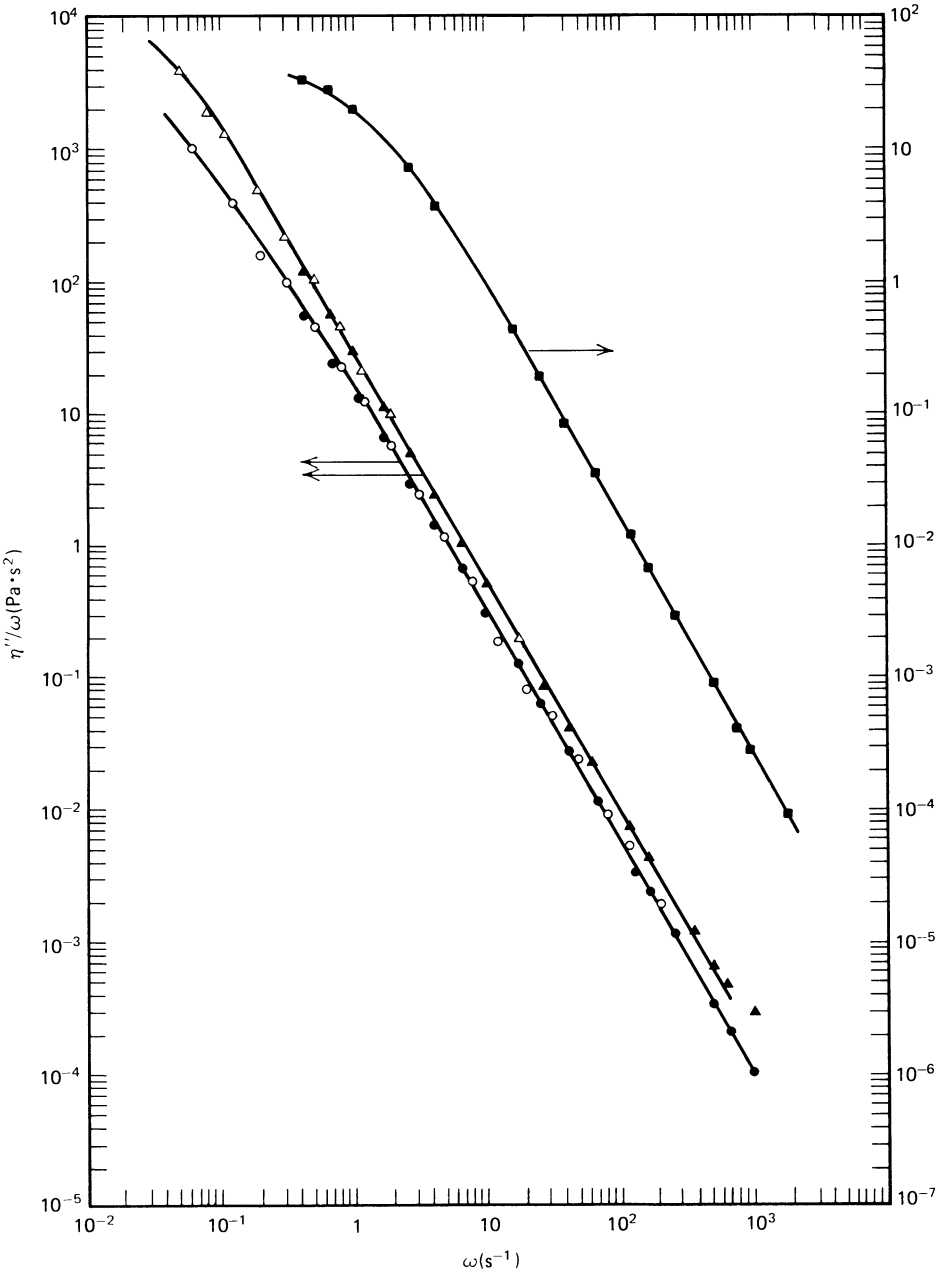

FIGURE 3.4-5. Plots of η''/ω as a function of frequency for the two polymer solutions and the aluminum soap solution shown in Fig. 3.4-4. [Data of J. D. Huppler, E. Ashare, and L. A. Holmes, *Trans. Soc. Rheol.*, **11**, 159–179 (1967).]

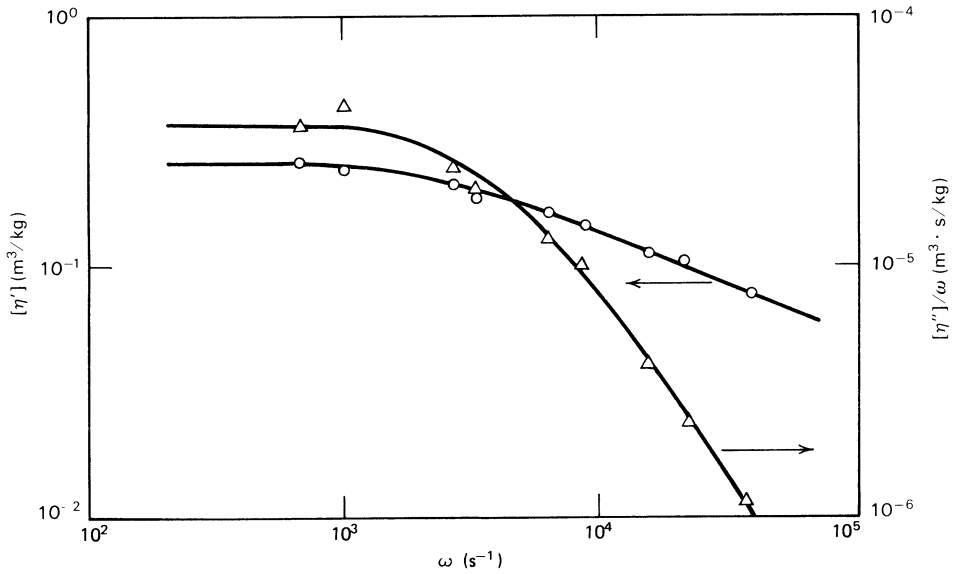

FIGURE 3.4-6. Real and imaginary parts of the intrinsic complex viscosity plotted as $[\eta']$ (circles) and $[\eta'']/\omega$ (triangles) versus frequency ω for poly-α-methylstyrene, with a narrow-distribution molecular weight of 1.43×10^6, in α-chloronaphthalene. [Data replotted from K. Osaki, J. L. Schrag, and J. D. Ferry, *Macromolecules*, **5**, 144–147 (1972).]

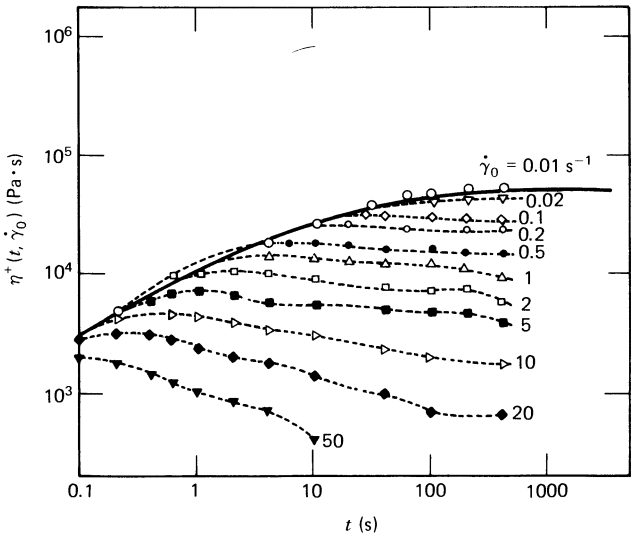

FIGURE 3.4-7. Shear stress growth function $\eta^+(t,\dot{\gamma}_0)$ data for a low-density polyethylene melt (Melt I). The maximum in η^+ occurs at smaller times as $\dot{\gamma}_0$ is increased. Note that all of the η^+ curves lie below the solid curve envelope, which is the value of η^+ in the linear viscoelastic limit. The solid curve is calculated from Eq. 5.3-25 with the spectrum in Table 5.3-2. The experimental data for small $\dot{\gamma}$ differ from the linear viscoelastic prediction at short times because of instrumental problems involved in the start-up of steady shear flow. [Reprinted with permission from M. H. Wagner and J. Meissner, *Macromol. Chem.*, **181**, 1533–1550 (1980), Hüthig and Wepf Verlag, Basel.]

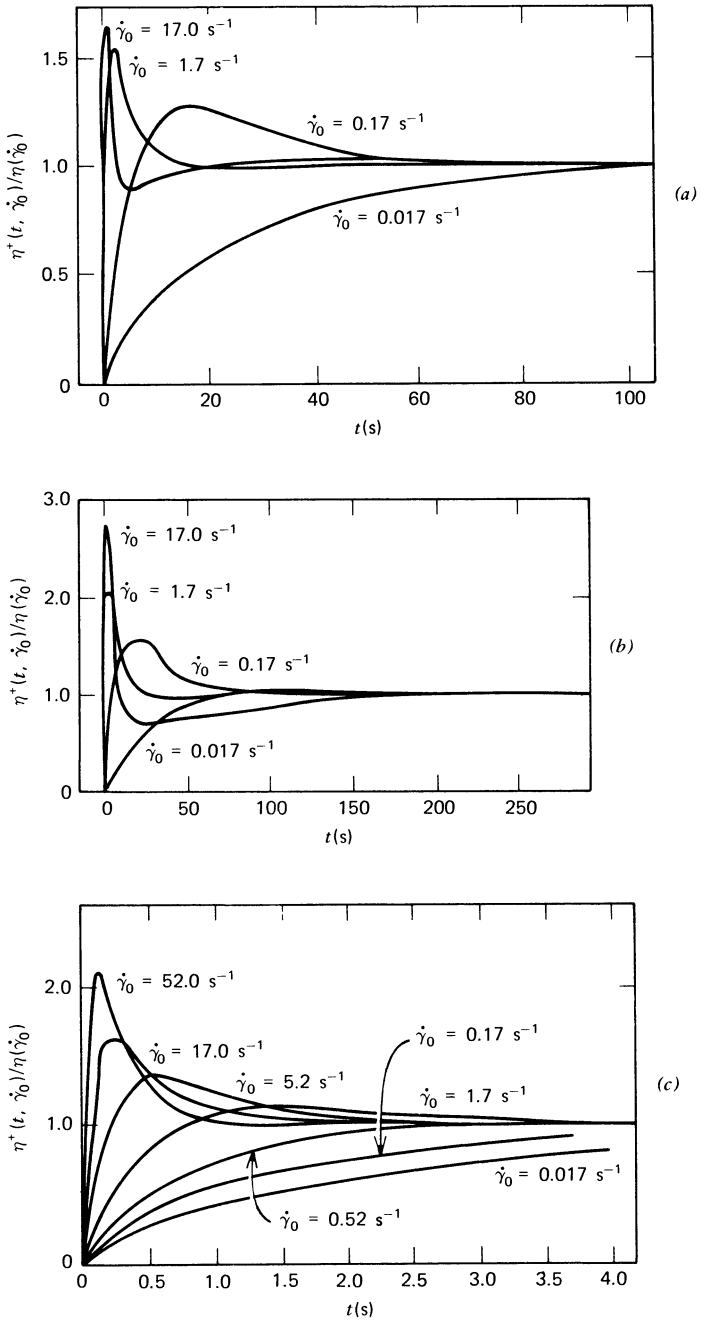

FIGURE 3.4-8. Shear stress growth function $\eta^+(t,\dot{\gamma}_0)/\eta(\dot{\gamma}_0)$ for two polymer solutions and an aluminum soap solution: (*a*) 1.5% polyacrylamide (Separan AP30) in a 50/50 mixture by weight of water and glycerin; (*b*) 2.0% polyisobutylene in Primol; and (*c*) 7% aluminum laurate in a mixture of decalin and *m*-cresol. All data were taken at 298 K. Note that the data are reduced with respect to $\eta(\dot{\gamma}_0)$ so that they all approach a common asymptote; all the data still lie within the linear viscoelastic envelope if plotted as $\eta^+(t, \dot{\gamma}_0)$. [Data of J. D. Huppler, I. F. Macdonald, E. Ashare, T. W. Spriggs, R. B. Bird, and L. A. Holmes, *Trans. Soc. Rheol.*, **11**, 181–204 (1967).]

$\dot{\gamma}_0$ is increased in such a way that the shear strain where non-linear effects are first detected is constant. For example, this critical strain for η^+ is about 1.5 for the low-density polyethylene melt in Fig. 3.4-7. For polymer melts in general, it appears that the maximum in η^+ also always occurs at about the same value of the shear strain $\gamma_{max} = t_{max}\dot{\gamma}_0$ for a given polymer,[7] and that γ_{max} is on the order of 2 to 3. Since the viscosity decreases with increasing shear rate, η^+ approaches successively lower steady-state asymptotes as $\dot{\gamma}_0$ is raised. The size of the shear-stress overshoot increases with increasing shear rate; this is reflected in plots of $\eta^+(t, \dot{\gamma}_0)/\eta(\dot{\gamma}_0)$, which are presented for three moderately concentrated solutions in Fig. 3.4-8.

The growing first normal stress difference shows the same qualitative dependence on $\dot{\gamma}_0$ as the shear stress (Figs. 3.4-9 and 10). The shear strains at which departure from the low-shear-rate envelope and at which the primary maximum occur for the first-normal-stress growth coefficient again appear to be independent of the imposed shear rate for melts, and they are larger than for the shear stress growth. For example, the deviation from the envelope occurs at about $\gamma = 2$ for Ψ_1^+ for the low-density polyethylene melt. The size of the maximum overshoot is larger for Ψ_1^+/Ψ_1 than η^+/η. Limited data[8] on $\Psi_2^+(t, \dot{\gamma}_0)$ indicate that $\Psi_2^+(t, \dot{\gamma}_0)/\Psi_1^+(t, \dot{\gamma}_0) = \Psi_2/\Psi_1$ for all $\dot{\gamma}_0$ and t.

Experiment d: Stress Relaxation after Cessation of Steady Shear Flow

In the *stress relaxation experiment* shown in Fig. 3.4-1d, the motion of a fluid that is undergoing steady shear flow with shear rate $\dot{\gamma}_0$ is suddenly stopped at say time $t = 0$ so that

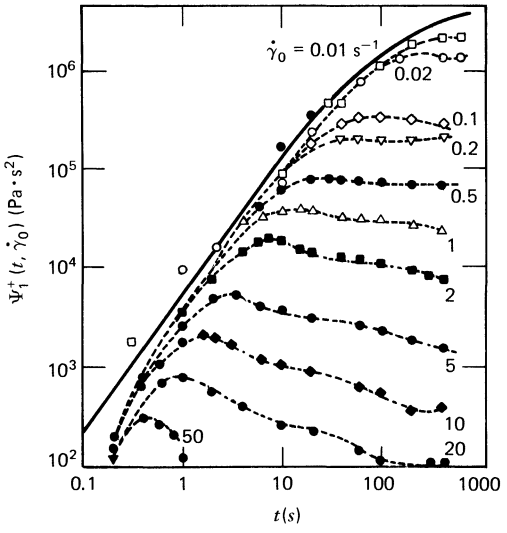

FIGURE 3.4-9. First normal stress growth function $\Psi_1^+(t, \dot{\gamma}_0)$ for the low-density polyethylene melt (Melt I) in Fig. 3.4-7. All Ψ_1^+ curves lie below the solid curve envelope which is approached for small shear rates; the solid curve is calculated from linear viscoelastic data (see Table 5.3-2) with the Lodge rubberlike liquid model (cf. Eqs. 8.2-1 and 4). [Reprinted with permission from M. H. Wagner and J. Meissner, *Macromol. Chem.*, **181**, 1533–1550 (1980), Hüthig and Wepf Verlag, Basel.]

[7] W. W. Graessley, *Adv. Polym. Sci.*, **16**, 1–179 (1974).

[8] W. R. Leppard and E. B. Christiansen, *AIChE J.*, **21**, 999–1006 (1975).

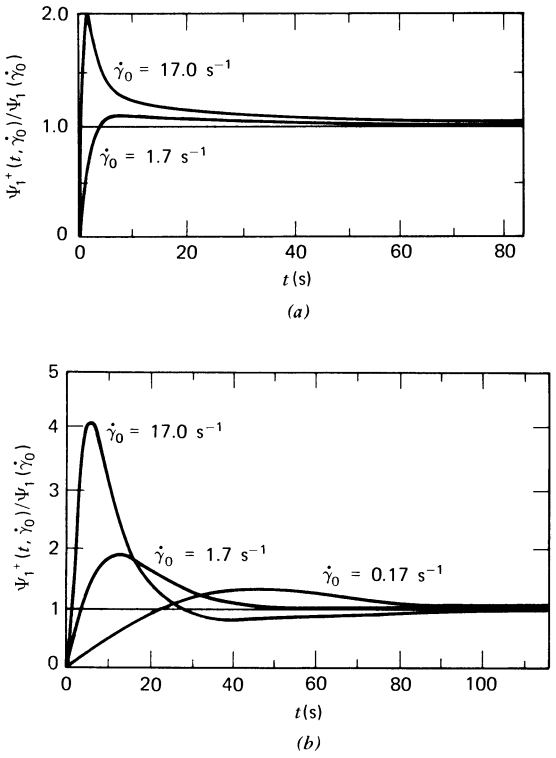

FIGURE 3.4-10. First normal stress growth function $\Psi_1^+(t, \dot{\gamma}_0)/\Psi_1(\dot{\gamma}_0)$ for (*a*) 1.5% polyacrylamide (Separan AP30) in a 50/50 mixture by weight of water and glycerin and (*b*) 2.0% polyisobutylene in Primol. All data were taken at 298 K. Note that Ψ_1^+ is reduced by the steady shear flow value Ψ_1 so that these curves show the relative sizes of the overshoot at different shear rates. [Data of J. D. Huppler, I. F. Macdonald, E. Ashare, T. W. Spriggs, R. B. Bird, and L. A. Holmes, *Trans. Soc. Rheol.*, **11**, 181-204 (1967).]

$\dot{\gamma} = 0$ for $t \geq 0$. The decay of the steady shear flow stresses to zero is then observed.[9] We can describe the relaxing stresses by the stress relaxation material functions $\eta^-(t, \dot{\gamma}_0)$, $\Psi_1^-(t, \dot{\gamma}_0)$, and $\Psi_2^-(t, \dot{\gamma}_0)$ (see Table 3.4-1) which are defined analogously to the viscometric functions. The superscripted minus sign is a reminder that the steady shear flow occurred for negative times. As in the definition of the stress growth functions, the $\dot{\gamma}_0$ in the argument of each material function indicates the parametric dependence on shear rate. For Newtonian fluids, $\eta^-(t, \dot{\gamma}_0) = \mu(1 - H(t))$, where $H(t)$ is the Heaviside unit step function, and $\Psi_1^-(t, \dot{\gamma}_0)$ and $\Psi_2^-(t, \dot{\gamma}_0)$ are both zero.

Experiments show that the stresses relax monotonically to zero and that they relax more rapidly as the shear rate $\dot{\gamma}_0$ in the preceding steady shear flow is increased. All the relaxation curves for η^- lie below the linear viscoelastic envelope approached in the limit $\dot{\gamma}_0 \to 0$. Furthermore it is found that the shear stress relaxes more rapidly than the first normal stress difference, which is similar to the slower response of the normal stresses in the stress growth experiment. Sample data for η^- and Ψ_1^- are shown in Figs. 3.4-11 to 14. Limited data on Ψ_2^- indicate[8] that $\Psi_2^-(t, \dot{\gamma}_0)/\Psi_1^-(t, \dot{\gamma}_0) = \Psi_2/\Psi_1$ for all $\dot{\gamma}_0$ and all t.

[9] For materials with a yield stress, the shear stress will not relax to zero but rather to the yield value. This method has been used to measure the yield stress of suspensions by N. Q. Duzy and D. V. Boger, *J. Rheol.*, **27**, 321-350 (1983), and of foams by S. A. Khan, Sc.D. Thesis, Massachusetts Institute of Technology, Cambridge (1985).

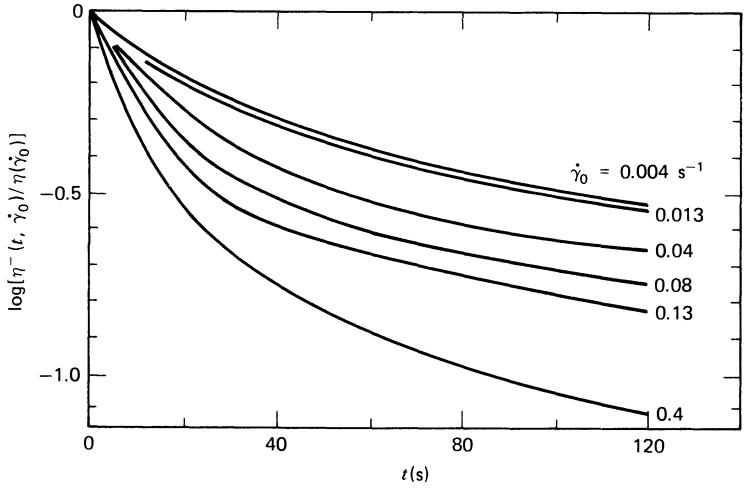

FIGURE 3.4-11. Shear stress relaxation function $\eta^-(t,\dot{\gamma}_0)/\eta(\dot{\gamma}_0)$ for a low molecular weight polyisobutylene melt ($\bar{M}_w \doteq 10^4$). [E. Mustafayev, A. Ya. Malkin, Ye. P. Plotnikova, and G. V. Vinogradov, *Vysokomol. Soedin.*, **6**, 1515–1521 (1964).]

Experiment e: Stress Relaxation after a Sudden Shearing Displacement

Another experiment in which we can observe relaxing stresses is *stress relaxation following a sudden shearing displacement* (Fig. 3.4-1e); this is sometimes referred to as *step-strain stress relaxation.* The shear strain γ_0 can be induced by applying a large, constant shear rate $\dot{\gamma}_0$ for a short time interval Δt, so that $\dot{\gamma}_0 \Delta t = \gamma_0$. As defined in Table 3.4-1, the time decay of the shear stress is described by the *relaxation modulus* $G(t, \gamma_0)$ and the relaxation of the first normal stress difference, by the function $G_{\Psi_1}(t, \gamma_0)$ for a step strain at $t = 0$.

Data for a low-density polyethylene melt and a polystyrene solution are shown in Figs. 3.4-15 and 16. For small shear strains, the relaxation modulus is found to be independent of γ_0

$$\lim_{\gamma_0 \to 0} G(t, \gamma_0) = G(t) \tag{3.4-7}$$

In this limit, the shear stress is linear in strain, so that the relaxation modulus is a function of time alone and contains the same linear viscoelastic information as G' and G'' (see Chapter 5). The effect of increasing strain on G and G_{Ψ_1} is to decrease them, but not to alter their time dependence, except at very short times. Thus the curves for G and G_{Ψ_1} in Fig. 3.4-15 and for G in Fig. 3.4-16 for different γ_0 are parallel and can be superposed by vertical shifting as demonstrated in Fig. 3.4-16. It is further observed that

$$\frac{G(t, \gamma_0)}{G_{\Psi_1}(t, \gamma_0)} = 1 \tag{3.4-8}$$

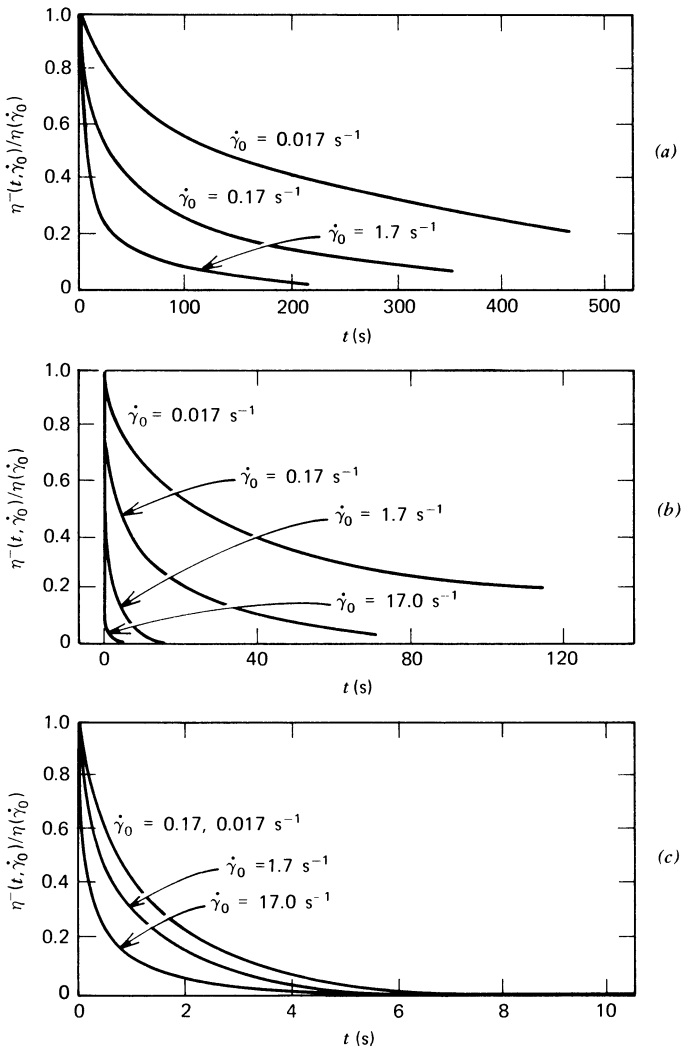

FIGURE 3.4-12. Shear stress relaxation function $\eta^-(t, \dot{\gamma}_0)/\eta(\dot{\gamma}_0)$ for two polymer solutions and an aluminum soap solution: (*a*) 1.5% polyacrylamide (Separan AP30) in a 50/50 mixture by weight of water and glycerin; (*b*) 2.0% polyisobutylene in Primol; and (*c*) 7% aluminum laurate in a mixture of decalin and *m*-cresol. All data were taken at 298 K. [Data of J. D. Huppler, I. F. Macdonald, E. Ashare, T. W. Spriggs, R. B. Bird, and L. A. Holmes, *Trans. Soc. Rheol.*, **11**, 181-204 (1967).]

that is, the relaxation behavior of the shear stress and normal stresses is given by the same function. This result, known as the *Lodge-Meissner rule*,[10] is found to hold for the few concentrated polymer solutions and melts for which it has been tested.

[10] A. S. Lodge and J. Meissner, *Rheol. Acta*, **11**, 351-352 (1972); see also A. S. Lodge, *Rheol. Acta*, **14**, 664-665 (1975), and O. Hassager and S. Pedersen, *J. Non-Newtonian Fluid Mech.*, **4**, 261-268 (1978). K. Osaki, S. Kimura, and M. Kurata, *J. Polym. Sci. Polym. Phys. Ed.*, **19**, 517-527 (1981), found that for concentrated solutions of polystyrene in Arochlor 1248 the ratio $-(\tau_{yy} - \tau_{zz})/(\tau_{xx} - \tau_{yy})$ is independent of time in stress relaxation following a step shear strain; that is, the two normal-stress differences relax with the same time dependence. However, the value of this ratio is found to depend on the size of the applied strain. For small strains this ratio is a constant, 0.17; for large strains, the ratio decreases with increasing strain.

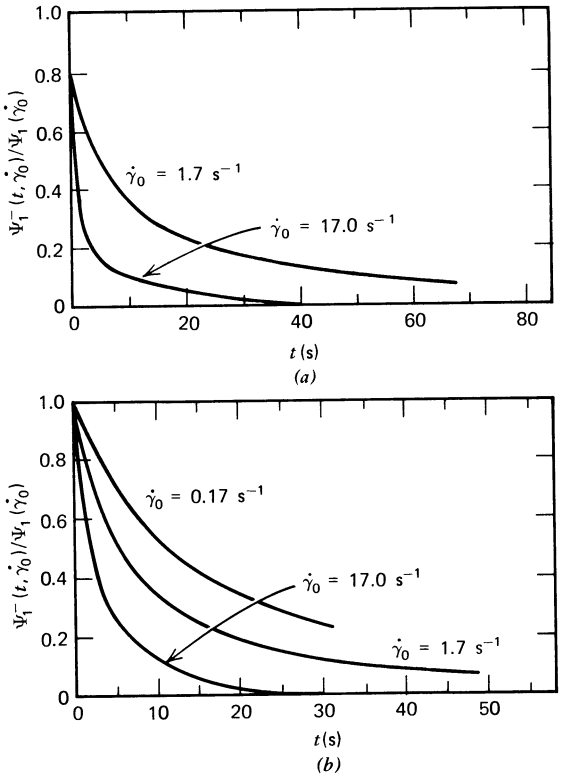

FIGURE 3.4-13. First normal stress relaxation function $\Psi_1^-(t, \dot{\gamma}_0)/\Psi_1(\dot{\gamma}_0)$ for (*a*) 1.5% polyacrylamide in water and glycerin and (*b*) 2.0% polyisobutylene in Primol. All data were taken at 298 K. [Data of J. D. Huppler, I. F. Macdonald, E. Ashare, T. W. Spriggs, R. B. Bird, and L. A. Holmes, *Trans. Soc. Rheol.*, **11**, 181–204 (1967).]

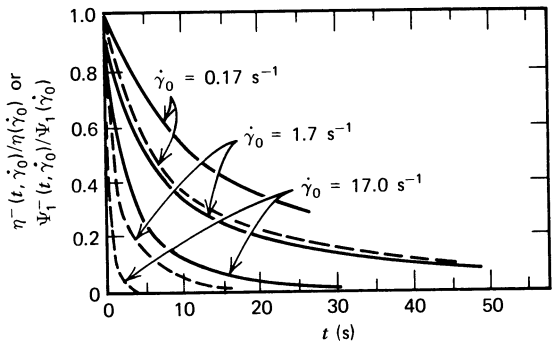

FIGURE 3.4-14. Comparison of first normal stress relaxation function $\Psi_1^-(t, \dot{\gamma}_0)/\Psi_1(\dot{\gamma}_0)$ and shear stress relaxation function $\eta^-(t, \dot{\gamma}_0)/\eta(\dot{\gamma}_0)$ for 2.0% polyisobutylene in Primol at 298 K. Note that the first normal stress difference (——) relaxes more slowly than the shear stress (----). [Data of J. D. Huppler, I. F. Macdonald, E. Ashare, T. W. Spriggs, R. B. Bird, and L. A. Holmes, *Trans Soc. Rheol.*, **11**, 181–204 (1967).]

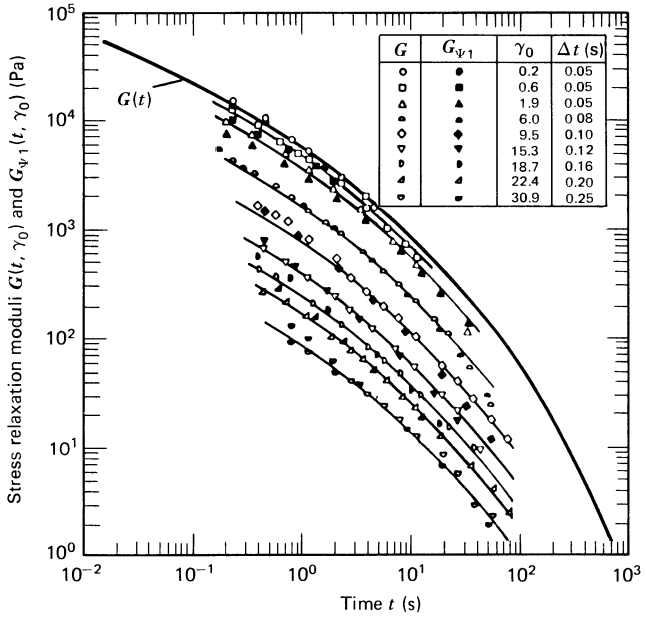

FIGURE 3.4-15. The relaxation modulus $G(t,\gamma_0)$ (open symbols) and normal stress relaxation function $G_{\Psi 1}(t, \gamma_0)$ (solid symbols) for a low-density polyethylene melt (Melt I). The indicated strains were obtained by applying a large, constant shear rate for time interval Δt; all data were taken at $T = 423$ K. The linear relaxation modulus curve $G(t)$ was calculated from the dynamic data in Fig. 3.4-3 (see Example 5.3-7). The solid curves connecting the sets of data points were obtained by shifting $G(t)$ vertically [H. M. Laun, *Rheol. Acta*, **17**, 1–15 (1978).]

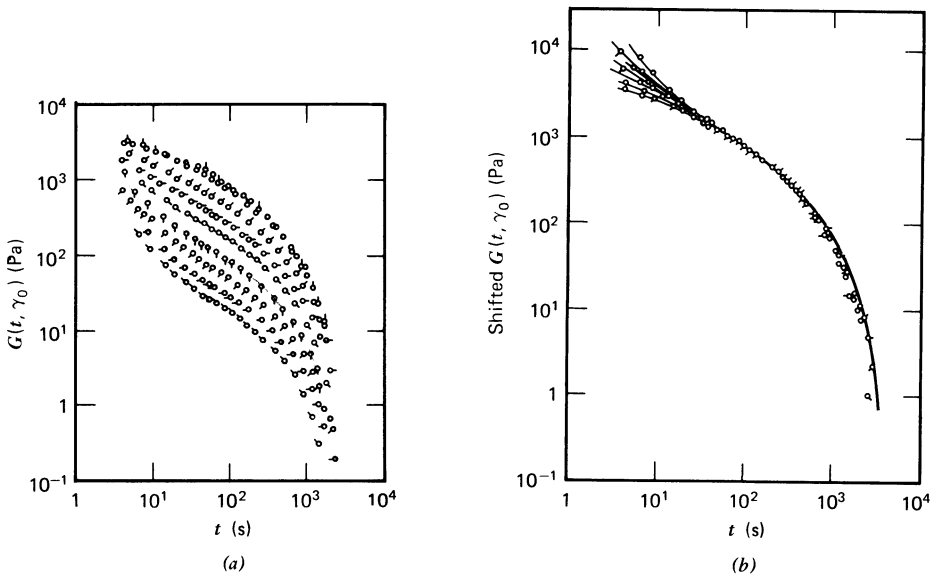

FIGURE 3.4-16. The stress relaxation modulus $G(t, \gamma_0)$ for 20% polystyrene (narrow distribution $\bar{M}_w = 1.8 \times 10^6$) in Aroclor. The imposed shear strains are (○) 0.41, (○) 1.87, (○) 3.34, (○) 5.22, (○) 6.68, (○) 10.0, (○) 13.4, (○) 18.7, and (○) 25.4. Part (*a*) shows how $G(t, \gamma_0)$ varies with shear strain; note that the data for γ_0 equal to 0.41 and 1.87 are in the linear regime. In (*b*) the data are superposed by vertical shifting to show the similarity in $G(t, \gamma_0)$ at large times regardless of the imposed shear strain. [Y. Einaga, K. Osaki, M. Kurata, S. Kimura, and M. Tamura, *Polym. J. Jpn.*, **2**, 550–552 (1971).]

Experiment f: Creep

Instead of controlling the shear rate and measuring the resulting stresses, we can apply a prescribed time-dependent shear stress and measure the resulting shear strain. In the *creep experiment* (Fig. 3.4-1f), a constant shear stress $\tau_{yx} = \tau_0$ is applied at $t = 0$ to a fluid that was previously at rest and stress-free. It is convenient to measure the shear strain in the material relative to the application of the shear stress at $t = 0$

$$\gamma_{yx}(0, t) = \int_0^t \dot{\gamma}_{yx}(t')dt' \tag{3.4-9}$$

The "give" of the sample in response to the applied stress is sometimes described by the *creep compliance* $J(t, \tau_0)$ as defined in Table 3.4-1. For small values of τ_0 the strain is proportional to stress so that

$$\lim_{\tau_0 \to 0} J(t, \tau_0) = J(t) \tag{3.4-10}$$

The linear viscoelastic function $J(t)$ contains the same information as $G(t)$, G', and G''.[11]

Creep data for a low-density polyethylene melt are shown in Fig. 3.4-17. By a reduced time of 200 s the strain is proportional to time, so that steady state has been reached. Comparison of this time with the corresponding time of 500 to 600 s to reach steady state in start-up of steady shear flow with constant shear rate of 1 s^{-1} (this gives the same steady state in the two experiments since $\eta(1\ s^{-1}) = 10^4$ Pa · s) in Fig. 3.4-7, indicates that the time constant for approach to steady state is different for the two different experiments. At least for the low-density polyethylene shown here steady state is achieved

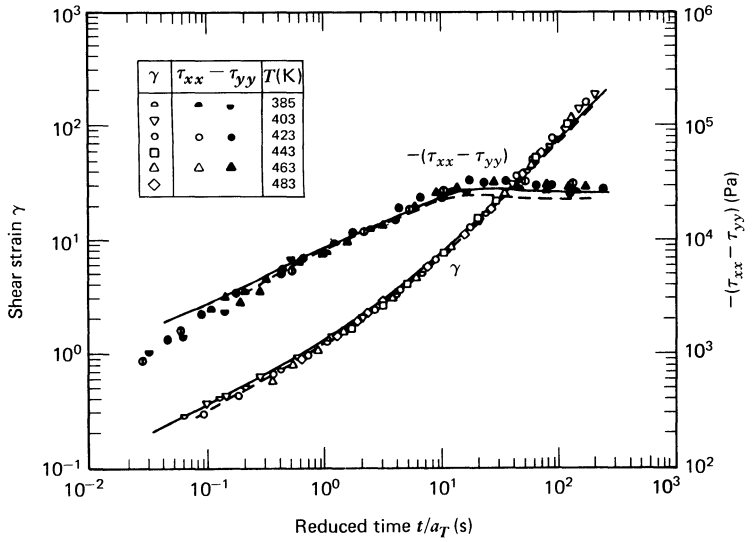

FIGURE 3.4-17. The shear strain and first normal stress difference for a low-density polyethylene melt (Melt I) as functions of reduced time t/a_T in a creep experiment. The data are all taken for an applied shear stress of 10^4 Pa, and shift factors a_T are the same as found in Fig. 3.3-2. The reference temperature is $T_0 = 423$ K. The solid and the dashed curves were calculated with the Wagner model (cf. Fig. 3.3-2). [M. H. Wagner and H. M. Laun, *Rheol. Acta*, **17**, 138–148 (1978).]

[11] J. D. Ferry, *Viscoelastic Properties of Polymers*, 3rd ed., Wiley, New York (1980), Chapt. 3.

faster in creep than in the constant shear rate test. Also shown in Fig. 3.4-17 is the transient first normal stress difference; note that it appears to show a small overshoot under these experimental conditions.

Experiment g: Constrained Recoil after Steady Shear Flow

If the shear stress is suddenly removed from a viscoelastic fluid undergoing steady shear flow (Fig. 3.4-1g) and if the separation between the plates is held constant, the fluid will recoil to some position it previously occupied. We have seen an example of this *constrained recoil* in tube flow of an aqueous carboxymethylcellulose solution in the sequence of photographs in §2.5. The recovery of the fluid is described by the shear strain $\gamma_r(0, t, \dot{\gamma}_0)$ during recoil measured relative to the time when the shear stress is removed; the time evolutions of the shear stress and shear strain are illustrated in Fig. 3.4-18.

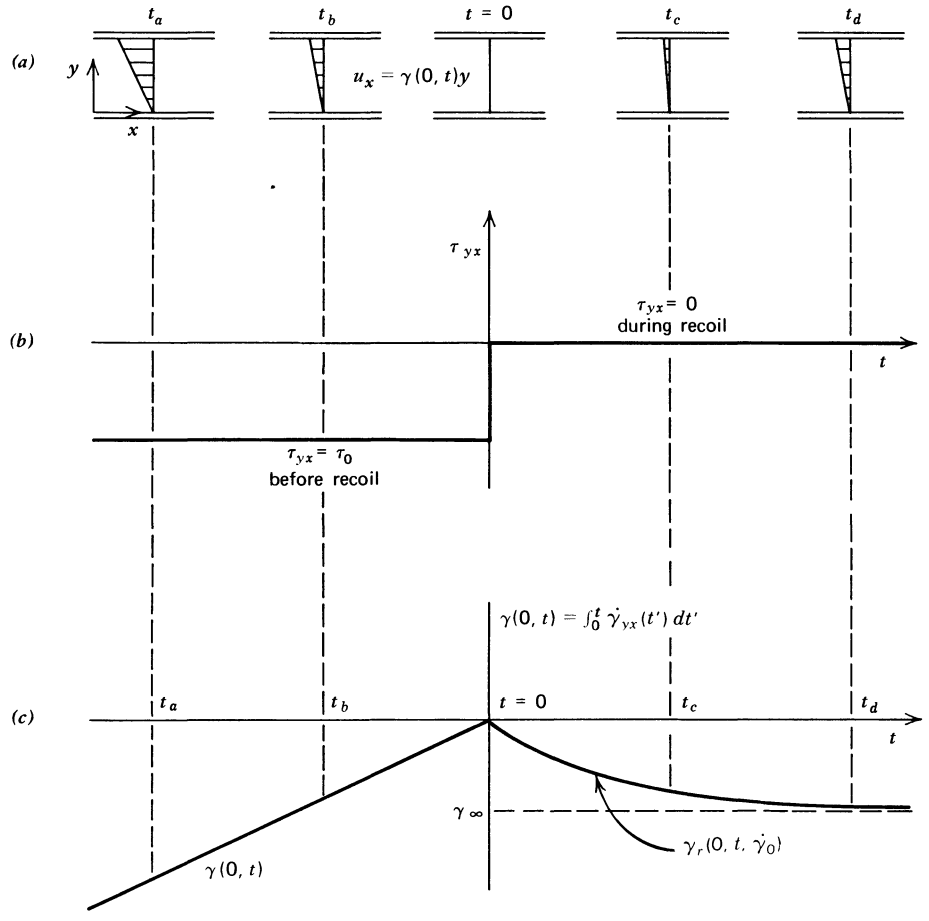

FIGURE 3.4-18. Constrained recoil after cessation of steady shear flow. (*a*) Diagram showing the fluid deformation before and after recoil begins. (*b*) Sketch of shear stress as a function of time. (*c*) Shear strain measured relative to the configuration at the time of shear stress removal $\gamma(0, t) = \int_0^t \dot{\gamma}_{yx}(t')\,dt'$; strain during recoil is denoted by γ_r and the ultimate recoil by γ_∞. Note that γ_r depends parametrically on the shear rate $\dot{\gamma}_0$ prior to the recoil experiment.

At long times the recoil approaches the *ultimate recoil* or *recoverable shear* $\gamma_\infty(\dot\gamma_0)$, which depends on the value of shear rate (or shear stress) in the steady shear flow preceding the recoil. The steady state compliance, J_e^0, is defined in terms of the ultimate recoil by

$$\begin{aligned}\gamma_\infty &= J_e^0(\tau_0)\tau_0 \\ &= -J_e^0(\dot\gamma_0)\eta(\dot\gamma_0)\dot\gamma_0\end{aligned} \tag{3.4-11}$$

In the limit of small τ_0 or $\dot\gamma_0$, the steady state compliance is a linear viscoelastic property equal to (see Eq. 5.3-33 and Table 5.3-1)

$$J_e^0 = \lim_{\omega\to 0}\frac{G'}{\omega^2\eta_0^2} = \frac{\Psi_{1,0}}{2\eta_0^2} \tag{3.4-12}$$

Note that in the linear limit the (steady state) recoverable shear is

$$\boxed{\gamma_\infty = -\frac{\Psi_{1,0}\dot\gamma_0}{2\eta_0}} \tag{3.4-13}$$

This formula for recoverable shear is often (incorrectly) used outside of the linear viscoelastic regime with $\Psi_{1,0}$ and η_0 replaced by $\Psi_1(\dot\gamma_0)$ and $\eta(\dot\gamma_0)$. Although this is conventional, the connection formula between J_e^0 and $\Psi_1/2\eta^2$ in Eq. 3.4-12 does not hold outside of the zero-shear-rate regime.

A consequence of constraining the fluid recovery by maintaining a fixed gap between the plates is that the normal stresses do not go to zero when the shear stress is made zero; rather, they relax over a period of time comparable to that required for the recoil. If all

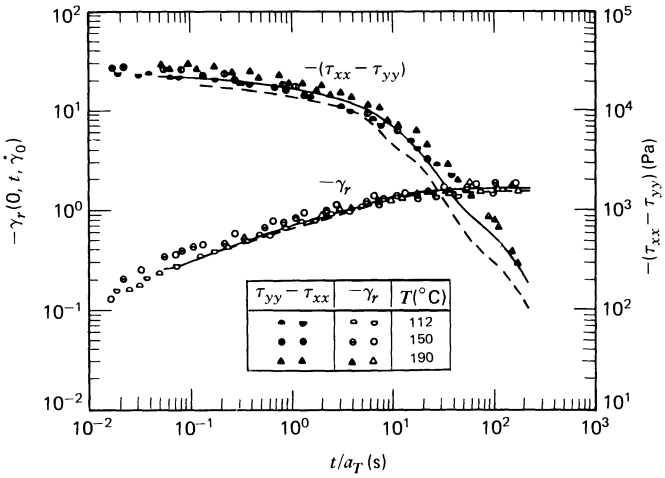

FIGURE 3.4-19. Constrained recoil after steady shear flow is achieved in the creep tests shown in Fig. 3.4-17. The shear strain is measured relative to the time at which the shear stress is set to zero; it is negative because recoil occurs in the direction opposite to the preceding shear flow. The data from three different temperatures are superposed on a single curve at reference temperature $T_0 = 150°C$ by use of the reduced time scale t/a_T. The relaxing first normal stress difference shows that $\tau_{xx} - \tau_{yy}$ does not become zero immediately when τ_{yx} is set to zero. The solid and dashed curves are calculated with the Wagner model (cf. Fig. 3.3-2). [M. H. Wagner and H. M. Laun, *Rheol. Acta*, **17**, 138–148 (1978).]

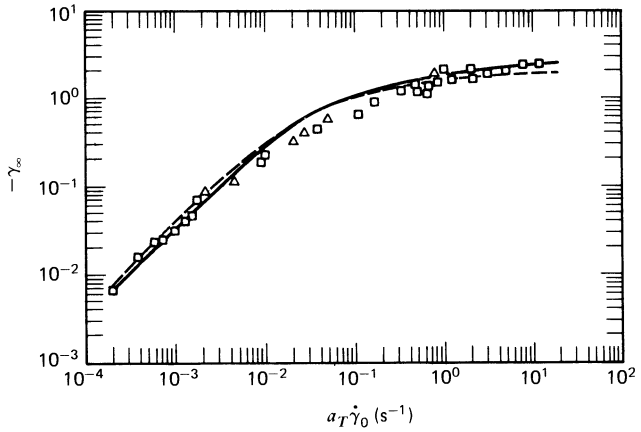

FIGURE 3.4-20. Dependence of the ultimate recoil γ_∞ on the shear rate $\dot{\gamma}_0$ of the steady shear flow preceding the recoil experiment for the low-density polyethylene melt shown in Fig. 3.4-19. Recoil data were taken at $T = 423$ K following steady shear flow obtained from both constant shear rate (□) and constant shear stress (○) experiments. The (○) data are from Fig. 3.4-19 and the (□) data from Fig. 3.4-21. The solid and dashed curves are calculated with the Wagner model (cf. Fig. 3.3-2). [M. H. Wagner and H. M. Laun, *Rheol. Acta*, **17**, 138–148 (1978).]

stresses were removed from the sample at $t = 0$, the fluid might expand laterally during the recoil.[12] Unconstrained or free recovery is thus not necessarily a shear flow. Since constrained recoil can be pictured as the opposite to a creep experiment, it is sometimes called "creep recovery".

Constrained recoil data for a low-density polyethylene melt are shown in Figs. 3.4-19 through 21. In Fig. 3.4-19 the recoil from the steady shear flow achieved after the creep

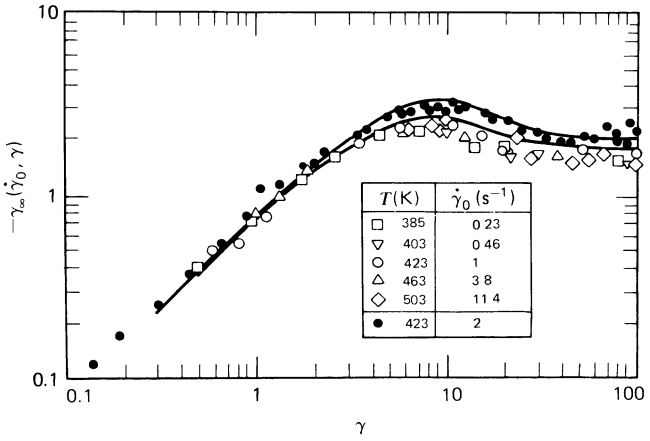

FIGURE 3.4-21. Ultimate recoil as a function of shear strain following start-up of steady shear flow; the shear stress was set to zero after the indicated strains in the start up of steady shear flow. The open symbols correspond to measurements made at the indicated temperatures and shear rates, and all correspond to a reduced shear rate of $a_T\dot{\gamma}_0 = 1\ s^{-1}$ at a reference temperature of $T_0 = 423$ K. The solid symbols were taken at $\dot{\gamma}_0 = 2\ s^{-1}$ and $T = 423$ K. The solid curves were calculated with the Wagner model (cf. Fig. 3.3-2). [M. H. Wagner and H. M. Laun, *Rheol. Acta*, **17**, 138–148 (1978).]

[12] A. S. Lodge, *Elastic Liquids*, Academic Press, New York (1964), pp. 131–138, 239–242.

experiments in Fig. 3.4-17 is shown. The time required to attain the ultimate recoil is approximately the same as the time to reach steady state in the creep experiments. The ultimate recoil increases with increasing value of the steady shear rate $\dot{\gamma}_0$ preceding the recovery as shown in Fig. 3.4-20; the larger the shear rate, the more strain is imposed on the sample within the memory span of the fluid. Recoil experiments can also be done on fluid that is not undergoing steady shear flow. For example start-up of steady shear flow experiments can be stopped short of steady state at various shear strains $\gamma(0, t) = \dot{\gamma}_0 t$ by setting τ_{yx} to zero and the ultimate[13] recoil $\gamma_\infty(\dot{\gamma}_0, \gamma)$ observed. These data are illustrated in Fig. 3.4-21 for two different shear rates where it is seen that a maximum value of $\gamma_\infty(\dot{\gamma}_0, \gamma)$ occurs at strains less than that required to attain steady shear flow.

§3.5 SHEARFREE FLOW MATERIAL FUNCTIONS

Since we assume that the fluid is isotropic, the stresses and material functions in simple shearfree flows depend only on $\dot{\varepsilon}(t)$ and the parameter b that defines the type of flow. For steady simple shearfree flows we define two viscosity functions $\bar{\eta}_1$ and $\bar{\eta}_2$ to describe the two normal stress differences introduced in §3.2

$$\boxed{\tau_{zz} - \tau_{xx} = -\bar{\eta}_1(\dot{\varepsilon}, b)\dot{\varepsilon}} \tag{3.5-1}$$

$$\boxed{\tau_{yy} - \tau_{xx} = -\bar{\eta}_2(\dot{\varepsilon}, b)\dot{\varepsilon}} \tag{3.5-2}$$

For the special steady-state shearfree flow where $b = 0$, $\bar{\eta}_2 = 0$ and $\bar{\eta}_1$ is equal to the *elongational viscosity* $\bar{\eta}$:

$$\boxed{\bar{\eta}(\dot{\varepsilon}) = \bar{\eta}_1(\dot{\varepsilon}, 0); \qquad \bar{\eta}_2(\dot{\varepsilon}, 0) = 0} \tag{3.5-3}$$

For $\dot{\varepsilon} > 0$, $\bar{\eta}$ describes elongational flow, and for $\dot{\varepsilon} < 0$, it describes biaxial stretching. The elongational viscosity is sometimes called the "Trouton viscosity" or the "extensional viscosity."

Sample data for $\bar{\eta}$ are shown in Fig. 3.5-1 for a polystyrene melt.[1] Also shown for comparison is the viscosity at the same temperature. At low elongation rates the elongational viscosity approaches a constant value known as the *zero-elongation-rate elongational viscosity* $\bar{\eta}_0$, which is three times the zero-shear-rate viscosity. Recall that $\bar{\eta} = 3\mu$ for Newtonian fluids (cf. Eq. 1B.7-3). As the elongation rate is increased, $\bar{\eta}(\dot{\varepsilon})$ is seen to increase somewhat, and then decrease at still higher elongation rates. This is contrasted in Fig. 3.5-1 with the viscosity $\eta(\dot{\gamma})$, which decreases with increasing shear rate. The shear stress at which η begins to "shear thin" is approximately the same as the stress difference $(\tau_{zz} - \tau_{xx})$ at which $\bar{\eta}$ begins to deviate from $\bar{\eta}_0$. For other polymer melts, different behavior for $\bar{\eta}(\dot{\varepsilon})$ is found. For example, for a polyisobutylene–isoprene copolymer[2] $\bar{\eta}$ appears to be independent of elongation rate and no maximum is observed; for high-density polyethylene,[3] $\bar{\eta}$ is observed to decrease with increasing $\dot{\varepsilon}$ without ever going through a

[13] We use the same terminology, ultimate recoil, for both $\gamma_\infty(\dot{\gamma}_0)$ and $\gamma_\infty(\dot{\gamma}_0, \gamma)$. The number of arguments indicates whether the recoil is measured following steady shear flow.

[1] H. Münstedt, *J. Rheol.*, **24**, 847–867 (1980).

[2] J. F. Stevenson, *AIChE J.*, **18**, 540–547 (1972).

[3] H. M. Laun in G. Astarita, G. Marrucci, and L. Nicolais, eds., *Rheology, Vol. 2: Fluids*, Plenum Press, New York (1980), pp. 419–424.

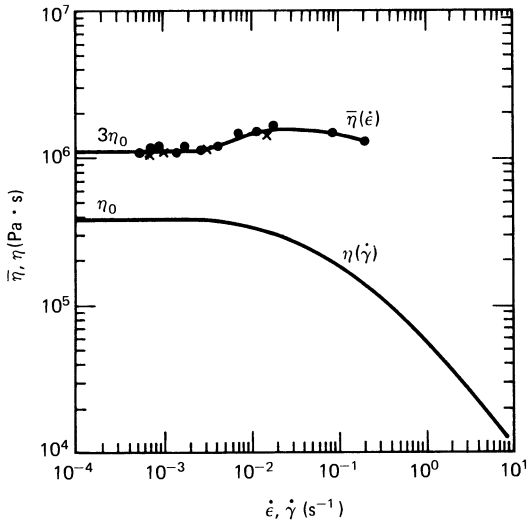

FIGURE 3.5-1. Elongational viscosity $\bar{\eta}$ and viscosity η for a polystyrene melt ($\bar{M}_w = 2.19 \times 10^5$, $\bar{M}_w/\bar{M}_n = 2.3$; sample denoted as PS IV in Fig. 3.5-2) as functions of elongation rate and shear rate, respectively. The experimentally determined zero-strain-rate values of $\bar{\eta}_0 = 1.1 \times 10^6$ Pa·s and $\eta_0 = 3.7 \times 10^5$ Pa·s agree closely with the relation $\bar{\eta}_0 = 3\eta_0$, as they must. The temperature is $T = 433$ K. [Data replotted from H. Münstedt, *J. Rheol.*, **24**, 847–867 (1980).]

TABLE 3.5-1

Definitions of Material Functions in Shearfree Flows

$v_x = -\frac{1}{2}\dot{\epsilon}(1 + b)x, \quad v_y = -\frac{1}{2}\dot{\epsilon}(1 - b)y, \quad v_z = \dot{\epsilon}z$

Flow	Material Function	Defining Equation
a. Steady shearfree flow $\dot{\epsilon}$ = constant	$\bar{\eta}_1(\dot{\epsilon})$ $\bar{\eta}_2(\dot{\epsilon})$	$\tau_{zz} - \tau_{xx} = -\bar{\eta}_1\dot{\epsilon}$ $\tau_{yy} - \tau_{xx} = -\bar{\eta}_2\dot{\epsilon}$
b. Stress growth on inception of steady shearfree flow $\dot{\epsilon} = \begin{cases} 0 & t < 0 \\ \dot{\epsilon}_0 & t \geq 0 \end{cases}$	$\bar{\eta}_1^+(t, \dot{\epsilon}_0)$ $\bar{\eta}_2^+(t, \dot{\epsilon}_0)$	$\tau_{zz} - \tau_{xx} = -\bar{\eta}_1^+\dot{\epsilon}_0$ $\tau_{yy} - \tau_{xx} = -\bar{\eta}_2^+\dot{\epsilon}_0$
c. Elongational creep ($b = 0$) $(\tau_{zz} - \tau_{xx}) = \begin{cases} 0 & t < 0 \\ \sigma_0 & t \geq 0 \end{cases}$	$D(t, \sigma_0)$	$\varepsilon(0, t) = -D\sigma_0$
d. Free recovery after steady elongational flow ($b = 0$) $(\tau_{zz} - \tau_{xx}) = \begin{cases} \sigma_0 & t < 0 \\ 0 & t \geq 0 \end{cases}$	$\varepsilon_r(0, t, \sigma_0)$ $\varepsilon_\infty(\sigma_0)$	$\varepsilon_r = \int_0^t \dot{\epsilon}(t')\,dt'$ $\varepsilon_\infty = \lim_{t\to\infty} \varepsilon_r$

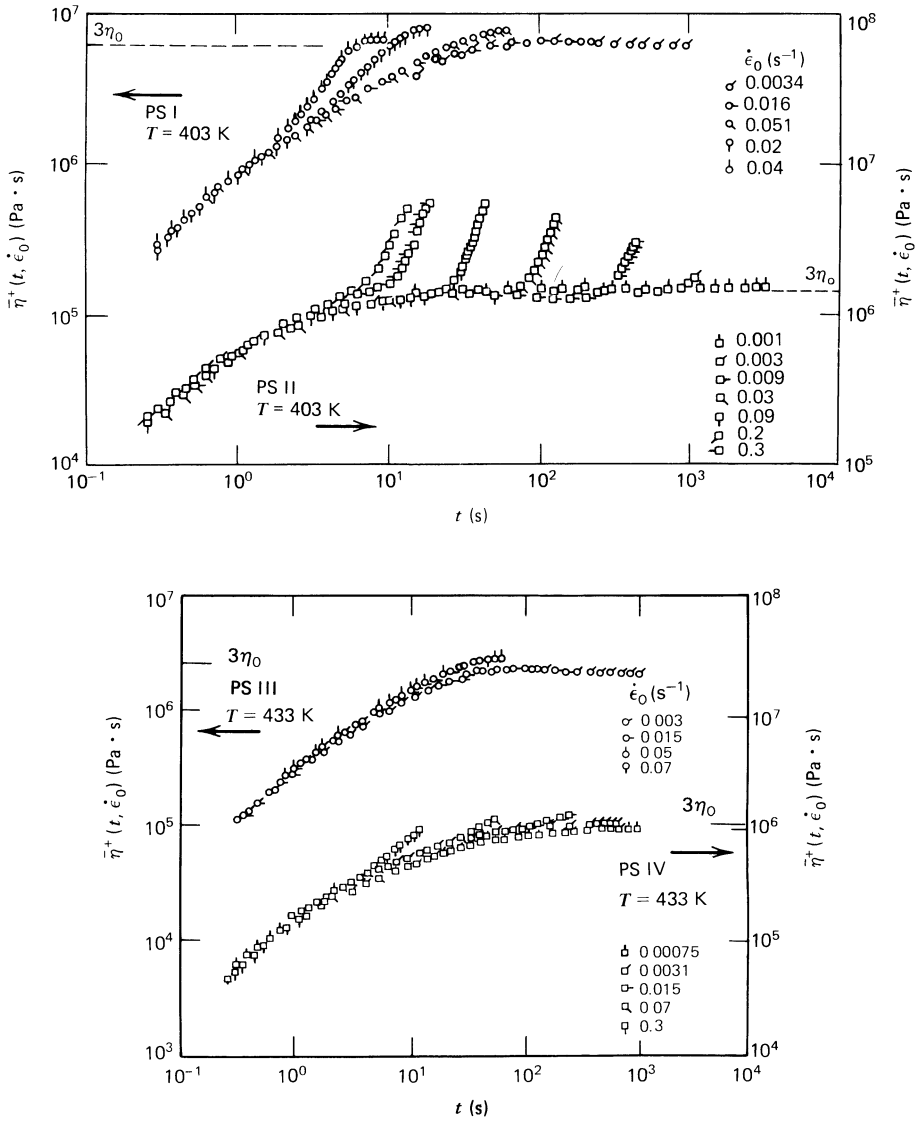

FIGURE 3.5-2. Time dependence of the elongational stress growth viscosity $\bar{\eta}^+$ for four polystyrene melts. The constant elongation rate $\dot{\epsilon}_0$ is applied to the samples for $t \geq 0$. The number average and weight average molecular weights of the samples are as follows:

	$\bar{M}_w$	$\bar{M}_w/\bar{M}_n$
PS I	7.4×10^4	1.2
PS II	3.9×10^4	1.1
PS III	2.53×10^5	1.9
PS IV	2.19×10^5	2.3

[Data from H. Münstedt, *J. Rheol.*, **24**, 847–867 (1980).]

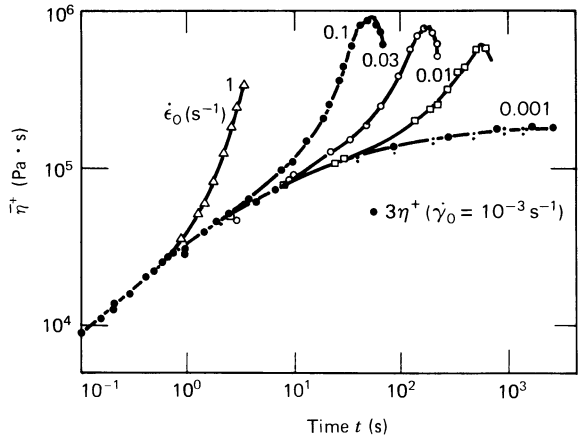

FIGURE 3.5-3. Elongational stress growth viscosity $\bar{\eta}^+$ as a function of time for a low-density polyethylene melt. Note the agreement between $\bar{\eta}^+$ and $3\eta^+$ at low $\dot{\epsilon}_0$ and $\dot{\gamma}_0$. All data were taken at $T = 423$ K. [J. Meissner, *Chem. Engr. Commun.*, **33**, 159–180 (1985).]

maximum. For other polymer melts, e.g, low-density polyethylene, and polymer solutions it has been impossible thus far to achieve steady elongational flow and measure $\bar{\eta}$.

Because of the difficulty in reaching steady state in many shearfree flows of polymeric liquids, transient shearfree flows are very important. Several of the most commonly used of these are summarized in Table 3.5-1. For start-up of steady elongational flow the transient stress is described by the *elongational stress growth function* $\bar{\eta}^+$. Data for this material function are illustrated in Fig. 3.5-2 for several polystyrene melts including the one shown in Fig. 3.5-1. At low strain rates the transient viscosity $\bar{\eta}^+$ is seen to approach the zero-elongation-rate elongational viscosity exponentially. The limiting shape of the $\bar{\eta}^+$ curve at small $\dot{\epsilon}_0$ is independent of $\dot{\epsilon}_0$ and is equal to $3\eta^+$ in the limit of zero shear rate; $\bar{\eta}^+(t, 0)$ can be predicted from linear viscoelasticity. (see Chapter 5).

The most striking feature of the $\bar{\eta}^+$ curves is the abrupt upturn, or "strain hardening," that occurs at a roughly constant value of *Hencky strain* $\varepsilon(0, t) = \dot{\epsilon}_0 t$, the value of which varies from fluid to fluid. Although steady state is approached in most of the tests shown, for the PS II sample there is no indication of a steady state even at the lowest applied strain rates. Note that the strains applied to the samples are quite large; the largest value of ε achieved of about 3.5 corresponds to a ratio of final to initial length of the sample of about $e^{3.5} = 33$ (see Eq. 3.1-4).

The unattainability of a steady state in $\bar{\eta}^+$ has been observed in other melts. The most striking example is the study of a low-density polyethylene melt[4] for which data are shown in Fig. 3.5-3. There $\bar{\eta}^+$ at $\dot{\epsilon}_0 = 10^{-3}\text{s}^{-1}$ is seen to agree well with $3\eta^+$ measured at a shear rate of $\dot{\gamma} = 10^{-3}\ \text{s}^{-1}$. For higher elongation rates the characteristic strain hardening is observed followed by a *maximum* in $\bar{\eta}^+$. No steady state is observed, and $\bar{\eta}^+$ is still decreasing at the highest values of strain. In these experiments strains of $\varepsilon = 7$ were achieved which correspond to increasing the sample length by a factor of 1100! It is not clear that $\bar{\eta}$ exists for some materials and conditions.

Measurements have also been made on the stress growth material functions for other types of shearfree flows. These are illustrated in Figs. 3.5-4 and 5 for a polyisobutylene. Figure 3.5-4 contains data for both elongational flow and biaxial elongational flow. The

[4] T. Raible, A. Demarmels, and J. Meissner, *Polym. Bull.*, **1**, 397–402 (1979); T. Raible, Ph.D. Dissertation No. 6751, ETH Zürich (1981).

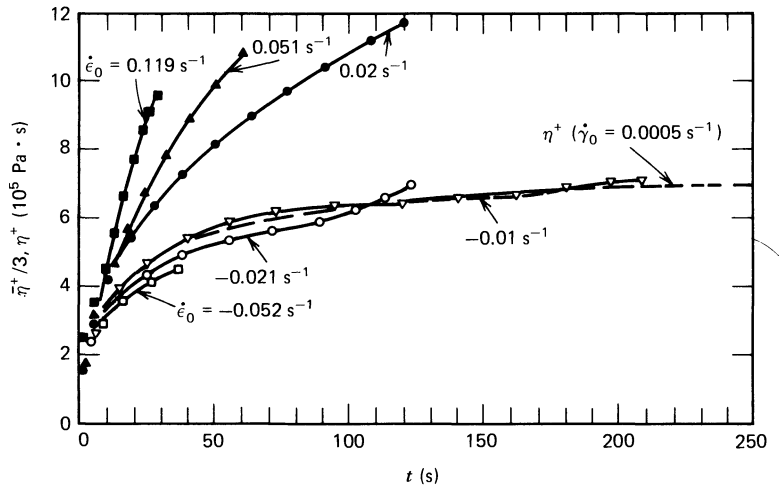

FIGURE 3.5-4. Elongational stress growth viscosity $\bar{\eta}^+$ for start-up of elongational ($\dot{\varepsilon}_0 > 0$) and biaxial elongational ($\dot{\varepsilon}_0 < 0$) flows. Data for η^+ at a very low shear rate are shown for comparison. The data for $\bar{\eta}^+$ are normalized so that they are equal to η^+ in the limit as $\dot{\varepsilon} \to 0$ and $\dot{\gamma} \to 0$. Data are for a polyisobutylene at $T = 296$ K. [J. Meissner, *Pure Appl. Chem.*, **56**, 369-384 (1984).]

data are normalized so that both sets should equal η^+ in the linear viscoelastic limit. Whereas $\bar{\eta}^+(\dot{\varepsilon}_0 > 0)$ rises above this limit as seen in the previous figures, $\bar{\eta}^+(\dot{\varepsilon}_0 < 0)$ falls below η^+ at small strains and then appears to exceed η^+ at large strains. For the planar elongational flow ($b = 1$) in Fig. 3.5-5, $\bar{\eta}_1^+/4$ at large $\dot{\varepsilon}_0$ exceeds η^+ at moderate strains but may fall below η^+ at larger strains. In contrast $\bar{\eta}_2^+/2$ appears to decrease from the linear viscoelastic envelope and remain below it. A few measurements have also been made on this polyisobutylene for shearfree flows with b between 0 and 1.[5]

Thus far we have considered the transient shearfree flows in which $\dot{\varepsilon}$ is varied and the stresses are measured. Next we consider two experiments in which the stress is varied and

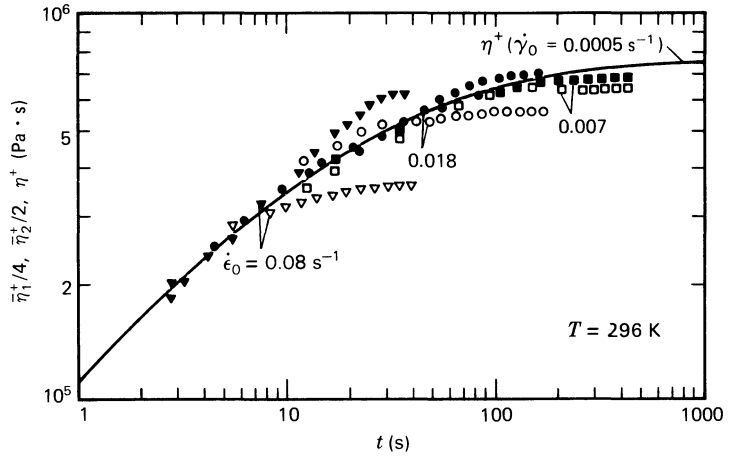

FIGURE 3.5-5. Stress growth viscosities $\bar{\eta}_1^+$ (filled symbols) and $\bar{\eta}_2^+$ (hollow symbols) for start-up of planar elongational flow ($b = 1$). Both $\bar{\eta}_1^+$ and $\bar{\eta}_2^+$ are normalized so they are equal to η^+ in the limit $\dot{\varepsilon}_0 \to 0$ and $\dot{\gamma}_0 \to 0$. Data are for the same material and temperature as Fig. 3.5-4. [J. Meissner, *Pure Appl. Chem.*, **56**, 369-384 (1984).]

[5] A. Demarmels, Ph.D. Dissertation No. 7345, ETH Zürich (1983).

the strain or strain rate is measured. We restrict attention to elongational flow, with $b = 0$, and we denote the normal stress difference $(\tau_{zz} - \tau_{xx})$ by σ. For a cylindrical sample being pulled in the z direction with its sides exposed to atmospheric pressure, σ is equal to the stress applied to the sample by the mechanical clamping arrangement. If σ is suddenly fixed at σ_0 for $t \geq 0$ on a sample that was at equilibrium prior to $t = 0$, then we have an *elongational creep* experiment. If after some amount of deformation ε in the creep experiment the stress σ is suddenly set to 0, then we can observe *free recovery* following elongational flow.

Data for the elongational creep compliance $D(t, \sigma_0)$ defined in Table 3.5-1 are shown in Fig. 3.5-6 for the four polystyrenes presented in Fig. 3.5-2. Steady state is achieved when the slope of log D vs log t is $+1$. As in the data presented in Fig. 3.5-2, no steady state is observed for the PS II sample except at the smallest value of σ.

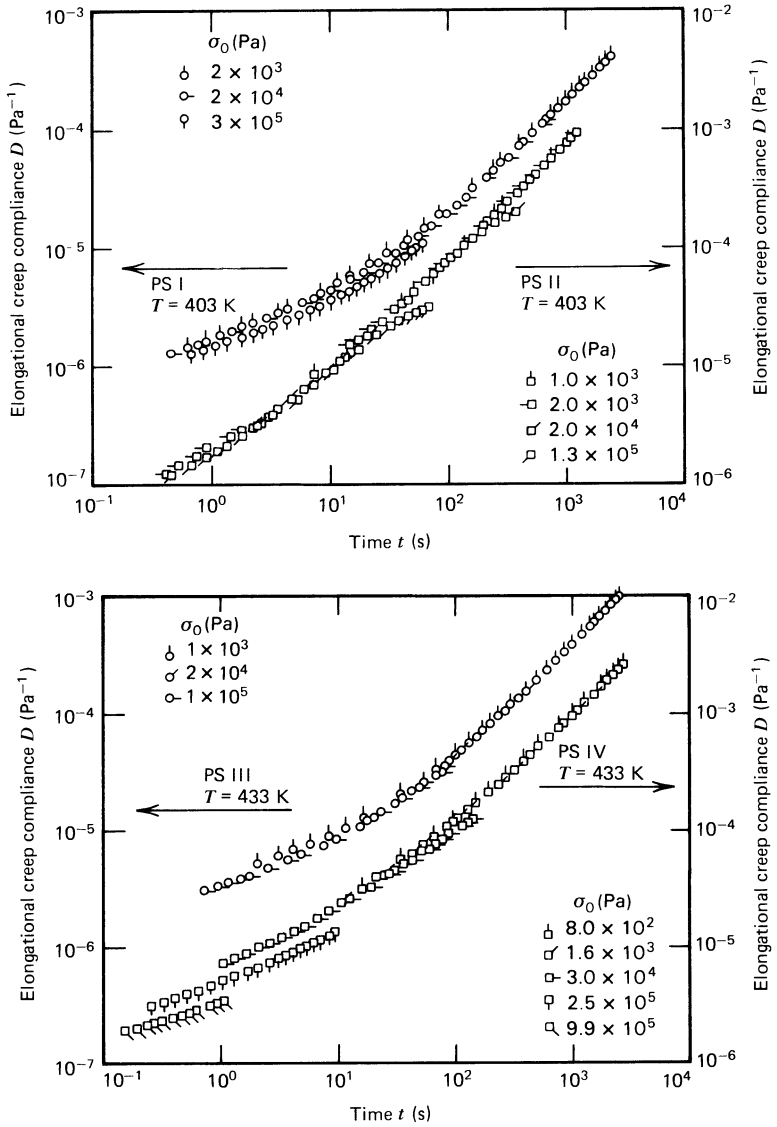

FIGURE 3.5-6. Elongational creep compliance $D(t, \sigma_0)$ for the same polystyrene melts shown in Fig. 3.5-2. [H. Münstedt, *J. Rheol.*, **24**, 847-867 (1980).]

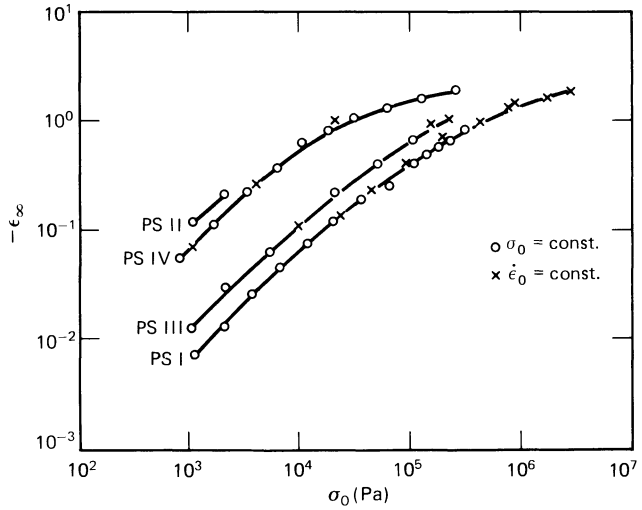

FIGURE 3.5-7. Ultimate recoil ε_∞ following steady elongational flow for the four polystyrene melts and conditions shown in Fig. 3.5-2. [H. Münstedt, *J. Rheol.*, **24**, 847-867 (1980).]

The *ultimate recoil* ε_∞ following steady elongational flow is shown in Fig. 3.5-7. Limited data on PS II is plotted since its steady state was generally not attained. Note that some of the recovery experiments were performed after start-up of steady elongational flow and some after elongational creep. Since steady state was reached prior to the recovery experiment, the two sets of data agree closely. The negative of the ultimate recoil increases monotonically with increasing applied strain rate or tensile stress. For large values of σ_0 the ultimate recoil approaches -2 for the PS I and PS IV samples. This means that the length of a specimen can decrease by more than seven fold following elongational flow! This is an amazing demonstration of "memory" in a liquid system.

Because it is difficult to achieve steady elongational flow, recovery experiments are often performed as a function of applied strain following the initiation of creep or constant

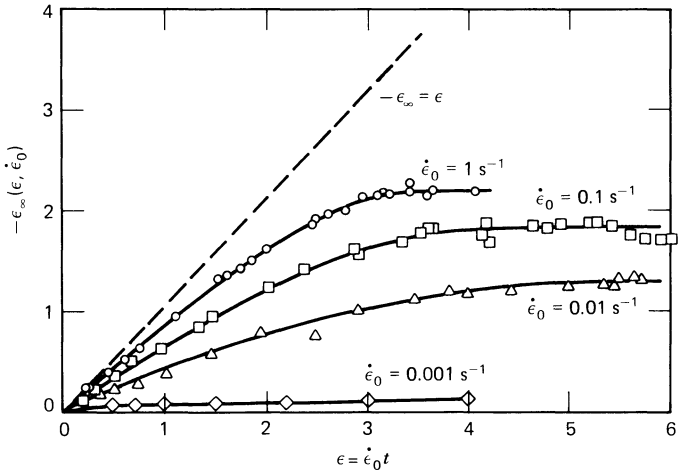

FIGURE 3.5-8. Ultimate recoil ε_∞ $(\varepsilon, \dot{\varepsilon}_0)$ after a strain of ε is applied in start-up of elongational flow with elongation rate $\dot{\varepsilon}_0$ for a low-density polyethylene melt (IUPAC A). All data are taken at $T = 423$ K. [Data from H. Münstedt and H. M. Laun, *Rheol. Acta*, **18**, 492-504 (1979).]

strain rate flow. In these experiments ultimate recoil results are presented as $\varepsilon_\infty(\varepsilon, \sigma_0)$ or $\varepsilon_\infty(\varepsilon, \dot{\varepsilon}_0)$, respectively. Here ε is the strain accrued from the beginning of the elongational flow to the point that σ_0 or $\dot{\varepsilon}_0$ is set to zero. Data for a low-density polyethylene melt for $\varepsilon_\infty(\varepsilon, \dot{\varepsilon}_0)$ are shown in Fig. 3.5-8. The highest amounts of recovery are around $-\varepsilon_\infty = 2.3$ which corresponds to a length contraction of a factor of 10! In this figure the $\varepsilon_\infty = -\varepsilon$ curve represents total recovery of the deformation. For high strain rates and short times, the actual recovery is seen to approach this limiting curve.

§3.6 USEFUL CORRELATIONS FOR MATERIAL FUNCTIONS[1–4]

In §§3.3 to 3.5 we described how the material functions depend on the kinematics, or fluid motion. These material properties also depend on the chemical constitution of the polymeric fluid—for example, solvent, type of polymer, molecular weight, and molecular weight distribution—and on the physical state of the fluid as measured by polymer concentration, temperature, and pressure. In this final section we wish to illustrate how these other variables affect the material functions.

a. Temperature Effects[5–7]

The material functions are strong functions of temperature. In Fig. 3.3-1, the influence of temperature on the viscosity of a low-density polyethylene melt is shown. There it can be seen that the zero-shear-rate viscosity decreases by two orders of magnitude as the temperature is raised from 388 to 513 K. More importantly, the viscosity-shear-rate curves evidently have similar shapes at the different temperatures. This similarity provides the basis for an important empirical method, known as the "method of reduced variables", for combining data taken at several different temperatures into one master curve for the sample. This method was described briefly in connection with Fig. 3.3-2.

In order to obtain a master curve for the viscosity function at an arbitrary reference temperature T_0 from plots of $\log \eta$ versus $\log \dot{\gamma}$ for a variety of temperatures T we follow a two step procedure: (1) the curve at temperature T is first shifted vertically upward by an amount $\log[\eta_0(T_0)/\eta_0(T)]$ and (2) the resulting curve is then shifted horizontally in such a way that any overlapping regions of the T_0-curve and shifted T-curve superpose. The amount by which $\eta(\dot{\gamma}, T)$ must be translated to the right in order to achieve superposition is defined as $\log a_T$.

Often it is found that the shift factor is given by[8]

$$a_T = \frac{\eta_0(T)T_0\rho_0}{\eta_0(T_0)T\rho} \tag{3.6-1}$$

[1] W. W. Graessley, *Adv. Polym. Sci.*, **16**, 1–179 (1974).
[2] S. Middleman, *The Flow of High Polymers*, Wiley-Interscience, New York (1968), Chapt. 5.
[3] A. Peterlin, *Adv. Macromol. Chem.*, **1**, 225–281 (1968).
[4] G. C. Berry and T. G. Fox, *Adv. Polym. Sci.*, **5**, 261–357 (1968).
[5] J. D. Ferry, *Viscoelastic Properties of Polymers*, 3rd ed., Wiley, New York (1980).
[6] G. V. Vinogradov and A. Ya. Malkin, *J. Polym. Sci.* Part A, **21**, 2357–2372 (1964); G. V. Vinogradov and A. Ya. Malkin, *Rheology of Polymers*, Mir Publishers, Moscow (1980), §§2.2, 3.2, 4.6.
[7] R. C. Armstrong and H. H. Winter in E. U. Schlünder, ed., *Heat Exchange Design Handbook*, Hemisphere, Washington, D.C. (1983), Chapt. 2.5.12.
[8] A theoretical basis for the method of reduced variables is provided by molecular theory (see Chapter 15). For dilute solutions Eq. 15.3-31 gives the same expression as Eq. 3.6-1 except that η_0 is replaced by $\eta_0 - \eta_s$ where η_s is the solvent viscosity.

where ρ is the density at temperature T, and ρ_0, the density at T_0. Thus the method of reduced variables predicts that a single *master curve* can be obtained by plotting reduced viscosity η_r vs. reduced shear rate $\dot{\gamma}_r$ where these are defined by

$$\eta_r = \eta(\dot{\gamma}, T)\frac{\eta_0(T_0)}{\eta_0(T)}$$

$$\doteq \frac{\eta(\dot{\gamma}, T)T_0}{a_T T} \tag{3.6-2}$$

$$\dot{\gamma}_r = a_T\dot{\gamma} \tag{3.6-3}$$

In the second line of Eq. 3.6-2 we have neglected the temperature dependence of density. Moreover the ratio $T_0\rho_0/T\rho$ is about unity and changes very little over ordinary temperature ranges. For example this ratio is 0.92 for low-density polyethylene at 150°C relative to 200°C, whereas the complete shift factor a_T has a value of 0.32 for the same temperature change.

If zero-shear-rate viscosity data are not available, then Eq. 3.6-2 cannot be used to calculate the reduced viscosity and empirical shifting along the viscosity and shear rate axes must be done simultaneously in order to determine a_T. A better procedure is to use the fact that the shear stress can be shifted without knowing η_0 (or a_T). From Eqs. 3.6-2 and 3 we define the reduced shear stress τ_r as

$$\tau_r(\dot{\gamma}, T_0) = \tau_{yx}(\dot{\gamma}, T)\frac{T_0\rho_0}{T\rho} \tag{3.6-4}$$

Thus τ_{yx} is fairly insensitive to temperature and can be shifted without knowing a_T. Horizontal shifting of different $\tau_r(\dot{\gamma}, T_0)$ curves will give a master curve of $\tau_r(\dot{\gamma}_r, T_0)$; the amount of shifting along the shear rate axis at each temperature gives a_T. Once this master curve is available it can be used to construct $\eta_r = -\tau_r/\dot{\gamma}_r$ vs. $\dot{\gamma}_r$.

The temperature dependence of a_T is illustrated in Figs. 3.6-1 and 2 for several polymer melts. Because of Eq. 3.6-1 these figures also give the temperature dependence of η_0. Two types of exponential functions have been used for describing the temperature dependence. Often an "Arrhenius dependence" of the form

$$a_T = \exp\left[\frac{\Delta\tilde{H}}{R}\left(\frac{1}{T} - \frac{1}{T_0}\right)\right] \tag{3.6-5}$$

is found to be appropriate (see Fig. 3.6-1). Here $\Delta\tilde{H}$ is known as the "activation energy for flow". This behavior is observed with low-molecular-weight fluids and with molten polymers 100 K or more above their glass transition temperatures. Typical values of $\Delta\tilde{H}/R$ are 4.5×10^3 K (low-density polyethylene), 2.83×10^3 K (high-density polyethylene), and 5.14×10^3 K (polypropylene). These values, of course, depend on molecular parameters of the polymer and therefore may change considerably within each class of polymer.

For temperatures between the glass-transition temperature T_g and $T_g + 100$, the *WLF equation* for a_T has been found to hold for a wide variety of polymers[9]

$$\log a_T = \frac{-c_1^0(T - T_0)}{c_2^0 + (T - T_0)} \tag{3.6-6}$$

[9] M. L. Williams, R. F. Landel, and J. D. Ferry, *J. Am. Chem. Soc.*, **77**, 3701-3707 (1955).

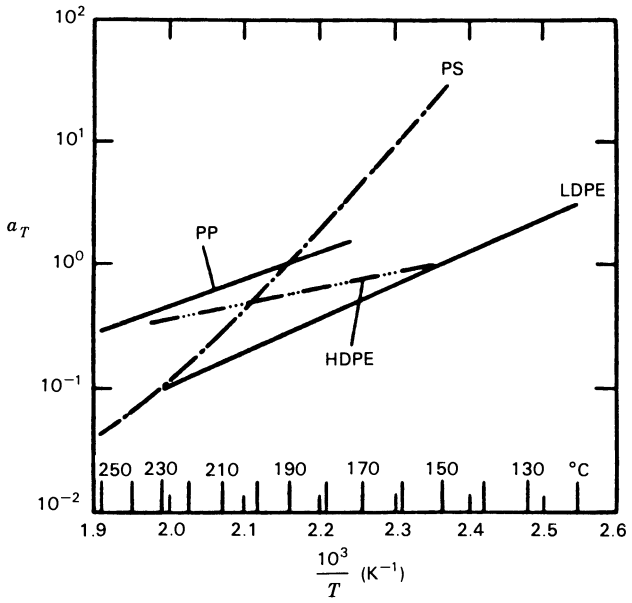

FIGURE 3.6-1. Arrhenius plot of the shift factors a_T for several molten polymers. The reference temperature T_0 is 423 K for low-density polyethylene (LDPE) and high-density polyethylene (HDPE) and 190°C for polypropylene (PP) and polystyrene (PS). [Reproduced with permission from H. Münstedt, *Kunststoffe*, **68**, 94 (1978), Hanser Publishers, Munich, GFR.]

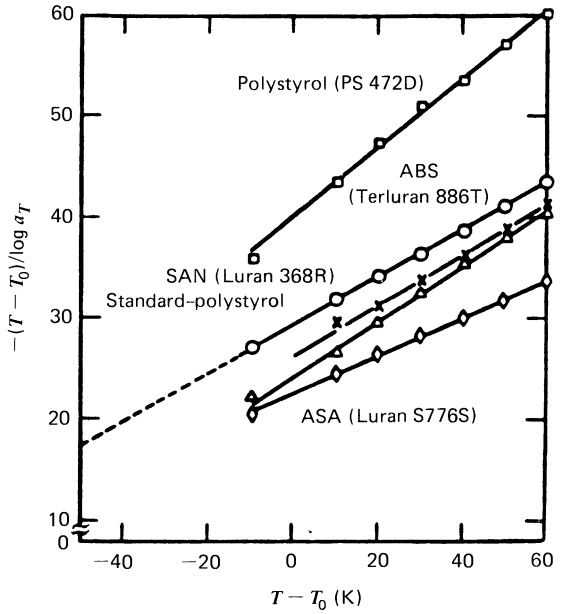

FIGURE 3.6-2. WLF plot of the shift factor a_T for molten polystyrenes. The polymers shown are polystyrene (PS 472D – □), acryonitrile-butadiene-styrene terpolymer (ABS – ○), styrene-acrylonitrile copolymer (SAN – ×), polystyrene (△), and acrylonitrile-styrene-acrylester terpolymer (ASA – ◇). The reference temperature T_0 is 463 K. [Reproduced with permission from H. Münstedt, *Kunststoffe*, **68**, 95 (1978), Hanser Publishers, Munich, GFR.]

If T_0 is taken to be the glass-transition temperature, then $c_1^0 = 17.44$ and $c_2^0 = 51.6$ K. These constants are useful when specific data on a polymer are not available. When some data are available, it is preferable to take $c_1^0 = 8.86$ and $c_2^0 = 101.6$ K, and then to choose T_0 to give a best fit of the data.

Styrene polymers are usually well described by the WLF equation. The agreement of the WLF equation is shown best by plotting $(T - T_0)/\log a_T$ vs. $(T - T_0)$ as shown in Fig. 3.6-2 for a variety of polystyrenes.

Master curves for other material functions are obtained similarly to η. To decide on a proper form for the reduced material functions we assume that all components of the stress are reduced in the same manner as the shear stress. For example, we assume the first normal stress difference $N_1 = +\Psi_1\dot{\gamma}^2$ shifts in the same way as τ_{yx}, so that the reduced first normal stress difference is given by

$$N_{1,r}(\dot{\gamma}, T_0) = N_1(\dot{\gamma}, T)\frac{T_0}{T}\frac{\rho_0}{\rho} \tag{3.6-7}$$

Thus the first normal stress coefficient is reduced as

$$\Psi_{1,r}(\dot{\gamma}, T_0) = \Psi_1\frac{T_0}{a_T^2 T} \tag{3.6-8}$$

where we have taken $\rho_0/\rho = 1$.

For the linear viscoelastic properties (for which the method of reduced variables was originally developed), the reduced moduli are defined by

$$G'_r(\omega, T_0) = G'(\omega, T)\frac{T_0\rho_0}{T\rho} \tag{3.6-9}$$

$$G''_r(\omega, T_0) = G''(\omega, T)\frac{T_0\rho_0}{T\rho} \tag{3.6-10}$$

Note that the moduli are reduced in exactly the same way as stress. Corresponding to Eqs. 3.6-9 and 10 we have (cf. Eq. 3.6-2)

$$\eta'_r(\omega, T_0) = \eta'(\omega, T)\frac{T_0}{a_T T} \tag{3.6-11}$$

$$\eta''_r(\omega, T_0) = \eta''(\omega, T)\frac{T_0}{a_T T} \tag{3.6-12}$$

where we have set $\rho/\rho_0 = 1$.

The success of the method of reduced variables in producing master curves is illustrated in Figs. 3.3-2, 3.4-3, 17, 19 and 20 for low-density polyethylene. A successful master curve of η_r and $N_{1,r}$ for a polystyrene solution is shown in Fig. 3.6-3.

The principal use for the method of reduced variables is that it allows us to extend the effective shear-rate or frequency range of an experimental geometry. Because of the factor a_T that multiplies $\dot{\gamma}$ in the master curve, varying temperature at a fixed shear rate is equivalent to varying shear rate at a fixed temperature. Thus, by measuring viscosity over two or three decades of shear rate at many different temperatures and then combining the

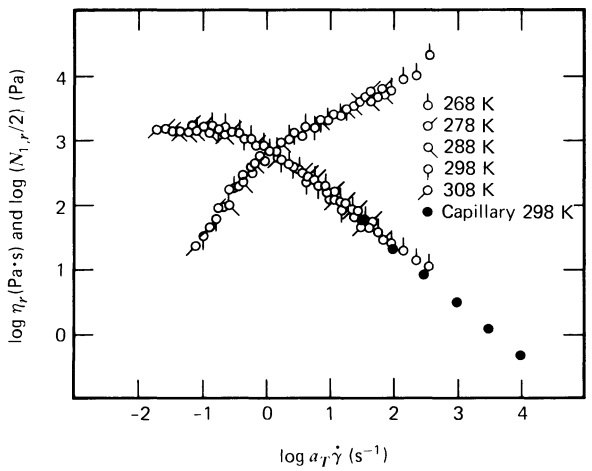

FIGURE 3.6-3. Master curves for viscosity and first normal stress difference for a solution of 2.0×10^6 molecular weight, monodisperse, linear polystyrene in 1-chloronaphthalene. The reduced quantities η_r and $N_{1,r}$ are defined in Eqs. 3.6-2 and 7. The concentration of polymer is 0.150 g/cm^3 and the reference temperature is $T_0 = 423$ K. High shear rate data taken in the capillary viscometer at 423 K were not shifted. [K. Yasuda, R. C. Armstrong, and R. E. Cohen, *Rheol. Acta*, **20**, 163–178 (1981).]

results from the separate tests into a composite curve, it is possible to obtain the viscosity function over six or more decades of shear rate. To obtain reliable results by this method, it is essential that substantial portions of the superposed segments overlap. Even then we must be careful in using results obtained this way, since the cumulative error in estimating several shifts may be large when a wide range of shear rates is used. Finally, when the method of reduced variables is used for dilute solutions, it is more convenient to work in terms of $\eta - \eta_s$ and $\eta_0 - \eta_s$ in place of η and η_0.

b. Effects of Concentration and Molecular Weight[10]

We have already been introduced to the effects of concentration on the viscosity function in §3.3 where we used the intrinsic viscosity to describe the initial rate of increase of η with increasing mass concentration c. In this subsection we shall extend that discussion to cover a full range of concentrations, from infinite dilution to the undiluted state. It is found that for homologous series of fractionated linear polymers, the relation between $[\eta]_0$ and molecular weight can be expressed as:[11]

$$[\eta]_0 = K'M^a \tag{3.6-13}$$

where the value of K' depends on the particular polymer–solvent pair. The parameter a, which is known as the *Mark–Houwink exponent*, lies in the range 0.5–0.8. Originally it was thought that $[\eta]_0$ was proportional to M, this linear relation being known as *Staudinger's rule*.[12]

[10] W. W. Graessley, *op cit.*, §§5 and 8. We have drawn heavily on Graessley's review article for this subsection.
[11] P. J. Flory, *Principles of Polymer Chemistry*, Cornell University Press, Ithaca, NY (1953), pp. 24, 310–314; C. Tanford, *Physical Chemistry of Macromolecules*, Wiley, New York (1961), pp. 407–412.
[12] H. Staudinger and W. Heuer, *Ber. Deutsch. Chem. Ges.*, **63**, 222–234 (1930); H. Staudinger, *Die hochmolekularen organischen Verbindungen*, Springer, Berlin (1932).

Equation 3.6-13 provides a convenient method for determining molecular weight of a polydisperse sample of a linear polymer.[11] For polydisperse samples the *viscosity average molecular weight* $\bar{M}_v$ is given by

$$[\eta]_0 = K'\bar{M}_v^a \tag{3.6-14}$$

where K' and a have the same values as for the monodisperse polymer.

Experimentally, it is found that at low concentrations (defined roughly as $c[\eta]_0 <$ 1 to 5) the material functions correlate well with $c[\eta]_0$ and at high concentrations they correlate with cM. Since it is found that $[\eta]_0$ is proportional to M^a, then we can combine the above and say that cM^x should be a good correlating parameter with x approximately equal to 0.68 at low concentration and x equal to unity at high concentrations. Because c and M occur together in both of these regimes, we shall discuss molecular weight and concentration effects together. The quantity $c[\eta]_0$, which gives a rough estimate of the degree to which the domains of different molecules are likely to overlap, is sometimes called the "coil overlap" parameter. Similarly cM gives an approximate measure of the number of intermolecular contacts per molecule. The fact that each is dominant in one concentration regime suggests two different kinds of interaction between molecules at high and low concentrations.

From the discussion in §3.3 we know that the non-Newtonian viscosity can be described to a very good approximation by giving three quantities: the zero-shear-rate viscosity η_0, the shear rate $\dot{\gamma}_0$ at which η begins to decrease from η_0, and the slope $n - 1$ (see §4.1) of the power-law region of a log η versus log $\dot{\gamma}$ curve. A convenient way to present solution data is to plot $(\eta - \eta_s)/(\eta_0 - \eta_s)$ as a function of a reduced shear rate $\lambda\dot{\gamma}$ where λ is some characteristic time constant for the polymer solution. The form of λ suggested by molecular theory (see Chapters 13 to 15) leads to a reduced shear rate $\beta \equiv \lambda\dot{\gamma} = (\eta_0 - \eta_s)M\dot{\gamma}/cRT$. Note that in the limit as c approaches zero this definition becomes $\beta = [\eta]_0\eta_s M\dot{\gamma}/RT$. This latter quantity was used in constructing Fig. 3.3-4 in which intrinsic viscosity data were presented for a variety of polystyrene solutions at different temperatures. We shall consider, then, the influence of concentration and molecular weight on η_0, $\dot{\gamma}_0$(or β_0), and $(n - 1)$.

The behavior of η_0 as a function of c and M is fairly well understood. At low concentrations an expression of the form $\eta_0 = \eta_0(c[\eta]_0)$ may be used to consolidate data for a given polymer-solvent system over a wide range of both concentration and molecular weight of the polymer. An example is the Martin equation:[13]

$$\eta_0 - \eta_s = \eta_s c[\eta]_0 e^{k''c[\eta]_0} \tag{3.6-15}$$

in which k'' is an arbitrary constant. Actually, a slightly better fit with data is obtained by replacing $[\eta]_0$ with $M^{a'}$ and choosing a' to fit data. It is found that a' is close to the Mark-Houwink exponent.

At high concentrations η_0 is governed by the product cM. The most striking feature of $\eta_0(cM)$ is illustrated in Fig. 3.6-4 for a variety of undiluted polymers. It is seen that η_0 goes from a linear to a 3.4 power dependence on M at some critical molecular weight M_c

$$\begin{aligned} \eta_0 &\propto M \qquad (M < M_c) \\ \eta_0 &\propto M^{3.4} \qquad (M > M_c) \end{aligned} \tag{3.6-16}$$

[13] L. Utracki and R. Simha, *J. Polym. Sci. Part A*, **1**, 1089-1098 (1963).

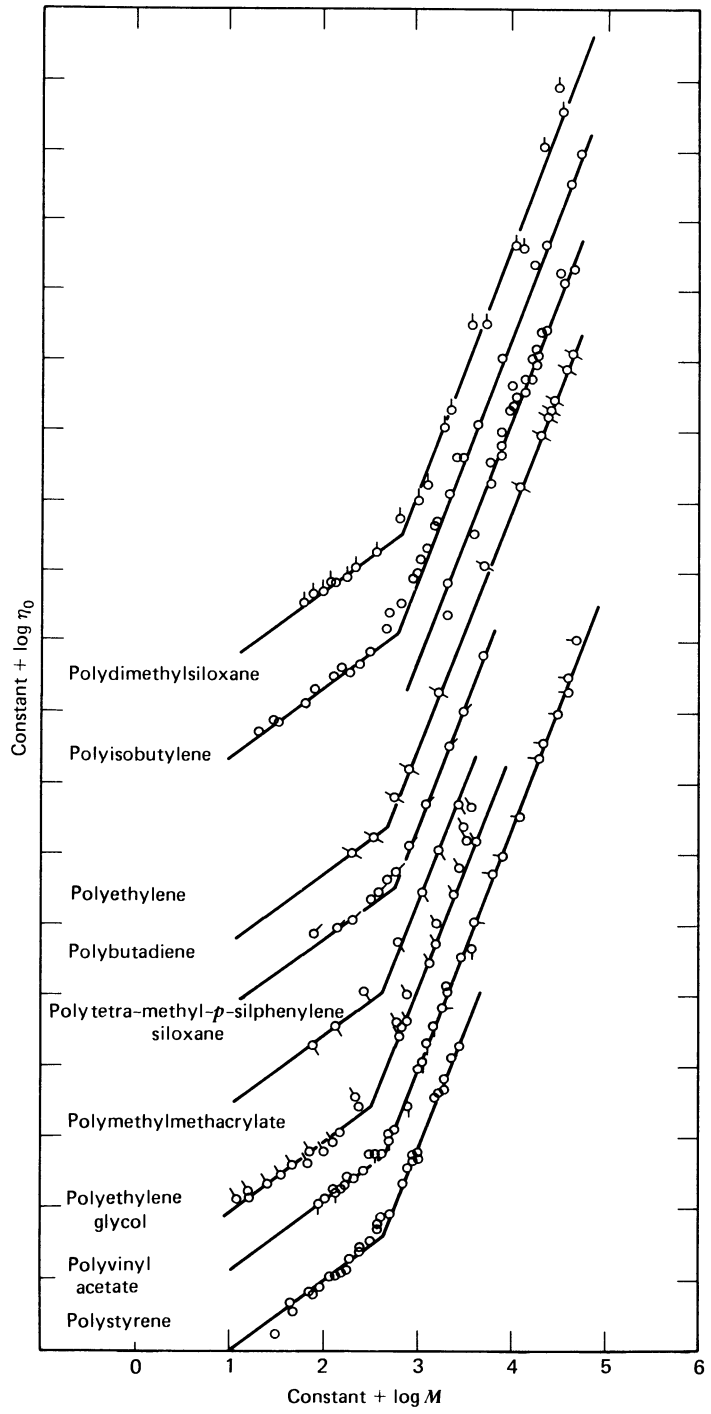

FIGURE 3.6-4. Plots of constant + log η_0 vs. constant + log M for nine different polymers. The two constants are different for each of the polymers, and the one appearing in the abscissa is proportional to concentration, which is constant for a given undiluted polymer. For each polymer the slopes of the left and right straight line regions are 1.0 and 3.4, respectively. [G. C. Berry and T. G. Fox, *Adv. Polym. Sci.*, **5**, 261–357 (1968).]

Actually there is no discontinuity in the slope of $\eta_0(cM)$; the transition is smooth and appears sharp because of the way in which the figure is plotted. The $M^{3.4}$ dependence is followed by an amazingly wide variety of linear polymers. For concentrated solutions, similar behavior is found with $(M_c)_{\text{solution}} = (\rho/c)M_c$ where ρ is the density of the solution. The $M^{3.4}$ behavior of melts and concentrated polymer solutions is thought by many polymer chemists to be due to the existence of "entanglements", or temporary, physical junctions between different polymer molecules (see Chapter 20). It is believed that M_c is a rough measure (within a factor of 2 or 3) of the molecular weight of polymer between two entanglement points. The molecular weight dependence of η_0 can also be interpreted in terms of the "reptation theory" for polymer melts (see Chapter 19).

Next we consider the variation[14] of the critical shear rate β_0 (or $\dot{\gamma}_0$) with c and M. For the sake of definiteness, β_0 is arbitrarily taken to be the value of the dimensionless shear rate at which $(\eta - \eta_s)/(\eta_0 - \eta_s) = 0.8$. At low concentrations β_0 is a constant between 1.5 and 2.0; this value persists down to infinite dilution. At the high concentrations, β_0 increases with cM; β_0 begins this increase at a value of cM slightly greater than ρM_c.

Finally, the power-law slope $(n - 1)$ is approximately -0.1 at infinite dilution. It decreases with $c[\eta]_0$ and approaches $(n - 1) = -0.8$ for $c[\eta]_0 > 20$. The fact that the power-law slope approaches a constant value at high concentrations and molecular weights suggests that for a given polymer–solvent system in the concentrated regime or for a given polymer melt, data taken at varying concentrations, molecular weights, and temperatures should all lie on a single curve when plotted as η/η_0 vs. $\dot{\gamma}/\dot{\gamma}_0$. This prediction is impressively confirmed in Fig. 3.6-5.

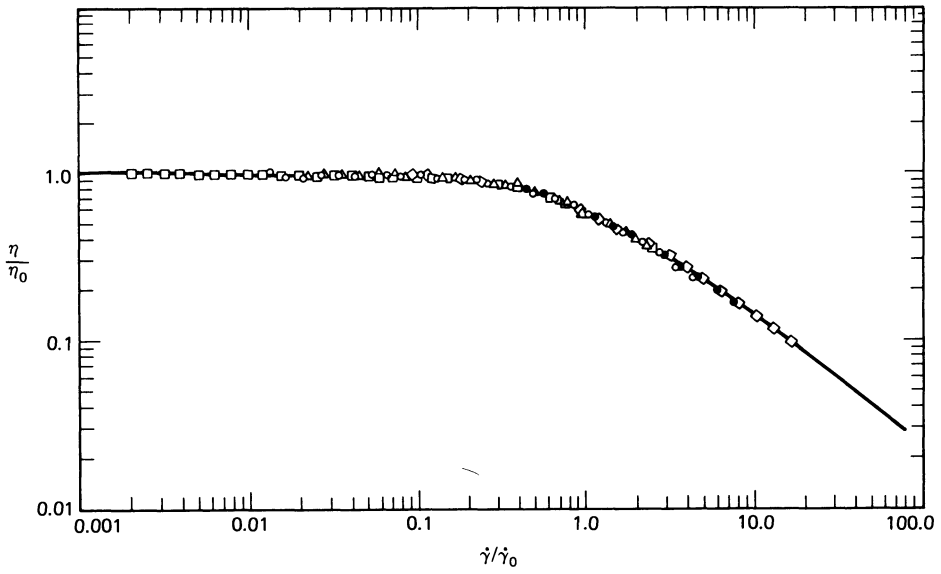

FIGURE 3.6-5. Composite plot of dimensionless viscosity η/η_0 versus dimensionless shear rate $\dot{\gamma}/\dot{\gamma}_0$ for several different concentrated polystyrene-*n*-butyl benzene solutions. Molecular weights varied from 1.6×10^5 to 2.4×10^6, concentrations from 0.255 to 0.55 g/cm^3, and temperatures from 303 to 333 K. [W. W. Graessley, *Adv. Polym. Sci.*, **16**, 1–179 (1974).]

[14] These results as well as those for the power-law slope are based on data for narrow molecular weight distribution polystyrene and poly-α-methylstyrene solutions and melts. See W. W. Graessley, *op. cit.*, and K. Yasuda, R. C. Armstrong, and R. E. Cohen, *Rheol. Acta*, **20**, 163–178 (1981).

Most of the above statements are for polymers with narrow molecular weight distributions. Roughly speaking, broadening the distribution lowers $\dot{\gamma}_0$ and broadens the range of shear rates over which the transition from η_0 to a power-law behavior occurs. Some work has been done on constructing phenomenological blending laws from which the properties of polymers of broad molecular weight distributions can be predicted from monodisperse polymer behavior. As an example of effort along these lines we mention the study of Harris on polystyrene solutions.[15] It was found that η_0 for a two-component blend could be related to η_0 of the separate components by

$$\log(\eta_0)_{\text{blend}} = w_1 \log(\eta_0)_1 + w_2 \log(\eta_0)_2 \tag{3.6-17}$$

where w_1 and w_2 are the weight fractions of the components of the blend. This relation does best when the difference between molecular weights of the components is not too great. The molecular weight distribution does not appear to affect either the power-law slope or $\dot{\gamma}_0$ inasmuch as $\dot{\gamma}_0$ is the same function of c and $\bar{M}_w$, and $(n-1)$ is the same function of $c\bar{M}_n$ as for narrow distribution polymers. This study included molecular weights in the range $3.94 \times 10^5 < \bar{M}_w < 1.9 \times 10^6$ and concentrations of polystyrene in Aroclor between 0.0357 and 0.1502 g/cm^3. The kinetic theory of polydisperse polymer melts is discussed in Chapter 19.

The dynamic viscosity $\eta'(\omega)$ can be described by η_0, a characteristic frequency ω_0 at which $\eta'(\omega)$ begins to decrease, and a power-law slope for high frequencies. The dynamic viscosity η' is often presented as $(\eta' - \eta_s)/(\eta_0 - \eta_s)$ versus $\lambda\omega$ where λ is given by molecular theory as before (see text above Eq. 3.6-15). Experimentally, it is found that the characteristic frequency ω_0 is practically the same as $\dot{\gamma}_0$ for *all* polymeric fluids.[16] Hence the only aspect of η' that we need to describe is the high frequency behavior.[17] For molecules that are not of too high a molecular weight, η' is proportional to $\omega^{-1/3}$ at low concentrations and high frequencies. At $c[\eta]_0$ approximately equal to 3, the dependence on ω begins to change until for high concentrations and undiluted polymers, η' varies as $\omega^{-1/2}$. This sequence is sometimes referred to as a transition from "Zimmlike" to "Rouselike" behavior, as the Zimm and Rouse molecular theories account for the respective dependences on ω (see Chapter 15). As one proceeds from low to high concentrations, the high frequency behavior of η''/ω goes from $\omega^{-4/3}$ to $\omega^{-3/2}$.

Master curves for the dynamic moduli for a series of linear, narrow-distribution polystyrenes having different molecular weights are shown in Fig. 3.6-6. The transition region between zero-frequency behavior ($G' \propto \omega^2$) and high frequency behavior ($G' \propto \omega^{1/2}$) becomes broader as molecular weight increases. There is a pronounced common region in which the curves for different molecular weights overlap and in which the storage modulus is constant. This value is known as the *plateau modulus* G_{eN}^0. Clearly this modulus is independent of the overall molecular weight of the polymer. It is believed to be proportional to the molecular weight of polymer segments between 'entanglements' or between points where the motion of the polymer is severely constrained by neighboring molecules[18] (see Chapters 19 and 20).

The molecular weight dependence of several other material functions is now briefly described. In Fig. 3.6-7 the molecular weight dependence of the zero-shear-rate first normal stress coefficient and the steady-state compliance is contrasted with that of η_0 for

[15] E. K. Harris, Jr., *J. Appl. Polym. Sci.*, **17**, 1679–1692 (1973).
[16] W. W. Graessley, *op. cit.*, p. 126.
[17] J. D. Ferry, *op. cit.*, Chapt. 11.
[18] J. D. Ferry, *op. cit.*, Chapt. 13.

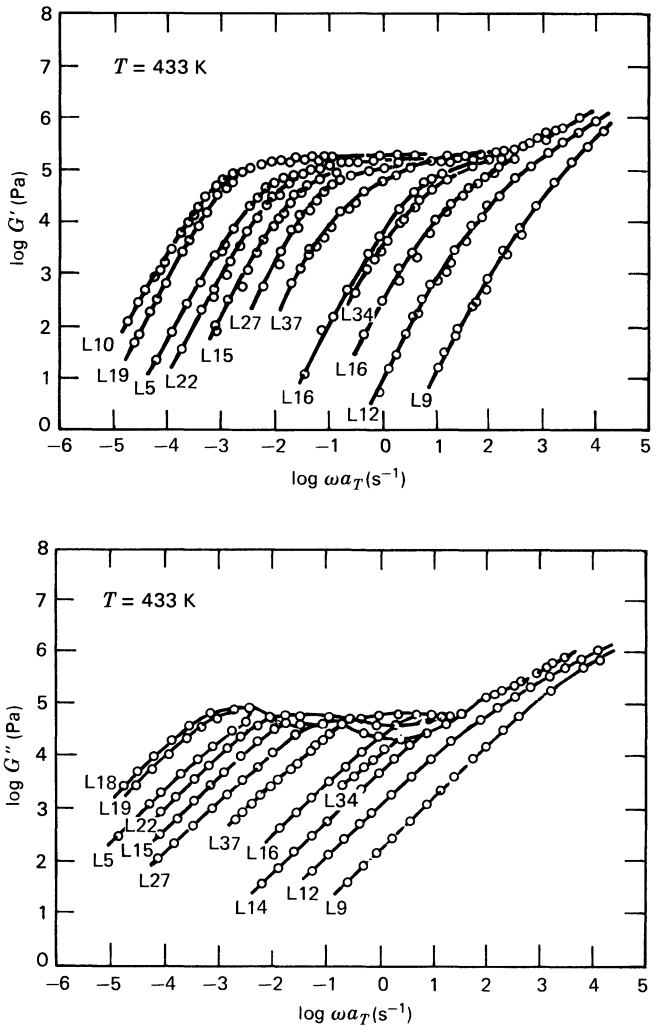

FIGURE 3.6-6. Master curves of G' and G'' for a series of narrow-distribution, linear polystyrenes. The value of G' in the frequency regime where it is constant is known as the plateau modulus. The viscosity average molecular weights of the samples are: L18-580,000; L19-510,000; L5-350,000; L22-275,000; L15-215,000; L27-167,000; L37-113,000; L16-58,700; L34-46,900; L14-28,900; L12-14,800; L9-8,900. The reference temperature is $T = 160°C$. [Reprinted with permission from S. Onogi, T. Masuda, and K. Kitagawa, *Macromolecules*, **3**, 109–116 (1970). Copyright (1970) American Chemical Society.]

polyamide-6 polymers. It is interesting that J_e^0 is independent of molecular weight and that $\Psi_{1,0}$ follows

$$\Psi_{1,0} \propto \bar{M}_w^{7.0} \propto \eta_0^2 \tag{3.6-18}$$

For polydisperse polymers $\Psi_{1,0}$ is more sensitive to high molecular weight fractions than either η_0 or J_e^0.

Since $\bar{\eta}_0 = 3\eta_0$, the molecular weight dependence of $\bar{\eta}_0$ should be the same as that for η_0. This is confirmed in Fig. 3.6-8 for the four polystyrene melts shown in Fig. 3.5-2. The

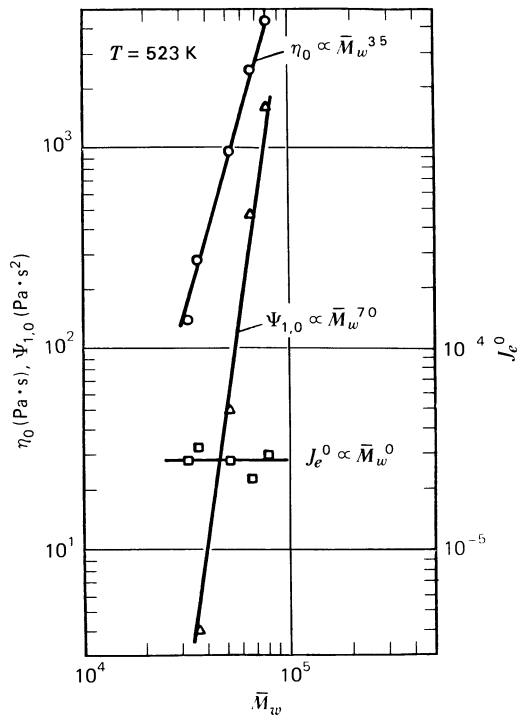

FIGURE 3.6-7. Molecular weight dependence of J_e^0, η_0, and $\Psi_{1,0}$ for polyamide-6 melts with Schultz-Flory molecular weight distributions. [Data from H. M. Laun, *J. Rheol.*, **30**, 459-501 (1986).]

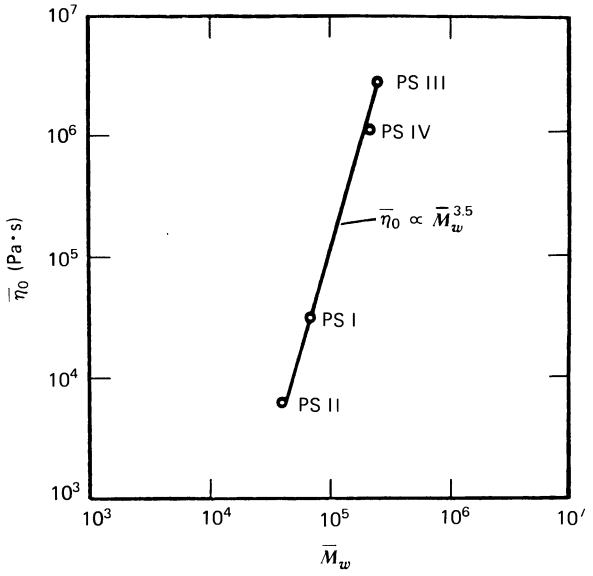

FIGURE 3.6-8. Molecular weight dependence of $\bar{\eta}_0$ for the polystyrenes shown in Fig. 3.5-2. $T = 433$ K. [H. Münstedt, *J. Rheol.*, **24**, 847-867 (1980).]

sensitivity of $\bar{\eta}^+$, D, and ε_∞ to molecular weight distribution has already been seen in Figs. 3.5-2, 6, and 7, respectively.

c. Relations between Linear Viscoelastic Properties and Viscometric Functions

From the sample viscosity and dynamic viscosity data presented in §§3.3 and 3.4 it is evident that $\eta(\dot{\gamma})$ and $\eta'(\omega)$ are similar functions of their arguments. In fact, we know that both approach η_0 as their arguments go to zero and also that both begin to decrease at comparable values of $\dot{\gamma}$ and ω. The main difference between these functions is their behavior at large shear rates and frequencies; it is found that η' decreases more rapidly with ω than η does with $\dot{\gamma}$. The *Cox-Merz rule*[19] has been suggested as a way of obtaining an improved relation between the linear viscoelastic properties and the viscosity. This empiricism predicts that the magnitude of the complex viscosity is equal to the viscosity at corresponding values of frequency and shear rate

$$\eta(\dot{\gamma}) = |\eta^*(\omega)|\Big|_{\omega=\dot{\gamma}} = \eta'(\omega)\left[1 + \left(\frac{\eta''}{\eta'}\right)^2\right]^{0.5}\Bigg|_{\omega=\dot{\gamma}} \tag{3.6-19}$$

The Cox-Merz rule has proven very useful in predicting $\eta(\dot{\gamma})$ when only linear viscoelastic data are available. In Fig. 3.6-9 we show an experimental test of Eq. 3.6-19 for three different polystyrene solutions. Also shown are data for the dynamic viscosity. It is clear that $|\eta^*(\omega)|$ follows $\eta(\dot{\gamma})$ more closely than $\eta'(\omega)$ does, and that the Cox-Merz rule is a good approximation. The agreement between $|\eta^*|$ and η is within experimental error for the linear polystyrene sample.

An interesting alternative to the Cox-Merz rule for predicting η from linear viscoelastic data is *Gleissele's mirror relation*:[20]

$$\eta(\dot{\gamma}) = \eta^+(t)|_{t=1/\dot{\gamma}} \tag{3.6-20}$$

in which $\eta^+(t)$ is the limiting curve of $\eta^+(t, \dot{\gamma})$ as $\dot{\gamma} \to 0$. Successful fits of the viscosity from the viscous stress growth coefficient have been constructed for a variety of polymers, including silicone oils, polyisobutylene, and polyethylene. The Cox-Merz and the Gleissele mirror relation are compared in Fig. 3.6-10 for low-density polyethylene.

It is desirable to be able to predict the normal stresses in steady shear flow from more easily made linear viscoelastic measurements. It may be recalled from §§3.3 and 3.4 that Ψ_1 and $2\eta''/\omega$ have the same values at low shear rates and frequencies and that the shapes of the curves are similar. This similarity is emphasized in Fig. 3.6-9 where $N_1/2$ and G' are compared; here $N_1 = +\Psi_1\dot{\gamma}^2$ is the negative of the first normal stress difference. The discrepancy between $N_1/2$ and G' is more pronounced than that between η and η'. A useful empiricism, analogous to the Cox-Merz rule, is *Laun's rule*[21]

$$\Psi_1(\dot{\gamma}) = \frac{2\eta''(\omega)}{\omega}\left[1 + \left(\frac{\eta''}{\eta'}\right)^2\right]^{0.7}\Bigg|_{\omega=\dot{\gamma}} \tag{3.6-21}$$

[19] W. P. Cox and E. H. Merz, *J. Polym. Sci.*, **28**, 619-622 (1958).
[20] W. Gleissele in G. Astarita, G. Marrucci, and L. Nicolais, eds., *Rheology, Vol. 2: Fluids*, Plenum Press, New York (1980), pp. 457-462.
[21] H. M. Laun, *J. Rheol.*, **30**, 459-501 (1986).

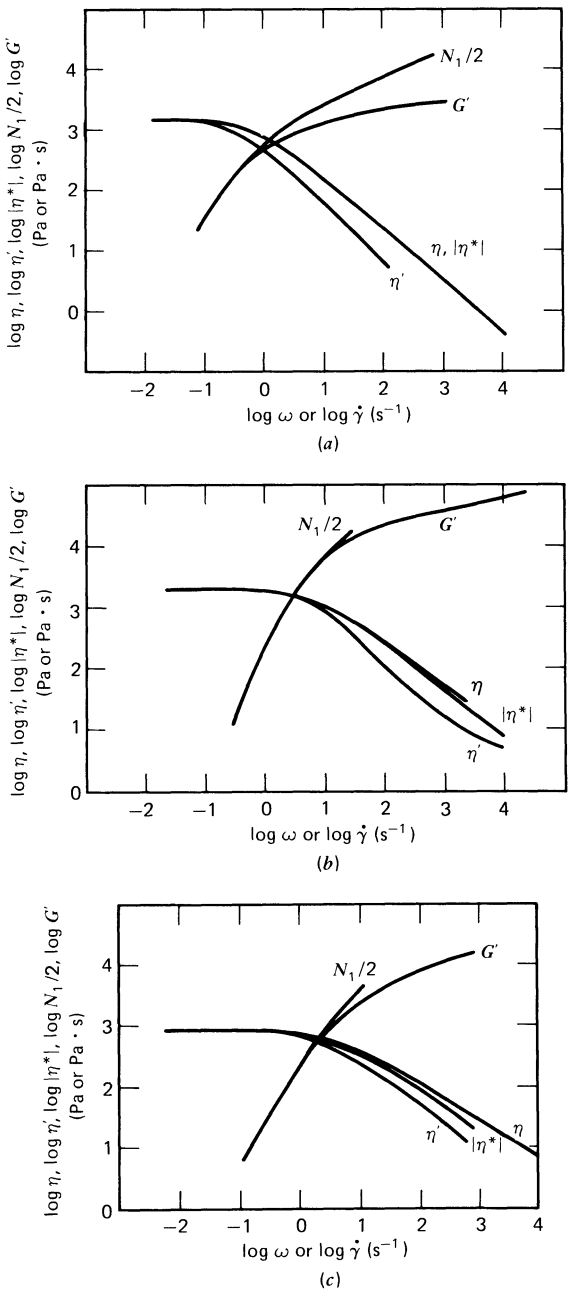

FIGURE 3.6-9. Comparison of the viscous properties $\eta(\dot{\gamma})$ and $\eta'(\omega)$ and the elastic properties $N_1(\dot{\gamma})/2$ and $G''(\omega)$ for several solutions of polystyrene in 1-chloronaphthalene. Also shown is the magnitude of the complex viscosity $|\eta^*|$ which should equal η according to the Cox-Merz rule. The solutions are (*a*) 0.15 g/ml of 2×10^6 $\bar{M}_w$ narrow distribution, linear polystyrene; (*b*) 0.45 g/ml of 7.9×10^5 $\bar{M}_w$ narrow distribution, star-branched polystyrene; and (*c*) 0.42 g/ml of 3.69×10^5 $\bar{M}_w$ broad distribution, linear polystyrene (Styron). [Data from K. Yasuda, R. C. Armstrong, and R. E. Cohen, *Rheol. Acta.*, **20**, 163-178 (1981).]

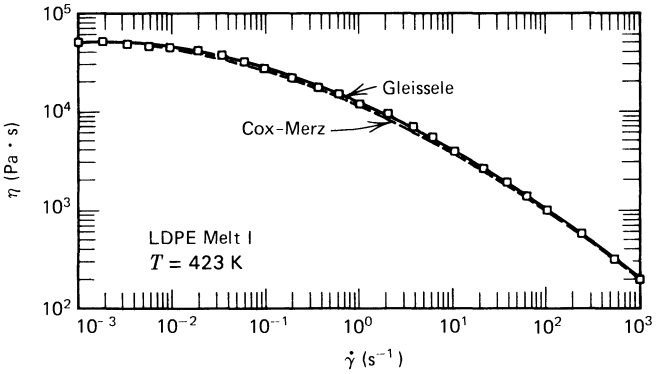

FIGURE 3.6-10. Comparison of the Cox-Merz rule (Eq. 3.6-19) and the Gleissele mirror rule (Eq. 3.6-20) for a low-density polyethylene melt (Melt I). The symbols are data; the dashed curve, Eq. 3.6-19; and the solid curve, Eq. 3.6-20. [H. M. Laun, *J. Rheol.*, **30**, 459–501 (1986).]

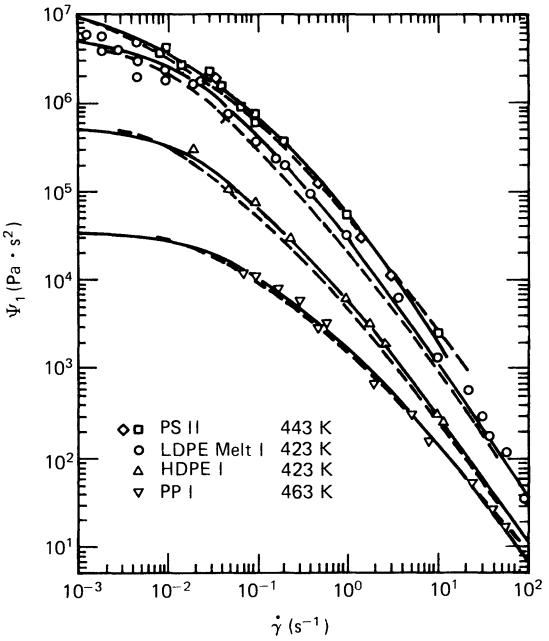

FIGURE 3.6-11. First normal stress coefficient vs. shear rate for polystyrene (PS), low-density polyethylene (LDPE), high-density polyethylene (HDPE), and polypropylene (PP). The symbols are measured values and the ---- curves are calculated from linear viscoelastic data by Eq. 3.6-21. The solid curves are calculated with the Wagner model with a single exponential damping function (see §8.3). [H. M. Laun, *J. Rheol.*, **30**, 459–501 (1986).]

Figure 3.6-11 shows a comparison between measured Ψ_1 and values computed from linear viscoelastic data according to Eq. 3.6-21. The agreement is excellent.

Gleissele[22] has also proposed a 'mirror relation' for Ψ_1 similar to Eq. 3.6-20:

$$\Psi_1(\dot{\gamma}) = \Psi_1^+(t)|_{t=k/\dot{\gamma}} \tag{3.6-22}$$

where k is an empirical constant which seems to be in the range of $2.5 \leq k \leq 3$ for many polymeric liquids. For silicone oils and low-density polyethylene a value of $k = 3$ gives a quantitative connection between Ψ_1 and Ψ_1^+.

Laun[23] has also reported an empiricism relating the recoverable shear γ_∞ to the complex viscosity

$$\begin{aligned} -\gamma_\infty(\dot{\gamma}) &= \frac{\eta''}{\eta'}\left[1 + \left(\frac{\eta''}{\eta'}\right)^2\right]^{1.5}\Bigg|_{\omega=\dot{\gamma}} \\ &= \frac{\Psi_1\dot{\gamma}}{2\eta}\left[1 + \left(\frac{\eta''}{\eta'}\right)^2\right]^{1.3}\Bigg|_{\omega=\dot{\gamma}} \end{aligned} \tag{3.6-23}$$

The second line of Eq. 3.6-23 is obtained by using Eqs. 3.6-19 and 21. Note the similarity between Eqs. 3.6-23 and 3.4-13.

§3.7 KINEMATICS AND CLASSIFICATION OF SHEAR AND SHEARFREE FLOWS

In §3.1 we introduced *simple* shear and shearfree flows; these flows were sufficient for defining the material functions in §§3.3-5. There are many other *non-simple* shear and shearfree flows for which these same material functions apply. The purpose of this section is to give a careful classification of these. This is important for two reasons: first, in later chapters we find constitutive equations that are valid for restricted types of flows, and we need to be able to identify those flows for which the constitutive equation can be legitimately applied; second, since the simple flows of §3.1 are not the most convenient for measuring the material functions, we need to be able to find alternative flows.

a. Shear Flows

In Table 3.7-1 we list all of the various categories of shear flows and give an example of each. This table should give some perspective to the definitions that follow. We begin by returning to the steady simple shear flow of Eq. 3.1-1 with $\dot{\gamma}$ independent of time. A number of characteristics[1] of this flow are:

[22] W. Gleissele, *op. cit.*

[23] H. M. Laun, *op. cit.*

[1] A thorough discussion of shear and other flows in terms of the response of material particles, lines, and planes is given in A. S. Lodge, *Elastic Liquids*, Academic Press, New York (1964); A. S. Lodge, *Body Tensor Fields in Continuum Mechanics*, Academic Press, New York (1974). See also R. I. Tanner, *Engineering Rheology*, Oxford University Press (1985), Chapter 3.

TABLE 3.7-1

Classification and Examples of Shear Flows

	Rheologically Unsteady	Rheologically Steady
General shear flow	N[a] Tangential annular flow with the inner cylinder vibrating axially. H[b] Eccentric-disk (orthogonal) rheometer flow. See Problem 3B.1.	
Unidirectional shear flow	N Oscillatory tangential annular flow. H Oscillatory cone-and-plate flow (approximate for small cone angles and high viscosity fluids). See Table 3.7-2d.	N Helical flow. See Table 3.7-2e.[c] H Tangential annular flow (approximate for narrow gaps and high viscosity fluids).[c]
Rectilinear shear flow	N Pulsatile pressure-driven flow in tubes or slits. H Wall-driven oscillatory flow between parallel plates (approximate for narrow gaps and high viscosity fluids).[d]	N Pressure-driven slit flow.[c] H Wall-driven flow between parallel plates.[c,d]

[a] N = nonhomogeneous.
[b] H = homogeneous.
[c] These are called "viscometric flows."
[d] These are called "simple shear flows."

(a) Fluid planes that are parallel to the bounding plates move rigidly; since these planes consist of the same set of fluid particles at all times, we call them material planes or surfaces. These form a one-parameter family of material surfaces, y = constant, and each member is denoted as a *shearing plane.* Note that the distance between any two particles in a shearing plane is constant.

(b) The volume of every material element remains constant throughout the flow. The constant volume condition is a requirement for a shear flow independent of the assumption of incompressibility used in this book.

(c) The direction of relative motion of the shearing planes is denoted by the unit vector $\boldsymbol{\delta}_x$ along the x-coordinate axis. If at any instant we trace out a curve to which $\boldsymbol{\delta}_x$ is everywhere tangent, we generate a straight line that we call a *line of shear*. In the present flow all of the lines of shear are parallel to the x-axis, and they are coincident with fluid particle pathlines. This latter property does not hold in all shear flows as we shall see in Example 3.7-1. In simple shear flow, the lines of shear are material lines.

(d) The shear rate $\dot{\gamma}$, which is equal to the relative sliding velocity of any two shearing planes divided by the distance between them, is a constant.

(e) Finally, in Cartesian coordinates the velocity gradient tensor has the form

$$\nabla \boldsymbol{v} = \dot{\gamma}_{yx} \begin{pmatrix} 0 & 0 & 0 \\ 1 & 0 & 0 \\ 0 & 0 & 0 \end{pmatrix} = \boldsymbol{\delta}_y \boldsymbol{\delta}_x \dot{\gamma}_{yx} \tag{3.7-1}$$

and hence,

$$\dot{\boldsymbol{\gamma}} = \dot{\gamma}_{yx} \begin{pmatrix} 0 & 1 & 0 \\ 1 & 0 & 0 \\ 0 & 0 & 0 \end{pmatrix} = (\boldsymbol{\delta}_x \boldsymbol{\delta}_y + \boldsymbol{\delta}_y \boldsymbol{\delta}_x) \dot{\gamma}_{yx} \tag{3.7-2}$$

By using Eq. 3.7-2, it is not difficult to show that the shear rate $\dot{\gamma} = |\dot{\gamma}_{yx}|$ is related to the second invariant of $\dot{\boldsymbol{\gamma}}$ (see Eq. A.3-21):

$$\dot{\gamma} = \sqrt{\tfrac{1}{2} II} = \sqrt{\tfrac{1}{2}(\dot{\boldsymbol{\gamma}} : \dot{\boldsymbol{\gamma}})} \tag{3.7-3}$$

One can take as a definition for steady simple shear flow, either properties **(a)** to **(d)** or property **(e)**.

Now that we have discussed steady simple shear flow in some detail we are ready to give the definition of general shear flow: one that is not necessarily steady-state, rectilinear, or homogeneous and that does not have plane shearing surfaces. To this general definition, we then add a sequence of further requirements that define special kinds of shear flow; this specialization process will end at our original example, steady simple shear flow.

We define a *shear flow* to be a flow in which:

i. There is a one-parameter family of material surfaces, the *shearing surfaces*, which move isometrically, that is, the distance between any two neighboring particles in the surface is constant; and

ii. The volume of every fluid element is constant.

As an alternative to **(i)** and **(ii)** one could use **(i)** and

ii′. The separation of any two neighboring shearing surfaces is constant.

At any instant, a family of curves can be drawn on each shearing surface so that they are tangent to the direction of relative sliding motion at each particle. These curves are known as *lines of shear*. For an arbitrary shear flow defined by **(i)** and **(ii)** above, the lines of shear are not necessarily material lines, that is, they do not necessarily consist of the same set of material particles at every instant. From the material point of view, then, the lines of shear are in general functions of time, since they must be drawn differently on the shearing surfaces at different times.

We now define a type of shear flow for which the lines of shear are "constant." These are *unidirectional shear flows*, and they have the following property in addition to (i) and (ii):

iii. The lines of shear are material lines.

Unidirectional shear flow is the most frequently encountered kind of shear flow. The lines of shear are constant in the sense that if a line of shear is drawn on a shearing surface at any particular time, then the same material particles that lie along the curve at that time also fall on the same line of shear at any other time.

In order to describe the kinematics of shear flows mathematically, it is useful to introduce a coordinate system based on the shapes of the shearing surfaces. We construct an orthogonal curvilinear coordinate system with unit vectors $\hat{\boldsymbol{\delta}}_1$, $\hat{\boldsymbol{\delta}}_2$, and $\hat{\boldsymbol{\delta}}_3$ at every particle so that at any time $\hat{\boldsymbol{\delta}}_1$ and $\hat{\boldsymbol{\delta}}_3$ are tangent to a shearing surface and $\hat{\boldsymbol{\delta}}_2$ is normal to the shearing surface. Furthermore we take the grid of $\hat{x}_1$- and $\hat{x}_3$-coordinate curves to be imprinted on the shearing surfaces so that these curves are made up of material particles. We shall refer to the $\hat{\boldsymbol{\delta}}_i$ set of axes as "shear axes"; notice that from a spatial point of view the shear axes may be functions of time as well as position. Since the lines of shear are material lines for unidirectional shear flow, we may choose the $\hat{x}_1$-curves to coincide with the lines of shear for this kind of shearing motion. We then call the direction denoted by $\hat{\boldsymbol{\delta}}_1$ "the direction of shear." Referred to the $\hat{\boldsymbol{\delta}}_1\hat{\boldsymbol{\delta}}_2\hat{\boldsymbol{\delta}}_3$-axes, the velocity gradient tensor at every particle has the following form in unidirectional shear flow:[2]

$$\boxed{\nabla\hat{\boldsymbol{v}} = \hat{\dot{\gamma}}_{21}(t)\begin{pmatrix}0 & 0 & 0\\ 1 & 0 & 0\\ 0 & 0 & 0\end{pmatrix} = \hat{\boldsymbol{\delta}}_2\hat{\boldsymbol{\delta}}_1\hat{\dot{\gamma}}_{21}(t)} \tag{3.7-4}$$

and the rate-of-strain tensor can be written

$$\boxed{\hat{\boldsymbol{\dot{\gamma}}} = \hat{\dot{\gamma}}_{21}(t)\begin{pmatrix}0 & 1 & 0\\ 1 & 0 & 0\\ 0 & 0 & 0\end{pmatrix} = (\hat{\boldsymbol{\delta}}_1\hat{\boldsymbol{\delta}}_2 + \hat{\boldsymbol{\delta}}_2\hat{\boldsymbol{\delta}}_1)\hat{\dot{\gamma}}_{21}(t)} \tag{3.7-5}$$

(See Problem 3C.2 for the corresponding form for $\dot{\boldsymbol{\gamma}}$ for arbitrary shear flows.) Here $\hat{\boldsymbol{v}}$ is the velocity as seen in the shear axes frame of reference. Since $\boldsymbol{v}$ and $\hat{\boldsymbol{v}}$ differ by at most a rigid rotation and rigid translation, $\nabla\boldsymbol{v}$ and $\nabla\hat{\boldsymbol{v}}$ may differ by a rigid rotation, but $\dot{\boldsymbol{\gamma}}$ and $\hat{\dot{\boldsymbol{\gamma}}}$ must be the same. Of course, the components $\dot{\gamma}_{ij}(t)$ and $\hat{\dot{\gamma}}_{ij}(t)$ will be different unless the $\boldsymbol{\delta}_i$ and $\hat{\boldsymbol{\delta}}_i$ are coincident at time t. Note that $\dot{\gamma} = |\hat{\dot{\gamma}}_{21}(t)|$ is related to the second invariant of the rate-of-strain tensor just as in steady simple shear flow; it can thus be computed using the definition of $\dot{\gamma}$ in Eq. 3.7-3 provided that $\dot{\boldsymbol{\gamma}}$ is known in *any* coordinate system. By comparing Eqs. 3.7-4 and 3.7-5 with Eqs. 3.7-1 and 3.7-2, we see that at every particle unidirectional shear flow is a simple shear flow when viewed from the particle shear axes.

The motion of a typical fluid element in unidirectional shear flow is depicted in Fig. 3.7-1. Note that the same fluid particles lie along $\hat{\boldsymbol{\delta}}_1$ and $\hat{\boldsymbol{\delta}}_3$ at times t and t'; whereas different fluid particles lie along $\hat{\boldsymbol{\delta}}_2$ at the two different times. From a particle point of view, different unidirectional shear flows are obtained by changing the time dependence of $\hat{\dot{\gamma}}_{21}$ in Eq. 3.7-4. The various time-dependent unidirectional shear flow experiments used in rheology are illustrated in Fig. 3.4-1 for simple shear flow.

[2] For the use of matrices to display the components of a tensor, see §A.9.

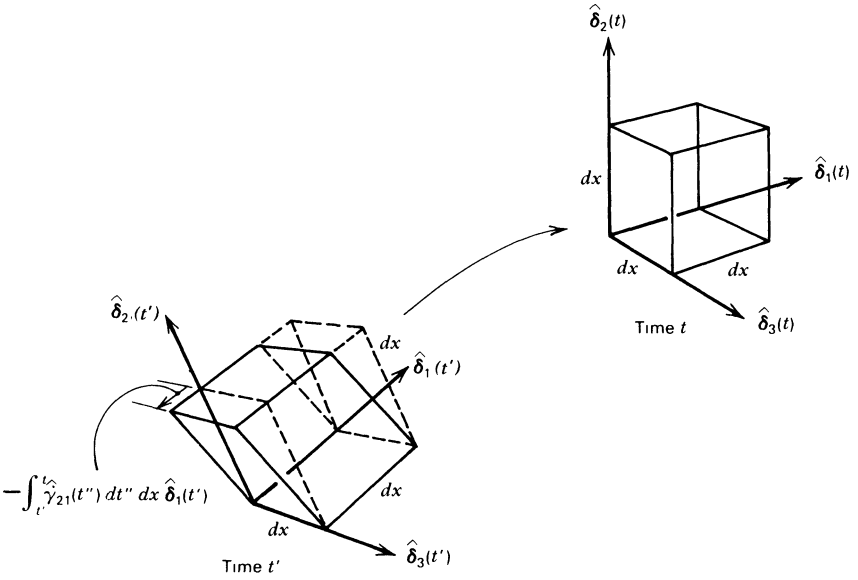

FIGURE 3.7-1. Motion of a typical fluid element of volume $(dx)^3$ undergoing unidirectional shear flow. The deformation that takes the element from its shape at some past time t' to its shape at the present time t is a simple shear flow with shear rate $\hat{\dot{\gamma}}_{21}(t)$. The unit vectors $\hat{\boldsymbol{\delta}}_1$, $\hat{\boldsymbol{\delta}}_2$, $\hat{\boldsymbol{\delta}}_3$ specify the coordinate system from which the flow is seen as simple shear. The same fluid particles lie along $\hat{\boldsymbol{\delta}}_1$ and $\hat{\boldsymbol{\delta}}_3$ at times t' and t, but different fluid particles mark $\hat{\boldsymbol{\delta}}_2$ at the two times. The top and bottom faces of the cube are parts of adjacent shearing surfaces.

Next, we define *rheologically steady shear flow* or *viscometric flow*[3] as a unidirectional shear flow for which:

iv. The velocity gradient $\hat{\dot{\gamma}}_{21}$ is independent of time at a given particle.

In view of Eq. 3.7-4, an alternative way[4] of defining viscometric flow is that the flow history at any particle be one of steady simple shear as seen from the shear axes at the particle.[5] Note that this definition requires the flow to be steady following a particle. In rheologically

[3] This definition of viscometric flow is not universal. It is the same definition used by B. D. Coleman, H. Markovitz, and W. Noll, *Viscometric Flows of Non-Newtonian Fluids*, Springer, New York (1966), and by Pipkin and Tanner (see footnote 5). Some rheologists use the word viscometric to stand for a unidirectional shear flow.

[4] For future reference the finite strain tensor $\boldsymbol{\gamma}^{[0]}(t, t')$, as defined in §8.1, has the form

$$\boldsymbol{\gamma}^{[0]} = \begin{pmatrix} 0 & -(t-t')\hat{\dot{\gamma}}_{21} & 0 \\ -(t-t')\hat{\dot{\gamma}}_{21} & (t-t')^2\hat{\dot{\gamma}}_{21}^2 & 0 \\ 0 & 0 & 0 \end{pmatrix} \tag{3.7-5a}$$

when referred to the shear axes. Requiring $\boldsymbol{\gamma}^{[0]}$ to be given in this way is equivalent to both definitions of viscometric flow given in the text. The rate-of-strain tensor may be calculated from $\boldsymbol{\gamma}^{[0]}$ using the relation given in Table 9.3-1 that

$$\dot{\boldsymbol{\gamma}}(t) = \left[\frac{\partial}{\partial t'}\boldsymbol{\gamma}^{[0]}(t, t')\right]\Bigg|_{t'=t} \tag{3.7-5b}$$

[5] This is the approach taken in the review article by A. C. Pipkin and R. I. Tanner, *Mech. Today*, **1**, 262-321 (1972). We have drawn on this review in Example 3.7-1.

complex fluids that exhibit memory effects (cf. §2.5), this definition of steady flow is preferable to the usual hydrodynamic one. We refer, then, to flows steady at a fluid particle as "rheologically steady." The velocity gradient $\hat{\dot{\gamma}}_{21}$ at a particle is constant; however, $\hat{\dot{\gamma}}_{21}$ can vary from particle to particle. If $\hat{\dot{\gamma}}_{21}$ does not vary from particle to particle, then the flow is homogeneous as well. An example of a flow that is steady in the hydrodynamical sense that $\partial \boldsymbol{v}(\boldsymbol{r}, t)/\partial t = 0$, but that is rheologically unsteady is eccentric-disk rheometer flow (see Problem 3B.1). Some examples of rheologically steady shear flows are steady-state tube flow, steady tangential annular flow, and steady axial annular flow.

TABLE 3.7-2

Examples of Viscometric Flow

Flow	Velocity Field	Shear Axes / Shear Rate	Shearing Surfaces / Lines of Shear
a. Steady tube flow 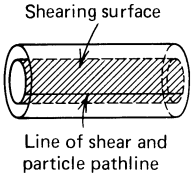 (*a*)	$v_z = v_z(r)$ $v_r = 0$ $v_\theta = 0$	$\hat{\boldsymbol{\delta}}_1 = \boldsymbol{\delta}_z$ $\hat{\boldsymbol{\delta}}_2 = \boldsymbol{\delta}_r$ $\hat{\boldsymbol{\delta}}_3 = \boldsymbol{\delta}_\theta$ $\dot{\gamma} = -\frac{d}{dr} v_z$	Concentric cylinders Straight lines parallel to the tube axis
b. Steady tangential annular flow 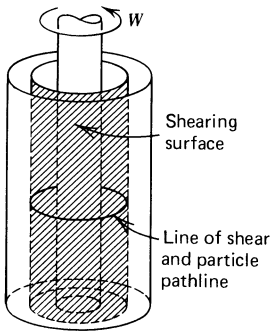 (*b*)	$v_\theta = v_\theta(r)$ $v_r = 0$ $v_z = 0$	$\hat{\boldsymbol{\delta}}_1 = \boldsymbol{\delta}_\theta$ $\hat{\boldsymbol{\delta}}_2 = \boldsymbol{\delta}_r$ $\hat{\boldsymbol{\delta}}_3 = -\boldsymbol{\delta}_z$ $\dot{\gamma} = -r \frac{d}{dr}\left(\frac{v_\theta}{r}\right)$	Concentric cylinders Circles of constant r and z
c. Steady torsional flow 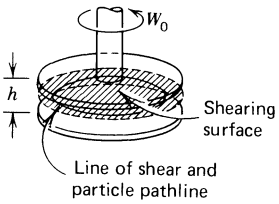	$v_\theta = \frac{rzW_0}{h}$ $v_r = 0$ $v_z = 0$	$\hat{\boldsymbol{\delta}}_1 = \boldsymbol{\delta}_\theta$ $\hat{\boldsymbol{\delta}}_2 = \boldsymbol{\delta}_z$ $\hat{\boldsymbol{\delta}}_3 = \boldsymbol{\delta}_r$ $\dot{\gamma} = rW_0/h$	Parallel disks Circles of constant r and z

TABLE 3.7-2 (*continued*)

d. Steady cone-and-plate flow (small cone angle) 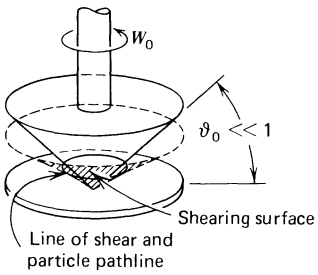 (*d*)	$v_\phi = rf(\theta)$ $v_\theta = 0$ $v_r = 0$	$\hat{\boldsymbol{\delta}}_1 = \boldsymbol{\delta}_\phi$ $\hat{\boldsymbol{\delta}}_2 = -\boldsymbol{\delta}_\theta$ $\hat{\boldsymbol{\delta}}_3 = \boldsymbol{\delta}_r$ $\dot{\gamma} = -\frac{1}{r}\frac{\partial v_\phi}{\partial \theta}$	Cones of constant θ Circles of constant r and z
e. Steady helical flow 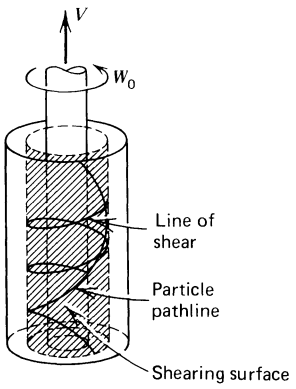 (*c*)	$v_\theta = v_\theta(r)$ $v_z = v_z(r)$ $v_r = 0$	$\hat{\boldsymbol{\delta}}_1 = \frac{1}{\dot{\gamma}}\left[\boldsymbol{\delta}_\theta r \frac{d}{dr}\left(\frac{v_\theta}{r}\right) + \boldsymbol{\delta}_z \frac{dv_z}{dr}\right]$ $\hat{\boldsymbol{\delta}}_2 = \boldsymbol{\delta}_r$ $\hat{\boldsymbol{\delta}}_3 = \frac{1}{\dot{\gamma}}\left[\boldsymbol{\delta}_\theta \frac{dv_z}{dr} - \boldsymbol{\delta}_z r \frac{d}{dr}\left(\frac{v_\theta}{r}\right)\right]$ $\dot{\gamma} = +\sqrt{\left(r\frac{d}{dr}\left(\frac{v_\theta}{r}\right)\right)^2 + \left(\frac{dv_z}{dr}\right)^2}$	Concentric cylinders Helices

The viscometric flows in Table 3.7-1 are especially marked. It is important to be able to identify these flows, as we shall later obtain a constitutive equation that describes viscometric flows for a wide class of polymeric materials (see §9.6). In Example 3.7-1 we show that steady tube flow, tangential annular flow, and helical flow are viscometric flows. These and some other viscometric flows are listed in Table 3.7-2 along with some of their identifying characteristics.

Before proceeding to Example 3.7-1, we point out that *rectilinear shear flows* are defined by (i), (ii), (iii), and

v. The fluid particle pathlines are straight lines.

Finally, *steady simple shear flow* is a viscometric flow for which, in addition to (i), (ii), (iii), and (iv), we require

vi. The shearing surfaces are planes, that is, the shear axes $\hat{\boldsymbol{\delta}}_1$, $\hat{\boldsymbol{\delta}}_2$, $\hat{\boldsymbol{\delta}}_3$ are everywhere identical to the rectangular Cartesian axes $\boldsymbol{\delta}_x$, $\boldsymbol{\delta}_y$, $\boldsymbol{\delta}_z$.

vii. The flow is homogeneous, that is, the velocity gradient $\hat{\gamma}_{21} = \dot{\gamma}_{yx}$ is independent of position.

EXAMPLE 3.7-1 Kinematics of Steady Tube Flow, Steady Tangential Annular Flow, and Steady Helical Flow

Consider the three fluid flows: **(a)** steady axial tube flow under a constant pressure gradient, **(b)** steady tangential annular flow between two concentric cylinders in relative rotation, and **(c)** steady helical flow between two coaxial cylinders, the inner one of which is rotating and is translating in the axial direction. In **(a)** the motion of the liquid will be such that $v_z = v_z(r)$, $v_r = 0$, and $v_\theta = 0$; in **(b)** the velocity field will have the form $v_\theta = v_\theta(r)$, $v_z = 0$, and $v_r = 0$; and in **(c)**, $v_\theta = v_\theta(r)$, $v_z = v_z(r)$, and $v_r = 0$. Show that all of these flows are viscometric according to the definition given in the text.

SOLUTION **(a)** Steady Tube Flow

Since the fluid velocity is in the z-direction only and varies in the r-direction only, the flow can be pictured as the relative axial sliding motion of concentric cylinders of fluid. These rigid cylindrical material surfaces are then the shearing surfaces and perform a telescoping motion. The shear axes correspond to the cylindrical coordinate axes as follows: $\hat{\boldsymbol{\delta}}_1 = \boldsymbol{\delta}_z$, $\hat{\boldsymbol{\delta}}_2 = \boldsymbol{\delta}_r$ and $\hat{\boldsymbol{\delta}}_3 = \boldsymbol{\delta}_\theta$. It is easy to see that the lines of shear are parallel to the z-axis and are also fluid pathlines. Referred to the shear axes, the velocity gradient tensor is

$$\dot{\boldsymbol{\gamma}} = \hat{\boldsymbol{\delta}}_2\hat{\boldsymbol{\delta}}_1\hat{\dot{\gamma}}_{21}(r) \tag{3.7-6}$$

where $\hat{\dot{\gamma}}_{21}(r) = dv_z(r)/dr = -\dot{\gamma}$ is constant for each material particle since each particle moves at constant r. Thus the flow history at every particle is a steady simple shearing moton and the flow is viscometric.

(b) Steady Tangential Annular Flow

Once again the shearing surfaces are concentric cylinders. At any time t, the shear axes at a particle P are related to the cylindrical coordinate axes at the position of the particle as follows: $\hat{\boldsymbol{\delta}}_1 = \boldsymbol{\delta}_\theta$, $\hat{\boldsymbol{\delta}}_2 = \boldsymbol{\delta}_r$, and $\hat{\boldsymbol{\delta}}_3 = -\boldsymbol{\delta}_z$. In order to compute the velocity gradient tensor relative to the shear axes at P, we note that a point fixed relative to the shear axes has velocity $(v_\theta/r)_P r$ referred to the space-fixed cylindrical coordinate system. Here $(v_\theta/r)_P$ is the constant angular velocity of P as it moves in its circular trajectory. Thus when viewed from the shear axes, the velocity field is $\hat{v}_1 = v_\theta - (v_\theta/r)_P r$, $\hat{v}_2 = \hat{v}_3 = 0$. Since at any instant the shear coordinate system is coincident with the cylindrical one, we can use the relations for the components of $\nabla \boldsymbol{v}$ given in Table A.7-2 to find

$$\nabla\hat{\boldsymbol{v}} = \hat{\boldsymbol{\delta}}_2\hat{\boldsymbol{\delta}}_1\frac{d\hat{v}_1}{dr} - \hat{\boldsymbol{\delta}}_1\hat{\boldsymbol{\delta}}_2\frac{\hat{v}_1}{r} \tag{3.7-7}$$

But

$$\frac{d\hat{v}_1}{dr} = \frac{d}{dr}\left[v_\theta - \left(\frac{v_\theta}{r}\right)_P r\right] = \frac{dv_\theta}{dr} - \left(\frac{v_\theta}{r}\right)_P = r\frac{d}{dr}\left(\frac{v_\theta}{r}\right) + \frac{v_\theta}{r} - \left(\frac{v_\theta}{r}\right)_P \tag{3.7-8}$$

When Eq. 3.7-8 is substituted into Eq. 3.7-7 and the velocity gradient tensor evaluated at the particle P, we find

$$(\nabla\hat{\boldsymbol{v}})\Big|_P = \hat{\boldsymbol{\delta}}_2\hat{\boldsymbol{\delta}}_1\hat{\dot{\gamma}}_{21}(r) \tag{3.7-9}$$

where $\hat{\dot{\gamma}}_{21} = rd(v_\theta/r)/dr$ is the constant shear rate at the particle and is equal to $-\dot{\gamma}$ if the inner cylinder is rotating and the outer one fixed. The flow at any particle P is thus steady simple shear as seen from the shear axes; according to the definition, then, tangential annular flow is a viscometric flow.

(c) Steady Helical Flow

In this flow the direction of shear is not so obvious as in the two preceding parts. Hence, in this part we show how the shear axes may be determined in the process of writing the velocity gradient tensor in the form appropriate to a steady simple shear flow. Again we compute the velocity gradient with respect to shear axes at an arbitrary particle P.

Because the shearing surfaces are concentric cylinders, at any time t the unit vector $\hat{\boldsymbol{\delta}}_2$ at P is coincident with $\boldsymbol{\delta}_r$. Furthermore, the unit vectors $\hat{\boldsymbol{\delta}}_1$ and $\hat{\boldsymbol{\delta}}_3$ are tangent to the cylindrical surfaces so that at any time $\boldsymbol{\delta}_\theta$ and $\boldsymbol{\delta}_z$ can be expressed in terms of them:

$$\begin{aligned} \boldsymbol{\delta}_\theta &= \hat{\boldsymbol{\delta}}_1 a + \hat{\boldsymbol{\delta}}_3 b \\ \boldsymbol{\delta}_z &= \hat{\boldsymbol{\delta}}_1 b - \hat{\boldsymbol{\delta}}_3 a \end{aligned} \tag{3.7-10}$$

where a and b depend on the details of the flow field and $\sqrt{a^2 + b^2} = 1$.

We now note that a point, which is stationary as seen from the shear axes at P, has velocity $\boldsymbol{v} = \boldsymbol{\delta}_\theta (v_\theta/r)_P r + \boldsymbol{\delta}_z (v_z)_P$ relative to the space-fixed cylindrical coordinate system. Thus the velocity $\hat{\boldsymbol{v}}$ of any fluid element relative to the shear axes at P may be written in terms of the cylindrical coordinate unit vectors:

$$\hat{\boldsymbol{v}} = \boldsymbol{\delta}_\theta \left[v_\theta - \left(\frac{v_\theta}{r}\right)_P r \right] + \boldsymbol{\delta}_z \left[v_z - (v_z)_P \right] \tag{3.7-11}$$

The velocity gradient relative to the shear axes is readily computed in the cylindrical coordinate system by using Table A.7-2:

$$\nabla \hat{\boldsymbol{v}} = \boldsymbol{\delta}_r \boldsymbol{\delta}_\theta \frac{d}{dr} \left[v_\theta - \left(\frac{v_\theta}{r}\right)_P r \right] + \boldsymbol{\delta}_r \boldsymbol{\delta}_z \frac{d}{dr} \left[v_z - (v_z)_P \right] + \boldsymbol{\delta}_\theta \boldsymbol{\delta}_r \left[-\frac{v_\theta}{r} + \left(\frac{v_\theta}{r}\right)_P \right] \tag{3.7-12}$$

When this is evaluated at the particle P we find

$$(\nabla \hat{\boldsymbol{v}})\Big|_P = \boldsymbol{\delta}_r \boldsymbol{\delta}_\theta r \frac{d}{dr}\left(\frac{v_\theta}{r}\right) + \boldsymbol{\delta}_r \boldsymbol{\delta}_z \frac{dv_z}{dr} = \hat{\boldsymbol{\delta}}_2 \hat{\boldsymbol{\delta}}_1 \hat{\dot{\gamma}}_{21} \tag{3.7-13}$$

where the last equality above emphasizes that when the velocity gradient is written in terms of the $\hat{\boldsymbol{\delta}}_i$, it must have the simple shear flow form. By substituting Eqs. 3.7-10 into Eq. 3.7-13 we can make the following identifications:

$$\hat{\boldsymbol{\delta}}_1 = \frac{1}{\dot{\gamma}} \left[\boldsymbol{\delta}_\theta r \frac{d}{dr}\left(\frac{v_\theta}{r}\right) + \boldsymbol{\delta}_z \frac{dv_z}{dr} \right] \tag{3.7-14}$$

$$\hat{\boldsymbol{\delta}}_3 = \frac{1}{\dot{\gamma}} \left[\boldsymbol{\delta}_\theta \frac{dv_z}{dr} - \boldsymbol{\delta}_z r \frac{d}{dr}\left(\frac{v_\theta}{r}\right) \right] \tag{3.7-15}$$

$$\dot{\gamma} = \sqrt{\left(r \frac{d}{dr}\left(\frac{v_\theta}{r}\right) \right)^2 + \left(\frac{dv_z}{dr}\right)^2} \tag{3.7-16}$$

Thus steady helical flow is a steady simple shear flow if seen from the shear axes given in Eqs. 3.7-14 and 3.7-15, and it is thus a viscometric flow. Note that Eq. 3.7-16 can also be obtained from the postulated velocity field, the definition of $\dot{\gamma}$ in Eq. 3.7-3, and Eqs. B.3-7 to 12. Equation 3.7-16 serves to emphasize that the terms "shear rate" and "velocity gradient" are not synonymous.

In parts **(a)** and **(b)** of this example, the lines of shear and the particle pathlines are identical, since $\hat{\boldsymbol{\delta}}_1$ is everywhere parallel to the local fluid velocity vector (see Table 3.7-2a and b). Steady helical flow, however, is a flow in which the particle pathlines and the lines of shear are different. The pathline

is the curve traced out by a given particle as it moves about in space. Since the flow considered here is steady, the velocity vector at any position is constant, and thus the pathline is the curve that is everywhere tangent to the velocity vector $\boldsymbol{v} = \boldsymbol{\delta}_\theta v_\theta + \boldsymbol{\delta}_z v_z$. On the other hand the line of shear is defined as the curve that, at any instant, is everywhere tangent to $\hat{\boldsymbol{\delta}}_1$. Since the flow is steady, the line of shear is independent of time. From Eq. 3.7-14 we see that $\hat{\boldsymbol{\delta}}_1$ is not in general parallel to $\boldsymbol{v}$ so that the line of shear is different than the particle pathline (see Table 3.7-2e).

b. Shearfree Flows

A *shearfree flow*[6] is defined as a flow for which it is possible to select for every fluid element an orthogonal set of unit vectors $\hat{\boldsymbol{\delta}}_i$ fixed in the element so that referred to these axes the rate-of-strain tensor has a diagonal form:

$$\dot{\boldsymbol{\gamma}} = \begin{pmatrix} \hat{\dot{\gamma}}_{11} & 0 & 0 \\ 0 & \hat{\dot{\gamma}}_{22} & 0 \\ 0 & 0 & \hat{\dot{\gamma}}_{33} \end{pmatrix} = \hat{\boldsymbol{\delta}}_1\hat{\boldsymbol{\delta}}_1\hat{\dot{\gamma}}_{11} + \hat{\boldsymbol{\delta}}_2\hat{\boldsymbol{\delta}}_2\hat{\dot{\gamma}}_{22} + \hat{\boldsymbol{\delta}}_3\hat{\boldsymbol{\delta}}_3\hat{\dot{\gamma}}_{33} \tag{3.7-17}$$

In addition we require that the volume remain constant in a shearfree flow so that $\hat{\dot{\gamma}}_{11} + \hat{\dot{\gamma}}_{22} + \hat{\dot{\gamma}}_{33} = 0$. By "fixed in a fluid element" we mean that at every time t the same fluid particles lie along each of the $\hat{\boldsymbol{\delta}}_i$'s.[7] The particle-fixed axes $\hat{\boldsymbol{\delta}}_i$ used in Eq. 3.7-17 are known as the *principal axes of rate of strain.* At any instant, the rate-of-strain tensor has the same form given above when referred to an orthogonal space-fixed coordinate system which has the same orientation everywhere as the principal axes of rate of strain.

A shearfree flow is *homogeneous* if the $\hat{\dot{\gamma}}_{ij}$ are independent of position. A homogeneous, shearfree flow for which the ratios of the $\hat{\dot{\gamma}}_{ij}$ (i.e., $\hat{\dot{\gamma}}_{11}/\hat{\dot{\gamma}}_{22}$, $\hat{\dot{\gamma}}_{22}/\hat{\dot{\gamma}}_{33}$) are independent of time is said to be a *simple shearfree flow.*

EXAMPLE 3.7-2. Kinematics of Flow into a Line Sink

A fluid is flowing into a line sink located at $r = 0$ in a cylindrical coordinate system. The strength of the sink is Q where Q is the volume rate of flow into the sink per unit length. Show that this flow is a shearfree flow.

SOLUTION The fluid velocity field is of the form $v_r = v_r(r)$, $v_\theta = v_z = 0$. From Table B.3 we have the rate-of-strain tensor in cylindrical coordinates:

$$\dot{\boldsymbol{\gamma}} = \begin{pmatrix} 2\dfrac{dv_r}{dr} & 0 & 0 \\ 0 & \dfrac{v_r}{r} & 0 \\ 0 & 0 & 0 \end{pmatrix} \tag{3.7-18}$$

[6] See also A. S. Lodge, *Elastic Liquids*, Academic Press, New York (1964), pp. 35–38; A. S. Lodge, *Body Tensor Fields in Continuum Mechanics*, Academic Press, New York (1974), pp. 81–83, 175–176; B. D. Coleman, *Proc. Roy. Soc.*, **A306**, 449-476 (1968). Coleman calls these flows "extensions." Thorough reviews of theoretical and experimental aspects of shearfree flows are given by J. M. Dealy, *Polym. Eng. Sci.*, **11**, 433-445 (1971); K. Walters, *Rheometry*, Chapman and Hall, London (1975), Chapt. 7; and C. J. S. Petrie, *Elongational Flows*, Pitman, London (1979).

[7] Since $\dot{\boldsymbol{\gamma}}$ is symmetric, it is always possible at any time t to select an orthogonal set of unit vectors at a given fluid element such that $\dot{\boldsymbol{\gamma}}$ is diagonal when referred to these axes. However, in general, these axes will not be tangent to curves defined by the same set of material particles at different times, and they are therefore not fixed in the